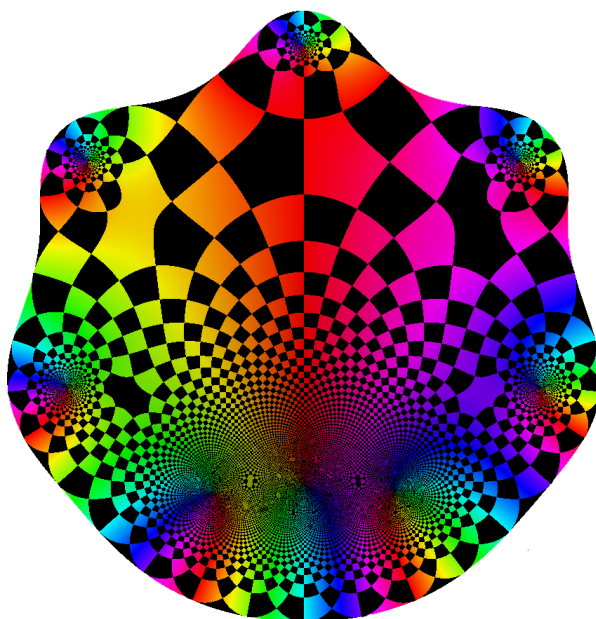


# Quiver vacua geometry *and* fermions on branes

Ph.D. Thesis

**Jamie Luke Edward Rogers**

October 2021



Thesis submitted in accordance with  
the requirements of the University of Liverpool  
for the degree of Doctor in Philosophy

Supervised by Dr. Radu Tatar



# Abstract

This thesis explores two topics from the intersection between string theory, quantum field theory, and geometry. While the two topics share some overarching themes, for practical purposes they are distinct areas of research. Therefore this work is presented in two parts, treated separately.

## Quiver vacua geometry

Supersymmetric quantum fields theories with eight supercharges are intimately related with numerous topics in geometry. Theories living in three dimensions and enjoying  $\mathcal{N} = 4$  supersymmetry are perhaps the most accessible such theories. The fields in these theories are arranged into hyper- and vector multiplets, both containing scalar fields. The field-content and symmetries of these theories may be denoted using a *quiver*, a type of graph in which edges and nodes have specific interpretations in terms of multiplets and symmetries. The possible lowest energy states (vacua) for these theories are associated to *vacuum expectation values* (VEVs) of the scalar fields. These possible vacua can be organised as an affine variety wherein each point corresponds to a particular set of scalar VEVs. This variety is called the *moduli space of vacua* for the theory in question. For the class of linear quivers, these varieties are known to be *nilpotent varieties* in  $\mathfrak{sl}_n$ . In Part I of this thesis, after introducing the necessary machinery, we explore the geometry of the moduli space of vacua of two sets of quiver gauge theories which appear as natural generalisations of the linear case. These are *circular* quiver gauge theories and D-type Dynkin quiver gauge theories. A central tool in our work is the *Kraft-Procesi transition* which can be thought of as a physical interpretation of the singularity structure of the affine variety associated to the possible vacua for a given theory.

## Fermions on branes

In Part II we make a detailed study of the fermionic fields living on brane worldvolumes. In string phenomenology many of the most promising candidates for the construction of a small, positive cosmological constant in a string theoretic setting rely on ingredients in which the fermionic couplings of fields living on brane worldvolumes play a critical role. We use the superspace formulation of supergravity in eleven and ten dimensions to compute fermion couplings on the M2-brane and on  $Dp$ -branes. Fermionic couplings arise naturally from the expansion of the superfields in orders of the fermionic coordinates of superspace. The techniques we use and develop can be applied to determine the fermionic couplings to background fields up to arbitrary fermionic order. We start with the superspace formulation of 11-dimensional supergravity and use a geometric technique known as the *normal coordinate* method to obtain the  $\theta$ -expansion of the M2-brane action. We then present a method which allows the translation of knowledge of fermionic couplings on the M2-brane to knowledge of such couplings on the D2-brane, and then to any  $Dp$ -brane. This method is based on superspace generalizations of both the compactification taking 11-dimensional supergravity to type IIA supergravity and the T-duality rules connecting the type IIA and type IIB supergravities.



# Declaration of originality

I, Jamie Luke Edward Rogers, hereby declare that all of the work presented in this thesis is the result of my own research unless reference to other work is provided. The material presented here has been used as the basis for the following collaborative publications:

- J. Rogers and R. Tatar, *Moduli space singularities for  $3d \mathcal{N} = 4$  circular quiver gauge theories*, *JHEP* **11** (2018) [[1807.01754](#)].
- J. Rogers and R. Tatar,  *$D_n$  Dynkin quiver moduli spaces*, *J. Phys. A* **52** (2019) [[1902.10019](#)].
- A. Retolaza, J. Rogers, R. Tatar and F. Tonioni, *Branes, fermions, and superspace dualities*, *JHEP* **10** (2021) [243](#) [[2106.02090](#)].

Large parts of these publications are included, verbatim, in this thesis. All work was carried out in the Theoretical Physics Division of the Department of Mathematical Sciences, University of Liverpool, UK, between October 2017 and September 2021.



*For my parents,  
for their unwavering support,  
unconditional love,  
and imperturbable pragmatism.*





My first and deepest thanks go to my supervisor these last four years, Radu Tatar. Thank you for your belief in me and thank you for expressing it often and unabashedly. Thank you for the freedom and flexibility you afforded me when I needed it, and for the guidance and advice when I needed that. Thank you for allowing me to only ever look forward to our meetings and discussions, for letting me ramble around subjects in my scatter-gun way, and for never once making me feel stupid for spending most of the time incorrect.

Next my thanks go to Flavio and to Ander, without whom the second half of this thesis would certainly not exist. It was a pleasure working with you through thick and thin, thank you for the support, thank you for all the hard work, and thank you for keeping my spirits up when I needed it, as I hope I did for you in return. Thank you also to the members of the quiver group at Imperial, but especially to Ami and Santi under whose wings I spent a short but formative time, and without whom the first half of this thesis would also not exist.

I have had the pleasure of working among some amazing people these last four years at Liverpool, I daren't begin thanking all of you individually for fear of never stopping. It would be amiss, however, to not thank Flavio again, for the encouragement and humour, for the companionship on countless late nights in the office beavering away, and for only rubbing Italy's victories in as much as was strictly necessary. And thank you especially to Giacomo for demonstrating to me better than anyone else that ambition need never come at the expense of creativity or kindness, you're genuinely inspiring.

This whole endeavour would have been impossible if not for the Swimming Team. The sanity preserving effects have been a life-saver, the mad nights-out near life-enders. The number of wonderful friends I have made has been invaluable, but once again I daren't try to list you all. Thank you Alex, Dan, Matt, and Sean, for your camaraderie, commitment, and skill, and for letting me cling on to the back of lane one in the early days. Thank you Cillian, your cool serenity and persistently excellent council have been vital on many occasions. Thank you Olly for the laughs and the memes, and for proving, in taking up a PhD of your own, that I didn't make the whole ordeal look too gruesome. Thank you Christy, for the good times and the mad, and for allowing me to foist the presidency onto you as it was foisted on to me.

Thank you enormously to my friends from Imperial and from Durham, who balance, guide, and inspire me. Whom I love and respect, and who are the best part of me. I know I can be bad at showing how much you all mean to me, forgive me again as you have so many times. I'm proud to know you all.

Most of all, thank you to my family who've supported me unfalteringly in everything I do. To my parents, whose oft-expressed pride burns fiercely in my heart, your contributions to what I do warrant coauthorships they are so essential. To my little brother Sam, for seeing the world through a very similar lens as me, for never being afraid of a competition, and, in winning most of them, for keeping me a damn sight more humble than I'd have otherwise been, as hard as you'll find that to believe. And thank you Grandma, for your patience and wisdom, for keeping me grounded, and for reminding me that there's a whole lot more to life than a bit of paper that means people will call you 'doctor', as nice a thing as that is to earn.

The front image is a plot of the complex function,

$$f(z) = \frac{1}{z^8 + 2z^2 + 4iz - 2}, \quad |f(z)| > \frac{1}{16}.$$

Plotter and details are available at [people.ucsc.edu/~wbolden/complex](http://people.ucsc.edu/~wbolden/complex).



# Contents

<b>I</b>	<b>Quiver vacua geometry</b>	<b>2</b>
<b>1</b>	<b>Introduction</b>	<b>3</b>
<b>2</b>	<b>Quivers, moduli spaces, and branes</b>	<b>5</b>
2.1	Multiplets . . . . .	5
2.2	Quivers . . . . .	6
2.3	Moduli space branches . . . . .	6
2.4	Brane constructions . . . . .	6
2.4.1	Example: $3d \mathcal{N} = 4$ SQED with 2 flavors . . . . .	8
2.4.2	Higgs mechanism . . . . .	9
2.4.3	Hanany-Witten transitions . . . . .	10
2.5	Example: $3d \mathcal{N} = 4$ SQED with $N$ flavors . . . . .	11
<b>3</b>	<b>Nilpotent varieties in Lie algebras</b>	<b>13</b>
3.1	Nilpotent elements of Lie algebras . . . . .	13
3.2	Integer partitions . . . . .	14
3.2.1	Hasse diagrams . . . . .	15
3.2.2	Restricted partitions . . . . .	15
3.3	Nilpotent orbits . . . . .	17
3.4	Closures of nilpotent orbits . . . . .	18
3.4.1	Singularity structure and labelled Hasse diagrams . . . . .	18
3.5	Slodowy slices and intersections . . . . .	21
3.5.1	Intersections for $\mathfrak{sl}_n$ . . . . .	22
3.5.2	Intersections for $\mathfrak{so}_{2n}$ . . . . .	24
<b>4</b>	<b>Linear quivers and the Kraft-Procesi transition</b>	<b>28</b>
4.1	Linear quivers . . . . .	28
4.1.1	An alternative class of linear theories . . . . .	29
4.2	Kraft-Procesi transitions in brane configurations . . . . .	32
4.3	Kraft-Procesi transitions in field theory . . . . .	35
4.4	Tables of descendant theories for $\mathfrak{sl}_N$ . . . . .	38

<b>5</b>	<b>Circular quivers</b>	<b>41</b>
5.1	The full class of good circular quiver gauge theories . . . . .	41
5.2	Moduli space dimension . . . . .	43
5.3	Performing transitions . . . . .	44
5.4	A minimal set of maximal theories . . . . .	44
5.4.1	Examples . . . . .	48
5.5	Hasse diagrams for family representatives . . . . .	49
5.5.1	The linear case: $L = 0$ . . . . .	51
5.5.2	A single wrapped brane: $L = 1$ . . . . .	51
5.5.3	$L = 1$ examples . . . . .	55
5.5.4	The schematic for $L = 2$ and orbit lattices . . . . .	55
5.5.5	Arbitrary $L$ and higher-level Hasse diagrams . . . . .	58
5.6	Hasse diagram modifications when $N_i \leq k + 2L - 1$ . . . . .	66
5.6.1	One bad edge: $N_i = k + 2L - 1$ . . . . .	67
5.6.2	A modification prescription . . . . .	69
<b>6</b>	<b>D-type Dynkin quivers</b>	<b>71</b>
6.1	Nilpotent varieties as Dynkin quiver Higgs branches . . . . .	71
6.1.1	$D_4$ quivers and nilpotent varieties of $\mathfrak{so}_8$ . . . . .	75
6.1.2	Quivers for maximal special slices . . . . .	76
6.1.3	Quivers for special slice nilpotent varieties in $\mathfrak{so}_{2n}$ . . . . .	77
6.2	Balanced $D_n$ Dynkin quivers . . . . .	79
6.2.1	Dimension matching for balanced theories . . . . .	85
6.3	From balanced to good quivers . . . . .	89
6.4	Good $D_n$ Dynkin quivers . . . . .	90
6.4.1	$D_n$ quivers of even type . . . . .	91
6.4.2	An alternative for even theories with odd partitions . . . . .	93
6.4.3	Good, even classification . . . . .	94
6.4.4	Dimension matching for good, even theories . . . . .	96
6.4.5	Recovering $\mathfrak{so}_{2n}$ nilpotent varieties . . . . .	98
6.4.6	Odd $D_n$ quiver Hasse diagram . . . . .	99
6.4.7	Good $D_n$ quivers of odd type . . . . .	102
6.4.8	Dimension matching for good, odd theories . . . . .	104
<b>7</b>	<b>Conclusions</b>	<b>105</b>
7.1	Summary . . . . .	105
7.2	Future directions . . . . .	107
<b>II</b>	<b>Fermions on branes</b>	<b>110</b>
<b>8</b>	<b>Introduction</b>	<b>111</b>

<b>9</b>	<b>Branes, fermions, and superspace</b>	<b>117</b>
9.1	Braney fermions . . . . .	117
9.1.1	Superspace perspective and the M2-brane action . . . . .	117
9.2	The bulk and $\kappa$ -symmetry . . . . .	118
9.3	Our approach . . . . .	119
<b>10</b>	<b>The ‘normal coordinate’ method</b>	<b>120</b>
10.1	Generalities . . . . .	120
10.2	A note on extra complexities . . . . .	122
10.3	Specifics . . . . .	122
<b>11</b>	<b>Eleven dimensional supergravity and the M2-brane</b>	<b>127</b>
11.1	M2-brane at fermionic order two . . . . .	129
11.2	Supersymmetry and $\kappa$ -symmetry . . . . .	130
11.3	M2-brane at fermionic order four . . . . .	132
<b>12</b>	<b>Superspace dimensional reduction and the D2-brane</b>	<b>134</b>
12.1	Reduction of 11-dim supergravity to type IIA supergravity . . . . .	134
12.2	Bosonic D2-brane action . . . . .	136
12.3	Superspace dimensional reduction and fermions on the D2-brane . . . . .	137
12.4	Order- $(\theta)^2$ terms . . . . .	139
12.5	Order- $(\theta)^4$ terms . . . . .	143
<b>13</b>	<b>Superspace T-duality and <math>Dp</math>-branes</b>	<b>150</b>
13.1	T-duality toolkit . . . . .	150
13.1.1	Bosons . . . . .	150
13.1.2	Spinors, supersymmetry operators, and spinor doublet notation . . . . .	151
13.1.3	T-duality and bosonic $Dp$ -branes . . . . .	155
13.2	A useful rearrangement . . . . .	157
13.3	Superspace T-duality and fermions on $Dp$ -branes . . . . .	158
13.3.1	Order- $(\theta)^2$ terms . . . . .	158
13.3.2	Order- $(\theta)^4$ terms . . . . .	161
<b>14</b>	<b>Conclusions</b>	<b>163</b>
14.1	Summary . . . . .	163
14.2	Future directions . . . . .	166
<b>15</b>	<b>Appendices</b>	<b>168</b>
15.1	Spinor conventions . . . . .	168
15.2	11-dimensional supergravity . . . . .	170
15.3	Order-4 vielbein manipulations . . . . .	172
15.3.1	Normal coordinate expansion of frame super-form . . . . .	172

15.3.2	Rearranging the expanded supervielbein using Bianchi identities . . . . .	173
15.4	Catalogue of dimensional reductions . . . . .	174
15.4.1	Basic dimensional reductions . . . . .	175
15.4.2	Supercovariant derivatives . . . . .	177
15.4.3	Pullbacks . . . . .	178
15.4.4	Order-4 combinations . . . . .	179
15.4.5	Dimensional reduction of the quartic 11-dimensional shifted fields for the dilaton .	180
15.5	Further comments on T-duality . . . . .	182

**References** **185**







# List of Figures

2.1	The ten spacetime dimensions for our brane set-up can be usefully illustrated . . . . .	8
2.2	SQED with 2 flavours . . . . .	9
2.3	Higgs mechanism . . . . .	10
2.4	$3d \mathcal{N} = 4$ SQED with $N$ flavours . . . . .	11
3.5	Two procedures in the Young tableaux . . . . .	15
3.6	The Hasse diagram for the partitions of $n = 6$ . . . . .	16
3.7	Hasse diagrams for restricted sets of partitions $\mathcal{P}_+(6)$ and $\mathcal{P}_+(8)$ . . . . .	16
3.8	Labelled Hasse diagrams for $\mathfrak{sl}_n$ and $\mathfrak{so}_{2n}$ . . . . .	20
3.9	A demonstration that $\mathfrak{sl}_6 \supset \bar{\mathcal{O}}_{(3^2)} \cap \mathcal{S}_{(3,1^3)} \sim \bar{\mathcal{O}}_{(3)} \subset \mathfrak{sl}_3$ . . . . .	23
3.10	Hasse diagrams for the maximal special slices, $\mathcal{S}_{(2m-1^2,1^2)} \in \mathfrak{so}_{4m}$ and $\mathcal{S}_{(2m^2,1^2)} \in \mathfrak{so}_{4m+2}$ . . . . .	26
4.11	An example theory, $\tau_{(4,2^2,1^2)}^{(3,2^3,1)}(10, 5, 5)$ . . . . .	30
4.12	Independence from $N_1$ or $N_2$ of the infrared physics in the class $\tau_{\mu^t}^\nu(M, N_1, N_2)$ . . . . .	31
4.13	$3d \mathcal{N} = 4$ SQED with $m + 1$ flavours (left) and its mirror dual (right) . . . . .	32
4.14	The Higgs brane configuration brane manipulation for Kraft-Procesi transitions . . . . .	33
4.15	Kraft-Procesi transitions to find $T_{(2^2,1)}^{(2,1^3)}(\text{SU}(5))$ within $T(\text{SU}(5))$ . . . . .	34
4.16	$\mathcal{K}(T(\text{SU}(2)))$ and $\mathcal{K}(T(\text{SU}(3)))$ . . . . .	39
4.17	$\mathcal{K}(T(\text{SU}(4)))$ . . . . .	40
4.18	$\mathcal{K}(T(\text{SU}(5)))$ . . . . .	40
5.19	The theory $\pi_{(4,2^2,1^2)}^{(3,2^3,1)}(10, 7, 7, 3)$ . . . . .	42
5.20	The breaking of degeneracy in the class of circular quivers when $L \neq 0$ . . . . .	43
5.21	The Higgs brane configuration and quiver for the theories $\pi(1, 2, 2, L)$ and $\pi(3, 2, 2, L)$ . . . . .	43
5.22	Coulomb branch singularities for $\pi(0, 3, 3, L)$ (top) and $\pi(1, 3, 3, L)$ . . . . .	45
5.23	The Young tableaux for the partitions that correspond to a possible set of maximal theories . . . . .	46
5.24	A demonstration using complementary tableaux . . . . .	47
5.25	Finding $\pi_{(3,2)}^{(2,1^3)}(5, 4, 4, L_1) \in \mathcal{K}(\pi(1, 4, 4, L_2))$ . . . . .	49
5.26	Finding $\pi_{(3,2,1)}^{(2^2,1^2)}(6, 3, 5, L_1) \in \mathcal{K}(\pi(0, 3, 5, L_2))$ . . . . .	50
5.27	The general form for the Higgs brane configuration and quiver for $\pi(k, N_1, N_2, L)$ . . . . .	50
5.28	The Hasse subdiagrams for the removal of one fully wrapped D3 brane . . . . .	52
5.29	The schematic for the general Hasse diagram for $\pi(k, N_1, N_2, 1)$ . . . . .	52
5.30	Coulomb (left) and Higgs (right) branch Hasse diagrams for $\pi(0, N_1, N_2, 1)$ . . . . .	55
5.31	Coulomb branch Hasse diagrams for $\pi(k, N_1, N_2, 1)$ for $k \in \{1, 2, 3, 4\}$ . . . . .	56

5.32	Schematic Hasse diagram for $L = 2$ . . . . .	57
5.33	Lattice schematic for Kraft-Procesi transitions . . . . .	59
5.34	The general structure of the higher-level Hasse diagram . . . . .	63
5.35	Editing when $N_2 = k + 2L - 1$ . . . . .	68
5.36	Editing $\pi(k, N_1, k + 3, 2)$ . . . . .	69
5.37	Editing $\pi(0, N_1, 3, 2)$ . . . . .	70
6.38	A general $3d \mathcal{N} = 4$ unitary $D_n$ Dynkin quiver . . . . .	71
6.39	$3d \mathcal{N} = 4$ quivers which realise $D_k, A_k \cup A_k$ and $A_k$ singularities as their Higgs branches . . . . .	73
6.40	Quiver addition of a $D_{n-2}$ singularity to the Higgs branch of a $D_n$ Dynkin quiver . . . . .	74
6.41	Quiver addition of one case of the $A_{n-3} \cup A_{n-3}$ singularity . . . . .	74
6.42	Hasse diagram for the maximal special slice in $\mathfrak{so}_8$ . . . . .	75
6.43	Dynkin quivers for all of the subvarieties of the maximal special slice of $\mathfrak{so}_8$ . . . . .	76
6.44	$D_n$ Dynkin quivers which realise the maximal special slices of $\mathfrak{so}_{4m}$ and $\mathfrak{so}_{4m+2}$ . . . . .	77
6.45	The general forms for the $D_n$ Dynkin quivers which realise $\mathfrak{so}_{2n}$ nilpotent varieties . . . . .	78
6.46	A bare $D_n$ Dynkin quiver is the $D_n$ singularity . . . . .	80
6.47	Hasse diagram for completely balanced $D_n$ Dynkin quivers . . . . .	81
6.48	The Hasse diagram resulting from balanced quiver addition for a generic $D_n$ Dynkin quiver . . . . .	82
6.49	The necessary form of a balanced $D_n$ Dynkin quiver. . . . .	83
6.50	The editing prescription for the balanced $D_n$ Hasse diagram given in Fig. 6.48 . . . . .	85
6.51	The editing prescription for the balanced Hasse diagram for $D_\kappa(4)$ for $ \kappa  \leq 8$ . . . . .	86
6.52	The general form for a good $D_n$ Dynkin quiver . . . . .	91
6.53	The general form of a good $D_n$ Dynkin quiver of even type . . . . .	91
6.54	Hasse diagram for quiver addition of even theories with an odd magnitude partition . . . . .	94
6.55	Hasse diagram for even theories with odd magnitude partitions . . . . .	95
6.56	The general structure of a $D_n$ Dynkin quiver of odd type . . . . .	99
6.57	Quiver addition for odd theories . . . . .	100
6.58	Quiver addition Hasse diagram for theories of odd type . . . . .	101
6.59	Editing odd theories . . . . .	102
6.60	Example of editing odd theories . . . . .	103
6.61	The general form of a good, odd $D_n$ Dynkin quiver. . . . .	103
8.62	A schematic of the web of dualities between the five 10-dimensional string theories . . . . .	113
14.63	A schematic map of the procedures investigated . . . . .	164





**Quiver**

**vacua**

**geometry**

# Introduction

## Overview

The first half of this thesis is dedicated, fittingly, to the first half of the research completed during my PhD. For this half we will be concerning ourselves with quantum field theories in two space dimensions and one time dimension. Specifically we will concern ourselves with those theories which enjoy  $\mathcal{N} = 4$  supersymmetry. We will be investigating the lowest energy states, or vacuum states, of these theories. The field content and gauge symmetries of the theories of concern will be expressed compactly using a *quiver*, a type of graph wherein nodes and edges have specific interpretations in terms of fields and symmetries. This area of research lies at the rich junction between particle physics by way of quantum field theory, mathematics by way of algebraic geometry, and string theory by way of the dynamics of branes. These three areas overlap and complement one another in myriad ways that prove to be a bountiful vein of new ideas and insights.

The  $3d \mathcal{N} = 4$  quiver gauge theories we will be investigating involve many fields. These fields are formally combined into representations of the supersymmetry called *hypermultiplets* and *vector multiplets*. Included among these fields are (potentially a great many) scalar fields arising in both types of multiplet. Generally there are numerous different possible vacuum states,  $|v\rangle$ , for such theories. These vacua are distinguished from one another by the *vacuum expectation values* (VEVs),  $\phi_v = \langle v | \phi(x) | v \rangle$ , for each of the scalar fields. These VEVs are independent of spacetime position. This plethora of vacua can be organised and understood through the introduction of the *moduli space of vacua*. The moduli space of vacua is an affine variety in which each point corresponds to a different set of VEVs for the scalar fields. The study of this space involves tools from algebraic geometry, and a detailed study of the singularity structure of this space allows us to investigate aspects such as gauge symmetry breaking in a highly regimented fashion. The theories we investigate also often have an interpretation as the low-energy dynamics of particular brane configurations in string theory.

## Outline

In Section 2 we first review the field content of the hypermultiplets and vector multiplets in  $3d \mathcal{N} = 4$  quantum field theories. After that we recall the bare-bones of how to represent the field content and symmetries of the specific theories of interest using quivers. We then say a little more about the broader structures that will appear in our study of the moduli spaces of vacua for these theories. We then review the brane config-

urations whose low-energy dynamics are given by the quiver gauge theories we are looking at. Finally we combine everything we have introduced into an example, specifically  $3d \mathcal{N} = 4$  supersymmetric quantum electrodynamics (SQED) with  $N$  flavors. For this example we write the quiver which characterises the field content and symmetries, provide a brane construction in type IIB string theory whose low energy dynamics is given by  $3d \mathcal{N} = 4$  SQED with  $N$  flavors, and perform an explicit calculation to determine the branch of the moduli space of vacua parameterised by those scalar fields which live inside the hypermultiplets of the theory. These well known results provide a firm grounding in the fundamental ideas of later sections.

In Section 3 we give an overview of the study of nilpotent varieties in Lie algebras, especially the theory of nilpotent orbits. These varieties form the algebro-geometric backbone of our work. The moduli spaces of vacua for a great many of the theories of interest either *are* these varieties, or are based upon them, and so a firm grasp of these objects is essential.

In Section 4 we review linear quivers and the *Kraft-Procesi transition* [4, 5]. This transition is a physical realisation of maneuvering which can be made within the singularity structure of the moduli space of vacua. We review the original brane realisation as well as providing a field-theory-only explanation. We conclude the section by enumerating those quiver gauge theories which realise nilpotent varieties in  $\mathfrak{sl}_n$  for small  $n$ .

In Section 5 we move from reviewing linear quivers with unitary gauge nodes to *circular* quivers with unitary gauge nodes [1]. These theories' moduli spaces of vacua have an unknown global structure. Nevertheless, we use the physical realisation of the local singularity structure by way of Kraft-Procesi transitions to build up an understanding of the moduli spaces of vacua for these theories. The process is delicate and complicated, however we successfully describe the singularity structure of vast affine varieties. Since the publication of this work it has been found that there are subtle problems with our constructions. We make more extensive remarks in the conclusions section to Part I.

In Section 6 we turn the previous considerations on their head somewhat when looking at quivers whose gauge nodes form a D-type Dynkin diagram [2]. Instead of considering some large class of quiver gauge theories and investigating the singularity structure via maneuvers which *remove* singularities (a 'top-down' approach), we first premise a quiver shape and then investigate which singularities can be *added* while maintaining the quiver shape. We investigate all those quivers whose gauge nodes and bifundamental hypermultiplets strictly form a D-type Dynkin diagram. We successfully characterise the singularity structure of the moduli space of vacua for all such theories. Note that this is a subtly different question to asking which quiver gauge theories have moduli spaces of vacua corresponding to nilpotent varieties in  $\mathfrak{so}_{2n}$ . While there is some overlap (in a region we call the *special slice*), in this work we take the quiver structure to be fixed and investigate the geometry, rather than trying to realise the geometry by changing the quiver structure. This means that we do not consider all possible *quiver additions* for these theories, but restrict ourselves to only those for which the gauge node structure is not changed.

Finally, in Section 7 we draw our conclusions for Part I, reviewing what we have discussed, and saying a few words about the strengths and short-comings of our analyses and potential future directions.



# Quivers, moduli spaces, and branes

In this section we are going to introduce some of the core concepts that will appear throughout the subsequent work. This should not be considered as a from-first-principles rendition of every detail of the topics at hand, instead this chapter will be a prompt reminder of the salient issues for a reader who is already familiar with them. We assume a working knowledge of supersymmetric quantum field theory. This is a vast and deep topic, some classic references are [6–8] and we refer the reader to the references in those texts for a history of the subject. First we will give a run-down of the field content of the multiplets present in the  $3d \mathcal{N} = 4$  theories with which we shall be working. After that we will review the use of quivers [9, 10] to encapsulate the field content and symmetries of the theories. Then we will make some general comments about the overall structure of the moduli spaces of vacua for these theories. Then we will cover how  $3d \mathcal{N} = 4$  quiver gauge theories arise as the low-energy dynamics of certain brane systems in type IIB superstring theory. As this final point may be less familiar to the reader than the earlier, more general topics, we enter into commensurately more detail. Finally we give an example combining everything we have mentioned, that of  $3d \mathcal{N} = 4$  SQED with  $N$  flavors.

## 2.1 Multiplets

Here we briefly enumerate the fields in the theories we will be examining. These fields are arranged into representations of the supersymmetry known as supermultiplets. As mentioned in the introduction, there are two types of multiplet with which we will be concerning ourselves, the *hypermultiplet* and the *vector multiplet*.

The  $3d \mathcal{N} = 4$  hypermultiplet consists of two complex scalars (for four total bosonic degrees of freedom) and two Dirac spinors (for four total fermionic degrees of freedom). This can also be viewed as two  $3d \mathcal{N} = 2$  chiral multiplets (consisting of one complex scalar and one Dirac spinor each). These two chiral multiplets transform in conjugate representations of the gauge group  $G$ .

The  $3d \mathcal{N} = 4$  vector multiplet can be viewed as a combination of a  $3d \mathcal{N} = 2$  chiral multiplet (a complex scalar and a Dirac spinor), and a  $3d \mathcal{N} = 2$  vector multiplet consisting of gauge field, a Dirac spinor, and a real scalar. In three dimensions, massless gauge fields have only one bosonic degree of freedom. This hints to their duality with scalar fields which we discuss in a moment.

## 2.2 Quivers

The field content and gauge and flavor symmetries for the  $3d \mathcal{N} = 4$  gauge field theories with which we shall be concerned may be represented by a particular kind of graph called a *quiver*. We will be considering theories with gauge groups given by  $\prod_{i \in I} U(i)$ , for  $I$  some set of positive integers. A circular node in the quiver with label  $k$  denotes a vector multiplet transforming in the adjoint of  $U(k)$ . There will be a single circular node, labelled  $k_i$ , for each  $U(k_i)$  factor of the gauge group. Square nodes labelled  $k$  represent a  $SU(k)$  flavour symmetry. Edges connecting two circular nodes correspond to hypermultiplets transforming in the bifundamental of the groups given by those nodes. Edges connecting a circular node and a square node represent hypermultiplets transforming in the fundamental representation of the gauge node.

## 2.3 Moduli space branches

A moduli space of vacua is an affine variety wherein each point represents a possible set of vacuum expectation values for the scalar fields in a theory. The study of moduli spaces of vacua for theories with eight supercharges have been closely studied for some decades [11, 12], including the study of  $3d \mathcal{N} = 4$  theories specifically [13, 14]. As we just mentioned, the scalar fields are packaged as part of either hyper- or vector multiplets. The hypermultiplet contains four scalar degrees of freedom and the vector multiplet contains three scalar and one vector degree of freedom. In three dimension a vector is dual to a scalar and as such both multiplets contribute four dimensions worth of parameters to the moduli space of vacua. The part of the moduli space of vacua parameterised by the scalars in the hypermultiplets is called the *Higgs branch*,  $\mathcal{M}_H$ , and the part of the moduli space of vacua parameterised by the fields in the vector multiplets is called the *Coulomb branch*,  $\mathcal{M}_C$ . These branches are exchanged under *mirror symmetry*. Generically these branches are highly singular algebraic varieties of some quaternionic dimension. Even more generically there may also be mixed branches of the moduli space where some of the non-zero scalar VEVs arise from hypermultiplets and others from vector multiplets. In this work we will concentrate on the Higgs and Coulomb branches, however.

## 2.4 Brane constructions

We are now going to describe a brane construction in a type IIB superstring background whose low energy dynamics are captured by  $3d \mathcal{N} = 4$  quiver gauge theories [14–16]. This construction will involve D3 branes, D5 branes, and NS5 branes. Generically, having three types of brane would break the supersymmetry in half [17, 18] three times, leaving only four out of the thirty-two supercharges in the bulk still associated with unbroken supersymmetry. However, in a particular arrangement described below, these three types of brane may leave eight supercharges preserved.

Consider the ten spacetime dimensions of the bulk type IIB background,  $(x^0, \dots, x^9)$ . Place the D3, D5, and NS5 branes such that they are extended in the direction marked with an  $\times$ .

	$x^0$	$x^1$	$x^2$	$x^3$	$x^4$	$x^5$	$x^6$	$x^7$	$x^8$	$x^9$
NS5	$\times$	$\times$	$\times$	$\times$	$\times$	$\times$	-	-	-	-
D5	$\times$	$\times$	$\times$	-	-	-	-	$\times$	$\times$	$\times$
D3	$\times$	$\times$	$\times$	-	-	-	$\times$	-	-	-



The NS5 branes, labelled with an  $i$ , take positions  $\vec{w}_i = (x_i^7, x_i^8, x_i^9)$  and the D5 branes, labelled with a  $j$ , take positions  $\vec{z}_j = (x_j^3, x_j^4, x_j^5)$ . Between them these branes only preserve eight of the bulk supercharges. In order for the D3 branes to not subsequently break to four supercharges, they must have constant positions in both the  $\vec{w}$  and  $\vec{z}$  directions. We label the D3 branes with a  $k$  and denote their positions as  $\vec{x}_k = (x_k^3, x_k^4, x_k^5)$  and  $\vec{y}_k = (x_k^7, x_k^8, x_k^9)$ . The only remaining option is that they are extended in the  $x^6$  as shown. A D3 brane can be suspended between two D5 branes if  $\vec{y} = \vec{z}_1 = \vec{z}_2$ , in this case it is free to move in the  $\vec{x}$  direction. A D3 brane can be suspended between two NS5 branes if  $\vec{x} = \vec{w}_1 = \vec{w}_2$ , in this case it is free to move in the  $\vec{y}$  direction. The low energy dynamics of this system is considered to be the theory living on these D3 branes. Due to their finite extent in  $x^6$  and the 8 preserved supercharges of the system, this is necessarily  $3d \mathcal{N} = 4$  quantum field theory. The freedoms of the D3 branes to move in certain directions now have interpretations as dynamical scalar fields in the effective field theory, and so part-parameterise the moduli space of vacua. A D3 brane suspended between a D5 and an NS5 brane is frozen and cannot move, as such these branes do not contribute to the low energy dynamics.

This brane set-up breaks the Lorentz group as  $SO(1, 9) \rightarrow SO(1, 2) \times SO(3) \times SO(3)$ . The  $SO(3)$  groups act on  $(x^3, x^4, x^5)$  and  $(x^7, x^8, x^9)$  respectively. The  $SO(4) = SU(2) \times SU(2)$  R-symmetry of  $3d \mathcal{N} = 4$  supersymmetry is realised as the double cover of this  $SO(3) \times SO(3)$ .

Let us now move to determine which fields and multiplets arise on which D3 branes. Consider an infinite D3 brane on which lives a four dimensional field theory. The four dimensional field theory is that of a  $U(1)$  vector multiplet [19]. Performing dimensional reduction from the vector multiplet to three dimensions yields the sum of a vector multiplet and a hypermultiplet. Now consider a D3 brane ending on 5-branes. Dirichlet or Neumann boundary conditions are imposed by the five branes. For  $\phi$ , a scalar field, Dirichlet conditions provide  $\phi = 0$  on the boundary and Neumann conditions provide  $\partial_i \phi = 0$  for directions normal to the boundary. A vector field,  $A_m$ , in four dimensions reduces to two fields in three dimensions. We are taking the D3 branes to be finite in  $x^6$  so these fields are a three dimensional  $U(1)$  gauge field  $a_\mu$  ( $\mu = 0, 1, 2$ ) and a scalar  $b$  such that  $\partial_\mu b = F_{\mu 6}$  where  $F_{mn}$  is the field strength of  $A_m$ . Dirichlet boundary conditions on  $A_m$  cause components of  $F_{mn}$  with  $m, n$  tangent to  $x^6$  to vanish, whereas Neumann conditions cause components of  $F_{mn}$  where only one of  $m$  or  $n$  is tangent to the boundary to vanish. Dirichlet conditions set  $a_\mu$  to zero whereas Neumann set  $b$  to zero. The three dimensional vector  $a_\mu$  lives in the  $3d \mathcal{N} = 4$  vector multiplet whereas  $b$  lives in the hypermultiplet. A three dimensional vector field is dual to a compact scalar field, we can write  $f_{\mu\nu} = \epsilon_{\mu\nu\rho} \partial^\rho \alpha$  for some zero-form  $\alpha$ . We therefore conclude that the field theory living on a D3 brane suspended between NS5 branes is that of a  $U(1)$  vector multiplet and the field theory living on a D3 brane suspended between D5 branes is that of a hypermultiplet. It is clear then that when the D3 branes are suspended between NS5 branes we are within the Coulomb branch of the moduli space of vacua and when they are suspended between D5 branes we are within the Higgs branch. For a D3 brane suspended between one of each type of 5-brane all of the massless modes are projected out by the boundary conditions which is why we stated earlier that they do not contribute to the low energy dynamics. They will be removed from our considerations via Hanany-Witten transitions, discussed in a moment.

Now we come to the potentially tricky business of illustrating our set-up. Happily there is a reasonably straight-forward way of capturing the essential features given in Fig. 2.1. We take the directions  $(x^3, x^4, x^5)$  to be one axis. Since the branes are either point-like in all three of these directions or infinite in all three of these

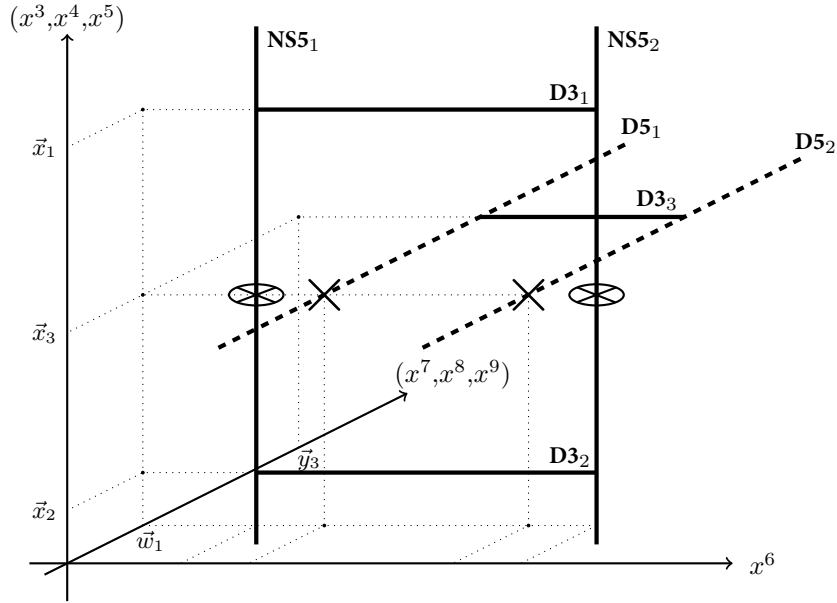


Figure 2.1: The ten spacetime dimensions for our brane set-up can be usefully illustrated using just three. Directions  $(x^0, x^1, x^2)$ , which are spanned by all branes, are suppressed. In the remainder of Part I we will reduce even this diagram to just two dimensions for illustrative purposes, one of which will be looking 'straight-on' to the  $(x^3, x^4, x^5) - x^6$  plane (and so the D5 branes will be denoted with  $\times$ ), and one of which will be 'top-down' onto the  $(x^7, x^8, x^9) - x^6$  plane (so the NS5 branes will be denoted with  $\otimes$ ).

directions, we can draw the branes as lines either parallel to the axis for NS5, or lines perpendicular to the axis in the case of D3 and D5. We take another axis to be the directions  $(x^7, x^8, x^9)$ . Using the same reasoning, D5 branes will be parallel to this axis whereas D3s and NS5s will be perpendicular. We take the third drawn axis to be  $x^6$  to which D5 and NS5 branes will be perpendicular and D3 will be parallel. We suppress  $x^0$ ,  $x^1$ , and  $x^2$  since all branes are infinite in these directions. The D5 branes will be drawn as dashed lines to distinguish them from solidly drawn NS5 branes. The D3 branes will always be distinguishable because they are horizontal in our diagrams, and will also be drawn solid.

It is simple to read the quiver for the gauge theory from the brane setup which is described at low energies by that theory. In the Coulomb brane configuration we have D3 branes on which there are vector multiplets transforming in the adjoint representation of some group. For  $N$  D3 branes in an interval between NS5 branes this group is naively  $U(1)^N$ , promoted to  $U(N)$  when the D3 branes converge. So for every interval between NS5 branes with  $N_i$  D3 branes, we draw a circular  $U(N_i)$  gauge node. If the interval contains  $k_i$  D5 branes, we draw a square  $SU(k_i)$  flavour node attached to the appropriate gauge node by an edge. We attach the gauge nodes of adjacent NS5 brane intervals by edges representing bifundamental hypermultiplets.

#### 2.4.1 Example: $3d \mathcal{N} = 4$ SQED with 2 flavors

Three dimensional  $\mathcal{N} = 4$  SQED with 2 flavours has two hypermultiplets transforming in the fundamental representation of the  $SU(2)$  flavour group and one vector multiplet transforming in the adjoint of the  $U(1)$  gauge group. The quiver and relevant brane configurations are given in Fig. 2.2

While the D3 brane is suspended between the NS5 branes, the vector multiplet is massless and the hypers

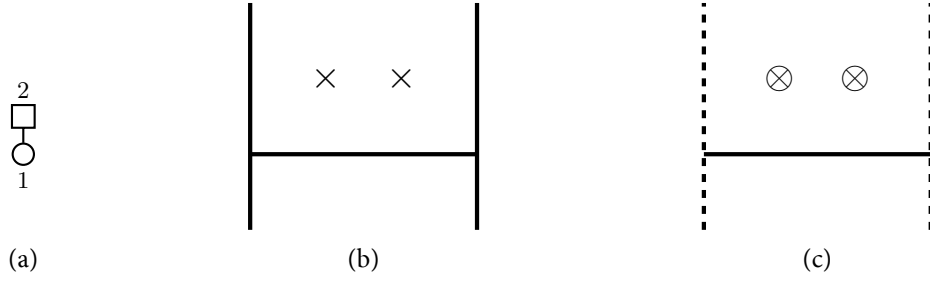


Figure 2.2: The (a) quiver, (b) Coulomb brane configuration and (c) Higgs brane configuration for  $3d \mathcal{N} = 4$  SQED with 2 flavours

acquire mass. Since the massless scalars on the D3 come from the vector multiplets, we are in the Coulomb branch of the moduli space. While the D3 brane is suspended between the D5 branes, one of the hypers is massless whilst the other is eaten by the vector multiplet which now acquires a mass via the Higgs mechanism. We are now in the Higgs branch of the moduli space.

There is a singular point in the moduli space where the D3 aligns with the NS5 branes and the D5 branes. All the fields become massless here and the Coulomb and the Higgs branches meet. Both branches have 4 real dimensions with a singular point. Any variety of the form  $\frac{\mathbb{C}^2}{\Gamma}$  with  $\Gamma$  a finite subgroup of  $SU(2)$  is a good candidate. We provide the answer here without ceremony. It is the simplest non-trivial group  $\mathbb{Z}_2$  and we have that both branches are

$$\mathcal{M}_C = \mathcal{M}_H = \frac{\mathbb{C}^2}{\mathbb{Z}_2}.$$

There is only one D3 brane and therefore there can be no circumstance wherein there are simultaneously D3 branes suspended between NS5 branes and D3 branes suspended between D5 branes. This tells us immediately that there are no mixed branches for this theory and that the full moduli space of vacua is a union of the Coulomb and Higgs branches,

$$\mathcal{M} = \frac{\mathbb{C}^2}{\mathbb{Z}_2} \cup \frac{\mathbb{C}^2}{\mathbb{Z}_2}.$$

We can also see that the Coulomb and Higgs branches intersect only at a single point (the singular point of both branches),

$$\mathcal{M}_C \cap \mathcal{M}_H = \{0\}.$$

### 2.4.2 Higgs mechanism

As hinted at in the example above, we can now give a physical, braney interpretation to the Higgs mechanism in our theories. From the Coulomb brane configuration we first align the D3 with the D5 branes. From the perspective of the moduli space this is realized as moving through the Coulomb branch to the singular point where it meets the Higgs branch. We then split the D3 across the D5 branes. The left and right hand pieces of the D3 are now frozen, since they have fixed positions for  $\vec{x}$  and  $\vec{y}$ . The middle segment is now free to move along  $(x^7, x^8, x^9)$  but has fixed position in  $(x^3, x^4, x^5)$ . From a moduli space perspective we have moved through the Coulomb branch to the singular point where it meets the Higgs branch and moved into the Higgs branch. This is illustrated in Fig. 2.3.

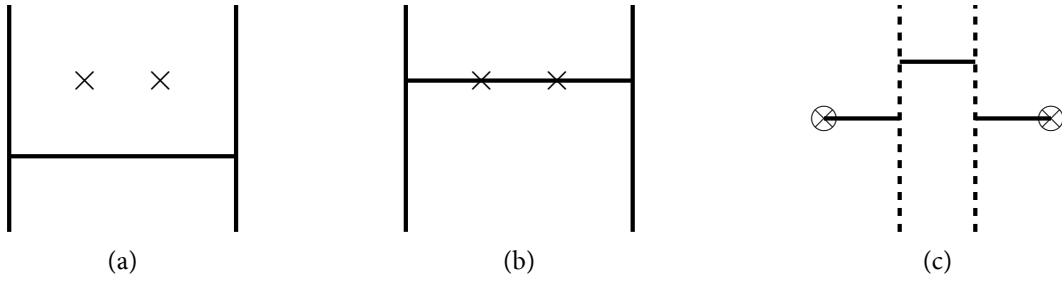
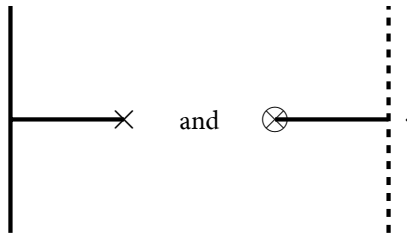


Figure 2.3: The brane configuration interpretation of the Higgs mechanism in our theories. In (a) we begin in the Coulomb brane configuration with a D3 brane suspended between NS5 branes. In (b) we move it to align with the D5 branes. In the moduli space this moves to the singular point of the Coulomb branch where it meets the Higgs branch. In (c) we split the D3 brane so that the center peice can move along the D5 branes. The remaining frozen sections must be removed via Hanany-Witten transitions.

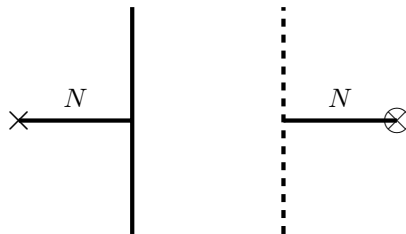
### 2.4.3 Hanany-Witten transitions

Let us consider the simplest possible system with a frozen D3 brane. The two brane configurations for this simple system are



Consider those quantities that are preserved when we move 5 branes around. There is the number of each type of 5 brane, denoted  $n_s$  and  $n_d$  for NS5 and D5 branes respectively, and the *linking number*. The linking number of a 5 brane is related to the magnetic charge on the brane and is therefore conserved, for further information the reader is directed to [15]. The linking number for a 5 brane is the net number of D3 branes ending on the 5 brane from the right (the number on the right minus the number on the left), plus the total number of the opposite type of 5 brane to its left. We denote the linking number of a brane as  $l_{d,i}$  for D5 branes and  $l_{s,i}$  for NS5 branes. Given a brane system we write the linking number of all of the branes of the same type as a tuple,  $l_d$  or  $l_s$ .

In our simple frozen D3 system, the conserved quantities are  $n_s = 1, n_d = 1, l_s = 1$  and  $l_d = 0$ . If we now move the D5 brane so it is left of the NS5 brane we have a new brane system, where  $N$  is a number of D3 branes that we need to determine using conservation of linking number.



In the new system,  $n_s = 1, n_d = 1, l_s = 1 - N$  and  $l_d = N$ , so by conservation of linking number,  $N = 0$ . We have annihilated the frozen D3 by exchanging the branes to which it is attached. The exact reverse

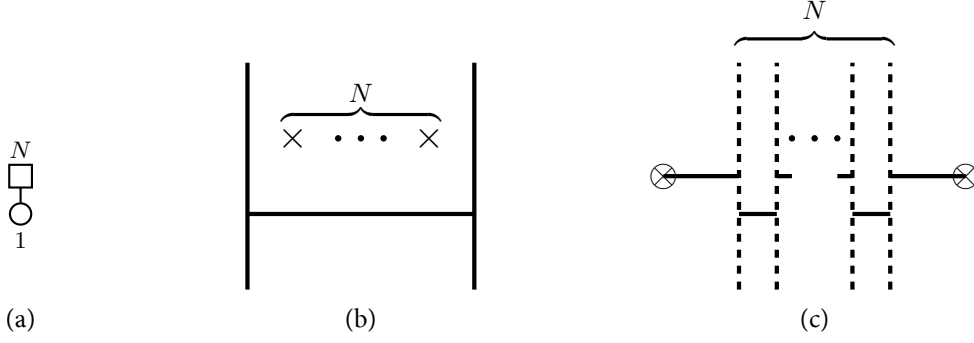


Figure 2.4: (a) Quiver (b) Coulomb brane configuration (c) Higgs brane configuration for  $3d \mathcal{N} = 4$  SQED with  $N$  flavours

of this process shows that exchanging a D5 and NS5 brane which do not have a D3 suspended between them results in the creation of a D3 brane. Also, there can be at most one D3 suspended between a given D5-NS5 pair. It is important we keep this in mind throughout.

## 2.5 Example: $3d \mathcal{N} = 4$ SQED with $N$ flavors

This is the generalization of the previous example with two flavours. Since theories can be completely determined by the linking number data, we shall begin by giving this data for this one parameter family of theories,  $n_s = 2$ ,  $n_d = N$ ,  $l_s = (1, 1, \dots, 1)$  and  $l_d = (1, N - 1)$ . The quiver, Coulomb brane configuration, and Higgs brane configuration are depicted in Fig. 2.4.

There is only one D3 brane in the Coulomb brane configuration and so the Coulomb branch has two complex dimensions in every theory in this family. There is also one singular point where the D3 brane aligns with all the D5 branes in the system. Once again the Coulomb branch must be a two dimensional with one singular point, and any variety of the form  $\frac{\mathbb{C}^2}{\Gamma}$  with  $\Gamma$  a finite subgroup of  $SU(2)$  is a good candidate. The *monopole formula* [20–25] can be used to show that the answer is in fact  $\Gamma = \mathbb{Z}_N$ . This exactly generalizes the result from the previous example. The Coulomb branches of these theories are exactly the A-type du Val singularities. But what about the Higgs branch? In our previous example with two flavours, the Higgs branch was  $\frac{\mathbb{C}^2}{\mathbb{Z}_2}$ . This will also generalize, but in a different way.

Geometric information concerning the Higgs branch has traditionally been calculated via a hyperkähler quotient [26–30]. We give a more rough-and-ready derivation of the Higgs branch in this specific instance, characterising it as a restricted set of matrices. First we have to identify all of the scalars arising from hypermultiplets that admit non-zero vacuum expectation values as these are the scalars that parametrize  $\mathcal{M}_H$ . This is more easily done from the point of view of the four supercharge theory ( $\mathcal{N} = 2$ ). In this perspective the hypermultiplet splits into 2 chiral multiplets and the vector multiplet splits into a chiral and a vector multiplet. An  $\mathcal{N} = 2$  chiral multiplet consists of a complex scalar and a Dirac spinor. The scalars we then have are,

- $N$  complex scalars, denoted  $Q_i$ , in the rep  $[1, 0, \dots, 0]$  of  $SU(N)$  with charge  $-1$  under  $U(1)$ .
- $N$  complex scalars, denoted  $\bar{Q}^j$ , in the rep  $[0, \dots, 0, 1]$  of  $SU(N)$  with charge  $1$  under  $U(1)$ .

- One complex scalar in the adjoint rep of  $U(1)$ , denoted  $\phi$ , that is the singlet of charge 0.

Now we must determine the affine variety parametrised by those scalars arising from the hypermultiplets, since this will be the Higgs branch. These scalars are  $Q_i$  and  $\bar{Q}_j$ . We are also only interested in those combinations of scalars whose VEVs are gauge invariant. The VEVs of  $Q_i$  and  $\bar{Q}_j$ , and therefore the VEVs of their combinations, are space-time independent. The ring of gauge invariant operators is generated by the combination  $Q_i \bar{Q}^j$ . We can characterise the corresponding variety in terms of a restricted set of matrices. Defining  $M^j_i = \bar{Q}^j Q_i$ , or as a matrix equation,  $M = \bar{Q} Q$ , the variety determined by possible values for the VEVs of these gauge invariant operators is the set of  $N \times N$  matrices with complex entries and with rank at most 1 (since  $\text{rank}(M) \leq \min(\text{rank}(\bar{Q}), \text{rank}(Q)) = 1$ ). This is not the Higgs branch however because we have not yet fixed ourselves to be in the vacuum state, that is, at a minimum of the scalar potential. The complex scalar part of the superpotential for this theory is proportional to,

$$W = \text{Tr}(Q_i \phi \bar{Q}^i), \quad (2.1)$$

and the zero energy conditions are,

$$\frac{\partial W}{\partial \phi} = 0, \quad \frac{\partial W}{\partial Q_i} = 0, \quad \frac{\partial W}{\partial \bar{Q}^j} = 0. \quad (2.2)$$

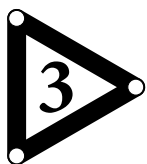
The field  $\phi$  arises from the  $\mathcal{N} = 4$  vector multiplet and so is set to zero when considering the Higgs branch of the theory. The only meaningful constraint is then,

$$Q_i \bar{Q}^i = 0. \quad (2.3)$$

With this extra constraint the Higgs branch may be characterised the set of  $N \times N$  complex matrices,  $\text{Rank}(M) = 0$  satisfying the zero energy condition. The relation  $Q_j \bar{Q}^j = 0$  implies that  $\text{Tr}(M) = 0$  and that  $M^2 = 0$ . Therefore

$$\mathcal{M}_H = \{M_{N \times N} \mid M^j_i \in \mathbb{C}, \quad \text{rank}(M) \leq 1, \quad \text{Tr}(M) = 0, \quad M^2 = 0\}. \quad (2.4)$$

These restricted sets of matrices are affine varieties known as *closures of nilpotent orbits*, in this case the closure of the smallest non-trivial nilpotent orbit in the Lie algebra  $\mathfrak{sl}(N, \mathbb{C})$ . These structures will be ubiquitous throughout the remainder of Part I. A detailed study of these and associated varieties is the subject of the next section.



# Nilpotent varieties in Lie algebras

In chapter 2 we reminded ourselves of the field content of  $3d \mathcal{N} = 4$  quantum field theories, discussed the brane constructions corresponding to  $3d \mathcal{N} = 4$  quiver gauge theories, and mentioned some features of the moduli spaces of vacua of these theories. Finally we made an explicit calculation for the Higgs branch of  $3d \mathcal{N} = 4$  SQED with  $N$  flavors and found that it could be characterised by a restricted set of matrices. In this section we introduce the necessary geometry to understand the moduli spaces of vacua that can be characterised similarly, namely nilpotent varieties in semisimple Lie algebras, and especially the closures of nilpotent orbits in those Lie algebras. The classic text for this subject is [31]. Other works on which this section is based are [32–38]. The relationship between these varieties and the theories we will be considering has been extensively studied in a large number of papers. A selection of these include [25, 39–51] and with especial reference made in [52–55].

## 3.1 Nilpotent elements of Lie algebras

In order to define a nilpotent orbits (and more general varieties of interest) of a complex semi-simple Lie algebra  $\mathfrak{g}$ , we must first define nilpotency. Take  $V$  to be a complex vector space. Take  $Y$  to be an element of  $\text{End}(V)$ . That is  $Y$  is a linear map from  $V$  to itself. We say  $Y$  is *nilpotent* if  $Y^m = Y \circ Y \circ Y \circ \dots \circ Y = 0$  for some  $m > 0$ .

Choosing a representation  $\rho : \mathfrak{g} \rightarrow \text{End}(V)$  we say an element  $X$  of  $\mathfrak{g}$  is nilpotent if  $\rho(X)^m = \rho(X) \circ \rho(X) \circ \dots \circ \rho(X) = 0$  for some  $m > 0$ . All such elements together make up the *nilpotent cone*,  $\mathcal{N}$ , of  $\mathfrak{g}$ . The adjoint representation (the instance where  $V$  is chosen to be  $\mathfrak{g}$  itself) seems an obvious choice since the adjoint rep is faithful for semi-simple Lie algebras. This neatly sidesteps the potential issue if  $X \in \ker(\rho)$ . In order to permanently sidestep the issue, we assume  $\rho$  is faithful, it can be shown that our definition of nilpotency is independant of the (faithful) rep  $\rho$  chosen. We will work with the adjoint rep unless otherwise stated.

An example of a nilpotent element in a Lie algebra is  $\begin{pmatrix} 0 & 1 \\ 0 & 0 \end{pmatrix} \in \mathfrak{sl}_2$ . Nilpotency can be checked by simple matrix multiplication  $\begin{pmatrix} 0 & 1 \\ 0 & 0 \end{pmatrix} \begin{pmatrix} 0 & 1 \\ 0 & 0 \end{pmatrix} = \begin{pmatrix} 0 & 0 \\ 0 & 0 \end{pmatrix}$ .

A more general example for  $\mathfrak{sl}_n$  is

$$X = \begin{pmatrix} J_{\lambda_1} & 0 & 0 & \dots & 0 & 0 \\ 0 & J_{\lambda_2} & 0 & \dots & 0 & 0 \\ 0 & 0 & J_{\lambda_3} & \dots & 0 & 0 \\ \vdots & \vdots & \vdots & \ddots & 0 & 0 \\ 0 & 0 & 0 & 0 & J_{\lambda_{k-1}} & 0 \\ 0 & 0 & 0 & 0 & 0 & J_{\lambda_k} \end{pmatrix} \quad (3.5)$$

where the  $\lambda_i$  are positive integers whose sum is  $n$ , and  $J_{\lambda_i}$  is the order  $\lambda_i$  Jordan normal block defined as the  $\lambda_i \times \lambda_i$  matrix with 1 on the off-diagonal,

$$J_{\lambda_i} = \begin{pmatrix} 0 & 1 & 0 & \dots & 0 \\ 0 & 0 & 1 & \dots & 0 \\ 0 & 0 & 0 & \dots & 0 \\ \vdots & \vdots & \vdots & \ddots & \vdots \\ 0 & 0 & 0 & 0 & 0 \end{pmatrix}. \quad (3.6)$$

It can be seen that  $X_\lambda$  is a nilpotent endomorphism of  $\mathbb{C}^n$  and so is a nilpotent element of  $\mathfrak{sl}_n$ .

Given set of  $\lambda_i$  the order in which they appear in  $X$  will be irrelevant due to the uniqueness of the Jordan normal form. We therefore see that the theory of nilpotent orbits for  $\mathfrak{sl}_n$  is intimately related to the study of integer partitions of  $n$ . We will also find that the theory of nilpotent orbits for  $\mathfrak{so}_{2n}$  is related to integer partitions of a restricted form. We present the details of integer partitions next.

## 3.2 Integer partitions

A partition,  $\mu$ , of magnitude  $n$ , is a weakly decreasing tuple of non-negative integers (parts)  $\mu = (\mu_1, \dots, \mu_j)$  such that  $\sum_{i=1}^j \mu_i = n$ . Partitions are usually written using *exponential notation* where each part is labelled with its multiplicity within the partition. A general partition of  $n$ , in exponential notation, is written

$$\mu = (n^{k_n}, (n-1)^{k_{n-1}}, \dots, 3^{k_3}, 2^{k_2}, 1^{k_1}, 0^{k_0}), \quad (3.7)$$

where  $\sum_{i=0}^n ik_i = n$ . The *length* of a partition is the number of non-zero parts it has, counted with multiplicity, so  $\text{length}(\mu) = \sum_{i=1}^n k_i := l(\mu)$ . The value of  $k_0 \in \mathbb{Z}_{\geq 0}$  can be changed without changing the magnitude of  $\mu$ , partitions are usually written with  $k_0 = 0$ , however it will also prove useful to take  $k_0 = n - l(\mu)$ . This is called ‘padding the partition’ with zeroes.

Partitions can be represented by Young tableaux, which are left-justified rows of boxes where the number of boxes in row  $i$  is  $\mu_i$ . The *transpose* of a partition,  $\mu^t$ , is found by reflecting the corresponding Young tableau in the NE-SW diagonal. Alternatively the transpose can be found by considering the tableau column-wise, or, without appealing to tableaux at all, by taking the difference between the  $i^{\text{th}}$  and  $(i+1)^{\text{th}}$  parts of  $\mu$  to be the multiplicity of  $i$  in  $\mu^t$ .

The set of partitions of  $n$ , denoted  $\mathcal{P}(n)$ , is a partially ordered set with ordering defined by the *dominance*



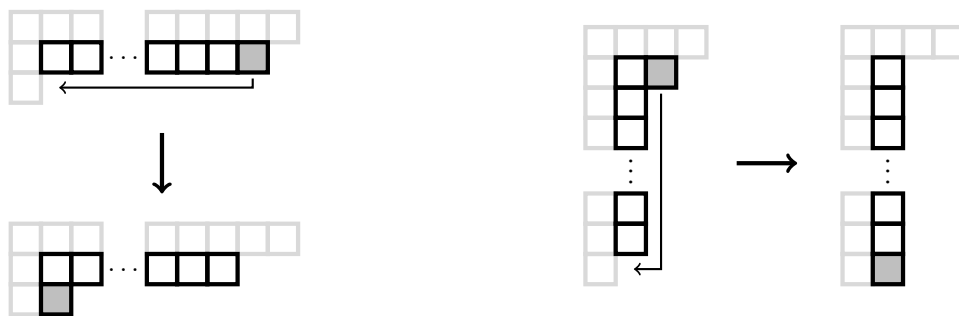


Figure 3.5: The two procedures in the Young tableaux that move from one partition to an adjacent partition in the dominance ordering.

relation for the partitions. A partition  $\mu$  dominates a partition  $\nu$  if,

$$\sum_{i=1}^m \mu_i \geq \sum_{i=1}^m \nu_i, \quad (3.8)$$

for all  $1 \leq m \leq n$ . If there is no partition  $\rho$  such that  $\mu > \rho > \nu$  the partitions  $\mu$  and  $\nu$  are said to be *adjacent* in the ordering. Adjacent partitions are related by one of two procedures at the level of the Young tableaux.

- (1) A single block is moved down one row and left at least one column.
- (2) A single block is moved down at least one row and left one column.

Tableaux demonstrating these two procedures are given in Fig 3.5.

### 3.2.1 Hasse diagrams

This (partial) ordering can be represented in a *Hasse diagram* in which the nodes are partitions, more dominant nodes are placed higher, and nodes are connected by edges if the partitions are adjacent. Given a magnitude  $n$ , there is a unique most dominant partition,  $(n)$ . This will always be at the top of the Hasse diagram. There is also a unique lowest partition,  $(1^n)$ , which will always be at the bottom of the diagram. Moreover, when considering all possible partitions of an integer, there are unique partitions  $(2, 1^{n-2})$ , one above the lowest partition, and  $(2^2, 1^{n-4})$ , two above the lowest partition. There are also unique partitions  $(n-1, 1)$ , one below the highest partition and  $(n-2, 2)$ , two below the highest partition. An example Hasse diagram for  $n = 6$  is given in Fig 3.6.

Transposition of the partitions is an involution on  $\mathcal{P}(n)$  where each partition gets mapped uniquely to a partition (perhaps itself). This involution reflects the Hasse diagram top-bottom. It is clear that if  $\mu > \nu$  then  $\mu^t < \nu^t$ .

### 3.2.2 Restricted partitions

A *restricted* set of partitions is one limited to partitions of  $n$  that fulfil certain criteria. The nilpotent orbits in  $\mathfrak{so}_{2n}$  are related to the set of partitions of  $2n$  where *even* parts occur with *even* multiplicity (including zero). This set is written  $\mathcal{P}_+(2n)$ . The dominance ordering can once again be used to realise the structure of a partially ordered set and hence construct a Hasse diagram. Some example Hasse diagrams are given in Fig 3.7. However there are complications in defining transpose in  $\mathcal{P}_+(2n)$  because  $\mu \in \mathcal{P}_+(2n)$  doesn't imply

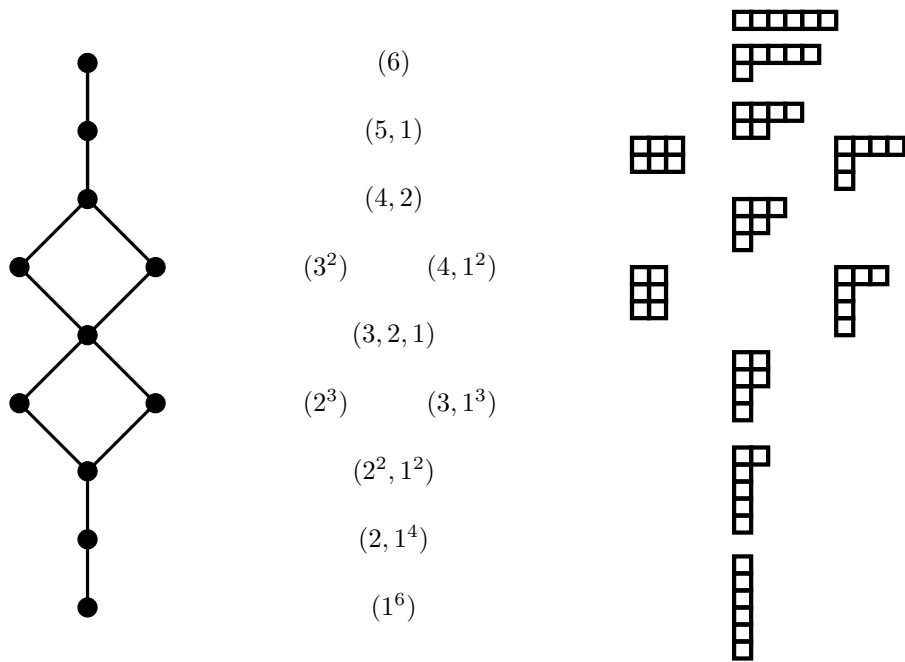


Figure 3.6: The Hasse diagram for the partitions of  $n = 6$ .

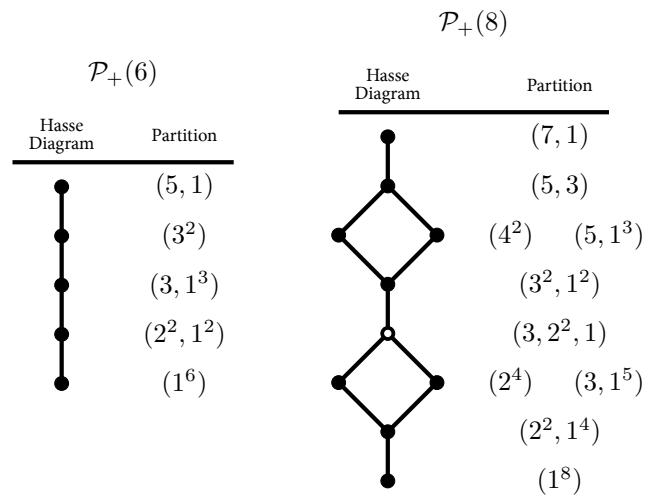


Figure 3.7: Hasse diagrams for restricted sets of partitions  $\mathcal{P}_+(6)$  and  $\mathcal{P}_+(8)$ . Hollow nodes ( $(3, 2^2, 1) \in \mathcal{P}_+(8)$ ) are *non-special*, see discussion.

that  $\mu^t \in \mathcal{P}_+(2n)$ . Since transpose maps  $\mathcal{P}_+(2n) \rightarrow \mathcal{P}(2n)$ , one defines another map called the *D-collapse* which maps  $\mathcal{P}(2n) \rightarrow \mathcal{P}_+(2n)$ . The D-collapse takes a partition  $\sigma$  to the largest partition in  $\mathcal{P}_+(2n)$  that is equal to, or dominated by,  $\sigma$ . Clearly  $\sigma_D = \sigma$  for  $\sigma \in \mathcal{P}_+(2n)$ . If  $\sigma \notin \mathcal{P}_+(2n)$  then (at least one) even part, say  $\sigma_j = 2r$ , must have odd multiplicity. In this case, take the final  $2r$  to  $2r - 1$  and take the largest part  $\sigma_i < 2r - 1$  to  $\sigma_i + 1$ . Repeat this process until the resulting partition is in  $\mathcal{P}_+(2n)$ . D-collapse is many-to-one.

The *Lusztig-Spaltenstein* map,  $d_{LS}$ , is transposition followed by D-collapse. It is a many-to-one (due to the D-collapse) map  $\mathcal{P}_+(2n) \rightarrow \mathcal{P}_+(2n)$ . Note that  $d_{LS}^3 = d_{LS}$ . A partition is called *special* if  $d_{LS}^2$  is the identity on the partition. Non-special partitions' nodes are drawn hollow in the Hasse diagram.

There are several important partitions to highlight. For every  $n \geq 4$  there are unique, special partitions which are the highest, next-to-highest, lowest and next-to lowest partitions in the set. These are  $(2n - 1, 1)$ ,  $(2n - 3, 3)$ ,  $(1^{2n})$  and  $(2^2, 1^{2n-4})$  respectively. For  $n \geq 4$  there are the highest and lowest non-special partitions. These always take the form  $(2n - 5, 2^2, 1)$  and  $(3, 2^2, 1^{2n-7})$  respectively (these coincide for  $n = 4$ ).

### 3.3 Nilpotent orbits

The standard text for nilpotent orbits in Lie algebras is [31]. The orbit,  $\mathcal{O}_X$ , of a nilpotent element  $X$  of some Lie algebra  $\mathfrak{g}$  is the conjugacy class of  $X$  under the natural action of the associated Lie group,  $G$ ,

$$\mathcal{O}_X = G \cdot X = \{A \cdot X \cdot A^{-1} | A \in G\}. \quad (3.9)$$

For example take  $X = \begin{pmatrix} 0 & 1 \\ 0 & 0 \end{pmatrix} \in \mathfrak{sl}_2$ . A simple calculation using  $A = \begin{pmatrix} a & b \\ c & d \end{pmatrix}$  with  $ad - bc = 1$  shows that a generic element of  $\mathcal{O}_X$  can be written as

$$\begin{pmatrix} -ac & a^2 \\ -c^2 & ac \end{pmatrix}. \quad (3.10)$$

It is simple to verify that all such matrices are nilpotent.

All of the nilpotent elements of  $\mathfrak{sl}_n$  are conjugate to one in Jordan block form with the ordering of the  $\lambda_i$  conventionally taken to be largest first. The nilpotent orbits of  $\mathfrak{sl}_n$  can therefore be placed in one-to-one correspondence with the partitions of  $n$ . The nilpotent orbit associated with the partition  $\mu$  is denoted  $\mathcal{O}_\mu$ .

Nilpotent orbits in  $\mathfrak{so}_{2n}$  are in one-to-one correspondence with the restricted set  $\mathcal{P}_+(2n)$  of partitions of  $2n$  in which *even* parts occur with *even* multiplicity. There are some caveats however. The exception comes for *very even* partitions, consisting of only even parts. Under the action of  $\text{SO}(2n)$  these partitions yield *two* orbits, but under the action of  $\text{O}(2n)$  these orbits combine into a single orbit. For example there are twelve nilpotent orbits in  $\mathfrak{so}_8$  under the action of  $\text{SO}(2n)$ , these are  $\mathcal{O}_{(7,1)}$ ,  $\mathcal{O}_{(5,3)}$ ,  $\mathcal{O}_{(4^2)}^I$ ,  $\mathcal{O}_{(4^2)}^{II}$ ,  $\mathcal{O}_{(5,1^3)}$ ,  $\mathcal{O}_{(3^2,1^2)}$ ,  $\mathcal{O}_{(3,2^2,1)}$ ,  $\mathcal{O}_{(2^4)}^I$ ,  $\mathcal{O}_{(2^4)}^{II}$ ,  $\mathcal{O}_{(3,1^5)}$ ,  $\mathcal{O}_{(2^2,1^4)}$  and  $\mathcal{O}_{(1^8)}$ . Under the action of  $\text{O}(2n)$  there are ten nilpotent orbits, all of the non-very-even orbits and the two orbits  $\mathcal{O}_{(4^2)}^I \cup \mathcal{O}_{(4^2)}^{II}$  and  $\mathcal{O}_{(2^4)}^I \cup \mathcal{O}_{(2^4)}^{II}$ . When discussing orbits in  $\mathfrak{so}_{2n}$  these unions of orbits will be what we mean by  $\mathcal{O}_\lambda$  for very even  $\lambda$ .

### 3.4 Closures of nilpotent orbits

The *closure* of a nilpotent orbit  $\mathcal{O}_\mu$  is defined as the union of that orbit with all of those orbits whose partitions its partition dominates,

$$\bar{\mathcal{O}}_\mu = \bigcup_{\nu \leq \mu} \mathcal{O}_\nu. \quad (3.11)$$

For  $\mathfrak{sl}_n$  the closure of a nilpotent orbit is a hyperkähler singular variety of quaternionic dimension

$$\dim_{\mathbb{H}}(\bar{\mathcal{O}}_\mu) = \frac{1}{2} \left( n^2 - \sum_i (\mu_i^t)^2 \right). \quad (3.12)$$

For  $\mathfrak{so}_{2n}$ , writing a general partition  $\mu = ((2n)^{r_{2n}}, \dots, 3^{r_3}, 2^{r_2}, 1^{r_1}, 0^{r_0})$ , the closures of nilpotent orbits are algebraic varieties of quaternionic dimension

$$\dim_{\mathbb{H}}(\bar{\mathcal{O}}_\mu) = \frac{1}{2} \left( 2n^2 - n - \frac{1}{2} \sum_i (\mu_i^t)^2 + \frac{1}{2} \sum_{i \text{ odd}} r_i \right). \quad (3.13)$$

The set of nilpotent orbit closures in  $\mathfrak{sl}_n$  has the same partial ordering as the partitions of  $n$  (for  $\mathfrak{so}_{2n}$ , the partitions in  $\mathcal{P}_+(2n)$ ), with the dominance relations taken as the inclusion relations between the orbit closures. Associating nilpotent orbits to the nodes in the Hasse diagram corresponding to their partitions, we may consider that the closure of the nilpotent orbit  $\mathcal{O}_\mu$  involves all of the orbits in a Hasse diagram from  $\mu$  down to  $(1^N)$ . Given  $\bar{\mathcal{O}}_\mu$  and  $\bar{\mathcal{O}}_\nu$  which form a *degeneration*,  $\bar{\mathcal{O}}_\nu \subset \bar{\mathcal{O}}_\mu$ , we call the degeneration *minimal* if there is no orbit closure  $\bar{\mathcal{O}}_\rho$  such that  $\bar{\mathcal{O}}_\nu \subset \bar{\mathcal{O}}_\rho \subset \bar{\mathcal{O}}_\mu$ . Minimal degenerations correspond to adjacent partitions.

Orbits associated to non-special partitions are themselves called non-special. Orbit closures which only have special nodes in their Hasse sub-diagram play an important role in our discussion of D-type Dynkin quiver moduli spaces of vacua. These are exactly the closures of those orbits with *height* two or less. The height of a nilpotent orbit in  $\mathfrak{so}_{2n}$  is

$$\text{ht}(\mathcal{O}_\mu) = \begin{cases} m_1 + m_2 - 2, & m_2 \geq m_1 - 1 \\ 2m_1 - 4, & m_2 \leq m_1 - 2 \end{cases}. \quad (3.14)$$

The  $m_i$  here are from the non-exponential notation for  $\mu$ . Low-height orbit closures are important because  $\text{ht}(\mathcal{O}_\mu) \leq 2$  nilpotent orbits always have a realisation as the Coulomb branch of a  $D_n$  Dynkin quiver.

#### 3.4.1 Singularity structure and labelled Hasse diagrams

An orbit closure is singular within the closure of an adjacent, dominating orbit closure. In [33–35], Kraft and Procesi determined  $\text{Sing}(\bar{\mathcal{O}}_\mu, \bar{\mathcal{O}}_\nu)$  for all minimal degenerations in the classical Lie algebras. The edges of the Hasse diagram for nilpotent orbit closures may be labelled with these singularities.

For  $\mathfrak{sl}_n$  the singularity of the closure of the *subregular* orbit,  $\bar{\mathcal{O}}_{(n-1,1)}$ , inside the closure of the *maximal*

(or *regular*) orbit,  $\bar{\mathcal{O}}_{(n)}$ , is, [32],

$$\text{Sing}(\bar{\mathcal{O}}_{(n)}, \bar{\mathcal{O}}_{(n-1,1)}) = A_{n-1} = \frac{\mathbb{C}^2}{\mathbb{Z}_n}. \quad (3.15)$$

There is a similar result concerning the zero orbit closure  $\bar{\mathcal{O}}_{(1^n)} = 0$ , and *minimal* orbit closure,  $\bar{\mathcal{O}}_{(2,1^{n-2})}$ . In this case, the type of singularity that zero is within the minimal orbit of  $\mathfrak{sl}_n$  can be taken as a definition and is denoted  $a_{n-1}$ ,

$$\text{Sing}(\bar{\mathcal{O}}_{(2,1^{n-2})}, \bar{\mathcal{O}}_{(1^n)}) := a_{n-1}. \quad (3.16)$$

It was exactly this variety which we determined was the Higgs branch of  $3d \mathcal{N} = 4$  SQED with  $N$  flavours in the example at the end of the previous chapter. Kraft and Procesi generalised these results in order to write down the type of singularity equivalent to any minimal degeneration in  $\mathfrak{sl}_n$ . Given a minimal degeneration  $\bar{\mathcal{O}}_\nu \subset \bar{\mathcal{O}}_\mu$ ,

$$\text{Sing}(\bar{\mathcal{O}}_\mu, \bar{\mathcal{O}}_\nu) = \begin{cases} A_m & \text{for some } m < n \text{ if } \dim_{\mathbb{H}}(\bar{\mathcal{O}}_\mu) - \dim_{\mathbb{H}}(\bar{\mathcal{O}}_\nu) = 1 \\ a_m & \text{for some } m < n \text{ if } \dim_{\mathbb{H}}(\bar{\mathcal{O}}_\mu) - \dim_{\mathbb{H}}(\bar{\mathcal{O}}_\nu) = m. \end{cases} \quad (3.17)$$

Moreover if  $\text{Sing}(\bar{\mathcal{O}}_\mu, \bar{\mathcal{O}}_\nu) = A_m$  then  $\text{Sing}(\bar{\mathcal{O}}_{\nu^t}, \bar{\mathcal{O}}_{\mu^t}) = a_m$  and vice versa.

For  $\mathfrak{so}_{2n}$  the situation is more complicated and also involves singularities such as  $\frac{\mathbb{C}^2}{\Gamma}$  for other finite subgroups of  $SU(2)$ , and the closure of the minimal nilpotent orbits in other semi simple Lie algebras. Examples (following obvious naming conventions) are given in Fig. 3.8.

In our previous example with  $\mathfrak{sl}_2$  we saw that the orbit of the element  $X_{(2)} = \begin{pmatrix} 0 & 1 \\ 0 & 0 \end{pmatrix}$ , which we now recognise as being associated to the partition (2) of  $n = 2$ , can be written as (3.10) with  $a$  and  $c$  not simultaneously 0 (as this would break the condition  $ad - bc = 1$ ). The other orbit of  $\mathfrak{sl}_n$  is associated to the partition  $(1^2)$ , and so the element  $\begin{pmatrix} 0 & 0 \\ 0 & 0 \end{pmatrix}$ , which is trivially nilpotent, and constitutes the whole of the orbit  $\mathcal{O}_{(1^2)}$  and its closure. We form the closure of  $\mathcal{O}_{(2)}$ , denoted  $\bar{\mathcal{O}}_{(2)}$ , by taking the union

$$\bar{\mathcal{O}}_{(2)} = \mathcal{O}_{(2)} \cup \mathcal{O}_{(1^2)}$$

Taking this closure is the same as allowing  $a$  and  $c$  in (3.10) to simultaneously be 0. We note then that  $\bar{\mathcal{O}}_{(2)}$  is generated by three generators

$$a^2 = q, \quad c^2 = r, \quad ac = s,$$

which satisfy the relation  $qr = s^2$ . This is exactly the variety  $A_1 = \frac{\mathbb{C}^2}{\mathbb{Z}_2}$ .

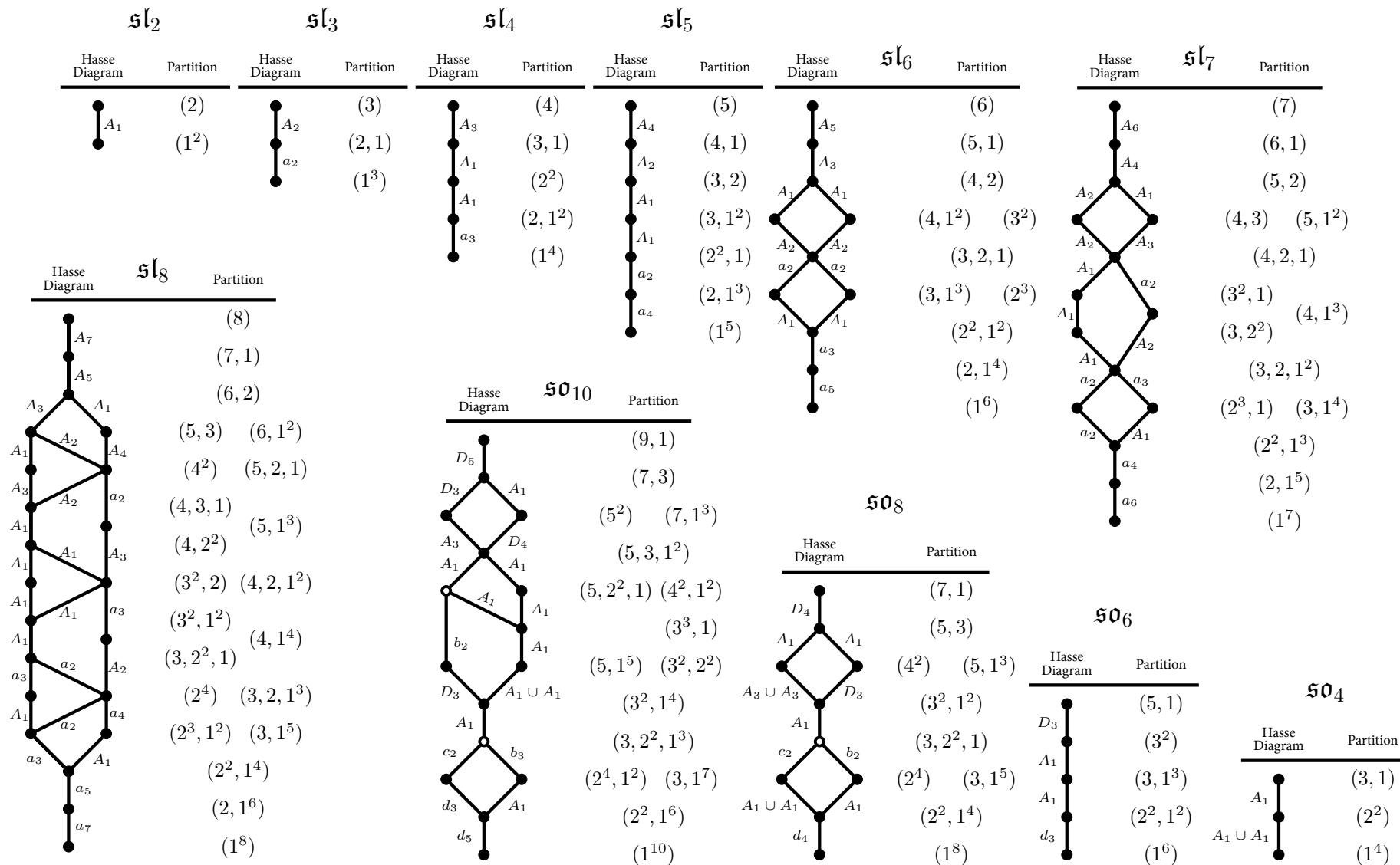


Figure 3.8: Labelled Hasse diagrams for  $\mathfrak{sl}_n$  for  $n = 2, \dots, 8$  and for  $\mathfrak{so}_{2n}$  for  $n = 2, \dots, 5$ .

### 3.5 Slodowy slices and intersections

We can now consider more general varieties arising as subvarieties of the nilpotent cone of some Lie algebra. Given  $X \in \mathcal{N}$  for a Lie algebra  $\mathfrak{g}$ , the Jacob-Morozov Theorem states that there are two elements,  $Y$  and  $H$ , such that  $(X, Y, H)$  form a standard  $\mathfrak{sl}_2$  triple. That is, given  $X$ , we are always able to find  $Y$  and  $H$  such that

$$[X, Y] = H, \quad [H, X] = 2X, \quad [H, Y] = -2Y.$$

Such triples are not unique, but are  $\mathrm{SL}_n(\mathbb{C})$  conjugate. We then define the Slodowy slice at  $X$  as

$$\mathcal{S}_X := X + \ker(\mathrm{ad}(Y)),$$

where  $\ker(\mathrm{ad}(Y))$  gives all those elements of  $\mathfrak{g}$  that commute with  $Y$ . Take  $X$  to be conjugate to the block Jordan normal form associated to the partition  $\lambda$ . Since this triple is unique up to conjugacy, this defines a transverse slice to the orbit  $\mathcal{O}_\lambda$ . We can label each slice with the partition associated to the conjugacy class of the  $X$  from which it is formed. The slice  $\mathcal{S}_\lambda$  meets all  $\mathcal{O}_\sigma$  for  $\sigma > \lambda$  transversely.

Let us explore an example for  $\mathfrak{sl}_n$ . For an  $(r+1) \times (r+1)$  Jordan normal block, we can realize these elements of the  $\mathfrak{sl}_2$  triple as

$$J_X = \begin{pmatrix} 0 & 1 & 0 & \dots & 0 \\ 0 & 0 & 1 & \dots & 0 \\ 0 & 0 & 0 & \dots & 0 \\ \vdots & \vdots & \vdots & \ddots & \vdots \\ 0 & 0 & 0 & 0 & 0 \end{pmatrix} \quad J_Y = \begin{pmatrix} r & 0 & 0 & \dots & 0 \\ 0 & r-2 & 0 & \dots & 0 \\ 0 & 0 & r-4 & \dots & 0 \\ \vdots & \vdots & \vdots & \ddots & \vdots \\ 0 & 0 & 0 & 0 & -r \end{pmatrix} \quad J_H = \begin{pmatrix} 0 & 0 & 0 & \dots & 0 \\ \mu_1 & 0 & 0 & \dots & 0 \\ 0 & \mu_2 & 0 & \dots & 0 \\ \vdots & \vdots & \vdots & \ddots & \vdots \\ 0 & 0 & 0 & \mu_r & 0 \end{pmatrix} \quad (3.18)$$

where  $\mu_i = i(r+1-i)$  for  $1 \leq i \leq r$ . For an element in the form (3.5) we follow an analogous construction from Jordan normal blocks to find the appropriate  $Y$  and  $H$  out of  $J_Y$  and  $J_H$ .

To give more specific examples consider the orbits of  $\mathfrak{sl}_3$ . There is the maximal orbit associated with the partition (3). The subregular and minimal orbits coincide and are associated with (2, 1), and the trivial orbit is associated to (1<sup>3</sup>). Simple calculations give us the following results:

For the maximal orbit

$$X = \begin{pmatrix} 0 & 1 & 0 \\ 0 & 0 & 1 \\ 0 & 0 & 0 \end{pmatrix} \quad \text{and} \quad Y = \begin{pmatrix} 0 & 0 & 0 \\ 2 & 0 & 0 \\ 0 & 2 & 0 \end{pmatrix}$$

$$\mathcal{S}_{(3)} = \left\{ \begin{pmatrix} 0 & 1 & 0 \\ a & 0 & 1 \\ b & a & 0 \end{pmatrix} \mid a, b \in \mathbb{C} \right\} \quad (3.19)$$

For the minimal / subregular orbit

$$X = \begin{pmatrix} 0 & 1 & 0 \\ 0 & 0 & 0 \\ 0 & 0 & 0 \end{pmatrix} \quad \text{and} \quad Y = \begin{pmatrix} 0 & 0 & 0 \\ 1 & 0 & 0 \\ 0 & 0 & 0 \end{pmatrix}$$

$$\mathcal{S}_{(2,1)} = \left\{ \begin{pmatrix} a & 1 & 0 \\ b & a & c \\ d & 0 & -2a \end{pmatrix} \mid a, b, c, d \in \mathbb{C} \right\} \quad (3.20)$$

For the trivial orbit

$$X = \begin{pmatrix} 0 & 0 & 0 \\ 0 & 0 & 0 \\ 0 & 0 & 0 \end{pmatrix} \quad \text{and} \quad Y = \begin{pmatrix} 0 & 0 & 0 \\ 0 & 0 & 0 \\ 0 & 0 & 0 \end{pmatrix}$$

and  $\mathcal{S}_{(1^3)}$  is the whole of  $\mathfrak{sl}_3$ .

These slices are not currently subvarieties of the nilpotent cone, we have to take the intersection with the nilpotent cone to obtain the varieties we are after.

### 3.5.1 Intersections for $\mathfrak{sl}_n$

The intersection of a Slodowy slice with the nilpotent cone,  $\mathcal{S}_\lambda \cap \mathcal{N} = \mathcal{S}_\lambda \cap \bar{\mathcal{O}}_{(n)}$ , is a hyperKähler singular variety of dimension,

$$\dim_{\mathbb{H}}(\mathcal{S}_\lambda \cap \bar{\mathcal{O}}_{(n)}) = \frac{1}{2} \left( \sum_i (\lambda_i^t)^2 - n \right). \quad (3.21)$$

On a Hasse diagram of the nilpotent cone as split into nilpotent orbit closures, we may consider that  $\mathcal{S}_\lambda \cap \bar{\mathcal{O}}_{(n)}$  involves all of the orbits from  $\lambda$  up to  $(n)$ .

To continue the above example we first restrict ourselves to this intersection by imposing on the matrices,  $M$ , given in (3.19) and (3.20) that  $\det(\lambda I - M) = \lambda^3$  (this being equivalent to nilpotency for a  $3 \times 3$  matrix) and determining relations between the variables. We needn't do this for the trivial orbit, we found  $\mathcal{S}_{(1^3)} = \mathfrak{sl}_3$  and so we easily see that  $\mathcal{S}_{(1^3)} \cap \mathcal{N} = \mathcal{N} = \bar{\mathcal{O}}_{(3)}$ .

For the maximal orbit we find  $a = 0$  and  $b = 0$ , giving us

$$\mathcal{S}_{(3)} \cap \mathcal{N} = \mathcal{S}_{(3)} \cap \bar{\mathcal{O}}_{(3)} = \begin{pmatrix} 0 & 1 & 0 \\ 0 & 0 & 1 \\ 0 & 0 & 0 \end{pmatrix} \quad (3.22)$$

which is exactly the  $X$  we used to define the slice in the first place. This is a general feature,  $\mathcal{S}_{(n)} \cap \bar{\mathcal{O}}_{(n)} = \{X\}$ . The intersection is therefore at a single point, which is the trivial variety.

For the minimal / subregular orbit we find  $-3a^2 - b = 0$  and  $2a(b - a^2) + cd = 0$ , plugging these into (3.20) we find

$$\mathcal{S}_{(2,1)} \cap \mathcal{N} = \mathcal{S}_{(2,1)} \cap \bar{\mathcal{O}}_{(3)} = \left\{ \begin{pmatrix} a & 1 & 0 \\ -3a^2 & a & c \\ d & 0 & -2a \end{pmatrix} \mid a, c, d \in \mathbb{C}, \quad (2a)^3 = cd \right\} \quad (3.23)$$

This is exactly the variety  $\frac{\mathbb{C}^2}{\mathbb{Z}_3}$ .

When we restrict in this manner to the intersection of the slice with the nilpotent cone, the complex



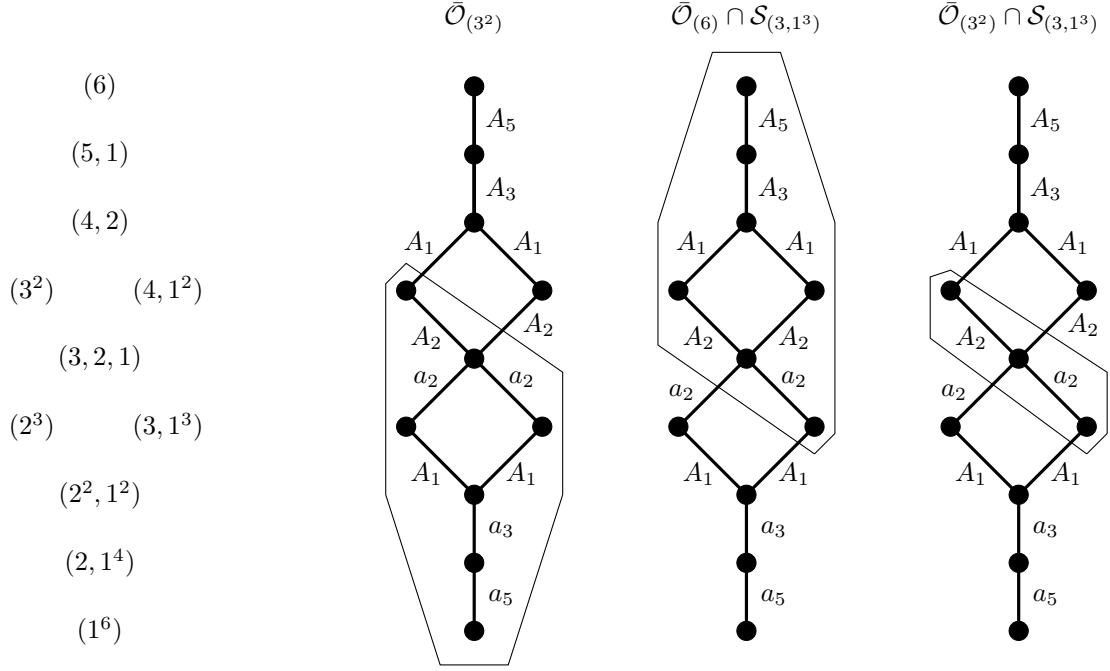


Figure 3.9: A demonstration in the Hasse diagrams of the minimal degenerations (edges) and orbits (nodes) involved in the varieties  $\bar{\mathcal{O}}_{(3^2)}$  (the closure of the  $(3^2)$  orbit),  $\bar{\mathcal{O}}_{(6)} \cap \mathcal{S}_{(3,1^3)}$  (the transverse slice to the  $(3, 1^3)$  orbit intersected with the nilpotent cone) and their intersection  $\bar{\mathcal{O}}_{(3^2)} \cap \mathcal{S}_{(3,1^3)}$ . It can be seen immediately that  $\mathfrak{sl}_6 \supset \bar{\mathcal{O}}_{(3^2)} \cap \mathcal{S}_{(3,1^3)} \sim \bar{\mathcal{O}}_{(3)} \subset \mathfrak{sl}_3$ .

dimension of the variety is

$$\begin{aligned}
 \dim(\mathcal{S}_\lambda \cap \mathcal{N}) &= \dim(\mathcal{N}) - \dim(\mathcal{O}_\lambda) \\
 &= \dim(\mathcal{O}_{(n)}) - \dim(\mathcal{O}_\lambda) \\
 &= n^2 - n - n^2 + \sum_i (\lambda_i^t)^2 \\
 &= \sum_i (\lambda_i^t)^2 - n.
 \end{aligned} \tag{3.24}$$

Finally we can consider the intersection of a given slice with a given orbit closure. This is a hyperKähler variety of dimension

$$\dim_{\mathbb{H}}(\mathcal{S}_\lambda \cap \bar{\mathcal{O}}_\mu) = \frac{1}{2} \left( \sum_i (\lambda_i^t)^2 - \sum_i (\mu_i^t)^2 \right). \tag{3.25}$$

This corresponds to a run on the Hasse diagram from the partition  $\lambda$  up to the partition  $\mu$ . Viewing the singularities above as  $\dim_{\mathbb{H}}(\bar{\mathcal{O}}_\mu) - \dim_{\mathbb{H}}(\bar{\mathcal{O}}_\nu)$  dimensional varieties, we interpret the work of Brieskorn [32] as the realisation that  $\mathcal{S}_{(n-1,1)} \cap \bar{\mathcal{O}}_{(n)} = \frac{\mathbb{C}^2}{\mathbb{Z}_n}$  and the work of Kraft and Procesi as the generalisation that  $\mathcal{S}_\nu \cap \bar{\mathcal{O}}_\mu$  is given by the right hand side of (3.17) when  $\mu$  and  $\nu$  are adjacent partitions. Some examples are given in Fig. 3.9.

For every variety  $\mathcal{S}_\lambda \cap \bar{\mathcal{O}}_\mu$  for  $\mu, \lambda \in \mathcal{P}(n)$  and  $\mu > \lambda$ , we can associate a pair of Young tableaux corresponding to those same partitions. The condition  $\mu > \lambda$  guarantees that there is a (not necessarily unique) sequence of moves of type (1) or (2) which takes us from the tableau for  $\mu$  to the tableau for  $\lambda$ .

Taking the association of these moves with the minimal singularities in (3.17), we can build up exactly the labelling of the edges between  $\mu$  and  $\lambda$  on the Hasse diagram. The moves of type (1) or (2) allow us to navigate the set of varieties  $\mathcal{S}_\lambda \cap \bar{\mathcal{O}}_\mu$ . Given the starting pair  $\mu = (n)$  and  $\lambda = (1^n)$ , corresponding to the variety  $\mathcal{S}_{(1^n)} \cap \bar{\mathcal{O}}_{(n)} = \bar{\mathcal{O}}_{(n)} = \mathcal{N}$ , we can manufacture the tableaux for any other variety  $\mathcal{S}_\lambda \cap \bar{\mathcal{O}}_\mu$  by performing moves on the tableau for  $(n)$  and reversals of the moves on the tableau for  $(1^n)$  until the tableaux correspond to the appropriate partitions. On the level of the Hasse diagram, this is the same as starting with a variety corresponding to the entire diagram and removing edges and nodes from our consideration by performing the appropriate moves in the Young tableaux. From the point of view of the varieties these moves correspond to the removal of transverse slices of the type found in (3.17) from the varieties.

Kraft-Procesi transitions are the physical realisation of the process of navigating these varieties. By performing certain manoeuvres in type IIB brane embeddings whose low-energy descriptions are field theories which have moduli space branches which are these nilpotent varieties, one can give ordering and structure to the class of such theories.

### 3.5.2 Intersections for $\mathfrak{so}_{2n}$

For  $\mathfrak{so}_{2n}$  the story is essentially similar. Restricting the Slodowy slice to nilpotent elements by intersecting the variety with the nilpotent cone,  $\mathcal{N} = \bar{\mathcal{O}}_{(2n-1,1)}$ , gives a variety which corresponds to a run from the node  $\nu$  up to the top of the Hasse diagram. From here on a slice written  $\mathcal{S}_\nu$  means the intersection of the full slice with the nilpotent cone.

Writing  $\nu$  in exponential notation with exponents  $t_i$ , the Slodowy slice  $\mathcal{S}_\nu$  is a hyperkähler singular variety of quaternionic dimension

$$\dim_{\mathbb{H}}(\mathcal{S}_\nu) = \frac{1}{2} \left( \frac{1}{2} \sum_i (\nu_i^t)^2 - \frac{1}{2} \sum_{i \text{ odd}} t_i - n \right). \quad (3.26)$$

Once again those varieties whose Hasse diagrams contain only special nodes will play an important role in our discussion. Slodowy slices that correspond to runs at the top of the Hasse diagram which contain no non-special nodes shall be referred to as *special slices*. These special slices (and their subvarieties) will have realisations as the Higgs branches of  $D_n$  Dynkin quivers.

There always exists a largest special slice in an algebra. This is due to the presence of a highest non-special partition whose node must be avoided. Recall that this non-special node was  $(2n-5, 2^2, 1)$ . In order for the Hasse diagram for a slice  $\mathcal{S}_\nu$  to avoid containing this node,  $\nu$  must not be dominated by  $(2n-5, 2^2, 1)$ . The lowest partition not dominated by  $(2n-5, 2^2, 1)$  always takes the form  $(n-1^2, 1^2)$ . Therefore the *maximal special slice* in an algebra  $\mathfrak{so}_{2n}$  is always  $\mathcal{S}_{(n-1^2, 1^2)} \in \mathfrak{so}_{2n}$ . It is this variety and its subvarieties that have realisations as the Higgs branches of  $D_n$  Dynkin quivers. Note that

$$\text{ht}(d_{LS}((n-1^2, 1^2))) = \begin{cases} \text{ht}((3^2, 2^{n-3})) = 4 > 2, & n \text{ odd} \\ \text{ht}((3^2, 2^{n-4}, 1^2)) = 4 > 2, & n \text{ even,} \end{cases} \quad (3.27)$$

so while all the Dynkin quivers which realise nilpotent orbit closures as their Coulomb branches also realise Slodowy slices with their Higgs branches, the reverse doesn't necessarily follow.

Happily, Hasse diagrams pertaining to maximal special slices in  $\mathfrak{so}_{2n}$  take regular forms which allow them to be written generally. It transpires that there are two forms for the Hasse diagrams for  $\mathcal{S}_{(2m-1^2, 1^2)} \in \mathfrak{so}_{4m}$  or  $\mathcal{S}_{(2m^2, 1^2)} \in \mathfrak{so}_{4m+2}$ . The Hasse diagrams are given in Fig. 3.10. The nilpotent varieties which appear as the Higgs branches of  $D_n$  Dynkin quivers are subvarieties of the maximal special slices and so their Hasse diagrams appear as subdiagrams of Fig. 3.10.

Some obvious subvarieties of the maximal special slice are all the Slodowy slices  $\mathcal{S}_\nu$  where  $\nu > (2m - 1^2, 1^2)$  (resp.  $(2m^2, 1^2)$ ). Further subvarieties can be found by considering slice and orbit-closure intersections.

The intersection of a Slodowy slice with a closure of a nilpotent orbit is a subvariety which corresponds to some run of nodes in the Hasse diagram. An intersection  $\bar{\mathcal{O}}_\mu \cap \mathcal{S}_\nu$  corresponds to a run from a node  $\mu$  down to a node  $\nu$  for  $\mu > \nu$ . The subvarieties of the maximal special slice are those varieties  $\bar{\mathcal{O}}_\mu \cap \mathcal{S}_\nu$  where  $\mu > \nu \geq (2m - 1^2, 1^2)$  (resp.  $(2m^2, 1^2)$ ). Intersections are hyperkähler varieties of dimension

$$\dim_{\mathbb{H}}(\bar{\mathcal{O}}_\mu \cap \mathcal{S}_\nu) = \frac{1}{2} \left( \frac{1}{2} \sum_i (\nu_i^t)^2 - \frac{1}{2} \sum_i (\mu_i^t)^2 + \frac{1}{2} \sum_{i \text{ odd}} r_i - \frac{1}{2} \sum_{i \text{ odd}} t_i \right), \quad (3.28)$$

when  $\mu$  and  $\nu$  are written using the aforementioned exponential notation. Note that this equation generalises (3.13) and (3.26), in which the nilpotent orbits' dimensions are obtained by setting  $\nu$  to be the minimal partition, and the Slodowy slices' dimensions obtained by setting  $\mu$  to be the maximal partition.

To characterise the general subvarieties of the maximal special slices note that the partitions in each maximal special slice fall into a small number of general forms. In  $\mathfrak{so}_{4m}$  the partitions are all of the form  $\psi_j = (4m - (2j + 1), 2j + 1)$  or  $\varphi_j = (4m - (2j + 3), 2j + 1, 1^2)$ , for  $0 \leq j \leq m - 1$ , or  $(2m^2)$ . There are therefore five general forms for subvarieties  $\mathcal{V} \subseteq \mathcal{S}_{(2m-1^2, 1^2)} \subset \mathfrak{so}_{4m}$ ,

$$\mathcal{V} = \begin{cases} \bar{\mathcal{O}}_{\psi_j} \cap \mathcal{S}_{\psi_k} & \text{for } k > j \\ \bar{\mathcal{O}}_{\psi_j} \cap \mathcal{S}_{\varphi_k} & \text{for } k > j - 1 \geq 0 \\ \bar{\mathcal{O}}_{\varphi_j} \cap \mathcal{S}_{\varphi_k} & \text{for } k > j \\ \bar{\mathcal{O}}_{\psi_j} \cap \mathcal{S}_{(2m^2)} \\ \bar{\mathcal{O}}_{(2m^2)} \cap \mathcal{S}_{(2m-1^2, 1^2)} = A_{2m-1} \cup A_{2m-1}. \end{cases} \quad (3.29)$$

In  $\mathfrak{so}_{4m+2}$  the maximal special slice partitions all take the form  $\psi'_j = (4m - (2j - 1), 2j + 1)$  or  $\varphi'_j = (4m - (2j + 1), 2j + 1, 1^2)$ , for  $0 \leq j \leq m$ , or  $(2m^2, 1^2)$ . There are therefore five general forms for subvarieties  $\mathcal{V} \subseteq \mathcal{S}_{(2m^2, 1^2)} \subset \mathfrak{so}_{4m+2}$ ,

$$\mathcal{V} = \begin{cases} \bar{\mathcal{O}}_{\psi'_j} \cap \mathcal{S}_{\psi'_k} & \text{for } k > j \\ \bar{\mathcal{O}}_{\psi'_j} \cap \mathcal{S}_{\varphi'_k} & \text{for } k > j - 1 \geq 0 \\ \bar{\mathcal{O}}_{\varphi'_j} \cap \mathcal{S}_{\varphi'_k} & \text{for } k > j \\ \bar{\mathcal{O}}_{\psi'_j} \cap \mathcal{S}_{(2m^2, 1^2)} \\ \bar{\mathcal{O}}_{\varphi'_j} \cap \mathcal{S}_{(2m^2, 1^2)}. \end{cases} \quad (3.30)$$

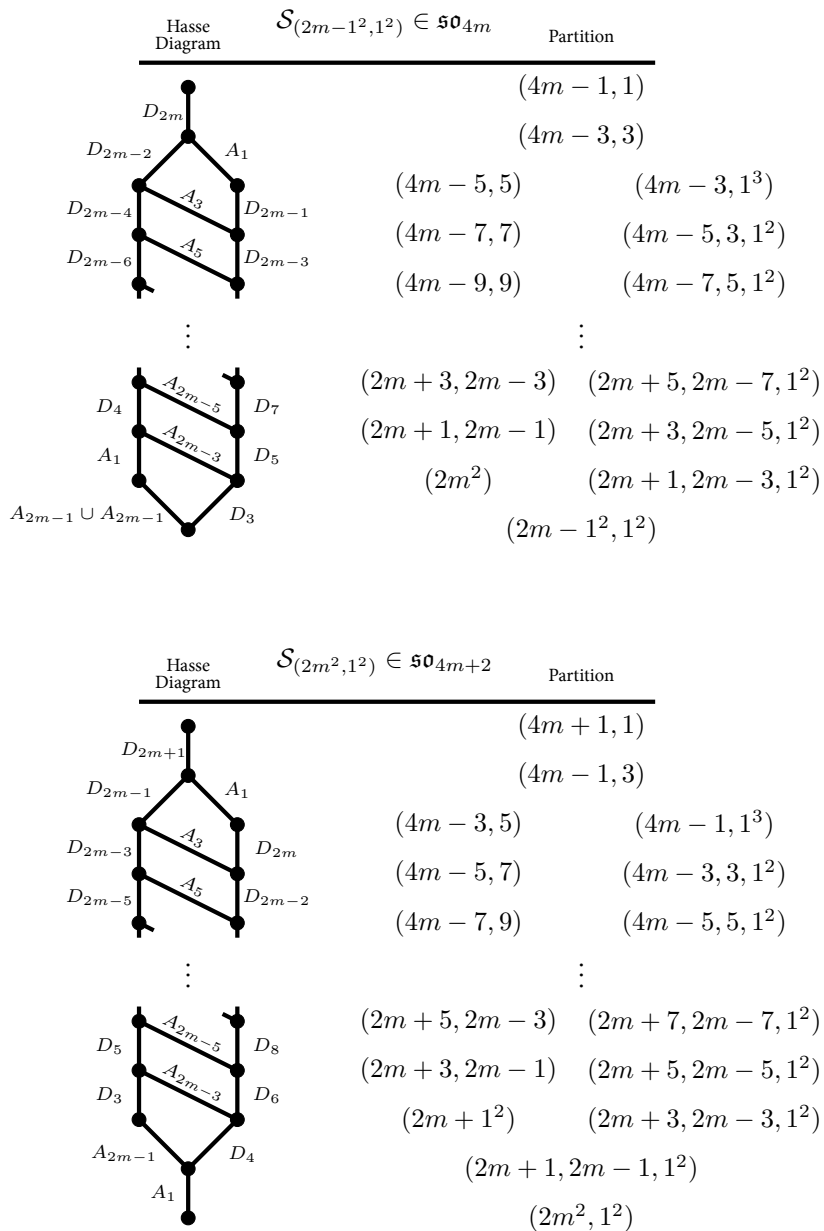


Figure 3.10: The Hasse diagrams for the maximal special slices,  $\mathcal{S}_{(2m-1^2, 1^2)} \in \mathfrak{so}_{4m}$  and  $\mathcal{S}_{(2m^2, 1^2)} \in \mathfrak{so}_{4m+2}$ . The Higgs branches of the  $D_n$  Dynkin quivers in this section will be subvarieties appearing as runs in these Hasse diagrams.

There are some varieties that appear in both maximal special slices. These are identified by looking for identical Hasse subdiagrams in the two maximal special slice Hasse diagrams. Hasse subdiagrams shared by both diagrams in Fig. 3.10 are: the individual singularities of types  $A_l$  and  $D_l$ , and varieties with Hasse diagrams that take the form of a chain of  $D_l$  singularities for odd or even  $l$ . Casting these shared subvarieties in the notation above gives the equalities

$$\begin{aligned}
 \bar{\mathcal{O}}_{\psi_j} \cap \mathcal{S}_{\psi_k} &= \bar{\mathcal{O}}_{\varphi'_j} \cap \mathcal{S}_{\varphi'_k}, \\
 \bar{\mathcal{O}}_{\varphi_j} \cap \mathcal{S}_{\varphi_k} &= \bar{\mathcal{O}}_{\psi'_{j+1}} \cap \mathcal{S}_{\psi'_{k+1}}, \\
 \bar{\mathcal{O}}_{\psi_j} \cap \mathcal{S}_{(2m^2)} &= \bar{\mathcal{O}}_{\varphi'_j} \cap \mathcal{S}_{(2m^2, 1^2)}.
 \end{aligned} \tag{3.31}$$



# Linear quivers and the Kraft-Procesi transition

We now review linear quivers and the Kraft-Procesi transition first developed in [4, 5]. This transition is the realisation in physical systems of the manipulations translating between nilpotent varieties as discussed above, wherein the moduli space of vacua of the field theoretic construction is the nilpotent variety. We will discuss the manifestation of this transition in the brane configurations discussed earlier, and through purely field theoretic considerations, in order to give complimentary perspectives on the subject. In this section we will concentrate on linear quivers as an illustrative example and relegate any further considerations specific to circular or D-type Dynkin quivers to later sections. We then use this transition to navigate the sets of linear quivers whose moduli spaces of vacua are nilpotent varieties for  $\mathfrak{sl}_n$  for small values of  $n$ . While well known, this will provide a robust grounding in the ideas central to later discussion.

## 4.1 Linear quivers

A linear quiver is one where the gauge nodes are connected in sequence such that the gauge group for the theory is  $U(k_1) \times U(k_2) \times \cdots \times U(k_{N-1})$ . Linear quivers are denoted as  $T_{\mu^t}^{\nu}(\mathrm{SU}(N))$  where  $\mu$  and  $\nu$  are partitions of  $N$ . These theories arise as the low energy dynamics of type IIB superstring embeddings involving D3, D5 and NS5 branes in a standard configuration already discussed. In these configurations the partitions are related to the *linking numbers* of the five branes. The linking number of a five brane can be defined as the net number D3 branes ending on the five brane from the right plus the number of the opposite type of five brane to the left. The linking numbers for each type of five brane are written as a tuple,  $l_s$  for NS5 branes and  $l_d$  for D5 branes. The  $i^{\mathrm{th}}$  part of the tuple is the linking number of the  $i^{\mathrm{th}}$  5-brane of a given type from the left. Set  $l_d = (N^N) - \nu$  and  $l_s = \overleftarrow{\mu^t}$ , where  $\leftrightarrow$  indicates order reversal. Pad the partitions with zeroes if necessary. To find the brane system in the Higgs brane configuration we can place all of the NS5 branes in the appropriate gaps between D5 branes then realise the D5 linking number by adding D3 branes suspended between D5 branes. The Coulomb brane configuration for a given theory can be found by performing a

*complete Higgsing* on the Higgs brane configuration. The quiver for the theory can be read from the Coulomb brane configuration. Recall that when reading the quiver each circular gauge node labelled  $n_i$  entails a stack of  $n_i$  D3 branes suspended between two NS5 branes and each square flavour node labelled  $m_i$  entails  $m_i$  D5 branes in the same gap as the gauge node to which it attaches.

The Higgs and Coulomb branches of these theories are therefore also related to the partition data. For a theory in the class  $T_{\mu^t}^\nu(\text{SU}(N))$ , the Higgs branch is given by

$$\mathcal{M}_H(T_{\mu^t}^\nu(\text{SU}(N))) = \bar{\mathcal{O}}_\mu \cap \mathcal{S}_\nu, \quad (4.32)$$

and the Coulomb branch by

$$\mathcal{M}_C(T_{\mu^t}^\nu(\text{SU}(N))) = \mathcal{S}_{\mu^t} \cap \bar{\mathcal{O}}_{\nu^t}. \quad (4.33)$$

A convenient visual intuition for these branches can be found by marking the orbits on the Hasse diagram for nilpotent orbits of  $\mathfrak{sl}_N$  which correspond to the Higgs and Coulomb branch varieties respectively. In this sense we may discuss how a given theory corresponds to a run of nodes and edges on a Hasse diagram.  $T_{\mu^t}^\nu(\text{SU}(N))$  corresponds to a run from a node labelled  $\nu$  up to a node labelled  $\mu$ . A number of aspects of these theories can now be realised in the manipulation of the Hasse diagram and associated visualisations.

For example, the mirror dual of  $T_{\mu^t}^\nu(\text{SU}(N))$  is  $T_{\nu^t}^{\mu^t}(\text{SU}(N))$ . The mirror theory is a theory in which the Higgs branch and Coulomb branch varieties have been exchanged. Mirror symmetry is realised as S-duality in these brane configurations, NS5 branes turn to D5 branes and vice versa while D3 branes remain the same. At the level of the Hasse diagram, mirror symmetry is therefore realised as the involution on  $\mathcal{P}(N)$  which flips the diagram top-bottom, that is, transposition of the partitions. The naming of the mirror class matches this. At the level of the Young tableaux, mirror symmetry is realised as the reflection in the NE-SW diagonal of *both* of the tableaux. The brane systems corresponding to the theories whose moduli space branches are the  $A_m$  and  $a_m$  minimal singularities must therefore be S-dual (mirror dual) to one another. Removal of an  $A_m$  minimal singularity from the Higgs branch means the removal of an  $a_m$  minimal singularity from the Coulomb branch and vice versa.

#### 4.1.1 An alternative class of linear theories

A theory in the class  $T_{\mu^t}^\nu(\text{SU}(N))$  requires two pieces of data to fully specify: two partitions,  $\mu$  and  $\nu$ , of equal magnitude,  $N$ . However this formulation will not generalise in a manner which captures the entire class of circular quivers. To prepare the ground for our discussion of circular quivers we will define a broader class of linear quiver gauge theories. In the linear case this broader class degenerates to the class  $T_{\mu^t}^\nu(\text{SU}(N))$ , however this degeneration doesn't hold for circular quivers so the broader class of linear quivers generalises more naturally to the circular case.

To define the broader class, we require that the two partitions  $\mu$  and  $\nu$  are of the same magnitude, now  $M$ , and that their Young tableaux may be contained within a frame  $N_1$  blocks wide and  $N_2$  blocks tall. The partitions of  $M$  can clearly be placed within an  $M \times M$  frame and so this restriction subsumes the traditional one. We temporarily call the class of theories attainable under these looser conditions  $\tau_{\mu^t}^\nu(M, N_1, N_2)$  and will show that this class contains exactly the same theories as  $T_{\mu^t}^\nu(\text{SU}(M))$ . These tableaux restrictions may

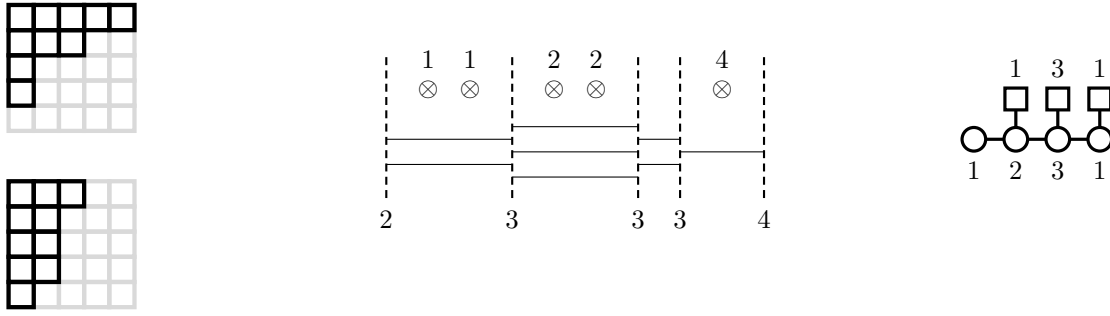


Figure 4.11: An example theory,  $\tau_{(4,2^2,1^2)}^{(3,2^3,1)}(10, 5, 5)$ . The Young tableaux and frames for each partition are given on the left. The Higgs brane configuration is given in the center along with the linking number of each of the five branes in the system. Finally the quiver itself is given, recall that the quiver must be read from the Coulomb brane configuration, so we have to fully Higgs the brane system displayed in order to read the quiver.

be realised as the following for the partitions:  $\mu$  must have no part that is larger than  $N_1$  and the partition  $\nu$  has no more than  $N_2$  parts. Since  $\mu$  is the highest partition, it will contain the (perhaps joint) largest part of those partitions bounded by  $\mu$  and  $\nu$ , and since  $\nu$  is the lowest, it will be the (perhaps joint) longest partition. The bounds imposed on the largest part of  $\mu$  and length of  $\nu$  are therefore bounds for these values for all of the partitions between  $\mu$  and  $\nu$ . The requirements also impose that  $0 \leq M \leq N_1 N_2$  since the partitions must be contained in the  $N_1 \times N_2$  frame. Fig. 4.11 contains an example.

The new requirements on the partitions have consequences in the brane configuration. The linking numbers of the five branes are now assigned as  $l_d = (N_1^{N_2}) - \nu$  and  $l_s = \overleftarrow{\mu^t}$ . Limiting the largest part of  $\mu$  to be no larger than  $N_1$  means that the length of  $\mu^t$  is no larger than  $N_1$ . The number of NS5 branes that receive non-zero linking number is exactly the length of  $\mu^t$ . As such, no more than  $N_1$  NS5 branes receive non-zero linking number. The number of D5 branes that receive a linking number other than  $N_1$  is exactly the length of the partition  $\nu$ , which is no more than  $N_2$ . Therefore restricting  $\nu$  to be no longer than  $N_2$  means no more than  $N_2$  D5 branes receive non- $N_1$  linking number. The only way for a D5 brane to have a linking number of  $N_1$ , given we assign linking numbers from left to right, is if it lies to the right of all NS5 branes and isn't attached to any D3 branes. Likewise the only way for an NS5 brane to have a linking number of zero is if it is to the left of all the D5 branes and isn't attached to any D3 branes. Therefore, for the linear case, NS5 branes with a linking number of 0 and D5 branes with a linking number of  $N_1$  do not play a role in the infrared physics as they don't meet D3 branes in the appropriate manner.

The effect this has on the class  $\mathcal{T}_{\mu^t}^\nu(M, N_1, N_2)$  is diagrammed in Fig. 4.12. Given  $\mu, \nu \in \mathcal{P}(M)$ , the linear quiver is *independent* of  $N_1$  and  $N_2$  providing they form a frame large enough to contain the partitions. The choice  $M = N_1 = N_2$  is the smallest for which this is guaranteed. This choice recovers  $T_{\mu^t}^\nu(\text{SU}(M))$ . For circular quiver gauge theories, there are no possible linking numbers for the five branes which make them irrelevant for the infrared physics. Therefore we are not free to choose the frame size arbitrarily as every different size of frame gives a different theory. The class of circular theories is therefore much larger than the class of linear theories.

The theories in the class  $T_{\mu^t}^\nu(\text{SU}(M))$  can be matched to the nilpotent varieties via consideration of their moduli space branches. There are diagrammatic techniques for navigating these varieties by manipulating the



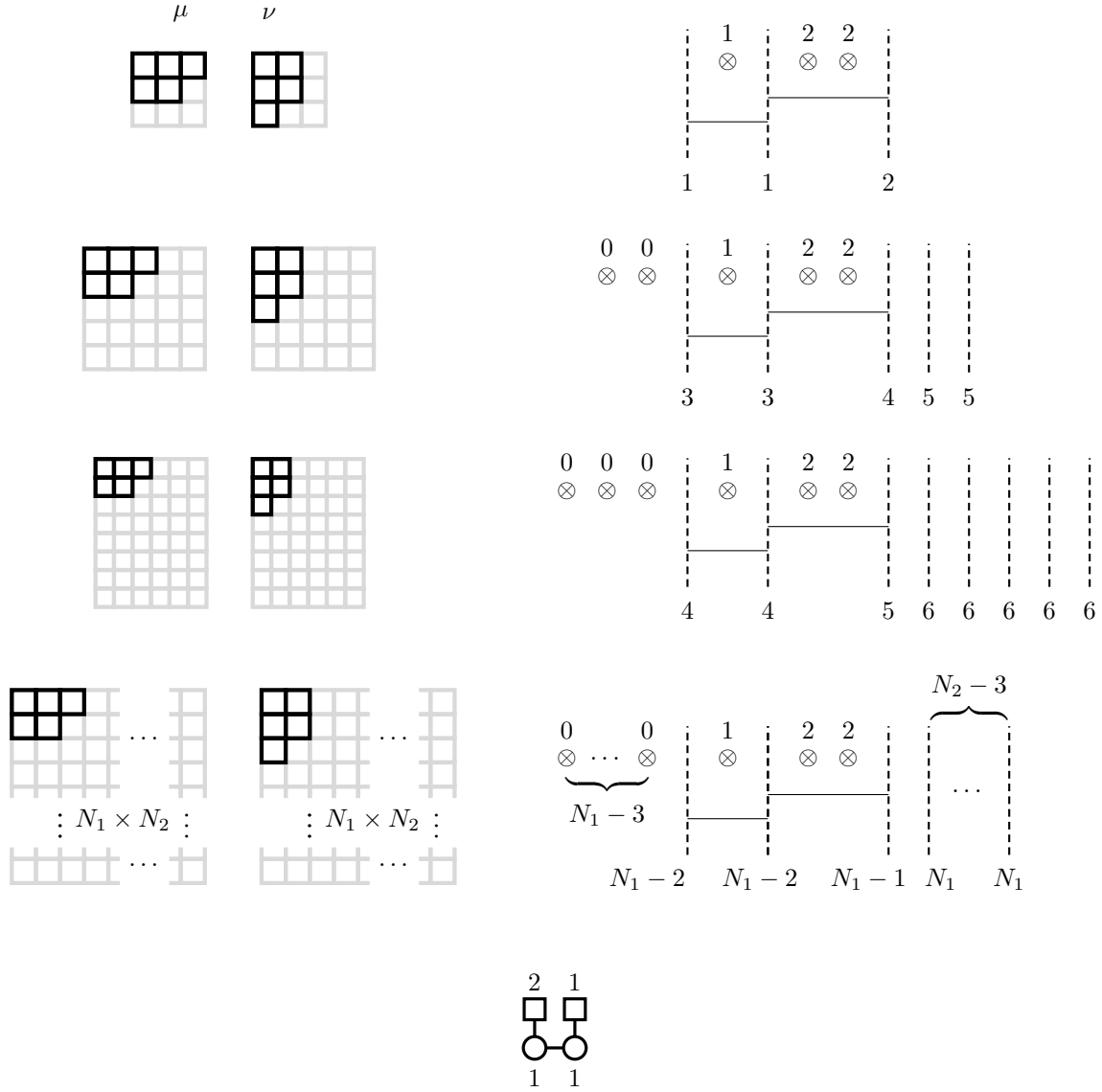


Figure 4.12: An explicit demonstration of the independence of the infrared physics in the class  $\tau_{\mu^i}^{\nu}(M, N_1, N_2)$  from  $N_1$  or  $N_2$ . The brane system and linking numbers for the theory  $\tau_{(2^2,1)}^{(2^2,1)}(5, 3, 3)$  along with the tableaux for both  $\mu$  and  $\nu$  is given first. Then the tableaux and the brane system for  $\tau_{(2^2,1)}^{(2^2,1)}(5, 5, 5)$  and then  $\tau_{(2^2,1)}^{(2^2,1)}(5, 6, 8)$  and finally for  $\tau_{(2^2,1)}^{(2^2,1)}(5, N_1, N_2)$  for any  $N_1 \geq 3$  and  $N_2 \geq 3$ . The quiver encapsulating the infrared physics of all of these brane constructions is given, which is the same for all of the brane set-ups.

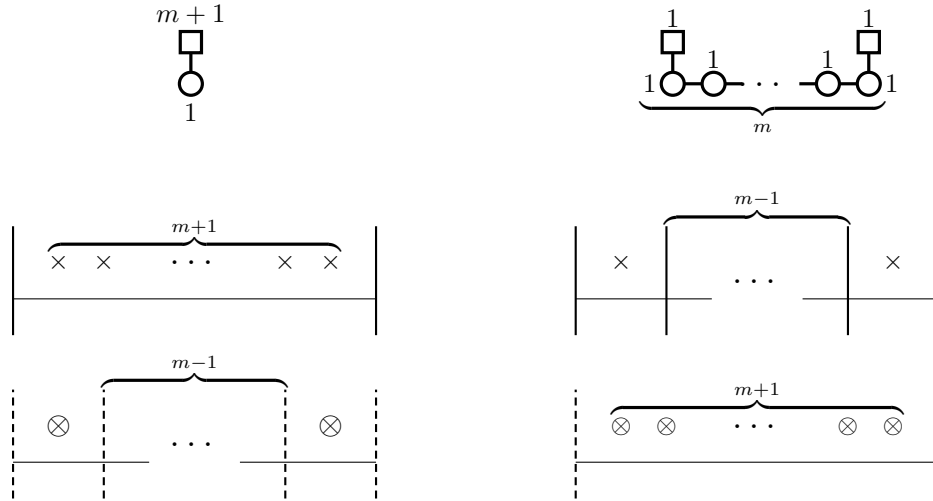


Figure 4.13: The quiver, Coulomb brane configuration, and Higgs brane configuration for 3d  $\mathcal{N} = 4$  SQED with  $m + 1$  flavours (left) and its mirror dual (right). The moduli space branches for 3d  $\mathcal{N} = 4$  SQED are  $\mathcal{M}_C = A_m$  and  $\mathcal{M}_H = a_m$  and vice versa for the mirror theory.

Young tableaux. These moves, as they changed the tableaux, changed the partitions. There is a prescription for writing the brane system with the appropriate low energy dynamics in terms of partitions by appealing to the linking number of the five branes. The Kraft-Procesi transition is a manipulation in the brane system which gives the appropriate change in linking number such that the change in partitions realises the transverse slice structure from chapter 3.

## 4.2 Kraft-Procesi transitions in brane configurations

A Kraft-Procesi transition involves two steps. The first step is the identification of a brane subsystem with a moduli space branch that is a transverse slice. The second is removing this subsystem via the Higgs mechanism in order to move to a different theory. The minimal singularities in  $\mathfrak{sl}_n$  come in two types,  $A_m$  and  $a_m$ , and so only two types of Kraft-Procesi transition need to be developed corresponding to brane subsystems whose moduli space branches are these varieties. The theories with these varieties as moduli space branches are 3d  $\mathcal{N} = 4$  SQED with  $m + 1$  flavours and its mirror dual. The brane configurations for the corresponding subsystems are given in Fig. 4.13.

To perform step two of a Kraft-Procesi transition, align the D3 branes for the subsystem corresponding to a minimal singularity with the five branes between which the D3 branes are *not* suspended given the configuration. For example, in the Higgs brane configuration, D3 branes are suspended between D5 branes so the initial process is to slide the D3 branes so they align with the NS5 branes. Then push the sections of D3 brane suspended between the five branes with which the D3 branes have been aligned to infinity along these branes, that is, into the other brane configuration. This removes them from the system. Starting in the Higgs brane configuration and pushing D3 branes to infinity in the Coulomb configuration removes the corresponding minimal singularity from the top of the Higgs branch Hasse diagram and bottom of the Coulomb branch Hasse diagram. Starting in the Coulomb configuration and pushing D3 branes to infinity in the Higgs brane

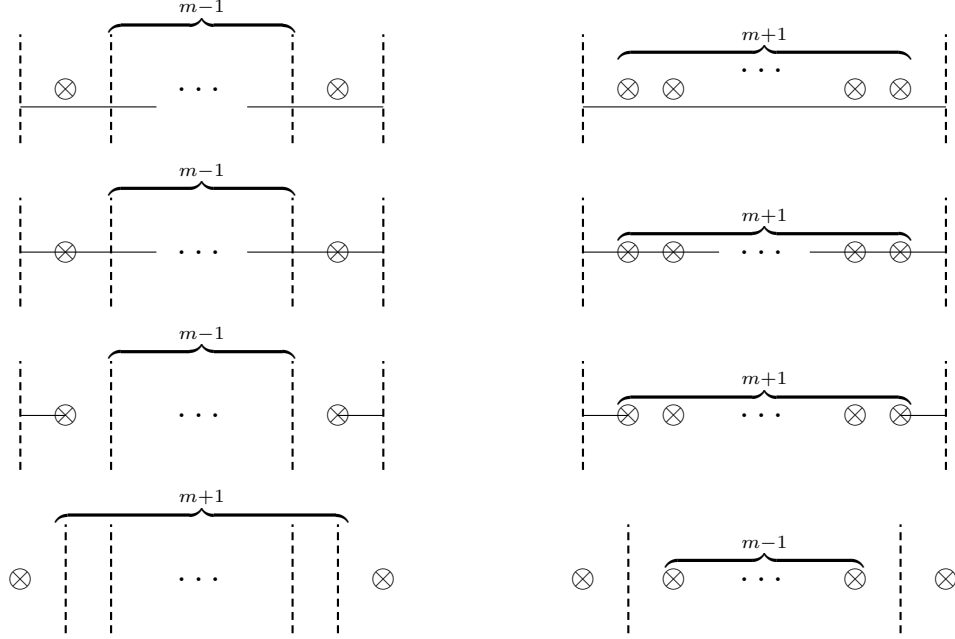


Figure 4.14: The Higgs brane configuration brane manipulation for an  $A_m$  Kraft-Procesi transition (right) and an  $a_m$  Kraft-Procesi transition (left). In both cases, the D3 branes are aligned with the NS5 branes and the centre parts are pushed to infinity. Hanany-Witten transitions are then performed to remove the frozen D3 segments.

configuration removes the corresponding minimal singularity from the top of the Coulomb branch Hasse diagram and bottom of the Higgs branch Hasse diagram. To complete the transition, perform Hanany-Witten transitions to remove the frozen sections of D3 brane that remain between the D5 and NS5 branes. Fig. 4.14 shows the process starting in the Higgs brane configuration.

Mirror symmetry, realised as S-duality in the brane configurations, swaps the Higgs and Coulomb branch varieties. Removal of an  $A_m$  ( $a_m$ ) minimal singularity in one branch is therefore the removal the same minimal singularity in the other branch of the mirror theory. Kraft-Procesi transitions remove minimal singularities from one branch starting at the top of the Hasse diagram, working down, and also remove minimal singularities from the other branch variety of that same theory, starting at the bottom of the Hasse diagram, working up. In order to find a  $T_{\mu^t}^{\nu}(\mathrm{SU}(M))$  theory from  $T(\mathrm{SU}(M))$ , for example, perform Kraft-Procesi transitions in the Higgs brane configuration down to the orbit  $\mu$  and Kraft-Procesi transitions in the Coulomb brane configuration down to the orbit  $\nu^t$ . A worked example is given in Fig. 4.15 in which Kraft-Procesi transitions are used to find  $T_{(2^2,1)}^{(2,1^3)}(\mathrm{SU}(5))$  starting from  $T(\mathrm{SU}(5))$ .

A *descendant theory* for a given theory  $\mathcal{T}$  is another theory,  $\mathcal{U}$ , which can be found by performing Kraft-Procesi transitions on  $\mathcal{T}$ . We denote the collection of descendant theories of  $\mathcal{T}$  as  $\mathcal{K}(\mathcal{T})$ . For this class of linear quivers

$$\mathcal{K}(T_{\mu^t}^{\nu}(\mathrm{SU}(M))) = \{T_{\rho^t}^{\sigma}(\mathrm{SU}(M)) \mid \rho \leq \mu, \sigma \geq \nu\}. \quad (4.34)$$

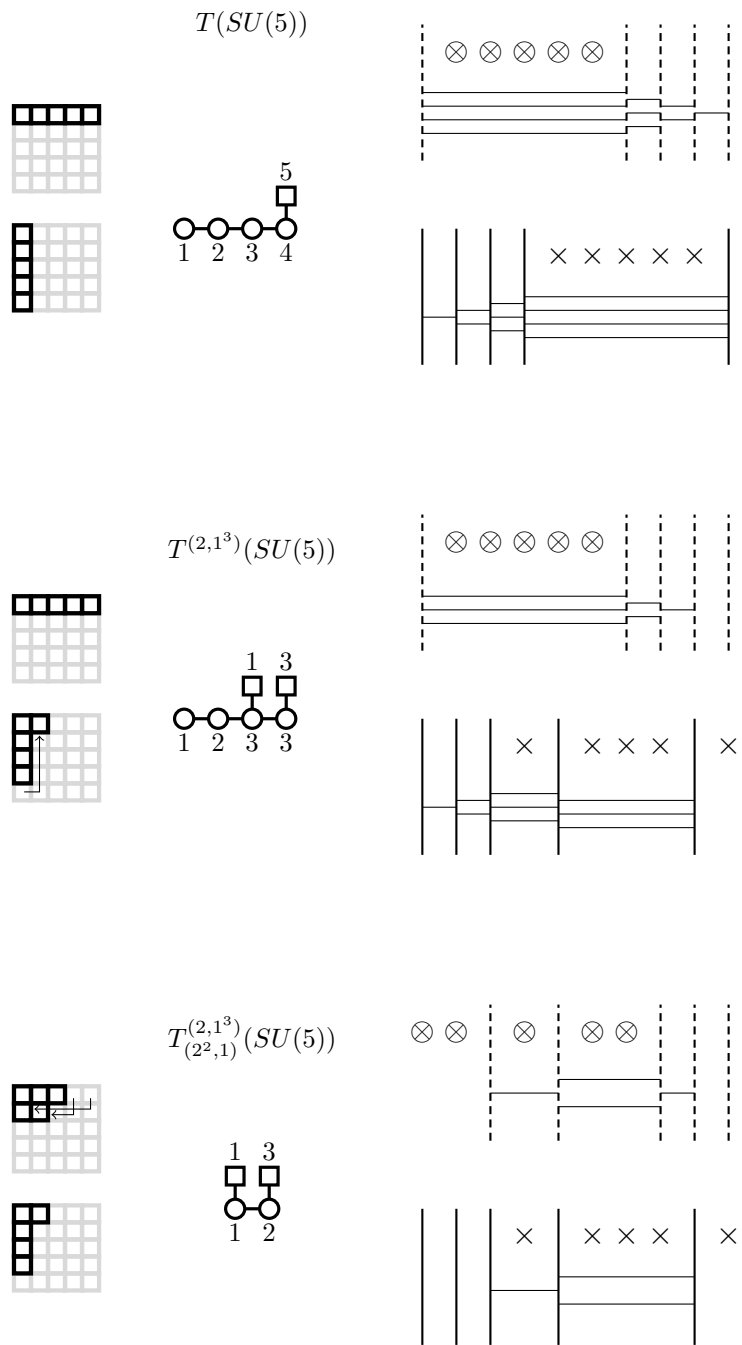
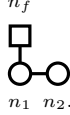


Figure 4.15: Demonstration of the use of Kraft-Procesi transitions to find  $T^{(2,1^3)}_{(2^2,1)}(SU(5))$  within  $T(SU(5))$ . The tableaux for the partitions defining the theories are given with corresponding block movements indicated. Then the quiver for each of the theories. Finally, on the right, the Higgs brane configuration (top) and Coulomb brane configuration (bottom) for the theories.

### 4.3 Kraft-Procesi transitions in field theory

Kraft-Procesi transitions can be interpreted in the field theory without reference to the brane configurations used in the previous section.

Consider a field theory with the gauge group  $U(n_1) \times U(n_2)$  with  $n_f$  fundamental flavours  $Q_i$  where  $i = 1, \dots, n_f$ , and their complex conjugate, for the group  $U(n_1)$ , and bifundamental fields  $A_{\tilde{a}}, B_{\tilde{a}}$  with  $a = 1, \dots, n_1; \tilde{a} = 1, \dots, n_2$  in the  $(n_1, \bar{n}_2)$  and  $(\bar{n}_1, n_2)$  representations of the gauge group. This set up corresponds to the  $3d \mathcal{N} = 4$  quiver:



A general discussion of moduli spaces for four dimensional  $\mathcal{N} = 1$  theories with product group  $U(n_1) \times U(n_2)$  and fundamental flavours has been developed in [56]. Their starting point was a four dimensional  $\mathcal{N} = 2$  theory with mass terms for the chiral adjoint fields and for fundamental fields. They also considered various limits for the masses of the adjoint field and the fundamental flavours. Here,  $\mathcal{N} = 4$  theories in three dimensions (which descend from  $\mathcal{N} = 2$  theories in four dimensions by dimensional reduction) are considered, when the masses of the adjoint fields and the masses of fundamental flavours are taken to zero. The field theory superpotential is, [56],

$$\text{Tr} \left( \sum_{i=1}^{n_f} Q_i \Phi_1 \tilde{Q}_i + A \Phi_1 B + B \Phi_2 A \right), \quad (4.35)$$

where the trace is over the gauge group. The F-term equations from derivatives with the fields  $\Phi_i$  imply

$$\sum_{i=1}^{n_f} Q_i^a \tilde{Q}_{ib} + \sum_{\tilde{a}} A_{\tilde{a}}^a B_{\tilde{a}}^b = 0 \quad \text{and} \quad \sum_{\tilde{a}} A_{\tilde{a}}^a B_{\tilde{a}}^b = 0. \quad (4.36)$$

The D-term equations for a supersymmetric vacuum are

$$[\Phi_1, \Phi_1^\dagger] = [\Phi_2, \Phi_2^\dagger] = 0, \quad (4.37)$$

$$A A^\dagger + \sum_{i=1}^{n_f} Q^i (Q^\dagger)_i - \sum_{i=1}^{n_f} (\tilde{Q}^\dagger)^i \tilde{Q}_i - B^\dagger B = 0. \quad (4.38)$$

The vanishing of the terms in equation (4.37) was explained in [57].

The difference between our case and the one of [56] concerns the moduli space. In [56] the authors considered the vacua with  $Q = 0$  when the bifundamental fields  $A, B$  could be simultaneously diagonalized by a colour rotation and have  $N = \min(n_1, n_2)$  diagonal entries. The only solution appears when  $A = B = 0$  and the Coulomb branch is a product of Abelian factors.

For our case, consider the Higgs branch when some or all of the expectation values for fields  $Q, \tilde{Q}$  are non zero and the fields  $A, B$  cannot be fully diagonalised. With  $Q, \tilde{Q}$  as  $n_1 \times n_f$  matrices, consider first the case

when the nonzero entry of  $Q$  is  $Q_1^1 = k_1$  and for  $\tilde{Q}$ ,  $\tilde{Q}_1^3 = k_1$  as in [57]. This breaks the flavour group to  $SU(n_f - 2)$  and the first gauge group to  $U(n_1 - 1)$ .

The bifundamental field  $A$  is an  $n_1 \times n_2$  matrix whereas  $B$  is an  $n_2 \times n_1$  matrix. When the fundamental fields have zero expectation values they can both be diagonalised by a  $U(n_1) \times U(n_2)$  gauge transformation. When  $Q_1^1 = k_1$  and  $\tilde{Q}_1^3 = k_1$ , equation (4.38) becomes

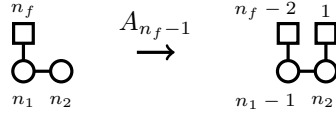
$$A A^\dagger - B^\dagger B = 0. \quad (4.39)$$

What about the diagonalisation of  $A$  and  $B$ ? The surviving  $U(n_1 - 1) \times U(n_2)$  gauge transformation can only partially diagonalise  $A$  and  $B$  and does not fix the values of the first row in  $A$  ( $A_1^1, \dots, A_{n_2}^1$ ) and the first column in  $B$  ( $B_1^1, \dots, B_1^{n_2}$ ). If we define

$$q_{\tilde{a}} = A_{\tilde{a}}^1, \quad \tilde{q}^{\tilde{a}} = B_1^{\tilde{a}}, \quad \tilde{a} = 1, \dots, n_2, \quad (4.40)$$

the equation (4.39) implies that a D-term equation for  $q$  is satisfied.  $q$  and  $\tilde{q}$  represent matter in the fundamental representation of  $U(n_2)$ .

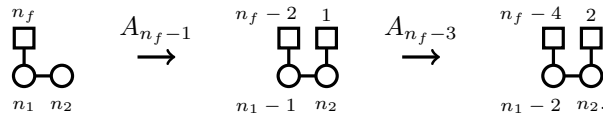
The conclusion is that when the product group  $U(n_1) \times U(n_2)$  with  $n_f$  fundamental flavours is broken to  $U(n_1 - 1) \times U(n_2)$  by a vacuum expectation value for a field in the fundamental representation of  $U(n_1)$ , there are  $n_f - 2$  fundamental flavours for  $U(n_1 - 1)$  and one for  $U(n_2)$ . This is exactly the result of an  $A_{n_f-1}$  Coulomb brane configuration Kraft-Procesi transition in the brane interval corresponding to the  $U(n_1)$  gauge group.



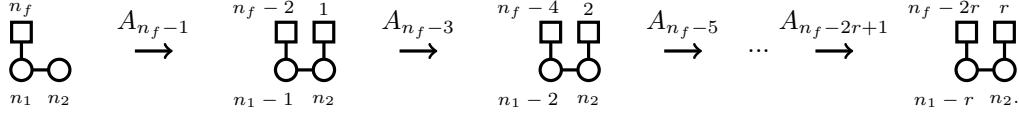
When more  $Q$  and  $\tilde{Q}$  fields have a nonzero expectation value,

$$Q_1^1 = k_1 = \tilde{Q}_1^3, \quad Q_2^2 = k_1 = \tilde{Q}_2^4, \quad (4.41)$$

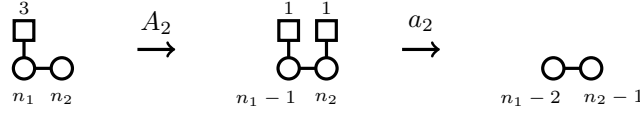
the gauge group is broken to  $U(n_1 - 2) \times U(n_2)$  and the gauge transformations leave more components of  $A$  and  $B$  unfixed. The first two rows in  $A$  and first two columns in  $B$  are not fixed and they correspond to an  $SU(2)$  fundamental flavour group for  $U(n_2)$  gauge group. The resulting theory is  $U(n_1 - 2) \times U(n_2)$  with  $n_f - 4$  fundamental flavours for  $U(n_1 - 2)$  and two for  $U(n_2)$ . This is exactly what is obtained by a succession of an  $A_{n_f-1}$  and an  $A_{n_f-3}$  Kraft-Procesi transition:



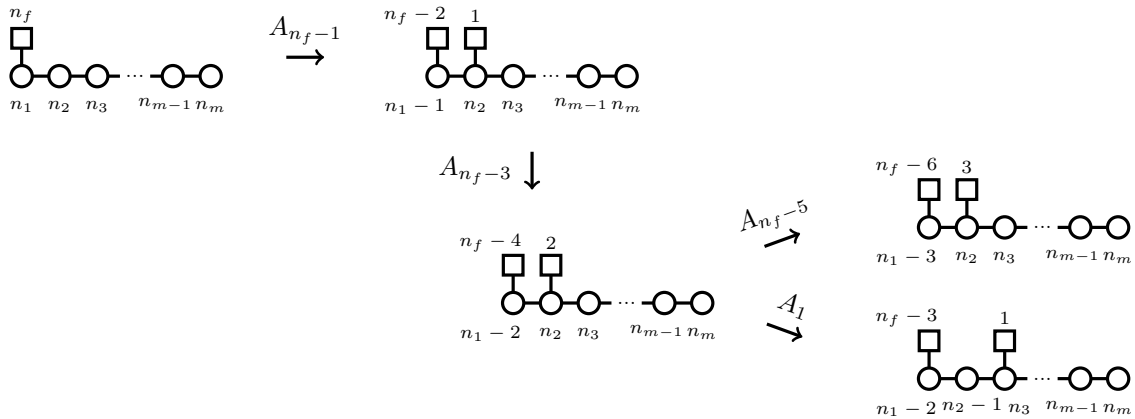
When there are an even number of fundamental flavours for  $U(n_1)$ ,  $n_f = 2r$ ,  $r < n_1$ , the case when all the fields  $Q, \tilde{Q}$  have an expectation value breaks the gauge group to  $U(n_1 - r) \times U(n_2)$ . Now  $r$  rows of  $A$  and  $r$  rows of  $B$  are not fixed which correspond to  $r$  fundamental flavours for  $U(n_2)$ . This could be obtained by a sequence of  $A_{n_f-1}, A_{n_f-3}, \dots, A_{n_f-r+1}$  Kraft-Procesi transitions.



Now consider the case of an odd number of flavours for  $U(n_1)$ ,  $n_f = 2r + 1$ . First consider  $r = 1$ ,  $n_f = 3$ . A VEV for one  $Q, \tilde{Q}$  leads us to  $U(n_1 - 1) \times U(n_2)$  with one remaining flavour  $Q_3$  for  $U(n_1 - 1)$  and one flavour  $q$  for  $U(n_2)$ . This step is familiar as the  $A_{n_f-1}$  transition just discussed. The fields  $A$  and  $B$  are  $(n_1 - 1) \times n_2$  and  $n_2 \times (n_1 - 1)$  matrices respectively,  $Q_3$  is a vector with  $n_1 - 1$  components and  $q$  a vector with  $n_2$  components. The D-term and F-term equations are satisfied if the first components of  $Q_3, \tilde{Q}_3, q, \tilde{q}$  and the elements  $A_1^1, B_1^1$  of the matrices  $A, B$  are nonzero. This breaks the gauge group to  $U(n_1 - 2) \times U(n_2 - 1)$  with no fundamental flavours for any of the groups. This is the same as the result of an  $a_2$  Coulomb brane configuration Kraft-Procesi transition. We have therefore considered an  $A_2$  transition followed by an  $a_2$  transition.

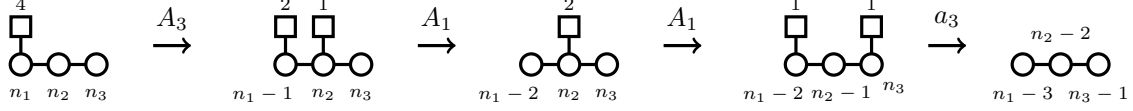


This can be generalised to any initial theory with product of gauge groups  $\prod_{k=1}^m U(n_k)$  and  $n_f$  flavours for the first gauge group  $U(n_1)$ . There are  $m - 1$  sets of bifundamental fields  $A_k, B_k$  in the  $(n_k, \bar{n}_{k+1})$  and  $(\bar{n}_k, n_{k+1})$  representations. As before, a vev for two fundamental and two antifundamental flavours will change the theory into one with  $U(n_1 - 2) \times \prod_{k=2}^m U(n_k)$  with  $n_f - 4$  flavours for  $U(n_1 - 2)$  and two for  $U(n_2)$ . The bifundamental fields  $A_1^{(1)}, B_1^{(1)}$  are now in the  $(n_1 - 1, \bar{n}_2)$  representation and its conjugate. What happens when the  $U(n_2)$  flavours get a vacuum expectation value and break the second group to  $U(n_2 - 1)$ ? The first row of  $A^{(1)}$  corresponds to a new fundamental flavour for  $U(n_1 - 1)$  and the first column of  $B^{(1)}$  to a new antifundamental flavour of  $U(n_1 - 1)$ . On the other hand, the same change should be applied to  $A_2, B_2$ , the bifundamental fields between  $U(n_2) \times U(n_3)$ . Their first row (column) will become the components of an (anti) fundamental field of  $U(n_3)$ :



The result is a theory with gauge group  $U(n_1 - 2) \times U(n_2 - 1) \times \prod_{k=3}^m U(n_k)$  with  $n_f - 3$  flavours for  $U(n_1 - 2)$  and one flavour for  $U(n_3)$ .

When  $n_f = 4$ ,  $m = 3$  there is a  $U(n_1 - 2) \times U(n_2 - 1) \times U(n_3)$  with one flavour  $Q$  for  $U(n_1 - 2)$  and one flavour  $q$  for  $U(n_3)$ . Making the products  $QA_1A_2q$  and  $\tilde{q}B_2B_1\tilde{Q}$  nonzero, the surviving group is  $U(n_1 - 3) \times U(n_1 - 2) \times U(n_3 - 1)$ . This is just an  $a_3$  Kraft-Procesi transition:



All the possible Kraft-Procesi transitions can be understood by looking at the various bifundamental fields in the theory. An  $A_k$  Kraft-Procesi transition occurs when one bifundamental field between two adjacent groups in the product group loses a row or a column which becomes a fundamental flavour for one of the adjacent groups. An  $a_k$  Kraft-Procesi transition occurs when several successive bifundamental fields have a nonzero entry such that their products with two fundamental fields are nonzero.

#### 4.4 Tables of descendant theories for $\mathfrak{sl}_N$

Starting with  $T(\text{SU}(M))$  and finding descendant theories should uncover the entire class  $T_{\mu^t}^\nu(\text{SU}(M))$ . Descendant theories were defined in (4.34). Every run on the Hasse diagram between nodes where one dominates the other corresponds to a theory ‘in’ that Hasse diagram. The number of (non trivial) descendant theories at a given  $M$  is given by

$$|\mathcal{K}(T(\text{SU}(M)))| = \sum_{\mu \in \mathcal{P}(M)} \#\{\nu | \nu < \mu\}. \quad (4.42)$$

Including the trivial theories replaces the requirement on  $\nu$  with  $\nu \leq \mu$ . The number of descendant theories when  $M \geq 4$  is bounded from below by the partition function,  $|\mathcal{K}(T(\text{SU}(M)))| \geq |\mathcal{P}(M)| = p(M)$ . As  $p(M)$  is asymptotically equivalent, ([31], 3.5.4), to  $\frac{1}{4\sqrt{3}M} \exp(\pi\sqrt{\frac{2M}{3}})$ , the number of theories in the class  $T_{\mu^t}^\nu(\text{SU}(M))$  for a given  $M$  quickly becomes large.

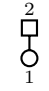
In order to rapidly perform the Kraft-Procesi transitions, we use the matrix method as developed in [4]. A brane configuration is written as a  $2 \times (M + 1)$  matrix with integer elements. The bottom row is the number of D3 branes in the 0th through to  $M$ th gap and the top row is the number of the other type of five brane in that gap, such that the brane configuration for, say,  $T(\text{SU}(4))$ , is written

$$\begin{pmatrix} 0 & 4 & 0 & 0 & 0 \\ 0 & 3 & 2 & 1 & 0 \end{pmatrix}. \quad (4.43)$$

The two types of Kraft-Procesi transition then correspond to

$$\begin{pmatrix} \dots & f_1 & m+1 & f_2 & \dots \\ \dots & g_1 & g_2 & g_3 & \dots \end{pmatrix} \xrightarrow{A_m} \begin{pmatrix} \dots & f_1+1 & m-1 & f_2+1 & \dots \\ \dots & g_1 & g_2-1 & g_3 & \dots \end{pmatrix} \quad (4.44)$$



$\nu \backslash \mu^t$	$(1^2)$	$(2)$
$(1^2)$		
$(2)$		

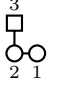
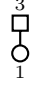
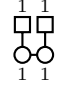
$\nu \backslash \mu^t$	$(1^3)$	$(2, 1)$	$(3)$
$(1^3)$			
$(2, 1)$			
$(3)$			

Figure 4.16:  $\mathcal{K}(T(\text{SU}(2)))$  and  $\mathcal{K}(T(\text{SU}(3)))$ . The tables of non-trivial descendant theories of  $T(\text{SU}(2))$  and  $T(\text{SU}(3))$ . For  $\mathcal{K}(T(\text{SU}(2)))$  there is only one non trivial theory,  $T(\text{SU}(2))$  itself. Since  $\mathcal{M}_C(T(\text{SU}(2))) = \mathcal{M}_H(T(\text{SU}(2))) = \bar{\mathcal{O}}_{(2)} = A_1$ , the theory is simply 3d SQED with 2 flavours. For  $T(\text{SU}(3))$  there are three non trivial theories,  $T(\text{SU}(3))$  and the theories with the two minimal singularities as moduli space branches.

$$\begin{pmatrix} \dots & f_1 & 1 & 0 & \dots & 0 & 1 & f_2 & \dots \\ \dots & g_0 & g_1 & g_2 & \dots & g_{m-1} & g_m & g_{m+1} & \dots \end{pmatrix}$$

$$\xrightarrow{a_m}$$

$$\begin{pmatrix} \dots & f_1 + 1 & 0 & 0 & \dots & 0 & 0 & f_2 + 1 & \dots \\ \dots & g_0 & g_1 - 1 & g_2 - 1 & \dots & g_{m-1} - 1 & g_m - 1 & g_{m+1} & \dots \end{pmatrix}.$$
(4.45)

Tables are arranged with  $\mu^t$  labelling columns and  $\nu$  labelling rows. All the theories in the tables are descendants of  $T(\text{SU}(M))$ , which appears in the top left corner. Theories whose Higgs branches are the closures of a nilpotent orbit (Coulomb branches are Slodowy slices) make up the top row of each table. Theories whose Coulomb branches are nilpotent orbit closures (Higgs branches are Slodowy slices) make up the left hand column of each table. Theories in the body of each table are those whose moduli space branches are other nilpotent varieties. The trivial theories have been left blank. Boxes corresponding to pairs of partitions where neither dominate have been crossed out. For  $M < 6$  mirror symmetric theories occupy boxes which are reflections of each other in the NW-SE diagonal. Larger Hasse diagrams branch in ways which obscure this. Performing a Higgs brane configuration Kraft-Procesi transition moves right through the table. For branching Hasse diagrams this is not necessarily the box immediately to the right. Performing Coulomb brane configuration Kraft-Procesi transitions moves down through the table, again not necessarily to the box immediately below for branching Hasse diagrams.

The goal for circular quivers will be to write down the general form for a collection of Hasse diagrams whose corresponding gauge theories' descendants encompass every good circular quiver gauge theory. In this way, the singularity structure of the general form will include the Hasse diagram for any circular theory.

$\nu \backslash \mu^t$	$(1^4)$	$(2, 1^2)$	$(2^2)$	$(3, 1)$	$(4)$
$(1^4)$					
$(2, 1^2)$					
$(2^2)$					
$(3, 1)$					
$(4)$					

Figure 4.17:  $\mathcal{K}(T(\text{SU}(4)))$ . The descendants of  $T(\text{SU}(4))$  contain the first quiver theory that is not in the classes  $T_\rho(\text{SU}(M))$  or  $T^\rho(\text{SU}(M))$ , nor a minimal singularity. Namely the theory  $T_{(2,1^2)}^{(2,1^2)}(\text{SU}(4))$  with the quiver  $[2] - (1) - (1) - [1]$  and the moduli space  $\bullet - A_1 - \bullet - A_1 - \bullet$ .

$\nu \backslash \mu^t$	$(1^5)$	$(2, 1^3)$	$(2^2, 1)$	$(3, 1^2)$	$(3, 2)$	$(4, 1)$	$(5)$
$(1^5)$							
$(2, 1^3)$							
$(2^2, 1)$							
$(3, 1^2)$							
$(3, 2)$							
$(4, 1)$							
$(5)$							

Figure 4.18:  $\mathcal{K}(T(\text{SU}(5)))$ . Table for the descendants of  $T(\text{SU}(5))$ .



# Circular quivers

Application of Kraft-Procesi transitions in the case of circular quiver gauge theories will be the subject of this chapter. Circular quivers should be thought of as linear quivers with an extra  $U(k_0)$  gauge node which connects to the first and last nodes of a linear quiver. They have been considered before for example in [58], however as we will see, their treatment there is incomplete. Much of the work of this section is taken directly from [1]. The field content and symmetries of circular quiver gauge theories is read in the same way as for linear quivers. There are now bifundamental hypermultiplets transforming under  $U(k_1) \times U(k_0)$  and under  $U(k_{N-1}) \times U(k_0)$  as well as an extra  $U(k_0)$  vector multiplet corresponding to the additional node. The extra node can also be attached to a square node representing flavour for  $U(k_0)$ .

Circular quivers can once again be realised as the low energy dynamics of a type IIB superstring embedding. This time the  $x^6$  direction is taken to be a circle. The extra node in the quiver corresponds to the ‘zeroth’ gap which can now contain D3 segments which are finite in the  $x^6$  direction and so contribute to the low energy dynamics, i.e. the effective  $3d \mathcal{N} = 4$  field theory. We wish to relate this embedding, via linking numbers, to some data as we saw in the linear case. However there are some immediately apparent differences that need to be addressed. The first is that the linking number for the five branes depended on a notion of ‘left of’ and ‘right of’ in the  $x^6$  direction, which breaks down when  $x^6$  is periodic. In order to define linking number a gap between five branes from which we will count needs to be chosen. We choose the zeroth gap.

Counting from the  $0^{th}$  gap for linking numbers means this gap will always have the (perhaps joint) minimum number of D3 branes in its stack. Correspondingly, the extra gauge node will always have (perhaps joint) minimal rank, that is,  $k_0 \leq k_i$  for  $i \neq 0$ . An equivalent statement to there being  $L$  D3 branes in the stack for the  $0^{th}$  gap is that there are  $L$  D3 branes that completely wrap the  $x^6$  direction. Starting with a good circular quiver and uniformly changing the rank of all the gauge nodes results in another good quiver. Note also that the fully wrapped D3 branes have no effect on the linking number of the five branes.

## 5.1 The full class of good circular quiver gauge theories

The brane configuration for circular quiver gauge theories can be thought of as consisting of a linear part and a wrapped part. The linear part is defined using the broader class definition discussed previously. The wrapped

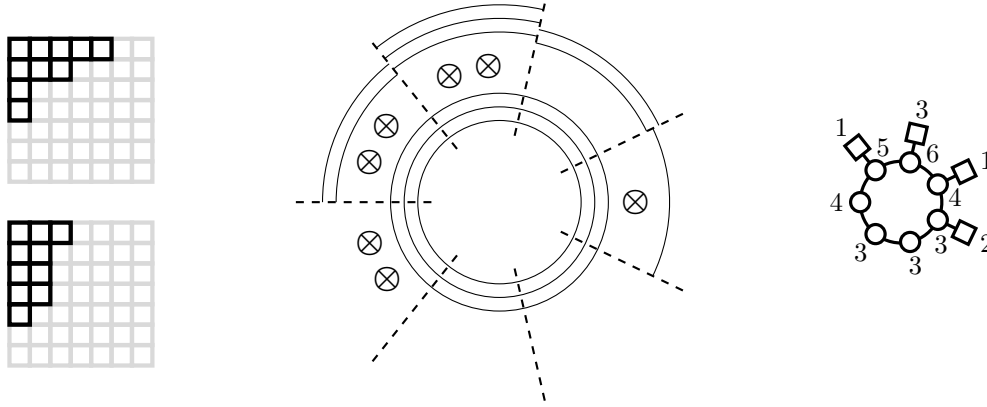


Figure 5.19: The theory  $\pi_{(4,2^2,1^2)}^{(3,2^3,1)}(10, 7, 7, 3)$ . The Higgs brane configuration (center) is drawn so the 1st gap is the one directly clockwise from the horizontal (as drawn) D5 brane. The 0<sup>th</sup> gap is therefore the one immediately anticlockwise from the horizontal D5 brane. This is the gap from which we start counting with regards to linking number. The quiver for the theory can be read from the Coulomb brane configuration after fully Higgsing the system.

part is captured by the non-negative integer  $L$  which counts the number of fully wrapped D3 branes.

For *linear* quivers there were places in the brane configuration where five branes could exist without entering into the infrared physics. NS5 branes with a linking number of zero or D5 branes with a linking number of  $N_2$  could not affect the quiver. For circular quivers this is no longer the case. The D3 branes wrapping the entire circle mean there are no gaps in which five branes can live where they do not affect the infrared physics and hence quiver. In the linear case the degeneracy led to the canonical identification  $N_1 = N_2 = M$ , for circular quivers with  $L \geq 1$  this is not possible. We call the class of circular quiver gauge theories  $\pi_{\mu^t}^{\nu}(M, N_1, N_2, L)$ <sup>1</sup>. An example theory is given in Fig. 5.19. Once again when one of the partitions is of the form  $(1^M)$  it is dropped from the notation so that  $\pi_{(1^M)}^{(1^M)}(M, N_1, N_2, L) = \pi(M, N_1, N_2, L)$ . This includes when  $M = 0$ . The degeneracy that was observed in the broader class of linear quivers is broken by the presence of  $L \geq 1$  fully wrapped D3 branes. In the Higgs brane configuration, a linking number for an NS5 brane of 0 or  $N_2$  means the brane resides in the 0<sup>th</sup> gap between the D5 branes (and vice versa for Coulomb brane configuration and  $N_1$ ), however for  $L \geq 1$  this still effects the low energy dynamics. When  $L = 0$  the rank of the extra gauge node,  $k_0$ , is zero, and circular quivers degenerate to linear quivers. Fig. 5.20 demonstrates that the same partitions and same  $L$  but different  $N_1$  and  $N_2$  result in markedly different circular quiver gauge theories, whereas analogous data for the linear case gave the same theory.

Mirror symmetry can once again be realised as S-duality, exchanging D5 branes and NS5 branes whilst leaving the D3 branes alone. Recall that, in the linear case, mirror symmetry corresponded to a involution on the Hasse diagram or equivalently a transposition of the partitions such that the mirror of  $T_{\mu^t}^{\nu}(\text{SU}(N))$  was  $T_{\nu^t}^{\mu}(\text{SU}(N))$ . In the circular case we can again interpret mirror symmetry as a transposition of the partitions, however the tableaux frame must also be transposed. Transposition on this frame exchanges  $N_1$  and  $N_2$ . The mirror dual to the theory  $\pi_{\mu^t}^{\nu}(M, N_1, N_2, L)$  is therefore  $\pi_{\nu^t}^{\mu}(M, N_2, N_1, L)$ .

Throughout our discussion we will work with theories where the D3 branes can be moved between brane

<sup>1</sup>In [58], the class  $C_{\mu^t}^{\nu}(\text{SU}(N), L)$  is discussed. This class can be found by setting  $M = N_1 = N_2 = N$  in the class  $\pi_{\mu^t}^{\nu}(M, N_1, N_2, L)$ . It is the most direct generalisation of the traditional linear quiver discussion, but does not include all of the possible good circular quivers.

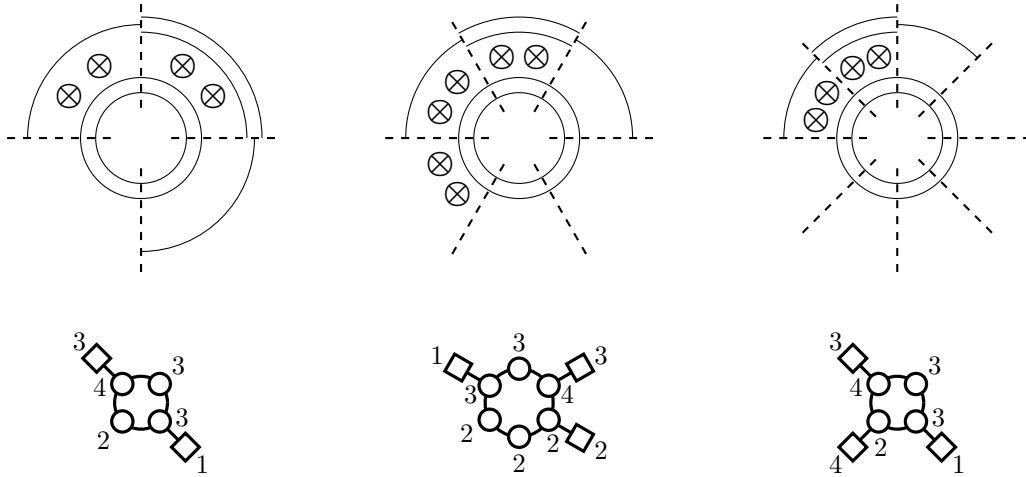


Figure 5.20: An explicit example of the breaking of degeneracy in the class of circular quivers when  $L \neq 0$ . The Higgs brane configuration for  $\pi_{(2^2, 1^2)}^{(3, 1^3)}(6, 4, 4, 2)$  is on the left,  $\pi_{(2^2, 1^2)}^{(3, 1^3)}(6, 6, 6, 2)$  is in the center and  $\pi_{(2^2, 1^2)}^{(3, 1^3)}(6, 4, 8, 2)$  is on the right. They do not yield the same quiver despite having the same partition data.  $N_1$  and  $N_2$  remain important parameters for defining a specific circular quiver gauge theory.

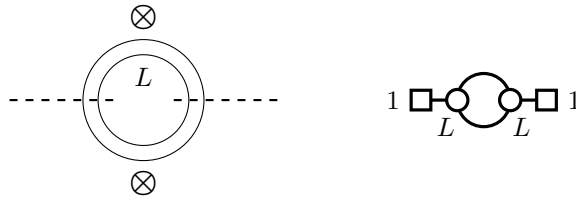


Figure 5.21: The Higgs brane configuration and quiver for the theories  $\pi(1, 2, 2, L)$  and  $\pi(3, 2, 2, L)$ . These theories are pathological from a Kraft-Procesi perspective because the D3 brane segments cannot be moved between brane configurations using the identified Kraft-Procesi transitions.

configurations using Kraft-Procesi transitions. This is only impossible when  $N_1$  and  $N_2$  are both very small. The criterion were first explored in [59] in the case of moving from the Coulomb to the Higgs branch, although the reverse is analogous. The requirement (3.4) in [59] translates to the requirements  $N_i \geq 2$ . When  $N_1 = N_2 = 2$  there are two further sets of pathological theories from a Kraft-Procesi point of view, these are  $\pi(1, 2, 2, L)$  and  $\pi(3, 2, 2, L)$ , their Higgs brane configuration and quiver are the same and given in Fig. 5.21. Since the D3 branes here cannot be Higgsed in the manner necessary for Kraft-Procesi transitions, they fall outside of this analysis.

## 5.2 Moduli space dimension

The quaternionic dimension of the moduli space branches is found by counting D3 segments in the appropriate brane configuration. Since circular theories can be considered as a linear part and a wrapped part, the

dimension of the Higgs and Coulomb branches are given by,

$$\begin{aligned} \dim_{\mathbb{H}}(\mathcal{M}_H(\pi_{\mu^t}^\nu(M, N_1, N_2, L))) &= \frac{1}{2} \left( \overbrace{\sum_i (\nu_i^t)^2 - \sum_i (\mu_i^t)^2}^{\text{Linear Part}} \right) + \overbrace{N_2 L}^{\text{Wrapped Part}}, \\ \dim_{\mathbb{H}}(\mathcal{M}_C(\pi_{\mu^t}^\nu(M, N_1, N_2, L))) &= \frac{1}{2} \left( \sum_i (\mu_i)^2 - \sum_i (\nu_i)^2 \right) + N_1 L. \end{aligned} \quad (5.46)$$

Checking that the dimensions for the Hasse diagrams constructed using Kraft-Procesi transitions are equal to these expectations is a simple and useful test. A generic path from the top to the bottom of the Hasse diagram should pass through transverse slices whose dimensions sum to (5.46).

### 5.3 Performing transitions

Performing Kraft-Procesi transitions in the brane configuration means identifying brane subsystems with  $A$  or  $a$  type transverse slices as moduli space branches and Higgsing them out of the system. These subsystems are precisely the same subsystems identified in the linear case. One can also identify the appropriate operation that can be performed in the field theory. Consider the following example.

**Example:**  $N_1 = N_2 = 3$  Consider two models for  $N_1 = N_2 = 3$ ,  $\pi(0, 3, 3, L)$  and  $\pi(1, 3, 3, L)$ . Both have the gauge group  $U(L)_1 \times U(L)_2 \times U(L)_3$  but the first has three flavours  $Q_1, Q_2, Q_3$  for  $U(L)_1$  and the second has two flavours for  $U(L)_1$  and one for  $U(L)_2$ . There are three bifundamental fields  $A_{12}, A_{23}, A_{31}$  and their conjugates. For both models, we first give expectation values to the flavours  $Q_1, Q_2$ . They break  $U(L)_1$  to  $U(L-1)_1$ , the fields  $A_{12}$  and the conjugate of  $A_{31}$  lose one row which become fundamental flavours for  $U(L)_2$  and  $U(L)_3$

This is an  $A_2$  Kraft-Procesi transition for the first model and the result is  $U(L-1)_1 \times U(L)_2 \times U(L)_3$  with one fundamental flavour for each gauge group  $q_1, q_2, q_3$ . The second step is a Kraft-Procesi  $a_2$  transition. We can choose this to correspond to a nonzero value of the product  $q_2 A_{23} q_3$  which can be reached when the first components of  $q_2$  and  $q_3$ , together with the 11 entry of  $A_{23}$  are all nonzero. The gauge group is broken to  $U(L-1)_1 \times U(L-1)_2 \times U(L-1)_3$  Both  $A_{12}$  and  $A_{31}$  lose one row which become fundamentals for  $U(L-1)_1$ . We can continue with a succession of  $A_2$  and  $a_2$  transitions until the whole gauge group is broken, as demonstrated in Fig. 5.22.

For the second model the first step is an  $A_1$  Kraft-Procesi transition which provides a  $U(L-1)_1 \times U(L)_2 \times U(L)_3$  with two fundamental flavour for  $U(N_2)$  and one for  $U(N_3)$ . The second fundamental flavour for  $U(N_2)$  and the fundamental flavour for  $U(N_3)$  come from the lost rows of the bifundamentals  $A_{12}, A_{31}$ . All subsequent steps until complete gauge breaking are  $A_1$  Kraft-Procesi transitions and involve giving vevs to flavours charged under the same gauge group, as demonstrated in Fig. 5.22.

### 5.4 A minimal set of maximal theories

Investigation of the moduli space singularities for any class of theories requires a starting point from which to perform the Kraft-Procesi transitions. The starting points for transitions in the linear case were the theories

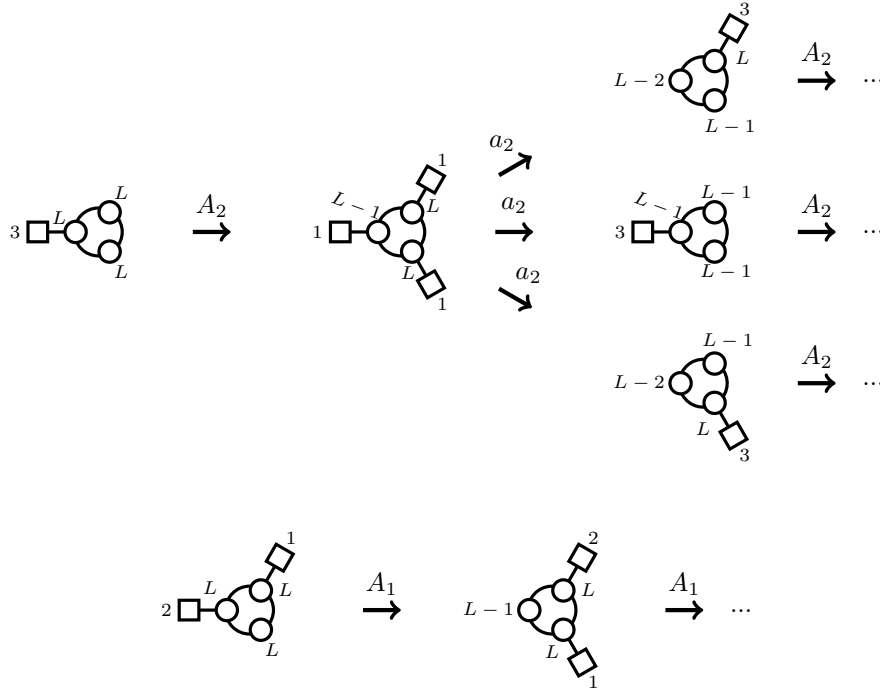


Figure 5.22: Quiver demonstrations for the start of the assessment of the Coulomb branch singularities for  $\pi(0, 3, 3, L)$  (top) and  $\pi(1, 3, 3, L)$  (bottom).

$T(\text{SU}(N))$  whose moduli space branches were closures of the maximal nilpotent orbits. This choice was obvious since the global structure of the moduli space branches of the class  $T_{\mu^i}^{\nu}(\text{SU}(N))$  was well known to be that of nilpotent varieties. Analogous global structure is less well understood for circular theories.

A maximal theory can be thought of as one for which there is no larger theory from which the maximal theory can be recovered using Kraft-Procesi transitions. It is informative to consider a method by which the set  $T(\text{SU}(N))$  can be established to be maximal in the linear case without appealing to the global structure. At the level of the tableaux, for a theory to be maximal means that there are no procedures which one could perform on the dominant partition or reverse procedures on the dominated partition to arrive at the partitions for the maximal theory. For linear quivers the arbitrary resizing of the frame becomes essential. The capacity for frame resizing means that the only possible pair of partitions  $(\mu, \nu)$  fulfilling the criteria is  $(\mu, \nu) = ((N), (1^N))$ . This corresponds exactly to  $T(\text{SU}(N))$ .

For circular quivers each pair of partitions for a given  $N_1$  and  $N_2$  give a different theory. The effects of changing  $L$  are considered momentarily. Resizing of the frame is not allowed. The tableaux procedures so far discussed cannot destroy or create boxes, therefore there are  $N_1 N_2 + 1$  seemingly non-equivalent possibilities for the value of  $M$ ,  $0 \leq M \leq N_1 N_2$ . For every  $N_1, N_2$  there are  $N_1 N_2 + 1$  apparent maximal theories, one for each value of  $M$ . These theories will have  $\mu$  given by the partition of  $M$  with the largest possible parts no larger than  $N_1$  and  $\nu$  the partition of  $M$  with the smallest possible parts but no more than  $N_2$  of them. Theories fulfilling these criteria take the form  $\pi_{\lambda_1}^{\lambda_2}(M, N_1, N_2, L)$  where

$$\lambda_i = \left( \left( \left[ \frac{M}{N_i} \right] + 1 \right)^{(M \bmod N_i)}, \left[ \frac{M}{N_i} \right]^{(N_i - (M \bmod N_i))} \right), \quad (5.47)$$

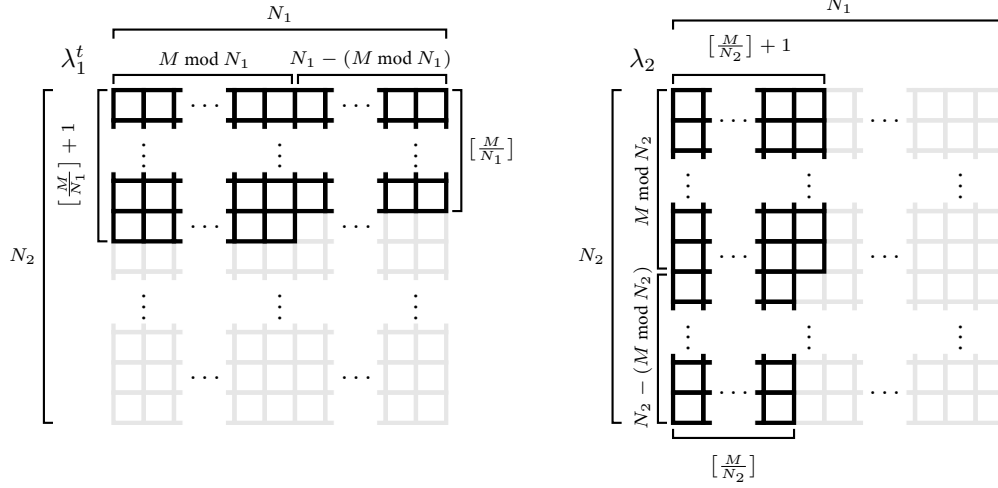


Figure 5.23: The Young tableaux for the partitions that correspond to a possible set of maximal theories. These partitions are the highest and lowest (with respect to the dominance ordering) partitions of  $M$  it is possible to put into an  $N_1 \times N_2$  frame. In exponential notation they are given by (5.47). These maximal theories don't account for Kraft-Procesi transitions which remove D3 branes from the zeroth gap and so the set isn't minimal.

where  $[\cdot]$  means the integer part, Fig. 5.23. It is easy to confirm that this is a partition of  $M$ . Any circular quiver gauge theory can be found via Kraft-Procesi transitions from a theory of this form. However this set of maximal theories is not minimal and there is much scope for reducing the number of theories whose Hasse diagrams need to be found in order to encompass all circular quiver gauge theories.

Given a partition pair in a frame defining a theory, we get precisely the same quiver by considering the complement to the tableaux inside the framing box, Fig. 5.24. The complement is the partition formed by those boxes inside the frame that are not part of the original partition. In the brane configurations, taking the complement of the partitions and assigning linking numbers from the left of the zeroth gap is equivalent to assigning the linking number from the right, or reversing the  $x^6$  direction. This is true in circular and linear quivers. There is an equivalence in the class of circular quiver gauge theories where, all other things being equal, taking

$$M \rightarrow N_1 N_2 - M, \quad \mu \rightarrow \mu^c, \quad \nu \rightarrow \nu^c, \quad (5.48)$$

gives the same theory. That is

$$\pi_{\mu^t}^{\nu} (M, N_1, N_2, L) = \pi_{(\mu^c)^t}^{\nu^c} (N_1 N_2 - M, N_1, N_2, L). \quad (5.49)$$

In the linear case  $T_{\mu^t}^{\nu}(\text{SU}(N)) = T_{(\mu^c)^t}^{\nu^c}(\text{SU}(N^2 - N))$ . This arises naturally in the study of the singularities of nilpotent varieties as the isomorphism  $\mathcal{S}_{\nu} \cap \bar{\mathcal{O}}_{\mu} \cong \mathcal{S}_{\nu^c} \cap \bar{\mathcal{O}}_{\mu^c}$ . The natural interpretation of this physically observable equivalence in terms of the singularity theory of the moduli space varieties for the linear case suggests a similar such isomorphism in the circular case. Applying this equivalence to the initial set of maximal theories reduces the number of different theories from  $N_1 N_2 + 1$  to  $[\frac{N_1 N_2}{2}] + 1$ . However this set is still not minimal.

Due to the periodicity of  $x^6$ , it is possible for Kraft-Procesi transitions to push five branes from the  $0^{th}$



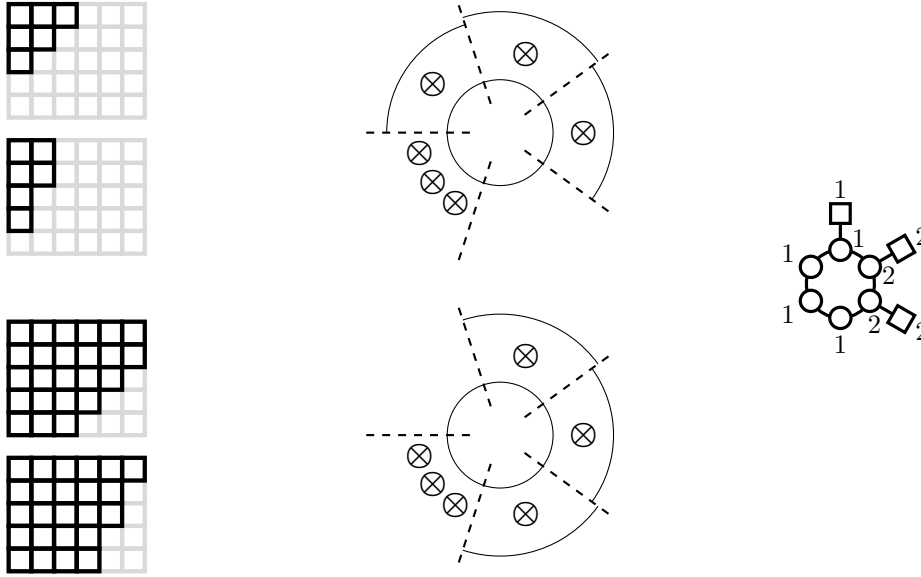


Figure 5.24: A demonstration that assigning linking numbers using complementary tableaux results in the same quiver gauge theory.

gap to the  $N_i - 1^{\text{th}}$  gap. In the brane picture this is the same as any other transition, only it involves moving branes ‘round the back’ of the circle. The interpretation in the tableaux is simple but fiddly and doesn’t provide any further insight to proceedings.

Kraft-Procesi transitions in the linear case always increase the linking number of one five brane by one whilst decreasing another by one. The total linking number (and hence the magnitude of the defining partitions) is unaffected by the transitions. At the level of the tableaux this is realised by the procedures not creating or destroying blocks and by procedures always making one row and one column one block shorter whilst making another row and column one longer. Transitions that move five branes ‘round the back’, however, change the linking number of one five brane by  $N_i - 1$  (depending on which branch we perform the transition in) and change the linking number of another five brane by 1. This means some transitions change the total linking number,  $M$ , by  $N_i$ . Theories with  $M = M'$  and theories with  $M = M' + sN_1 + rN_2$  (with  $r$  and  $s$  integers such that  $0 \leq M' + sN_1 + rN_2 \leq N_1N_2$ ) can be related using Kraft-Procesi transitions.

Incorporating the effects of changing  $L$  requires us to change our view of what it means to be a maximal theory. Any theory of the form  $\pi_{\lambda_1}^{\lambda_2}(M, N_1, N_2, L_1)$  can always be found in the descendants of the theory  $\pi_{\lambda_1}^{\lambda_2}(M, N_1, N_2, L_2)$  with  $L_2 > L_1$ . Instead we will say that two circular quiver gauge theories,  $\pi_{\mu^t}^{\nu}(M_1, N_1, N_2, L_1)$  and  $\pi_{\rho^t}^{\sigma}(M_2, N_1, N_2, L_2)$  are in the same *family* under Kraft-Procesi transitions, if for every  $L_1$  there exists a  $L_2$  such that

$$\pi_{\mu^t}^{\nu}(M_1, N_1, N_2, L_1) \in \mathcal{K}(\pi_{\rho^t}^{\sigma}(M_2, N_1, N_2, L_2)), \quad (5.50)$$

and vice versa. In essence, two theories are in the same family if we could rearrange the 5 branes using Kraft-Procesi transitions such that the partition data becomes the same.

The theories that belong to the same family will have moduli space varieties which appear as subvarieties of one another for sufficiently large  $L_i$ . This is what it is to be findable via Kraft-Procesi transitions. Theories

that are not in the same family have moduli space varieties that have no such containment relationship, they will therefore form entirely separate Hasse diagrams. Given  $N_1$  and  $N_2$ , finding the Hasse diagram for a representative theory from each family for general  $L$  will capture the singularity structure of all theories with those  $N_1$  and  $N_2$  values.

Recall that every circular quiver theory can be found as a descendant of one of the  $N_1 N_2 + 1$  ‘maximal’ theories so far considered. Classifying these into families is sufficient to classify all circular theories. Once classified, picking a representative theory from each family gives a minimal set of maximal theories.

**Proposition** Two sets of theories  $\pi_{\lambda_1}^{\lambda_2}(M, N_1, N_2, L)$  and  $\pi_{\lambda_1'}^{\lambda_2'}(M', N_1, N_2, L')$  are in the same family iff  $M' - M \equiv 0 \pmod{\gcd(N_1, N_2)}$ .

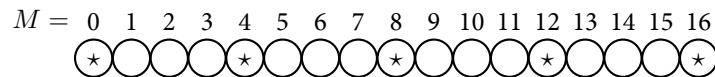
**Corollary** For a given  $N_1$  and  $N_2$ , there are  $\lceil \frac{\gcd(N_1, N_2)}{2} \rceil + 1$  families of circular quiver gauge theories under Kraft-Procesi transitions. One set of representatives for these families are the theories  $\pi(k, N_1, N_2, L)$  for  $k \in \{0, \dots, \lceil \frac{\gcd(N_1, N_2)}{2} \rceil\}$ .

Proving the proposition is straight-forward. Kraft-Procesi transitions can only change  $M$  by multiples of  $N_1$  or  $N_2$ , hence if  $M' - M \not\equiv 0 \pmod{\gcd(N_1, N_2)}$  we have no method of moving from a theory with  $M$  to one with  $M'$ . If they are in the same family we must have  $M' - M \equiv 0 \pmod{\gcd(N_1, N_2)}$ . The proposition also asserts that if  $M_2 - M_1 \equiv 0 \pmod{\gcd(N_1, N_2)}$  then the two sets of naive starters *must* belong to the same family. Consider that given sufficient  $L$  there is always a sequence of the Kraft-Procesi transitions in the Higgs brane configuration which can end with a transition that changes total linking number by exactly  $N_2$  or transitions in the Coulomb brane configuration that change the total by  $N_1$ . Given a starting point and sufficient  $L$ , all values for  $M$  of the form  $0 \leq M + sN_1 + rN_2 \leq N_1 N_2$  can be found.

To prove the corollary consider that every theory can be found by performing Kraft-Procesi transitions on the theories  $\pi_{\lambda_1}^{\lambda_2}(M, N_1, N_2, L)$ . For each  $(N_1, N_2)$  there are  $N_1 N_2 + 1$  such theories corresponding to values for  $M$  in the range  $\{0, 1, \dots, N_1 N_2 - 1, N_1 N_2\}$ . There are three circumstances under which these theories are in the same family. These can be modelled as the equivalence relations on values in this range. Conjugate theories can be modelled by  $M \sim N_1 N_2 - M$ . Kraft-Procesi transitions that change the total linking number can be modelled by  $M \sim M + N_1$  and  $M \sim M + N_2$  which combine to give  $M \sim M + \gcd(N_1, N_2)$ . Under these equivalence relations, values in this range form  $\lceil \frac{\gcd(N_1, N_2)}{2} \rceil + 1$  equivalence classes. These classes are those equivalent to values in the range  $\{0, \dots, \lceil \frac{\gcd(N_1, N_2)}{2} \rceil\}$ . Some examples demonstrating this are provided next.

### 5.4.1 Examples

$N_1 = N_2 = 4$  For  $N_1 = N_2 = 4$ ,  $\gcd(N_1, N_2) = 4$ . There are 3 families with representatives  $\pi(k, 4, 4, L)$  for  $k \in \{0, 1, 2\}$ . To see this explicitly, first consider those values of  $M$  in the same family as 0. All of these theories are labelled on a diagram whereby all the values of  $M$  in the same family have the same symbol. Recalling that  $0 \leq M \leq N_1 N_2$ ,



are in the same family as zero. Considering the family with representative  $k = 1$ ,

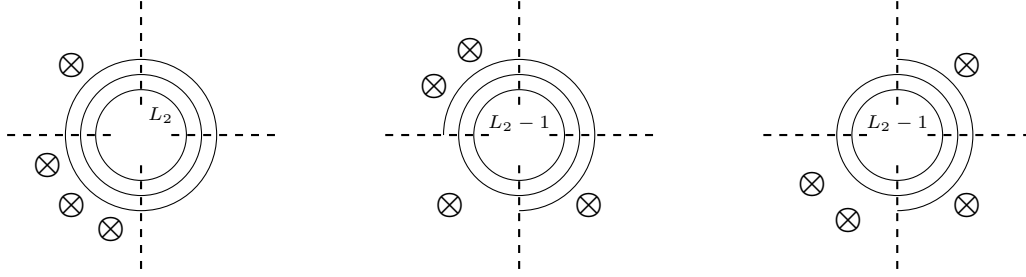


Figure 5.25: The Higgs brane configurations for the explicit demonstration of finding  $\pi_{(3,2)}^{(2,1^3)}(5, 4, 4, L_1) \in \mathcal{K}(\pi(1, 4, 4, L_2))$ . One has to perform an  $A_2$  transition followed by an  $A_1$  transition in the Higgs brane configuration. We require  $L_2 \geq L_1 + 1$  in order to perform the appropriate transitions.

$$M = 0 \quad 1 \quad 2 \quad 3 \quad 4 \quad 5 \quad 6 \quad 7 \quad 8 \quad 9 \quad 10 \quad 11 \quad 12 \quad 13 \quad 14 \quad 15 \quad 16$$

$$\begin{array}{cccccccccccccccc} \circledast & \clubsuit & \circ & \clubsuit & \circledast & \clubsuit & \circ & \clubsuit & \circledast & \clubsuit & \circ & \clubsuit & \circledast & \clubsuit & \circ & \clubsuit & \circledast \end{array}$$

and finally those values of  $M$  corresponding to theories in the same family as  $k = 2$  complete our considerations.

$$M = 0 \quad 1 \quad 2 \quad 3 \quad 4 \quad 5 \quad 6 \quad 7 \quad 8 \quad 9 \quad 10 \quad 11 \quad 12 \quad 13 \quad 14 \quad 15 \quad 16$$

$$\begin{array}{cccccccccccccccc} \circledast & \clubsuit & \triangle & \clubsuit & \circledast & \clubsuit & \triangle & \clubsuit & \circledast & \clubsuit & \triangle & \clubsuit & \circledast & \clubsuit & \triangle & \clubsuit & \circledast \end{array}$$

The families of the three representatives cover all the possible theories. Choosing a theory with  $M = 5$ , say,  $\pi_{(3,2)}^{(2,1^3)}(5, 4, 4, L_1)$ , this theory ought to be findable from the theory  $\pi(1, 4, 4, L_2)$  for some  $L_2 \geq L_1$ . The Higgs brane configurations are given in Fig. 5.25. An  $A_2$  followed by an  $A_1$  transition yields the theory and reveals that we require that  $L_2 = L_1 + 1$  at minimum.

$N_1 = 3 \quad N_2 = 5$  For  $N_1 = 3$  and  $N_2 = 5$ ,  $\gcd N_1, N_2 = 1$  and so all theories with these values of  $N_1$  and  $N_2$  appear in the descendants of  $\pi(0, 3, 5, L)$  for sufficient  $L$ . The Higgs brane configurations for finding  $\pi_{(3,2,1)}^{(2^2,1^2)}(6, 3, 5, L_1)$  by performing Kraft-Procesi transitions on  $\pi(0, 3, 5, L_2)$  are given in Fig. 5.26. The removal of the  $a_4$  and  $a_2$  from the bottom of the Higgs branch and the  $A_2$  from the top of the Higgs branch reveals that we require  $L_2 \geq L_1 + 2$ .

## 5.5 Hasse diagrams for family representatives

Calculating the Hasse diagrams for the moduli space branches of a set of family representatives will encompass the diagrams for all good circular quiver gauge theories. Theories  $\pi(k, N_1, N_2, L)$  for  $k \in \{0, \dots, \lfloor \frac{\gcd(N_1, N_2)}{2} \rfloor\}$  have a general Higgs brane configuration and quiver given in Fig. 5.27. The Hasse diagrams will be written for the Coulomb branch, once again mirror symmetry can be viewed as an involution on the Hasse diagram top-bottom along with an exchange of  $A_n$  for  $a_n$ . The dimension of the starting theories can be used as a check for the Hasse diagrams. Any single path from the top to the bottom of the Hasse diagram should have a dimension given by (5.46). As the starting theories' partitions are always in the form  $\nu = (1^k)$ ,  $\mu = (k)$ , application of (5.46) gives  $\dim_{\mathbb{H}}(\mathcal{M}_H) = \frac{1}{2}(k^2 - k) + N_2L$  and  $\dim_{\mathbb{H}}(\mathcal{M}_C) = \frac{1}{2}(k^2 - k) + N_1L$ . Recall also that  $\dim_{\mathbb{H}}(A_z) = 1$  for any  $z$  and  $\dim_{\mathbb{H}}(a_z) = z$  for any  $z$ .

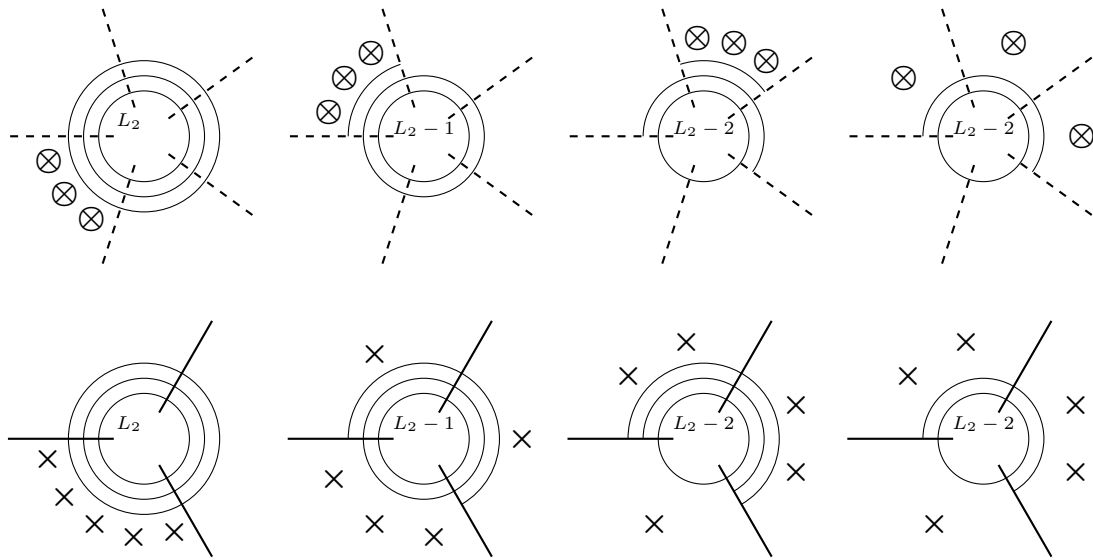


Figure 5.26: The Higgs and Coulomb brane configurations for the explicit demonstration of finding  $\pi_{(3,2,1)}^{(2^2,1^2)}(6, 3, 5, L_1) \in \mathcal{K}(\pi(0, 3, 5, L_2))$ . Starting with a Coulomb branch  $A_4$  transition (so a removal of an  $a_4$  singularity from the bottom of the Higgs branch) then a Coulomb branch  $A_2$  transition, followed by an  $A_2$  Higgs branch transition.  $L_2 \geq L_1 + 2$  is required to perform the transitions.

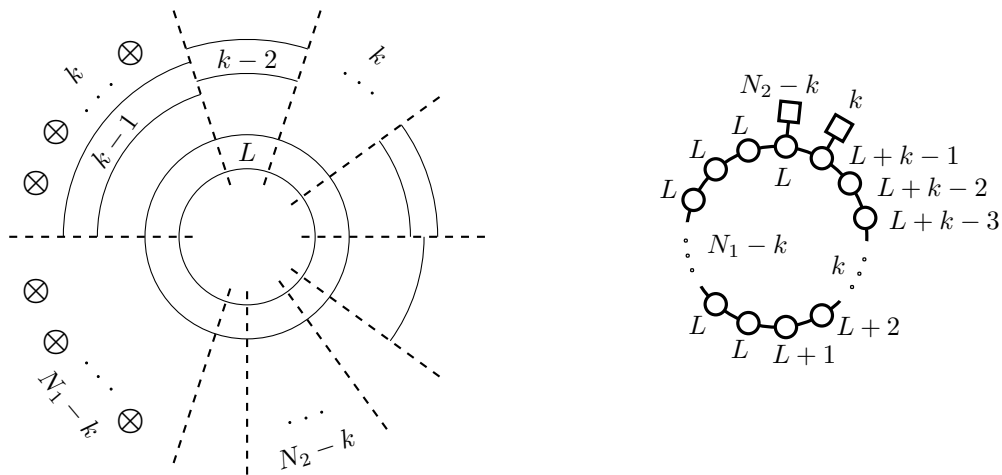


Figure 5.27: The general form for the Higgs brane configuration and quiver for our choice of a minimal set of maximal theories,  $\pi(k, N_1, N_2, L)$ , where  $k$  takes values in the range  $\{0, \dots, [\frac{\text{gcd}(N_1, N_2)}{2}]\}$ . The system has  $N_1$  NS5 branes and  $N_2$  D5 branes and hence the quiver has  $N_1$  gauge nodes and the sum of the flavour nodes is  $N_2$ . The mirror theories can be found by exchanging the labels 1 and 2. In the case that  $N_1 = N_2$  the theory is self-mirror dual. All good circular quiver theories can be found by performing Kraft-Procesi transitions on a theory of this form for some  $L$ .

### 5.5.1 The linear case: $L = 0$

Setting  $L = 0$  gives rise to the linear quiver case. In Fig. 5.27, setting  $L = 0$  leaves only the linear quiver for  $T(\mathrm{SU}(k))$  remaining. The independence of this theory from  $N_1$  and  $N_2$  is also evident. The only different maximal theories which arise when  $L = 0$  are those pertaining to different values of  $k$ , as expected.

### 5.5.2 A single wrapped brane: $L = 1$

Writing down the Hasse diagram for the Coulomb branch of the  $L = 1$  case requires assessing all of the different manners by which all the D3 branes may be removed from the Coulomb brane configuration using Kraft-Procesi transitions. Consider Fig. 5.27 when  $L = 1$ , the D3 branes in the Coulomb brane configuration can be considered as a linear part and a wrapped part. Initially the linear part takes the form of the theory  $T(\mathrm{SU}(k))$ . The Coulomb branch of these theories and their descendants are nilpotent varieties of  $\mathfrak{sl}_n$ , which are subvarieties of the closure of the maximal nilpotent orbit. Brane subsystems with moduli space branches that are maximal nilpotent orbit closures will be referred to as *orbit subsystems* and the section of the Hasse diagram corresponding the transitions performed in these subsystems will be referred to as *orbit subdiagrams*.

The D3 branes in this system can be removed in many different orders, however there are two sequences of brane removals that stand out immediately. Removal of the entire  $\bar{\mathcal{O}}_{(k)}$  orbit subsystem followed by the wrapped brane, or removal of the entire wrapped brane followed by the orbit subsystem. The wrapped D3 branes do not contribute to the linking number of either type of five brane, therefore completely removing an entire wrapped brane using Kraft-Procesi transitions does not move any of the five branes' positions relative to one another in the end. Removal of a maximal orbit subsystem moves  $k - 1$  D5 branes into the gap adjacent to their starting gap *away* from the D3 brane tail, and one D5 brane to the other end of the subsystem.

There is a third order of removing the D3 branes which will prove useful to consider. By initially performing an  $A_{N_2-k-1}$  transition in the zeroth gap, the single D3 brane in that gap is removed. This procedure moves one D5 brane into the gaps either side. This results in there being  $k + 1$  D5 branes in the first gap. There is now an  $\bar{\mathcal{O}}_{(k+1)}$  orbit subsystem in the brane configuration. After removing this, a final  $a_{N_1-k-1}$  transition removes the final D3 branes. These three orders of D3 brane removal form the backbone of a Hasse diagram schematic for  $L = 1$  theories.

To begin to construct the Hasse diagram it is useful to consider the subdiagrams for the different parts of the three removal orderings discussed above. The orbit subdiagrams are known to be the Hasse diagrams for nilpotent orbit closures. The subdiagrams corresponding to the removal of the wrapped brane either before or after the  $\bar{\mathcal{O}}_{(k)}$  subsystem are given in Fig. 5.28. These subdiagrams will exist at the very top and very bottom of the full Hasse diagram as they correspond to some of the first or last transitions it is possible to make.

The schematic for the full Hasse diagram for the  $L = 1$  case is given in Fig. 5.29. The three orbit subdiagrams and the subdiagrams for the removal of the wrapped brane are all evident. This is not a complete Hasse diagram however, there are many edges which link between orbit subdiagrams which are yet to be filled in. These edges will be referred to as *traversing structure* as they traverse from one orbit subdiagram to another. From here on the Hasse diagrams that are constructed will be formulated in terms of an orbit subdiagram skeleton which has been fleshed out with traversing structure.

There are two 'regions' of traversing structure in the  $L = 1$  Hasse diagram. The structure between the

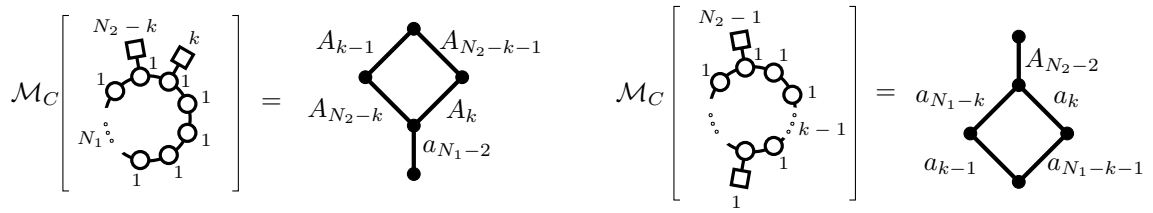


Figure 5.28: The Hasse subdiagrams for the removal of one fully wrapped D3 brane either entirely before (left) or entirely after (right) the removal of the  $\bar{\mathcal{O}}_{(k)}$  subsystem. On the right, removal of the orbit subsystem first has resulted in D5 branes being moved in the manner discussed. The two diagrams are mirror-duals of one another indicating that they exist at opposite ends of the full Hasse diagram such that they are mapped into one another under mirror symmetry.

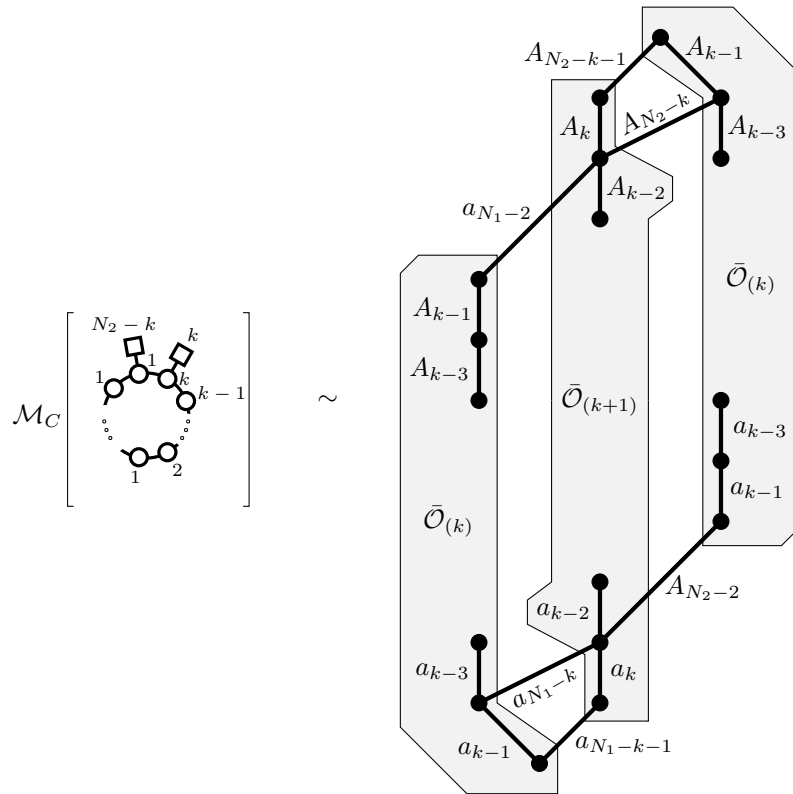


Figure 5.29: The schematic for the general Hasse diagram for  $\pi(k, N_1, N_2, 1)$ . The orbit subdiagrams are indicated using grey boxes. The subdiagrams corresponding to the removal of the wrapped brane before or after the orbit subsystems are evident. The edges which connect between orbit subdiagrams are mostly omitted in this schematic for simplicity (see discussion). The three orderings in the discussion correspond to moving down the first  $\bar{\mathcal{O}}_{(k)}$  subdiagram then down to the bottom (this is removing the orbit subsystem first, then the wrapped brane). Moving across to the top of the lower  $\bar{\mathcal{O}}_{(k)}$  subdiagram then down to the bottom (that is removing the wrapped brane first then the orbit subsystem). Or moving across to the  $\bar{\mathcal{O}}_{(k+1)}$  subsystem, down, then across to the bottom (this is performing an initial zeroth gap transition, removing the now larger orbit subsystem, then removing the final part of the wrapped brane).

higher  $\bar{\mathcal{O}}_{(k)}$  orbit subdiagram and the  $\bar{\mathcal{O}}_{(k+1)}$  subdiagram, and the structure between the  $\bar{\mathcal{O}}_{(k+1)}$  orbit subdiagram and the lower  $\bar{\mathcal{O}}_{(k)}$  subdiagram. Three of the edges in each of these regions have been found already when considering the removal of the wrapped brane. These two regions of traversing structure go into one another under mirror symmetry, therefore assessing one of them gives the other with simple adjustment.

Consider the traversing structure between the higher  $\bar{\mathcal{O}}_{(k)}$  orbit subdiagram and the  $\bar{\mathcal{O}}_{(k+1)}$  subdiagram. These edges can be found in general by considering the Coulomb brane configuration carefully. The upper  $\bar{\mathcal{O}}_{(k)}$  orbit subdiagram corresponds to removing the  $\bar{\mathcal{O}}_{(k)}$  orbit subsystem before removing any of the wrapped brane. However at any point during the process of removing the orbit subsystem, it is possible to start to remove the wrapped brane. There are always D5 branes in the zeroth gap<sup>2</sup> and the only D3 segment in the zeroth gap is part of the wrapped brane. Therefore at any point during the removal of the orbit subdiagram, there is the option to perform the zeroth gap transition and this option is never part of the orbit subsystem removal. This option forms the upper traversing structure in the Hasse diagram.

The nodes within an  $\bar{\mathcal{O}}_{(k)}$  orbital subdiagram can be labelled with partitions of  $k$  in the normal way. In order to write down a general form for the edges in the upper traversing structure it is useful to consider the nodes in the  $\bar{\mathcal{O}}_{(k)}$  subdiagram to be labelled as such. The option to perform a zeroth gap transition exists at all times during the  $\bar{\mathcal{O}}_{(k)}$  subsystem removal. Therefore every node in the upper  $\bar{\mathcal{O}}_{(k)}$  subdiagram has a traversing edge coming from it. This traversing edge corresponds to performing a zeroth gap transition after having removed some amount of the orbit subsystem. To fully characterise the edge requires two calculations, one to determine the label which the edge should carry and another to determine which node in  $\bar{\mathcal{O}}_{(k+1)}$  the edge should attach to.

**Label** Consider the traversing edge connecting the node in the upper  $\bar{\mathcal{O}}_{(k)}$  subdiagram labelled with a partition  $\kappa$  of  $k$ . The label this edge carries is determined by the number of D5 branes in the zeroth gap when the transition is performed. The process of removing the orbit subdiagram moves D5 branes into the zeroth gap. The number of D5 branes which have been moved into the zeroth gap by removing the orbit subsystem down to the node  $\kappa$  can be determined by considering the relationship between  $\kappa$  and the subsystem linking number of the D5 branes. Consider the linking number of five branes as considered just within the orbit subsystem. D5 branes that have been moved into the zeroth gap correspond to those with linking number zero. The number of D5 branes in the  $i^{\text{th}}$  subsystem gap is given by  $\kappa_i^t$ . The number of D5 branes that have been moved into the zeroth gap by descending to a node  $\kappa$  is therefore  $\kappa_0^t = k - l(\kappa^t)$ . Before removing any of the orbit subsystem there were  $N_2 - k$  D5 branes in the zeroth gap. The label for the traversing edge connecting to the  $\bar{\mathcal{O}}_{(k)}$  node  $\kappa$  is therefore  $A_{N_2 - k - 1 + k - l(\kappa^t)} = A_{N_2 - l(\kappa^t) - 1}$ .

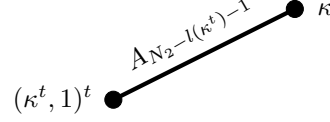
**$\bar{\mathcal{O}}_{(k+1)}$  node** Performing this transition will move a D5 brane into gaps either side of the zeroth gap. The D5 brane moved into the  $N_1 - 1^{\text{th}}$  gap will not be involved in the orbit subsystem<sup>3</sup>. However the D5 brane moved into the first gap *will* be involved in the orbit subsystem. Moving this D5 brane from the zeroth to the first gap increases its orbit subsystem linking number by one without decreasing the linking number of another D5 in the orbit subsystem. The magnitude of the total linking number, and hence magnitude of the partitions labelling orbit subdiagram nodes, has increased by one. This confirms that the edge traverses to the  $\bar{\mathcal{O}}_{(k+1)}$  subdiagram. The  $\bar{\mathcal{O}}_{(k+1)}$  to which it connects can be determined by considering the change of

<sup>2</sup>This is a temporary simplifying assumption about the size of  $N_2$ , what happens when it doesn't hold will be dealt with later.

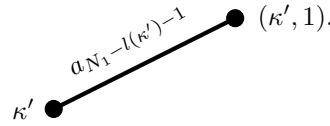
<sup>3</sup>This is part of a temporary simplifying assumption about the size of  $N_1$ , the breaking of which will be discussed later.

the partition induced by the moving of the D5 brane. The partition corresponding to the linking number of the D5 branes in the orbit subsystem has had a zero turn into a one. The edge traversing from a node  $\kappa$  in the  $\bar{\mathcal{O}}_{(k)}$  subsystem therefore connects to a node  $(\kappa^t, 1)^t$  in the  $\bar{\mathcal{O}}_{(k+1)}$  subsystem.

The complete  $L = 1$  Hasse diagram is given by Fig. 5.29 with the addition of the traversing edges



from every node in the top  $\bar{\mathcal{O}}_{(k)}$  subdiagram to the appropriate nodes in  $\bar{\mathcal{O}}_{(k+1)}$ , and adding the appropriate mirror dual edges from every node in the lower  $\bar{\mathcal{O}}_{(k)}$  up to the appropriate nodes in  $\bar{\mathcal{O}}_{(k+1)}$ :



These edges could also have been derived from brane configuration considerations.

**Dimensional Check** To perform a dimensional check on the construction, choose a general route  $R$  from the top to the bottom of the Hasse diagram. Such a route can be found by starting at the top, descending to a node of the upper  $\bar{\mathcal{O}}_{(k)}$  subdiagram labelled with a partition  $\kappa$ , traversing into the  $\bar{\mathcal{O}}_{(k+1)}$  subdiagram, descending further to the node labelled  $(\kappa', 1)$ , traversing again to the lower  $\bar{\mathcal{O}}_{(k)}$  at the node  $\kappa'$ , and from there to the bottom. The dimension of this general route is given by

$$\begin{aligned} \dim_{\mathbb{H}}(R) &= \dim_{\mathbb{H}}(\bar{\mathcal{O}}_{(k)} \cap \mathcal{S}_{\kappa}) + \dim_{\mathbb{H}}(A_{N_2 - l(\kappa^t) - 1}) + \dim_{\mathbb{H}}(\bar{\mathcal{O}}_{(\kappa^t, 1)^t} \cap \mathcal{S}_{(\kappa^t, 1)}) \\ &\quad + \dim_{\mathbb{H}}(a_{N_1 - l(\kappa') - 1}) + \dim_{\mathbb{H}}(\bar{\mathcal{O}}_{(\kappa')}) \\ &= \frac{1}{2} \left( \sum_i (\kappa_i^t)^2 - k + 2 + \sum_j ((\kappa', 1)_j^t)^2 - \sum_j ((\kappa^t, 1)_j)^2 \right. \\ &\quad \left. + 2N_1 - 2l(\kappa') - 2 + k^2 - \sum_i (\kappa_i'^t)^2 \right). \end{aligned} \quad (5.51)$$

Note that  $\sum_j ((\kappa^t, 1)_j)^2 = \sum_i (\kappa_i^t)^2 + 1$  and  $\sum_j ((\kappa', 1)_j^t)^2 = 1 + 2l(\kappa') + \sum_i (\kappa_i'^t)^2$ . The second equality takes a little work, to see it consider the following, writing  $\kappa' = (k^{p_k}, \dots, 1^{p_1})$  means

$$\overleftarrow{(\kappa', 1)^t} = \left( \left( \sum_{m=k}^k p_m \right), \left( \sum_{m=k-1}^k p_m \right), \dots, \left( \sum_{m=2}^k p_m \right), \left( \sum_{m=1}^k p_m \right) + 1 \right), \quad (5.52)$$

and so,

$$\begin{aligned} \sum_j ((\kappa', 1)_j^t)^2 &= \left( \left( \sum_{m=1}^k p_m \right) + 1 \right)^2 + \sum_{q=2}^k \left( \sum_{m=q}^k p_m \right)^2 \\ &= 1 + 2 \sum_{m=1}^k p_m + \sum_{q=1}^k \left( \sum_{m=q}^k p_m \right)^2 \\ &= 1 + 2l(\kappa') + \sum_i (\kappa_i'^t)^2. \end{aligned} \quad (5.53)$$



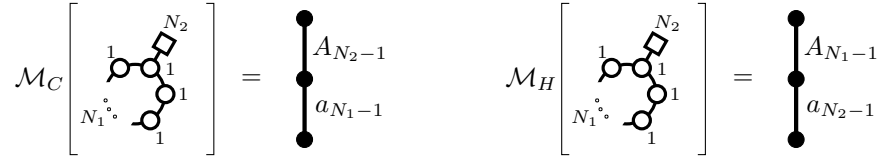


Figure 5.30: Coulomb (left) and Higgs (right) branch Hasse diagrams for  $\pi(0, N_1, N_2, 1)$ .

Applying these simplifications to (5.51) gives,

$$\dim_{\mathbb{H}}(R) = \frac{1}{2}(k^2 - k) + N_1. \quad (5.54)$$

This is exactly the result expected both from previous dimensional discussion and from a simple counting of the D3 branes in the Coulomb brane configuration.

### 5.5.3 $L = 1$ examples

**$k = 0$**  The moduli space branches for these quivers have been calculated before, [60], and found to be  $\mathcal{M}_H = A_{N_1-1} \times a_{N_2-1}$  and hence  $\mathcal{M}_C = A_{N_2-1} \times a_{N_1-1}$  as reiterated in [61]. This can easily be reproduced using Kraft-Procesi transitions directly or from the general construction above. Reading from the general construction, the three orbit subdiagrams all consist of a single node. The upper and lower  $\bar{\mathcal{O}}_{(k)}$  subdiagram nodes both carry the partition (0) and the center  $\bar{\mathcal{O}}_{(k+1)}$  subdiagram the partition (1). Note that  $l((0)) = 0$ . The traversing structure is then easily filled in. The result is given in Fig. 5.30.

**$k = 1, 2, 3, 4$**  The results for small values of  $k$  when  $L = 1$  are given in Fig. 5.31.

### 5.5.4 The schematic for $L = 2$ and orbit lattices

The schematic for  $L = 2$  can be constructed using similar considerations to the  $L = 1$  case. A skeleton can be found by considering some simple orderings of D3 removal, then traversing structure can be added to account for more complicated orderings.

Two simplest orders for D3 brane removal are analogous to the simplest cases in  $L = 1$ . Remove the entire orbit subsystem first, then both wrapped branes, or vice versa. The subdiagram for removal of two wrapped branes is much more complicated than removal of one brane. One method of removing two wrapped branes is to remove one at a time, so the subdiagram for two wrapped branes should contain a subdiagram which looks like two of the single-brane removal subdiagrams strung end to end. However any sequence which begins removing the second wrapped brane before the first has been fully removed will give extra structure not seen in  $L = 1$  case. Furthermore there is the option to remove one wrapped brane, the orbit subsystem, then the other wrapped brane. The Hasse diagram for  $L = 2$  therefore ought to contain two copies of the  $L = 1$  Hasse diagram with the lower  $\bar{\mathcal{O}}_{(k)}$  subdiagram of one being the upper  $\bar{\mathcal{O}}_{(k)}$  subdiagram of the next.

In the  $L = 1$  case, performing the transition in the zeroth gap moved a D5 brane into the first gap. This resulted in the  $\bar{\mathcal{O}}_{(k)}$  subsystem being promoted to a  $\bar{\mathcal{O}}_{(k+1)}$  subsystem. In the  $L = 2$  case a second zeroth gap transition can be performed. This will promote the  $\bar{\mathcal{O}}_{(k+1)}$  subsystem to a  $\bar{\mathcal{O}}_{(k+2)}$  subsystem. However this second zeroth gap transition also moves a second D5 brane into the  $N_1 - 1^{\text{th}}$  gap. This means that an  $A_1$

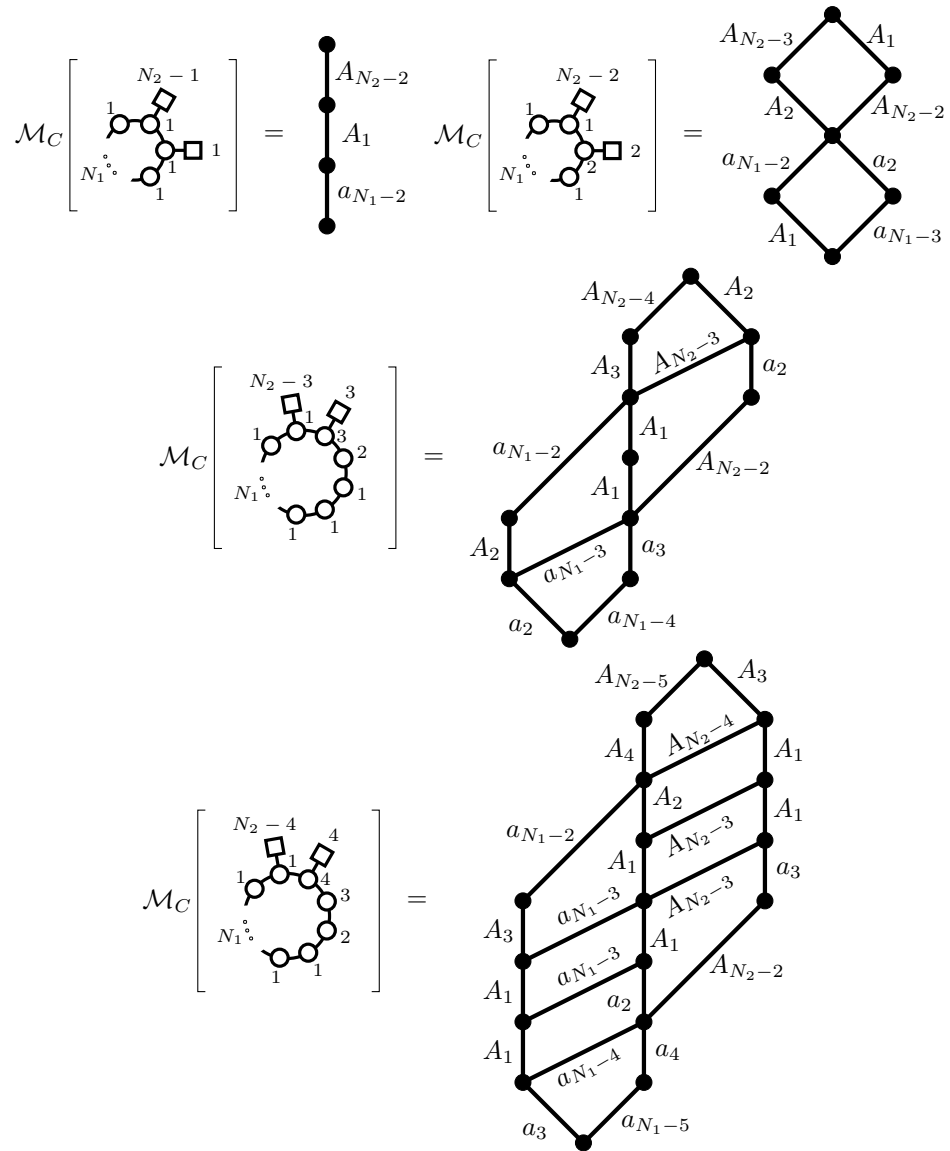


Figure 5.31: Coulomb branch Hasse diagrams for  $\pi(k, N_1, N_2, 1)$  for  $k \in \{1, 2, 3, 4\}$ .



called a *lattice* of orbit subdiagrams. A lattice denoted  $(\bar{\mathcal{O}}_{(p)}; \bar{\mathcal{O}}_{(q)})$  for  $p \geq q$  will consist of  $|\mathcal{P}(p)|$  copies of  $\bar{\mathcal{O}}_{(q)}$  and  $|\mathcal{P}(q)|$  copies of  $\bar{\mathcal{O}}_{(p)}$  arranged such that every node of an  $\bar{\mathcal{O}}_{(p)}$  subdiagram labelled with the same partition of  $p$  is also in the same  $\bar{\mathcal{O}}_{(q)}$  subdiagram, and vice versa, in the obvious manner. In this case the two copies of  $\bar{\mathcal{O}}_{(k+2)}$  are part of a  $(\bar{\mathcal{O}}_{(k+2)}; \bar{\mathcal{O}}_{(2)})$  lattice. Also, each copy of  $\bar{\mathcal{O}}_{(k+1)}$  (resp.  $\bar{\mathcal{O}}_{(k)}$ ) can be considered to be part of the lattices  $(\bar{\mathcal{O}}_{(k+1)}; \bar{\mathcal{O}}_{(1)})$  (resp.  $(\bar{\mathcal{O}}_{(k)}; \bar{\mathcal{O}}_{(0)})$ ). In these cases the lattices have degenerated into single orbit subdiagrams because  $\bar{\mathcal{O}}_{(1)}$  (resp.  $\bar{\mathcal{O}}_{(0)}$ ) both consist of only one node, that is  $|\mathcal{P}(1)| = 1 = |\mathcal{P}(0)|$ .

These lattices arise as the Hasse subdiagrams associated to two disjoint orbit subsystems in the brane configuration. Kraft-Procesi transitions may be performed in one orbit subsystem or the other in any order, hence the lattice. Both of the orbit subsystems in the brane configuration are adjacent to the zeroth gap, with tails which point away from the zeroth gap and so in opposite directions around the circle. It is assumed during this discussion that  $N_1$  and  $N_2$  are sufficiently large that these two orbit subsystems remain disjoint in both brane configurations. The consequences of this not being the case are discussed later.

The traversing edges now need to be considered to be between lattice subdiagrams rather than orbit subdiagrams. The generalisation is exactly analogous to the set-up in the  $L = 1$  case only there are now two orbit subsystems to contend with. We forgo this generalisation until the case of general  $L$ .

### 5.5.5 Arbitrary $L$ and higher-level Hasse diagrams

The case of general  $L$  may be treated in the same manner as for specific low values of  $L$ . Consider the brane configuration for  $\pi(k, N_1, N_2, L)$  given in Fig. 5.27. Because  $\pi(k, N_1, N_2, L)$  is self mirror dual up to exchange of  $N_1$  and  $N_2$ , replacing the D5 branes with NS5 branes and vice versa, and swapping  $N_1$  and  $N_2$  in the Higgs brane configuration in Fig. 5.27 gives the Coulomb brane configuration for the theory.

Consider performing initial Kraft-Procesi transitions in the zeroth gap. The edges representing these transitions are the highest traversing edges in the Hasse diagram. By definition there are exactly  $L$  D3 branes in the zeroth gap. Assuming for now that  $N_2$  is sufficiently large, this sequence of transitions forms a line of  $L$  nodes at the top of the Hasse diagram. The edges between these nodes are labelled  $A_{N_2-k-1}, A_{N_2-k-3}, A_{N_2-k-5}, \dots, A_{N_2-k-2L-1}$ . Consider a node in this line corresponding to having performed  $k'$  transitions in the zeroth gap. At this point, the transitions have moved  $k'$  D5 branes into both of the adjacent gaps. This has promoted the orbit subsystem from  $\bar{\mathcal{O}}_{(k)}$  to  $\bar{\mathcal{O}}_{(k+k')}$ , and created a  $\bar{\mathcal{O}}_{(k')}$  subsystem. Assuming for now that  $N_1$  is sufficiently large, these subsystems are disjoint and the Hasse subdiagram for these two subsystems is the lattice  $(\bar{\mathcal{O}}_{(k+k')}; \bar{\mathcal{O}}_{(k')})$ . Performing one more zeroth gap transition would push one more D5 brane into each adjacent gap. The lattice subdiagram would then be  $(\bar{\mathcal{O}}_{(k+k'+1)}; \bar{\mathcal{O}}_{(k'+1)})$ . This is demonstrated in Fig. 5.33.

For arbitrary  $L$ , part of the Hasse diagram will consist of this sequence of lattices of increasing size. The traversing structure between lattices therefore needs to be investigated. Doing so is similar to the  $L = 1$  case, only there are now two orbit subsystems with which to contend.

In the same way that nodes in an orbit subdiagram were labelled with a partition  $\kappa$  in the  $L = 1$  case, nodes in a lattice may be labelled with a pair of partitions,  $(\kappa; \rho) \in (\mathcal{P}(k+k'); \mathcal{P}(k'))$  one for each of the orbit diagrams which make up the lattice.

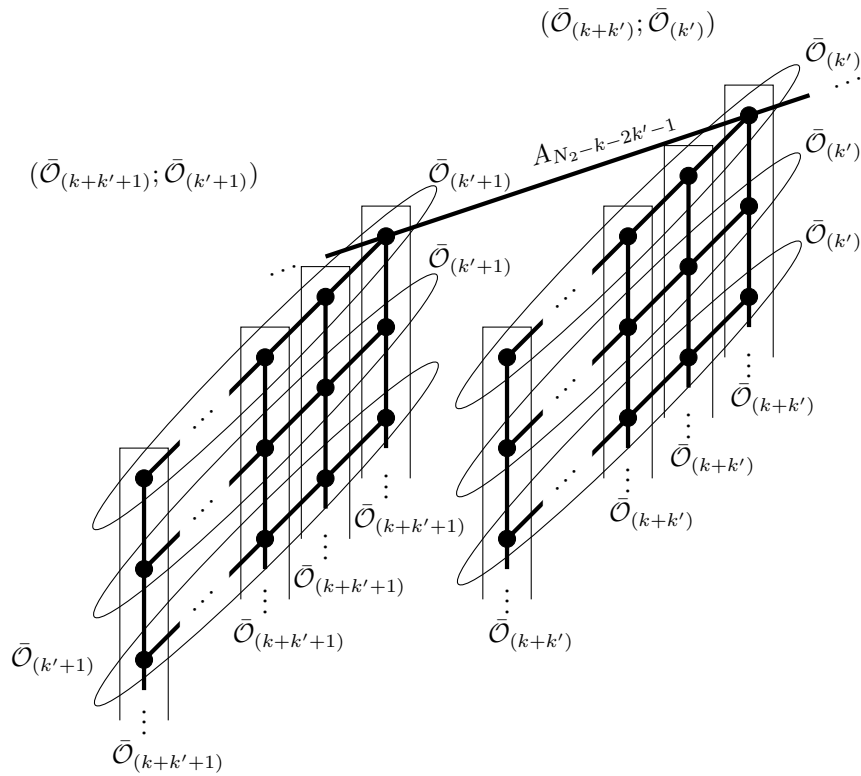


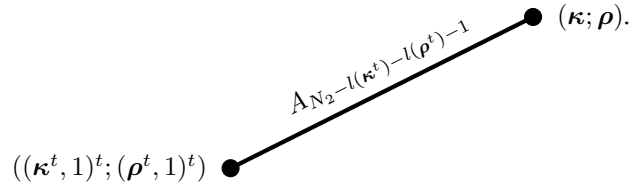
Figure 5.33:  $k'$  initial zeroth gap Kraft-Procetti transitions moves to a node from which descends a  $(\bar{\mathcal{O}}_{(k+k')}; \bar{\mathcal{O}}_{(k')})$  lattice. Performing one more transition in the zeroth gap moves to a node from which descends a  $(\bar{\mathcal{O}}_{(k+k'+1)}; \bar{\mathcal{O}}_{(k'+1)})$  lattice. Every node in the  $(\bar{\mathcal{O}}_{(k+k')}; \bar{\mathcal{O}}_{(k')})$  lattice has a traversing edge which attaches to an appropriate node in the  $(\bar{\mathcal{O}}_{(k+k'+1)}; \bar{\mathcal{O}}_{(k'+1)})$  lattice depending on the partition data related to the  $\bar{\mathcal{O}}_{(k+k')}$  and  $\bar{\mathcal{O}}_{(k')}$  orbits. These edges have been omitted for clarity here.

After  $k'$  zeroth gap transitions there is always the option to start removing from the orbit subsystems. This corresponds to moving from the line of traversing structure, discussed above, to moving down a lattice. At any point during the lattice removal there is the option to continue performing transitions in the zeroth gap. Deciding to go back to the zeroth gap is what it is to have the traversing structure between the lattices. Since the option to perform the zeroth gap transition exists at any point during the lattice removal, every node in the higher lattice will have a traversing edge coming from it (when in the top half of the overall diagram). Consider performing  $k'$  initial zeroth gap transitions, followed by removal from the  $(\bar{\mathcal{O}}_{(k+k')}; \bar{\mathcal{O}}_{(k')})$  lattice down to a node labelled by the pair  $(\kappa; \rho)$ . The traversing edge from this node to the  $(\bar{\mathcal{O}}_{(k+k'+1)}; \bar{\mathcal{O}}_{(k'+1)})$  lattice will be labelled with  $A_{x-1}$  where  $x$  is given by the number of D5 branes in the zeroth gap at that point. Since the removal of part of the orbit subsystems shifts D5 branes back into the zeroth gap, this will be

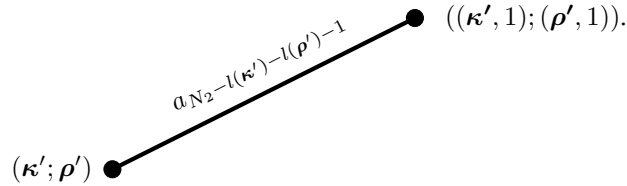
$$\begin{aligned} x &= \overbrace{N_2 - k}^{\text{Initial D5s}} - \overbrace{2k'}^{\text{First Removals}} + \overbrace{(k + k' - l(\kappa^t))}^{\text{From } \bar{\mathcal{O}}_{(k+k')}} + \overbrace{(k' - l(\rho^t))}^{\text{From } \bar{\mathcal{O}}_{(k')}} \\ &= N_2 - l(\kappa^t) - l(\rho^t). \end{aligned} \quad (5.55)$$

The considerations are precisely the same as those in the **label** paragraph of the  $L = 1$  section, only this time two orbits have to be considered.

A transition in the zeroth gap will move one D5 brane into each of the orbit subsystems. This again entails appending a one to both of the transpose partitions. The total traversing structure between the  $(\bar{\mathcal{O}}_{(k+k')}; \bar{\mathcal{O}}_{(k')})$  grid and the  $(\bar{\mathcal{O}}_{(k+k'+1)}; \bar{\mathcal{O}}_{(k'+1)})$  grid can be summarised in the edge diagram:



Along with these edges, there are their mirror counterparts which descend from a  $(\bar{\mathcal{O}}_{(k+k'+1)}; \bar{\mathcal{O}}_{(k'+1)})$  lattice to a  $(\bar{\mathcal{O}}_{(k+k')}; \bar{\mathcal{O}}_{(k')})$  lattice. These can be summarised in the edge diagram:

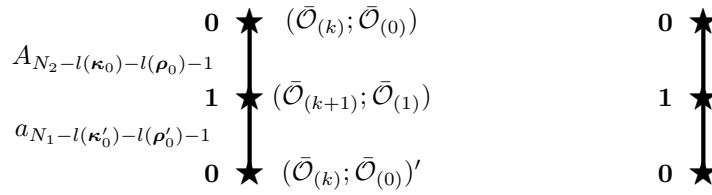


**Example:  $L = 2$**  In the  $L = 2$  case, the traversing edges from the  $(\bar{\mathcal{O}}_{(k+1)}; \bar{\mathcal{O}}_{(1)})$  lattice to the  $(\bar{\mathcal{O}}_{(k+2)}; \bar{\mathcal{O}}_{(2)})$  lattice can now be established. Here  $k' = 1$  and for the  $\bar{\mathcal{O}}_{(1)}$  orbit,  $\rho = (1)$ , because the Hasse diagram for the partitions of one contains one node. Therefore  $l(\rho^t) = 1$  for all cases. The transition from the  $\kappa = (k + 1)$  node has  $l(\kappa^t) = l((1^{k+1})) = k + 1$  and so should be labelled with  $A_{N_2 - 1 - (k+1) - 1} = A_{N_2 - k - 3}$ . This is exactly as was found. The node it attaches to is  $((\kappa^t, 1)^t; (\rho^t, 1)^t) = ((1^{k+1}, 1)^t; (1, 1)^t) = ((k + 2); (2))$  which is also as expected from previous calculations.

When  $L$  becomes large, the explicit Hasse diagrams rapidly become cumbersome. However the essential features may be represented in a *higher-level Hasse diagram*. In a higher level Hasse diagram, each node

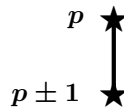
represents an entire lattice and each edge represents the whole traversing structure between lattices. Whilst not every node in the higher lattice strictly dominates every node in the lower lattice, no node in the lower lattice dominates any node in the higher lattice. To distinguish them from explicit Hasse diagrams, the nodes in a higher level Hasse diagram will be stars. A node representing the lattice  $(\bar{\mathcal{O}}_{(k+p)}; \bar{\mathcal{O}}_{(p)})$  will be labelled with the integer  $p$ . So for example the  $\bar{\mathcal{O}}_{(k)} = (\bar{\mathcal{O}}_{(k)}; \bar{\mathcal{O}}_{(0)})$  lattice will be represented by a star node with the label  $0$ . In each instance a value of  $k$  has to be specified for the entire diagram. Applying the above considerations in the  $L = 0, 1$  and  $2$  cases yields the following:

**Example:  $L = 1$**  When  $L = 1$  the Hasse diagram, Fig. 5.29, consists of an  $(\bar{\mathcal{O}}_{(k+0)}; \bar{\mathcal{O}}_{(0)})$  lattice which traverses down to an  $(\bar{\mathcal{O}}_{(k+1)}; \bar{\mathcal{O}}_{(1)})$  lattice and from there to another  $(\bar{\mathcal{O}}_{(k+0)}; \bar{\mathcal{O}}_{(0)})$  lattice. The higher level Hasse diagram is therefore:



The notation can be condensed considerably to just the integers labelling the nodes. This is because, once  $k$  is specified, all the other information can be extracted from this label.

The traversing edges from  $(\bar{\mathcal{O}}_{(k+p)}; \bar{\mathcal{O}}_{(p)})$  will always traverse to either  $(\bar{\mathcal{O}}_{(k+p+1)}; \bar{\mathcal{O}}_{(p+1)})$  or  $(\bar{\mathcal{O}}_{(k+p-1)}; \bar{\mathcal{O}}_{(p-1)})$ . Therefore every edge in a higher level Hasse diagram may be written as

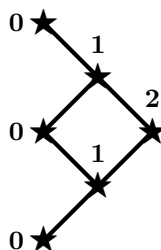


For a given  $k$ , all of the details of the structure in the explicit Hasse diagram to which these nodes and edges correspond may be extracted. Taking the  $+$  corresponds a  $(\bar{\mathcal{O}}_{(k+p)}; \bar{\mathcal{O}}_{(p)})$  lattice traversing down to a  $(\bar{\mathcal{O}}_{(k+p+1)}; \bar{\mathcal{O}}_{(p+1)})$  lattice. Traversing edges are labelled  $A_{N_2-l(kappa_p^t)-l(rho_p^t)-1}$ . For  $-$ , this corresponds to a  $(\bar{\mathcal{O}}_{(k+p)}; \bar{\mathcal{O}}_{(p)})$  lattice traversing down to a  $(\bar{\mathcal{O}}_{(k+p-1)}; \bar{\mathcal{O}}_{(p-1)})$  lattice, the edge is  $a_{N_1-l(kappa_{p-1})-l(rho_{p-1})-1}$ . The partitions in the indices of the edge labels have subscripts indicating which lattice they belong to.

**Example:  $L = 0$**  When  $L = 0$  the Hasse diagram is just the orbit diagram for  $\bar{\mathcal{O}}_{(k)} = (\bar{\mathcal{O}}_{(k+0)}; \bar{\mathcal{O}}_{(0)})$ . There is no traversing structure. Once  $k$  is specified, the higher level Hasse diagram is therefore a single star labelled with a  $0$ .



**Example:  $L = 2$**  The higher level Hasse diagram for  $L = 2$  is:



Given  $k$ , and once the notation is unpackaged, this diagram contains all of the same information as Fig. 5.32.

Consider once more the  $L = 2$  case. What does it mean, in the brane configuration, to choose different routes through the higher level Hasse diagram? The answer concerns the order and grouping of the removal of fully wrapped D3 branes. In the  $L = 2$  case there are two possible routes from the top to the bottom of the higher level Hasse diagram, either  $\mathbf{0} \rightarrow \mathbf{1} \rightarrow \mathbf{0} \rightarrow \mathbf{1} \rightarrow \mathbf{0}$  or  $\mathbf{0} \rightarrow \mathbf{1} \rightarrow \mathbf{2} \rightarrow \mathbf{1} \rightarrow \mathbf{0}$ . Similarly, when  $L = 2$  there are two manners in which the 2 wrapped branes may be removed. They may be removed *one at a time*, where the second wrapped brane only starts being removed once the first wrapped brane has been fully removed. Or they may be removed *concurrently* where the second wrapped brane starts being removed before the first wrapped brane has been fully removed. The structure associated to removal of the orbit subdiagrams is contained in the nodes and may be ignored in the following. Consider that one method to reach the  $\mathbf{2}$  node is to perform two Kraft-Procesi transitions in the zeroth gap immediately. This means we arrive at the top of the  $(\bar{\mathcal{O}}_{(k+2)}; \bar{\mathcal{O}}_{(2)})$  lattice in the explicit Hasse diagram and at the  $\mathbf{2}$  node in the higher-level Hasse diagram. After these transitions there are no more D3 branes in the zeroth gap, the wrapped branes are being removed concurrently. The structure of the higher level Hasse diagram captures the manner in which the wrapped branes are removed. Note however that Kraft-Procesi transitions only remove one D3 brane from a gap at a time. Hence even when two wrapped branes are removed concurrently, one always starts and finishes being removed before the other. Therefore the first edge and the final edge of both routes coincide.

To write down the higher level Hasse diagram for  $\pi(k, N_1, N_2, L)$ , it is sufficient to consider those different manners in which  $L$  wrapped branes may be removed that are in correspondence with the *unordered* partitions of  $L$ . For example, 4 wrapped branes may be removed as: 4 concurrently, 3 concurrently then 1, 1 then 3 concurrently, two concurrent pairs, 1 then 1 then 2, 1 then 2 then 1, 2 then 1 then 1 or one at a time. All of these options constitute a different route through the higher level Hasse diagram. These routes may be written

$$\begin{aligned} & \mathbf{0} \rightarrow \mathbf{1} \rightarrow \mathbf{2} \rightarrow \mathbf{3} \rightarrow \mathbf{4} \rightarrow \mathbf{3} \rightarrow \mathbf{2} \rightarrow \mathbf{1} \rightarrow \mathbf{0} \\ & \mathbf{0} \rightarrow \mathbf{1} \rightarrow \mathbf{2} \rightarrow \mathbf{3} \rightarrow \mathbf{2} \rightarrow \mathbf{1} \rightarrow \mathbf{0} \rightarrow \mathbf{1} \rightarrow \mathbf{0} \\ & \mathbf{0} \rightarrow \mathbf{1} \rightarrow \mathbf{0} \rightarrow \mathbf{1} \rightarrow \mathbf{2} \rightarrow \mathbf{3} \rightarrow \mathbf{2} \rightarrow \mathbf{1} \rightarrow \mathbf{0} \\ & \mathbf{0} \rightarrow \mathbf{1} \rightarrow \mathbf{2} \rightarrow \mathbf{1} \rightarrow \mathbf{0} \rightarrow \mathbf{1} \rightarrow \mathbf{2} \rightarrow \mathbf{1} \rightarrow \mathbf{0} \\ & \mathbf{0} \rightarrow \mathbf{1} \rightarrow \mathbf{2} \rightarrow \mathbf{1} \rightarrow \mathbf{0} \rightarrow \mathbf{1} \rightarrow \mathbf{0} \rightarrow \mathbf{1} \rightarrow \mathbf{0} \\ & \mathbf{0} \rightarrow \mathbf{1} \rightarrow \mathbf{0} \rightarrow \mathbf{1} \rightarrow \mathbf{2} \rightarrow \mathbf{1} \rightarrow \mathbf{0} \rightarrow \mathbf{1} \rightarrow \mathbf{0} \\ & \mathbf{0} \rightarrow \mathbf{1} \rightarrow \mathbf{0} \rightarrow \mathbf{1} \rightarrow \mathbf{0} \rightarrow \mathbf{1} \rightarrow \mathbf{2} \rightarrow \mathbf{1} \rightarrow \mathbf{0} \\ & \mathbf{0} \rightarrow \mathbf{1} \rightarrow \mathbf{0} \rightarrow \mathbf{1} \rightarrow \mathbf{0} \rightarrow \mathbf{1} \rightarrow \mathbf{0} \rightarrow \mathbf{1} \rightarrow \mathbf{0} \end{aligned}$$

Consider two routes, of the  $i^{\text{th}}$  and  $i + 1^{\text{th}}$  number in the routes are the same, then the arrow between the numbers in both routes corresponds to the same edge in the higher level Hasse diagram. Using these considerations for arbitrary  $L$ , the higher level Hasse diagram for  $\pi(k, N_1, N_2, L)$  is given in Fig. 5.34.

Each route through Fig. 5.34 is a different manner in which the fully wrapped D3 branes may be removed. Some of these manners correspond to the unordered partitions of  $L$ . For example moving from top to bottom only using the nodes labelled with  $\mathbf{0}$  and  $\mathbf{1}$  corresponds to removing each wrapped brane one at a time. Some





of the manners do not correspond to an unordered partition of  $L$ . For example, moving down to the first node labelled **2**, then to the second node labelled **1**, then to the second **2**, then down to the bottom following the zeroes and ones corresponds to the following removal sequence: beginning to remove a second wrapped brane before finishing the first, then beginning to remove a third wrapped brane before finishing the second but after finishing the first, then only beginning removing a fourth wrapped brane having fully removed the first three, and finally removing the remaining branes one at a time. In this sense, the label of the node in a route at any given point is the number of fully wrapped D3 branes in the process of being removed at that point in the route.

**Dimensional Check** In order to perform a dimensional check on this construction, a general route  $\mathcal{R}$  through Fig. 5.34 must be defined. Such a route must pass through  $2L+1$  star nodes and may be defined by a sequence  $\mathbf{R}_i, i = 1, \dots, 2L+1$  with the requirements that  $\mathbf{R}_i \geq \mathbf{0}$ ,  $\mathbf{R}_1 = \mathbf{0} = \mathbf{R}_{2L+1}$  and  $\mathbf{R}_{i+1} = \mathbf{R}_i \pm \mathbf{1}$ , then

$$\mathcal{R} = \mathbf{R}_1 \rightarrow \mathbf{R}_2 \rightarrow \mathbf{R}_3 \rightarrow \dots \rightarrow \mathbf{R}_{2L-1} \rightarrow \mathbf{R}_{2L} \rightarrow \mathbf{R}_{2L+1}. \quad (5.56)$$

$\dim_{\mathbb{H}}(\mathcal{R})$  will have contributions from edges and nodes,

$$\dim_{\mathbb{H}}(\mathcal{R}) = \dim_{\mathbb{H}}^e(\mathcal{R}) + \dim_{\mathbb{H}}^\star(\mathcal{R}). \quad (5.57)$$

The route must travel through exactly  $L$  edges that represent traversing structure carrying  $A$ -type labels and  $L$  edges corresponding to traversing structure carrying  $a$ -type labels. Each node represents a lattice in the explicit Hasse diagram. The route will meet exactly  $2L + 1$  nodes in the higher level Hasse diagram. In each case the route will join the  $i$ th lattice at a node  $(\kappa_i; \rho_i)$  and leave it again from a node  $(\sigma_i; \gamma_i)$ . The two contributions to the total dimension of the route can be written as:

$$\begin{aligned} \dim_{\mathbb{H}}^e(\mathcal{R}) &= \sum_{\{i|\mathbf{R}_i - \mathbf{R}_{i+1} = -\mathbf{1}\}} 1 + \sum_{\{i|\mathbf{R}_i - \mathbf{R}_{i+1} = \mathbf{1}\}} N_1 - l(\kappa_{i+1}) - l(\rho_{i+1}) - 1 \\ &= \sum_{i=1}^{2L} \left[ \left( \frac{1}{-2} \right) (\mathbf{R}_i - \mathbf{R}_{i+1} - 1) + \frac{1}{2} (\mathbf{R}_i - \mathbf{R}_{i+1} + 1) (N_1 - l(\kappa_{i+1}) - l(\rho_{i+1}) - 1) \right] \\ &= (\mathbf{R}_{2L+1} - \mathbf{R}_1) + LN_1 - \frac{1}{2} \sum_{i=1}^{2L} (\mathbf{R}_i - \mathbf{R}_{i+1} + 1) (l(\kappa_{i+1}) + l(\rho_{i+1})) \\ &= N_1 L - \frac{1}{2} \sum_{i=1}^{2L} (\mathbf{R}_i - \mathbf{R}_{i+1} + 1) (l(\kappa_{i+1}) + l(\rho_{i+1})) \end{aligned} \quad (5.58)$$

Where there is a contribution of 1 to  $\dim_{\mathbb{H}}^e(\mathcal{R})$  when an edge is of  $A$ -type and a contribution of  $N_1 - l(\kappa_{i+1}) - l(\rho_{i+1}) - 1$  when the  $i$ th edge is of  $a$ -type. In line two the sums are simplified and combined by multiplying by a factor which picks out the correct values in each case. This factor is  $\mathbf{R}_i - \mathbf{R}_{i+1} - 1 = 0$  when the  $i$ th edge is of  $a$ -type and  $-2$  when it's of  $A$ -type and  $\mathbf{R}_i - \mathbf{R}_{i+1} + 1 = 0$  when the  $i$ th edge is of  $A$ -type and 2 when it's of  $a$ -type. The second term in line three is equal to  $LN_1$  because and route  $\mathcal{R}$  must pass through  $L$

edges for which  $\mathbf{R}_i - \mathbf{R}_{i+1} + 1 = 2$ . Final simplification yields the result. And,

$$\begin{aligned}
\dim_{\mathbb{H}}^{\star}(\mathcal{R}) &= \frac{1}{2} \sum_{i=1}^{2L+1} \left[ \sum_{j=1}^{l(\sigma_i^t)} (\sigma_{ij}^t)^2 - \sum_{j=1}^{l(\kappa_i^t)} (\kappa_{ij}^t)^2 + \sum_{j=1}^{l(\gamma_i^t)} (\gamma_{ij}^t)^2 - \sum_{j=1}^{l(\rho_i^t)} (\rho_{ij}^t)^2 \right] \\
&= \frac{1}{2} \sum_{\{i|\mathbf{R}_i - \mathbf{R}_{i+1} = -1\}} \left[ \sum_j (\sigma_{ij}^t)^2 - \sum_j ((\sigma_{i-1}^t, 1))_j^2 + \sum_j (\gamma_{ij}^t)^2 - \sum_j ((\gamma_{i-1}^t, 1))_j^2 \right] \\
&\quad + \frac{1}{2} \sum_{\{i|\mathbf{R}_i - \mathbf{R}_{i+1} = 1\}} \left[ \sum_j ((\kappa_{i+1}, 1)^t)_j^2 - \sum_j (\kappa_{ij}^t)^2 + \sum_j ((\rho_{i+1}, 1)^t)_j^2 - \sum_j (\rho_{ij}^t)^2 \right] \\
&= \frac{1}{2} \sum_{i=2}^{2L+1} \left[ \left( \frac{1}{-2} \right) (\mathbf{R}_{i-1} - \mathbf{R}_i - 1) \left[ \sum_j (\sigma_{ij}^t)^2 - \sum_j ((\sigma_{i-1}^t, 1))_j^2 + \sum_j (\gamma_{ij}^t)^2 - \sum_j ((\gamma_{i-1}^t, 1))_j^2 \right] \right] \\
&\quad + \frac{1}{2} \left( \sum_j (\sigma_{1j}^t)^2 - \sum_j (\kappa_{1j}^t)^2 \right) + \frac{1}{2} \left( \sum_j (\gamma_{1j}^t)^2 - \sum_j (\rho_{1j}^t)^2 \right) \\
&\quad + \frac{1}{2} \sum_{i=1}^{2L} \left[ \left( \frac{1}{2} \right) (\mathbf{R}_i - \mathbf{R}_{i+1} + 1) \left[ \sum_j ((\kappa_{i+1}, 1)^t)_j^2 - \sum_j (\kappa_{ij}^t)^2 + \sum_j ((\rho_{i+1}, 1)^t)_j^2 - \sum_j (\rho_{ij}^t)^2 \right] \right] \\
&\quad + \frac{1}{2} \left( \sum_j (\sigma_{2L+1j}^t)^2 - \sum_j (\kappa_{2L+1j}^t)^2 \right) + \frac{1}{2} \left( \sum_j (\gamma_{2L+1j}^t)^2 - \sum_j (\rho_{2L+1j}^t)^2 \right) \\
&= \frac{1}{2} \sum_{i=2}^{2L+1} \left[ \left( \frac{1}{-2} \right) (\mathbf{R}_{i-1} - \mathbf{R}_i - 1) \left[ \sum_j (\sigma_{ij}^t)^2 - 1 + \sum_j (\sigma_{i-1}^t)_j^2 + \sum_j (\gamma_{ij}^t)^2 - 1 + \sum_j (\gamma_{i-1}^t)_j^2 \right] \right] \\
&\quad + \frac{1}{2} \left( \sum_j (\sigma_{1j}^t)^2 - k \right) + \frac{1}{2} \left( \sum_j (\gamma_{1j}^t)^2 - 0 \right) + \frac{1}{2} \left( k^2 - \sum_j (\kappa_{2L+1j}^t)^2 \right) + \frac{1}{2} \left( 0 - \sum_j (\rho_{2L+1j}^t)^2 \right) \\
&\quad + \frac{1}{2} \sum_{i=1}^{2L} \left[ \left( \frac{1}{2} \right) (\mathbf{R}_i - \mathbf{R}_{i+1} + 1) \left[ 1 + l(\kappa_{i+1}) + \sum_j ((\kappa_{i+1}^t)_j^2 - \sum_j (\kappa_{ij}^t)^2 \right. \right. \\
&\quad \quad \left. \left. + 1 + l(\rho_{i+1}) + \sum_j ((\rho_{i+1}^t)_j^2 - \sum_j (\rho_{ij}^t)^2) \right] \right] \\
&= \frac{1}{2} \left( \frac{1}{-2} \right) (\mathbf{R}_{2L} - \mathbf{R}_{2L+1} - 1) \left[ \sum_j (\sigma_{2L+1j}^t)^2 + \sum_j (\gamma_{2L+1j}^t)^2 \right] + \frac{1}{2} \sum_{i=2}^{2L+1} (\mathbf{R}_{i-1} - \mathbf{R}_i - 1) - \frac{1}{2} k \\
&\quad + \frac{1}{2} \left( \frac{1}{2} \right) (\mathbf{R}_1 - \mathbf{R}_2 + 1) \left[ \sum_j (\kappa_{1j}^t)^2 + \sum_j (\rho_{1j}^t)^2 \right] + \frac{1}{2} \sum_{i=1}^{2L} (\mathbf{R}_i - \mathbf{R}_{i+1} + 1) \\
&\quad + \frac{1}{2} k^2 + \frac{1}{2} \sum_{i=1}^{2L} (\mathbf{R}_i - \mathbf{R}_{i+1} + 1) (l(\kappa_{i+1}) + l(\rho_{i+1})) \\
&= \frac{1}{2} (k^2 - k) + \frac{1}{2} \sum_{i=1}^{2L} (\mathbf{R}_i - \mathbf{R}_{i+1} + 1) (l(\kappa_{i+1}) + l(\rho_{i+1})) + \frac{1}{2} (2\mathbf{R}_1 - 2\mathbf{R}_{2L+1}) - \frac{1}{2} (2L) + \frac{1}{2} (2L) \\
&= \frac{1}{2} (k^2 - k) + \frac{1}{2} \sum_{i=1}^{2L} (\mathbf{R}_i - \mathbf{R}_{i+1} + 1) (l(\kappa_{i+1}) + l(\rho_{i+1}))
\end{aligned} \tag{5.59}$$

Where the traversing structure between lattices allows some or all of the partitions for nodes in one lattice to be written in terms of the partitions for nodes in adjacent lattices. If the  $i^{\text{th}}$  edge in  $\dim_{\mathbb{H}}(\mathcal{R})$  is of  $A$ -type then the partitions for the node to which it connects in the  $i + 1^{\text{th}}$  lattice is known in terms of the partitions of the node from which it traverses in the  $i^{\text{th}}$  lattice. If the  $i^{\text{th}}$  edge is of  $a$ -type then the partitions for the node

from which it traverses in the  $i^{\text{th}}$  lattice is known in terms of the partitions of the node to which it connects in the  $i + 1^{\text{th}}$  lattice. Line two uses this to rewrite the  $i$  sum as two sums, one over  $A$ -type edges and one over  $a$ -type edges. Doing so allows the substitution into the calculation of the relations between nodes in adjacent lattices. Throughout the calculation the sum over  $j$  is taken to mean the sum over all non-zero parts of the partition.

In line three the same trick as in the calculation for  $\dim_{\mathbb{H}}^e(\mathcal{R})$  is employed to rewrite the sums with multiplicative factors dependant on  $\mathbf{R}_i$ . The contribution for the first and final lattices are separated from the rest. This is because the top partitions in the first lattice and the bottom partitions in the final lattice have to be the top and bottom of the diagram so these contributions play a special role. In line four assessing some of the sums that have been separated off yields  $k$  and  $k^2$  since  $\kappa_1 = (k)$  and  $\sigma_{2L+1} = (1^k)$ . Also in line four the relations  $\sum_j ((\lambda^t, 1)_j)^2 = \sum_i (\lambda_i^t)^2 + 1$  and  $\sum_j ((\lambda, 1)_j^t)^2 = 1 + 2l(\lambda) + \sum_i (\lambda_i^t)^2$  have been employed.

In line five the  $i$  sum has been assessed for the  $j$  sum contributions. Much of these sums cancel with one another leaving only the  $i = 2L + 1$  contributions from  $\kappa$  and  $\rho$  and the  $i = 1$  contribution from  $\sigma$  and  $\gamma$ , the remaining  $i$  sums have been separated out for clarity. In line six the first and fourth terms in line five have been assessed to be zero. This is because  $\mathbf{R}_{2L} - \mathbf{R}_{2L+1} - 1 = 0 = \mathbf{R}_1 - \mathbf{R}_2 + 1$ . Terms two and five in line five mostly cancel amongst themselves leaving terms three, four, and five in line six. These three terms all cancel to zero yielding the result in line seven.

Together, then, these results do indeed yield

$$\dim_{\mathbb{H}}(\mathcal{R}) = \frac{1}{2}(k^2 - k) + N_1 L, \quad (5.60)$$

as expected. In essence all contributions cancel in the same style as (5.51) - (5.54). The only contributions that don't are from the requirement that  $\mathcal{R}$  starts at the partition  $((k); (0))$  in the first lattice, ends at the partition  $((1^k); (0))$  in the final lattice, and passes through precisely  $L$   $a$ -type traversing edges.

## 5.6 Hasse diagram modifications when $N_i \leq k + 2L - 1$

So far, simplifying assumptions about the size of  $N_1$  and  $N_2$  have been made. In the Coulomb brane configuration these were:  $N_1$  was always large enough that the two orbit subsystems  $\bar{\mathcal{O}}_{(k+L)}$  and  $\bar{\mathcal{O}}_{(L)}$  remained disjoint and  $N_2$  was always large enough that performing  $L$  initial zeroth gap Kraft-Procesi transitions was possible without having to move D5 branes back into the zeroth gap by starting to remove the orbit subsystems.

However these two assumptions do not hold in all cases, especially as  $L$  becomes large. The failure of these assumptions to hold is reflected in the explicit Hasse diagrams. When these assumptions break, the indices carried by the labels for some edges become zero or negative. The transverse slice which the edge represents is therefore not defined. In the brane configuration this corresponds to the Kraft-Procesi transition to which the edge corresponds no longer being possible. The precise values of  $N_1$  and  $N_2$  at which this starts to become an issue can be ascertained from considering either brane configuration constraints or Hasse diagram constraints.

In the Hasse diagram, only traversing edges carry dependence on  $N_i$  or  $L$ . Consider the top most travers-

ing edges of  $A$ -type. The topmost traversing edge between the  $k^{\text{th}}$  and  $k' + 1^{\text{th}}$  lattices carries the label  $A_{N_2 - k - 2k' - 1}$ . Note  $k'$  can take a maximum value of  $L - 1$ . The  $A$ -type traversing edge with the smallest index in the whole Hasse diagram is therefore the top most traversing edge between the upper  $(\bar{\mathcal{O}}_{(k+L-1)}; \bar{\mathcal{O}}_{(L-1)})$  lattice and the  $(\bar{\mathcal{O}}_{(k+L)}; \bar{\mathcal{O}}_{(L)})$  lattice. The edge carries the label  $A_{N_2 - k - 2L + 1}$ . If this edge is to remain well defined then  $N_2 > k + 2L - 1$ . Seeing as  $L$  can become arbitrarily large for any value of  $N_2$ , increasing  $L$  will always violate this requirement eventually. Consider the interpretation of this bound in the brane configuration. The top most traversing edges between each lattice correspond to performing zeroth gap Kraft-Processi transitions without performing any orbit subsystem transitions. Each time a zeroth gap transition is performed it moves two D5 branes out of the zeroth gap. There are  $L$  D3 branes in the zeroth gap. To successfully perform the  $L^{\text{th}}$  transition, there needs to be at least  $2L$  D5 branes in the zeroth gap initially. There are  $N_2 - k$  D5 branes in the zeroth gap initially. Therefore  $N_2 - k \geq 2L$  and so once again  $N_2 > k + 2L - 1$ . The constraints on  $N_1$  are exactly analogous when performed in the Higgs brane configuration since  $\pi(k, N_1, N_2, L)$  is mirror dual to  $\pi(k, N_2, N_1, L)$ . Therefore  $N_1 > k + 2L - 1$  is necessary for the edges to remain well defined. The edges that carry the smallest indices with  $N_1$  dependence are in the position mirror to the top most edges considered when discussing  $N_2$ .

When  $N_i \leq k + 2L - 1$  the explicit Hasse diagram for  $\pi(k, N_1, N_2, L)$ , which can be unpacked from Fig. 5.34, needs to be modified. These modifications involve either removing the structure where edges become badly defined or replacing it in a systematic way. The effects of  $N_1$  and  $N_2$  being too small are mapped into one another by mirror symmetry. Assessing the effects of one of them being too small therefore fully uncovers the effect of the other being too small. Here the effects of  $N_2$  being too small are assessed using the Coulomb brane configuration.

### 5.6.1 One bad edge: $N_i = k + 2L - 1$

When  $N_2 = k + 2L - 1$  (and  $N_1 > k + 2L - 1$ ) the only edge in the Hasse diagram which is undefined is the topmost traversing edge between the upper  $(\bar{\mathcal{O}}_{(k+L-1)}; \bar{\mathcal{O}}_{(L-1)})$  lattice and the  $(\bar{\mathcal{O}}_{(k+L)}; \bar{\mathcal{O}}_{(L)})$  lattice. In the general Hasse diagram prescription from Fig. 5.34, this edge is now labelled with " $A_0$ " which isn't a defined transverse slice. In the brane configuration this edge corresponds to an  $L^{\text{th}}$  consecutive initial  $A$ -type Kraft-Processi transition in the zeroth gap. When  $N_2 = k + 2L - 1$ , the  $L - 1^{\text{th}}$  transition leaves only one D5 brane left in the zeroth gap and a further transition cannot be performed. Instead the only options available are to perform the first transition in one of the orbit subsystems. This will move one D5 brane back into the zeroth gap and allow the  $A_1$  transition which traverses from the two second-highest nodes in the  $(\bar{\mathcal{O}}_{(k+L-1)}; \bar{\mathcal{O}}_{(L-1)})$  lattice. The Hasse diagram modification in this case is removing the offending edge, the topmost node in the  $(\bar{\mathcal{O}}_{(k+L)}; \bar{\mathcal{O}}_{(L)})$  lattice, and both the lattice edges which descend from this node, Fig. 5.35.

However in the specific case of  $N_2 = k + 3$  (so  $L = 2$ ) this changes again. This case is shown in Fig. 5.36. Removal of the offending structure leaves a node in the  $(\bar{\mathcal{O}}_{(k+2)}; \bar{\mathcal{O}}_{(k)})$  lattice without any edge which descends into it. However in assessing the brane configuration it is apparent that the first  $A_2$  transition moves one D5 brane into the  $N_1 - 1^{\text{th}}$  gap, leaves one in the zeroth gap and moves one into the first gap. The second D3 brane in the zeroth gap can therefore be removed either by performing the first orbit transition, then an

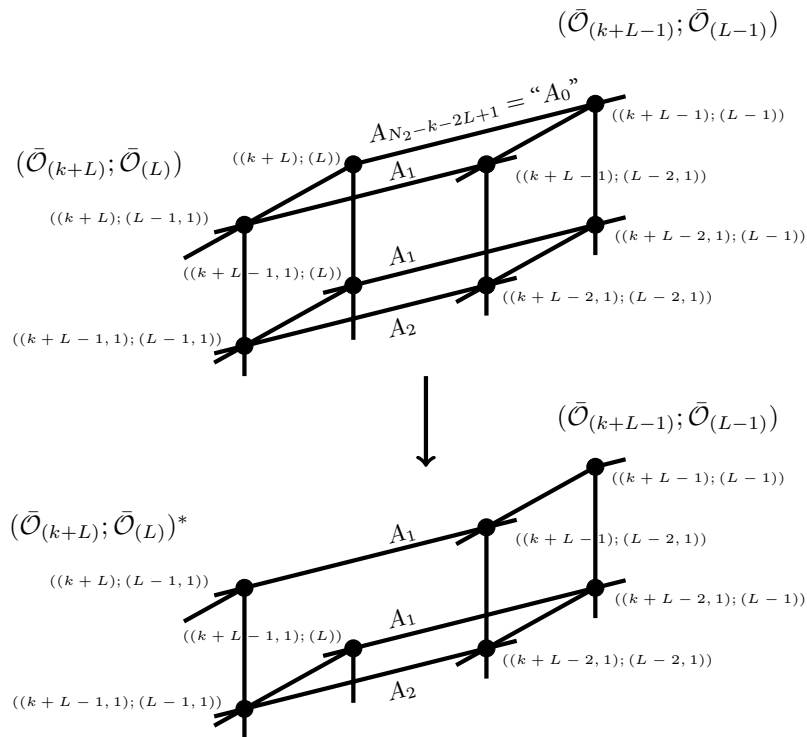


Figure 5.35: When  $N_2 = k + 2L - 1$ , the topmost traversing edge between the upper  $(\bar{\mathcal{O}}_{(k+L-1)}; \bar{\mathcal{O}}_{(L-1)})$  lattice and the  $(\bar{\mathcal{O}}_{(k+L)}; \bar{\mathcal{O}}_{(L)})$  lattice carries an undefined label. In the brane configuration, the Kraft-Procesi transition to which this edge corresponds is no longer possible. The result is that the edge is deleted. The  $((k+L); (L))$  node is therefore also deleted, as the brane configuration to which this node corresponds is no longer possible. Finally the two edges which descend from this node are also deleted.  $(\bar{\mathcal{O}}_{(k+L)}; \bar{\mathcal{O}}_{(L)})^*$  is used to indicate the lattice after the modifying.

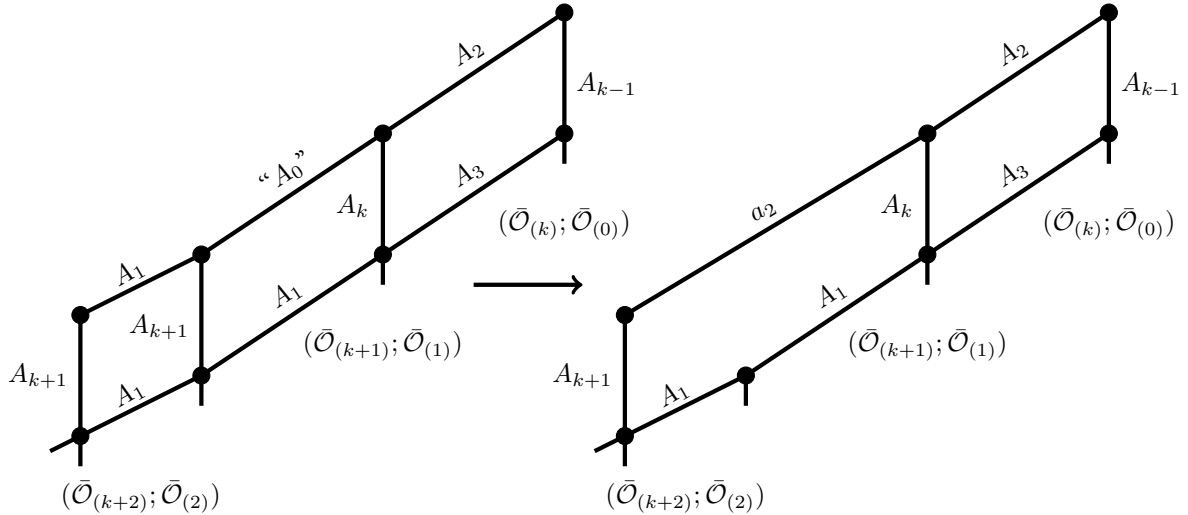


Figure 5.36: For the theory  $\pi(k, N_1, k+3, 2)$ , removing the offending structure leaves the node  $((k+2); (1^2))$  without an edge descending into it. An edge of appropriate dimension is therefore added, in this case  $a_2$ . In the general prescription, whenever a node is left 'floating' like this, extra structure must be added to the Hasse diagram (see discussion).

$A_1$ , or by performing an  $a_2$  transition in the  $N_1 - 1^{\text{th}}$  and zeroth gaps.

## 5.6.2 A modification prescription

The prescription for modifying the Hasse diagram when  $N_2$  becomes too small comes in two parts. It can be derived from considering what happens in the brane configuration, and which Kraft-Procesi transitions are allowed, under the different circumstances. The prescription is as follows:

(1) Having constructed the general Hasse diagram for the appropriate values of  $k, N_1, N_2$  and  $L$ , identify all of the edges which carry undefined labels. Remove these edges, the nodes to which they traversed, the edges which descend from those nodes and any nodes which are left without edges as a result.

(2) For every node that remains which no longer has any edge descending into it, identify the shortest route in the original general prescription from this node to a node in the lattice above it. Add an  $a_y$  edge between these two nodes where  $y$  is the sum of the dimensions of the edges in the original general Hasse diagram which this edge replaces.

The modifications necessary when  $N_1$  is too small can be found by performing the same prescription under mirror symmetry.

**Example:  $\pi(0, N_1, 3, 2)$**  The case of  $\pi(0, N_1, 3, 2)$  is given in Fig. 5.37. Here the removal of the offending structure leaves two nodes without edges descending into them. Two  $a_2$  edges are therefore added following the prescription. The right-hand Hasse diagram of Fig. 5.37 can be confirmed to be correct for  $\mathcal{M}_C(\pi(0, N_1, 3, 2))$  by explicit calculation using Kraft-Procesi transitions.

This completes the construction for any  $\pi(k, N_1, N_2, L)$  theory for  $N_i > 2$ . Since

$$\pi_{\mu^t}^\nu(M, N_1, N_2, L') \in \mathcal{K}(\pi(k, N_1, N_2, L))$$

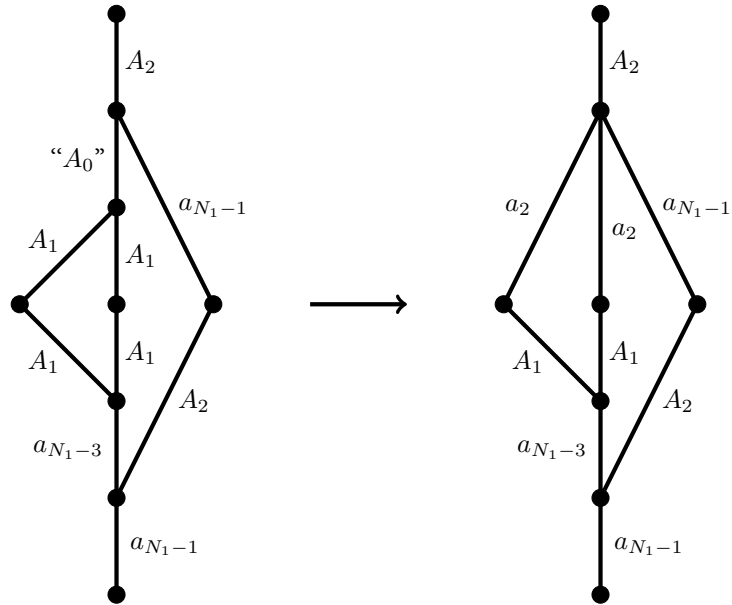


Figure 5.37: An example of applying the modifying procedure to a general Hasse diagram for the theory  $\pi(0, N_1, 3, 2)$ . On the left, the general Hasse diagram has an edge with an undefined label “ $A_0$ ”. Removing this edge, the node into which it descends and the edges descending from this node leaves two nodes floating. These are the  $((2); (1^2))$  and the  $((1^2); (2))$  nodes. Edges of dimension two therefore need to be added to the Hasse diagram.

for sufficient  $L$  given  $L'$ , this construction encompasses the Hasse diagram for *any* good circular quiver gauge theory.





# D-type Dynkin quivers

We now turn our attention to quivers whose gauge nodes and bifundamental hypermultiplets form a  $D_n$  Dynkin diagram. The moduli spaces of vacua of some small D-type Dynkin quivers with unitary gauge nodes have been explored before in, for example, [40, 51, 52, 54, 55, 62–64]. Here we give a comprehensive study for general  $n$ .

## 6.1 Nilpotent varieties as Dynkin quiver Higgs branches

The  $\mathfrak{so}_{2n}$  nilpotent varieties in (3.29) and (3.30) can be realised as the Higgs branches of  $D_n$  Dynkin quivers. A general  $D_n$  Dynkin quiver is given in Fig. 6.38.

The moduli space branches of  $D_n$  Dynkin quivers have been discussed before in numerous contexts. Their capacity to realise closures of  $\mathfrak{so}_{2n}$  nilpotent orbits of (characteristic) height  $\text{ht}(\bar{\mathcal{O}}_\rho) \leq 2$  as their *Coulomb* branches was considered in [52, 63, 64], to realise  $\mathfrak{so}_{2n}$  Slodowy slices as their Higgs branches in [54], and in the context of brane constructions for which they are IR descriptions in, for example, [62]. The discussion in this section will concern the Dynkin quivers which realise nilpotent varieties appearing as a subvariety of the maximal special slice as a Higgs branch. The  $D_n$  Dynkin quivers with  $\text{ht}(\bar{\mathcal{O}}_\rho) \leq 2$  nilpotent orbit Coulomb branches are a subset of those which realise the Slodowy slices as Higgs branches thanks to (3.27) and so the

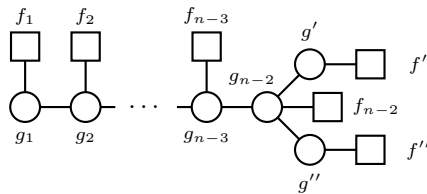


Figure 6.38: A general  $3d\mathcal{N} = 4$  unitary  $D_n$  Dynkin quiver. The field content can be read in the standard way. A circular gauge node labelled  $g$  represents a  $U(g)$  gauge group and carries an adjoint  $U(g)$  vectormultiplet. Square nodes labelled  $f$  represent  $SU(f)$  flavour symmetry. Edges between circular nodes are bifundamental hypermultiplets and edges between a circular and a square node are fundamental hypermultiplets. The gauge nodes and bifundamental hypermultiplets form the Dynkin diagram so a  $D_n$  Dynkin quiver has  $n$  gauge nodes total and a gauge group of  $U(g') \times U(g'') \times \prod_{i=1}^{n-2} U(g_i)$ .

discussion automatically generalises the Coulomb branch results in the same manner.

A central tool to write down these quivers is the Kraft-Procesi transition [4], [5], and its generalization, quiver subtraction, [64]. These processes identify and remove the transverse slice structure of the moduli space branches. This work introduces the reverse procedure, *quiver addition* whereby transverse slices are ‘added’ onto known moduli spaces by the introduction of appropriate fields at the level of the quiver. To demonstrate the technique’s effectiveness, quiver addition will be used to find the appropriate form for quivers realising Slodowy slices, then quiver subtraction will be used to identify quivers for subvarieties of the maximal special slice. In order to perform the addition the quivers for the minimal degenerations must be determined.

The maximal special slice  $\mathcal{S}_{(2m-1^2, 1^2)} \in \mathfrak{so}_{4m}$  has a Hasse diagram given in Fig. 3.10. It is clear that there are only three types of minimal degenerations needed in order to construct these varieties,  $D_l$ ,  $A_{2l-1}$  and  $A_{2l-1} \cup A_{2l-1}$ .

Note that the Hasse diagram for partitions and the Hasse diagram of inclusion relations for Slodowy slices are flipped. The Hasse subdiagram describing the singularity structure of  $\mathcal{S}_{(2m-1^2, 1^2)}$  places the partition  $(4m-1, 1)$  at the top, as it is the most dominant partition. However the Higgs branches are Slodowy slices<sup>4</sup> and as such this topmost node corresponds to a theory with *trivial* Higgs branch. If instead one drew a Hasse diagram corresponding to the inclusion relations of the Higgs branches of the quivers, the largest branch would be the slice  $\mathcal{S}_{(2m-1^2, 1^2)}$  and this theory would be placed at the top. Labelling the edges of this quiver Hasse diagram with the transverse slice between the quiver’s Higgs branches then yields a Hasse diagram which is exactly the partition diagram flipped upside down. When adding transverse slices in order to build up Higgs branches one builds the Hasse diagram for the slice from the *top* and the theory with the largest (with respect to the moduli space inclusion relation) Higgs branch will be associated to the node at the *bottom*. This is the convention which preserves the notation for the hierarchy of singularities within the varieties.

The three types of minimal degeneration that are realised as the Higgs branches of the Dynkin quivers are given in Fig. 6.39. The top and bottom quivers are familiar, however the middle one is not. In the context of  $\mathfrak{so}_{2n}$  nilpotent varieties, the  $A_k \cup A_k$  singularity is associated to very even partitions and hence to the subtlety regarding the nilpotent orbits for such partitions discussed previously. However in the broader context of  $D_n$  quivers the  $A_k \cup A_k$  singularity is associated with the choice that exists due to the equivalence of the two end nodes. Simplistically, swapping the two end nodes doesn’t change the field theory for a  $D_n$  Dynkin quiver, however in the more concrete diagrammatic context of quiver arithmetic, only one at a time will be realised. There is therefore an important implicit assumption in the remaining discussion: When the flavour content and/or gauge group of the two end nodes is different, there are implicitly *two*  $D_n$  Dynkin quivers available, which represent the same field theory. These quivers, when they are both drawn, are labelled *I* and *II*, following the very even nilpotent orbit naming convention. The  $A_k \cup A_k$  singularity exists in two scenarios, firstly when the end nodes differ and one of the flavours on an end node is 1<sup>5</sup>. The implicit choice that exists due to the difference in end nodes allows the observation that the true singularity is  $A_k \cup A_k$ , not just  $A_k$ . Alternatively, if *both* end node flavours are 1 this also corresponds to an  $A_k \cup A_k$  singularity if either could be considered as forming an  $A_k$  singularity with flavour in the tail of the quiver.

<sup>4</sup>Which can be considered to be all the edges and nodes from a given node *up* in the Hasse diagram.

<sup>5</sup>And this makes an  $A_k$  singularity with a flavour node on the tail.

$$\begin{aligned}
\mathcal{Q}_{\mathcal{M}_H}(D_k) &= \text{Diagram 1} \\
\mathcal{Q}_{\mathcal{M}_H}(A_k \cup A_k) &= \begin{aligned} &I \text{ Diagram 2} \\ &II \text{ Diagram 3} \end{aligned} \\
\mathcal{Q}_{\mathcal{M}_H}(A_k) &= \text{Diagram 4}
\end{aligned}$$

Figure 6.39: The  $3d \mathcal{N} = 4$  quivers which realise  $D_k$ ,  $A_k \cup A_k$  and  $A_k$  singularities as their Higgs branches. Each quiver has  $k$  nodes in each case. The  $A_k$  is familiar from linear quivers. The  $D_k$  case has been discussed before, for example [54]. The  $A_k \cup A_k$  singularity is a little more complicated, see discussion.

Note that there are  $B$  and  $C$  type Dynkin quivers which realise as *Coulomb* branches two other minimal degenerations  $b_n$  and  $c_n$  that appear in  $BCD$ -type orbit Hasse diagrams. However both involve non-simply laced edges and so do not map onto the topology of the  $D_n$  Dynkin quiver. Since the non-special nodes for the  $D_n$  always appear in the Hasse diagram as the end of an edge labelled with one of these singularities, this failure of quiver arithmetic is exactly the restriction that non-special nodes can't be included in the moduli space branch Hasse diagrams. Hence the diagrams are limited to  $\text{ht}(\bar{\mathcal{O}}_\rho) \leq 2$  nilpotent orbits and their subvarieties for Coulomb branches, and to the maximal special slice and its subvarieties for Higgs branches.

During quiver addition, the slice added to a given quiver must be such that its removal from the resulting quiver would give back the flavour arrangement of the quiver being added to. It is important to establish what happens to the flavour arrangement on the quivers when the slices are removed. Fig. 6.40 and Fig. 6.41 give two such examples.

The conclusion is that the  $D_k$  and  $A_k$  slices 'push' a single flavour onto the first gauge node(s) attached to them which are not part of the slice.  $A_{2k-1} \cup A_{2k-1}$  is a little more complicated, the transition still pushes flavour onto the first gauge nodes attached but not involved, however every time one of these slices is removed there is an option as to which leg of the Dynkin diagram is chosen. For example if a flavour node 1 is attached to both, the flavour on the one chosen gets pushed out of the diagram while the flavour on the one that wasn't chosen remains and is enhanced.

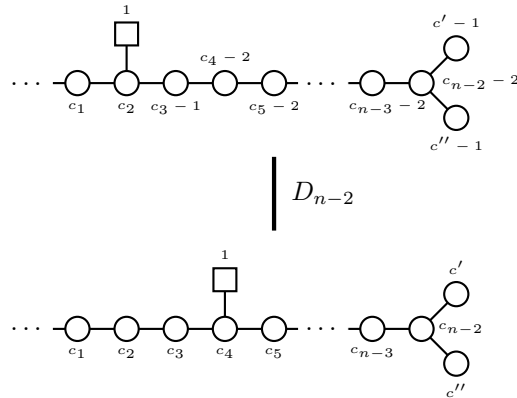


Figure 6.40: Quiver addition of a  $D_{n-2}$  singularity to the Higgs branch of a  $D_n$  Dynkin quiver. As per the discussion, the theory with the larger Higgs branch is placed lower and quiver subtraction works from the bottom, up. Reinterpreting the diagram as the *removal* of the singularity via the Higgs mechanism the behaviour of the flavour becomes clear.

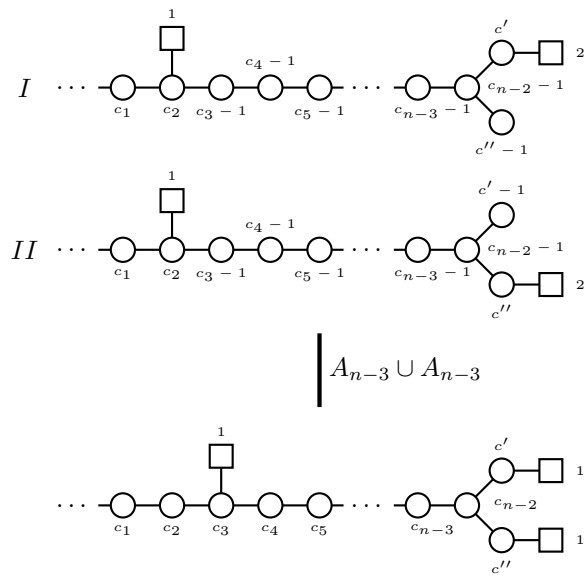


Figure 6.41: Quiver addition of one case of the  $A_{n-3} \cup A_{n-3}$  singularity to the Higgs branch of a  $D_n$  Dynkin quiver. Reinterpreting the diagram as the *removal* of the singularity via the Higgs mechanism (working up), the behaviour of the flavour is clear. The  $A_k \cup A_k$  transition for uneven initial end flavour is exactly analogous, only the bottom quiver here has uneven end flavour (with one still 1) and so also comes with two versions, as per the discussion.

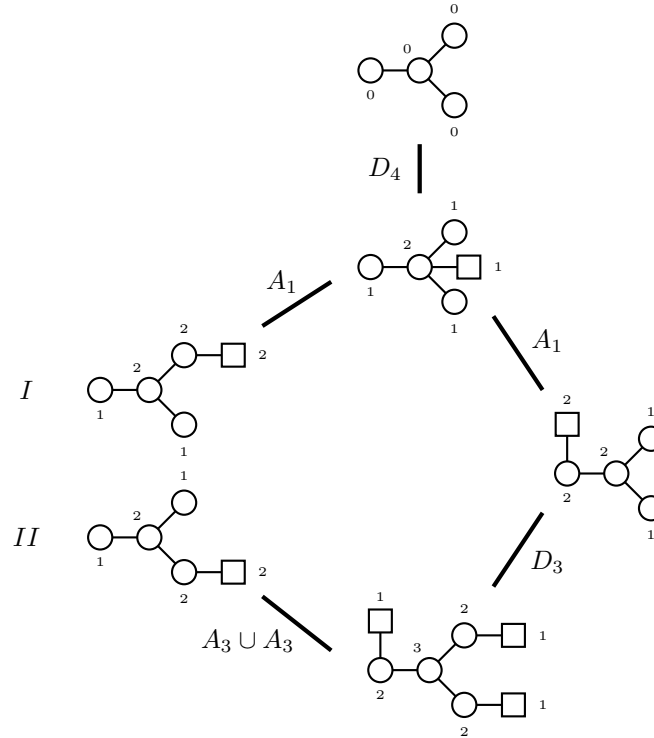
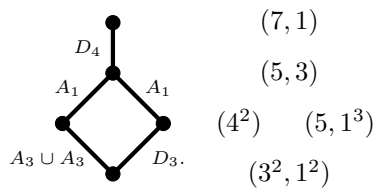


Figure 6.42: The Hasse diagram for the maximal special slice in  $\mathfrak{so}_8$  filled in with the  $3d\mathcal{N} = 4$  quivers which realise the Slodowy slices corresponding to each node. The singularity structure of the Higgs branches of the quivers is therefore exactly all of the structure which dominates the node at which the quiver lives.

### 6.1.1 $D_4$ quivers and nilpotent varieties of $\mathfrak{so}_8$

$D_4$  Dynkin quivers will be used several times as examples throughout. Here the quivers which realise  $\mathfrak{so}_8$  nilpotent varieties are studied in detail.

The special slice Hasse diagram for  $\mathfrak{so}_8$  is:



Beginning with a bare  $D_4$  Dynkin quiver, the only slice which can push *all* the flavour out of a  $D_4$  quiver is a  $D_4$  transition so this is the topmost singularity in Fig. 6.42. There are now three prior quivers which might have given this flavour arrangement by subtraction. At first they might all seem equivalent, however they can be distinguished by considering what may be added to them in subsequent steps. The full sequence is given in Fig. 6.42. Quiver subtraction can now be used in order to determine the quivers for any subvariety of the maximal special slice in  $\mathfrak{so}_8$ . An example of determining one such slice, namely the quiver with the Higgs branch  $\mathcal{S}_{(3^2, 1^2)} \cap \bar{\mathcal{O}}_{(5, 3)}$  is

$\nu \backslash \mu$	(7, 1)	(5, 3)	(4 <sup>2</sup> )	(5, 1 <sup>3</sup> )	(3 <sup>2</sup> , 1 <sup>2</sup> )
(3 <sup>2</sup> , 1 <sup>2</sup> )					
(5, 1 <sup>3</sup> )			X		
(4 <sup>2</sup> )					
(5, 3)					
(7, 1)					

Figure 6.43: A table that gives the  $D_4$ -type Dynkin quivers for all of the subvarieties of the maximal special slice of  $\mathfrak{so}_8$ . The left hand column contains those theories which realise Slodowy slices and so appear in Fig. 6.42. Almost all of the remaining quivers are quivers for singularities, the only one that isn't is the quiver  $Q_{\mathcal{M}_H}(\mathcal{S}_{(3^2,1^2)} \cap \bar{\mathcal{O}}_{(5,3)})$ . Trivial theories have been left blank and boxes which don't correspond to a possible variety have been crossed. Unlike the linear case, the subvarieties of the maximal special slice of  $\mathfrak{so}_{2n}$  fall into a small number of different types and so writing down more general quivers for each of these types supersedes the need to enumerate quivers for small algebras in tables.

$$Q_{\mathcal{M}_H}(\mathcal{S}_{(3^2,1^2)} \cap \bar{\mathcal{O}}_{(5,3)}) = Q_{\mathcal{M}_H}(\mathcal{S}_{(3^2,1^2)}) - Q_{\mathcal{M}_H}(\mathcal{S}_{(5,3)})$$

$$= \begin{array}{c} \begin{array}{c} \square \\ | \\ \bigcirc \\ | \\ \bigcirc \\ | \\ \bigcirc \\ | \\ \bigcirc \\ | \\ \bigcirc \\ | \\ \square \end{array} \\ \begin{array}{c} 1 \\ 2 \\ 3 \\ 2 \\ 1 \end{array} \end{array} - \begin{array}{c} \begin{array}{c} \bigcirc \\ | \\ \bigcirc \\ | \\ \bigcirc \\ | \\ \bigcirc \\ | \\ \bigcirc \\ | \\ \square \end{array} \\ \begin{array}{c} 1 \\ 2 \\ 1 \\ 1 \end{array} \end{array}$$

$$= \begin{array}{c} \begin{array}{c} \square \\ | \\ \bigcirc \\ | \\ \bigcirc \\ | \\ \bigcirc \\ | \\ \square \end{array} \\ \begin{array}{c} 1 \\ 1 \\ 1 \\ 1 \end{array} \end{array}$$

The full table of such slices is given in Fig. 6.43. The partitions which define the transverse slices  $\bar{\mathcal{O}}_\mu \cap \mathcal{S}_\nu$ , that appear as the Higgs branches, are given as column and row headings.

### 6.1.2 Quivers for maximal special slices

When writing down the general quiver for a maximal special slice there are two options arising from the two different Hasse diagrams for a maximal special slices given in Fig. 3.10,  $\mathcal{S}_{(2m-1^2,1^2)} \in \mathfrak{so}_{4m}$  and  $\mathcal{S}_{(2m^2,1^2)} \in \mathfrak{so}_{4m+2}$ . The quivers associated to each of these general slices are given in Fig. 6.44. These can be established

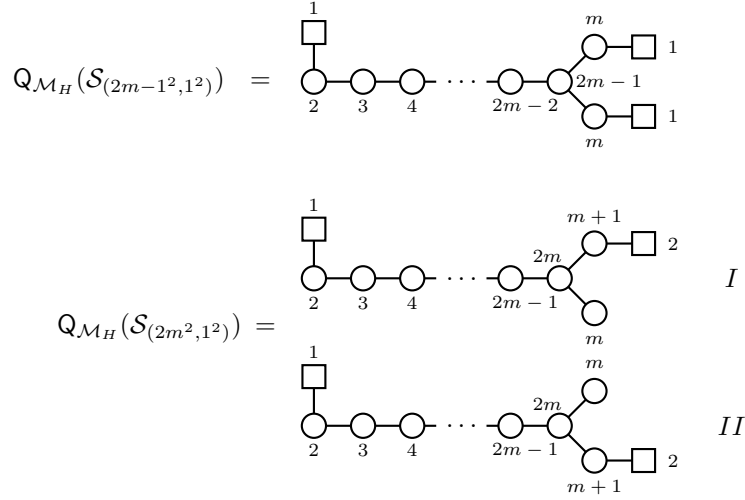


Figure 6.44: The  $D_n$  Dynkin quivers which realise the maximal special slices of  $\mathfrak{so}_{4m}$  and  $\mathfrak{so}_{4m+2}$  respectively as their Higgs branches.

by adding singularity quivers down any given route in the Hasse diagrams in Fig. 3.10, and can be checked in numerous ways. The first is balance, for a gauge node labelled  $c_i$  with flavour  $f_i$  balance means

$$2c_i = f_i + \sum_{c_j \text{ linked to } c_i} c_j. \quad (6.61)$$

It is easy to see that the quivers  $Q(\mathcal{S}_{(2m-1^2, 1^2)})$  and  $Q(\mathcal{S}_{(2m^2, 1^2)})$  in Fig. 6.44 fulfil this. Another test is Higgs branch dimension. For a general balanced unitary quiver, the Higgs branch dimension is given by

$$\dim_{\mathbb{H}}(\mathcal{M}_H(Q_{\text{bal}})) = \frac{1}{2} \sum_i c_i f_i.$$

$\dim_{\mathbb{H}}(\mathcal{S}_{(2m^2, 1^2)}) = m + 2$  and  $\dim_{\mathbb{H}}(\mathcal{S}_{(2m-1^2, 1^2)}) = m + 1$ , which the quivers for the maximal special slices also satisfy.

### 6.1.3 Quivers for special slice nilpotent varieties in $\mathfrak{so}_{2n}$

A theory  $Q_1$  descends from another theory,  $Q_2$ , if  $\mathcal{M}_H(Q_1) \subset \mathcal{M}_H(Q_2)$ . Clearly all the  $D_n$  Dynkin quivers concerned here<sup>6</sup> are descendants of  $Q_{\mathcal{M}_H}(\mathcal{S}_{(2m-1^2, 1^2)})$  (resp.  $Q_{\mathcal{M}_H}(\mathcal{S}_{(2m^2, 1^2)})$ ), given in Fig. 6.44. Instead of giving tables for small algebras, it is possible to write the general form for any theory one would expect to find as a descendant of  $Q_{\mathcal{M}_H}(\mathcal{S}_{(2m-1^2, 1^2)})$  or  $Q_{\mathcal{M}_H}(\mathcal{S}_{(2m^2, 1^2)})$ .

Because of (3.31), one needs to establish quivers for only 7 of the varieties listed in (3.29) and (3.30). The minimal degeneration  $\bar{\mathcal{O}}_{(2m^2)} \cap \mathcal{S}_{(2m-1^2, 1^2)} = A_{2m-1} \cup A_{2m-1}$  has been discussed, so only 6 general quivers need to be found. It transpires that all six can be written as one of two general forms given in Fig. 6.45. There are some conventions for reading these quivers also given in Fig. 6.45. The quivers for the six

<sup>6</sup> $Q(\mathcal{V})$  for  $\mathcal{V}$  a subvariety of the maximal special slice  $\mathcal{S}_{(2m-1^2, 1^2)}$  (resp.  $\mathcal{S}_{(2m^2, 1^2)}$ ), enumerated in (3.29) and (3.30).

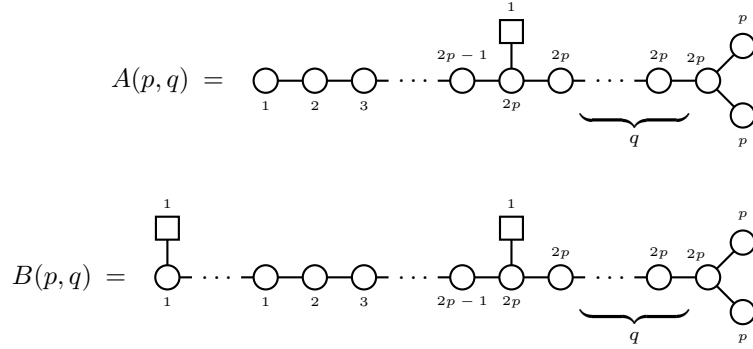


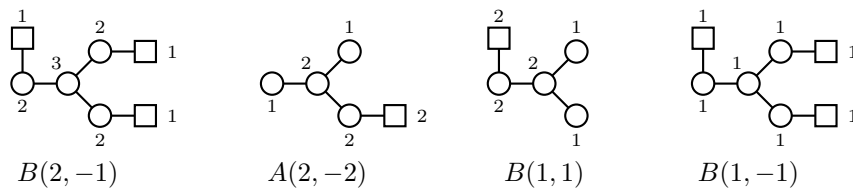
Figure 6.45: The general forms for the  $D_n$  Dynkin quivers which realise  $\mathfrak{so}_{2n}$  nilpotent varieties as their Higgs branches. The  $B(p, q)$  quiver always has  $2m$  (resp.  $2m + 1$ ) nodes for varieties in  $\mathfrak{so}_{4m}$  (resp.  $\mathfrak{so}_{4m+2}$ ). The conventions are that, in both quivers, when  $q = -1$  this corresponds to having a flavour of 1 on both end nodes, and when  $q = -2$  this corresponds to having a flavour 2 on one end node.

general nilpotent varieties that are left to find take the forms

$$\begin{aligned}
 \mathcal{Q}_{\mathcal{M}_H}(\bar{\mathcal{O}}_{\psi_j} \cap \mathcal{S}_{(2m^2)}) &= A(m - j, -2) \\
 \mathcal{Q}_{\mathcal{M}_H}(\bar{\mathcal{O}}_{\psi'_j} \cap \mathcal{S}_{(2m^2, 1^2)}) &= B(m - j + 1, 2m + 1) \\
 \mathcal{Q}_{\mathcal{M}_H}(\bar{\mathcal{O}}_{\psi_j} \cap \mathcal{S}_{\psi_k}) &= A(k - j, 2m - 2k - 2) \\
 \mathcal{Q}_{\mathcal{M}_H}(\bar{\mathcal{O}}_{\varphi_j} \cap \mathcal{S}_{\varphi_k}) &= A(k - j, 2m - 2k - 3) \\
 \mathcal{Q}_{\mathcal{M}_H}(\bar{\mathcal{O}}_{\psi_j} \cap \mathcal{S}_{\varphi_k}) &= B(k - j + 1, 2m - 2k - 3) \\
 \mathcal{Q}_{\mathcal{M}_H}(\bar{\mathcal{O}}_{\psi'_j} \cap \mathcal{S}_{\varphi'_k}) &= B(k - j, 2m - 2k - 4).
 \end{aligned}
 \tag{6.62}$$

These have been established using quiver addition and using the Hasse subdiagrams of Fig. 3.10 which correspond to each subvariety as a guide. The claim that these are all the  $\mathfrak{so}_{2n}$  nilpotent varieties appearing as moduli space branches of  $D_4$  Dynkin quivers is confirmed in the next section. There, the singularity structure of general good  $D_n$  Dynkin quivers is found and a comparison with the known singularity structure of any further  $\mathfrak{so}_{2n}$  nilpotent varieties is made. This shows that none of the  $D_n$  Dynkin quivers have further  $\mathfrak{so}_{2n}$  varieties as moduli space branches.

**$D_4$  example** (6.62) can be used to reproduce the results for  $D_4$  quivers relatively easily. There were only 4  $D_4$  Dynkin quivers which realised nilpotent varieties of  $\mathfrak{so}_{4m}$  (so  $m = 2$ ) which weren't also singularities. These were the quivers





whose appearance as the quivers which realised  $\mathfrak{so}_8$  nilpotent varieties as their Higgs branches can be checked:

$$\begin{aligned}
\mathbb{Q}_{\mathcal{M}_H}(\bar{\mathcal{O}}_{(7,1)} \cap \mathcal{S}_{(3^2,1^2)}) &= \mathbb{Q}_{\mathcal{M}_H}(\bar{\mathcal{O}}_{\psi_0} \cap \mathcal{S}_{\varphi_1}) = B(2, -1) \\
\mathbb{Q}_{\mathcal{M}_H}(\bar{\mathcal{O}}_{(7,1)} \cap \mathcal{S}_{(4^2)}) &= \mathbb{Q}_{\mathcal{M}_H}(\bar{\mathcal{O}}_{\psi_0} \cap \mathcal{S}_{(2m^2)}) = A(2, -2) \\
\mathbb{Q}_{\mathcal{M}_H}(\bar{\mathcal{O}}_{(7,1)} \cap \mathcal{S}_{(5,1^3)}) &= \mathbb{Q}_{\mathcal{M}_H}(\bar{\mathcal{O}}_{\psi_0} \cap \mathcal{S}_{\varphi_0}) = B(1, 1) \\
\mathbb{Q}_{\mathcal{M}_H}(\bar{\mathcal{O}}_{(5,3)} \cap \mathcal{S}_{(3^2,1^2)}) &= \mathbb{Q}_{\mathcal{M}_H}(\bar{\mathcal{O}}_{\psi_1} \cap \mathcal{S}_{\varphi_1}) = B(1, -1).
\end{aligned} \tag{6.63}$$

Here the variety is written in the form of (3.29), the type of quiver read from (6.62) and Fig. 6.45 used to draw the quiver. This reproduces the familiar  $D_4$  results.

## 6.2 Balanced $D_n$ Dynkin quivers

Which varieties *do*  $D_n$  Dynkin quivers realise with their moduli space branches? And is there a way of writing down a simple, complete description of every possible good  $D_n$  Dynkin quiver which also provides a simple means by which to extract moduli space information<sup>7</sup>? This section tackles both problems simultaneously. The full singularity structure of the moduli space varieties of  $D_n$  Dynkin quivers is provided and a classification based on that structure established. The analysis is performed without explicit reference to a brane construction in order to inform generalisations to quivers with no such description.

When discussing  $D_n$  Dynkin quivers with nilpotent varieties of  $\mathfrak{so}_{2n}$  as their moduli space branches, essential building blocks were those quivers which correspond to the minimal degenerations, or singularities. The singularities are  $A_k$ ,  $a_k$ ,  $A_k \cup A_k$  and  $D_k$ . These are the basic building blocks used to investigate the local structure of the moduli spaces for  $D_n$  Dynkin quivers. In conjuncture with this structure, there is a natural characterisation of all good  $D_n$  Dynkin quivers. The simplest subclass to tackle is that of *balanced*  $D_n$  Dynkin quivers, which are investigated first.

At the level of the quiver, balance is the requirement that the sum of all the nodes connected to a given gauge node by an edge (flavours and other gauge nodes) is exactly double the rank of the given gauge node. This is referred to as the gauge node having zero *excess*. Consider a general quiver with gauge nodes with positive rank  $g^i$ , where the upper index refers to some ordering of the gauge nodes. Attached to these gauge nodes are flavour nodes with non-negative label  $f^i$ . For each gauge node  $g^i$ , consider the set of gauge nodes which are connected to  $g^i$  via an edge. This will be a collection of gauge nodes labelled with indices in the set  $j_i$ . The condition of balance is then

$$e^i = f^i - 2g^i + \sum_{k \in j_i} g^k = 0. \tag{6.64}$$

Balance imposes a general restriction to  $D_n$  Dynkin quivers. The difference in the flavour attached to each of the end nodes must be even. For the quiver in Fig. 6.38 this means that  $f' - f'' \equiv 0 \pmod{2}$ . For concreteness take  $f'' \geq f'$ . Consider the situation where the difference in flavour is odd, that is,  $f'' = f' + 2b + 1$ . Balancing the end nodes requires that  $g' = \frac{1}{2}(f' + g_{n-2})$  and so  $f' + g_{n-2}$  must be even, but also that  $g'' = \frac{1}{2}(f' + 2b + 1 + g_{n-2})$ , so  $f' + g_{n-2}$  must be odd. An odd difference in flavour is therefore

<sup>7</sup>In analogy to the way the moduli space varieties of a linear ( $A_n$  Dynkin) quiver and the name of that quiver are related.

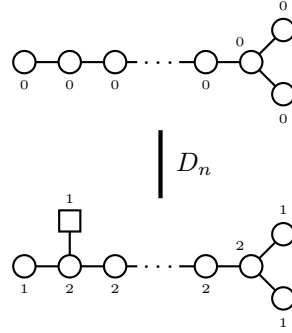


Figure 6.46: The only possible balanced singularity to consistently (maintaining balance) add to a bare  $D_n$  Dynkin quiver is the  $D_n$  singularity. This is drawn below the bare quiver when constructing the Hasse diagram because the Higgs branches of the quivers realise Slodowy slices which correspond to edges in the Hasse diagram *dominating* the node at which the quiver sits, as per the discussion.

unbalanceable. This will become important later for good  $D_n$  Dynkin quivers, but for now all it means is that the balanced quivers must have  $f' - f''$  even. Using nomenclature that will be introduced in more detail in the discussion of good quivers, this is the restriction that all balanced  $D_n$  Dynkin quivers must be of *even type*.

The local moduli space analysis and classification of balanced  $D_n$  Dynkin quivers arises via the imbuing of poset structure onto the set of balanced quivers. In this analysis, this structure will be based on the inclusion relations of the Higgs branches of the theories. This structure will be illustrated using a Hasse diagram built up using quiver addition.

The premise of quiver addition is that, for a given quiver, there exists at least one ‘larger’ quiver from which the first quiver could have been found via the removal of a singularity from the larger quiver. Using the realisation of singularities as (sub)quivers, one can find all of the larger quivers for a given quiver by ‘adding back’ the singularities. If one does this starting with some minimal quiver, and does so while insisting on maintaining balance at all times, one can recover *any* balanced  $D_n$  Dynkin quiver. This procedure also gives the set of balanced  $D_n$  Dynkin quivers the desired poset structure, which is illustrated by the Hasse diagram one constructs by adding the slices back. Furthermore, since this procedure is based off of the transverse slice structure of the Higgs branches of the theories, one has automatically generated the Hasse diagram representing the singularity structure of the varieties that these quivers realise as moduli space branches. Once this poset structure is uncovered, the classification of balanced  $D_n$  Dynkin quivers follows simply. As each node in the Hasse diagram represents a unique balanced  $D_n$  Dynkin quiver, and every quiver is in the diagram, a unique label for every node gives a unique label for every quiver.

The smallest balanced  $D_n$  Dynkin quiver is the flavourless trivial quiver at the top of Fig. 6.46. All gauge nodes are trivially balanced. Note that a gauge node of rank zero cannot be balanced unless all gauge nodes are zero. Therefore the only transverse slice it is possible to add whilst maintaining balance is  $D_n$ , this addition is given in Fig. 6.46. Recall that the manipulation of the quivers is performed in the Higgs branch geometry so the Hasse diagram is drawn descending from the trivial theory at the top.

From here there are two options. The single flavour on the second node might have been the result of an  $A_1$  transition in the end node of the tail, or a  $D_{n-2}$  transition in the third through  $n^{\text{th}}$  nodes. Both of these

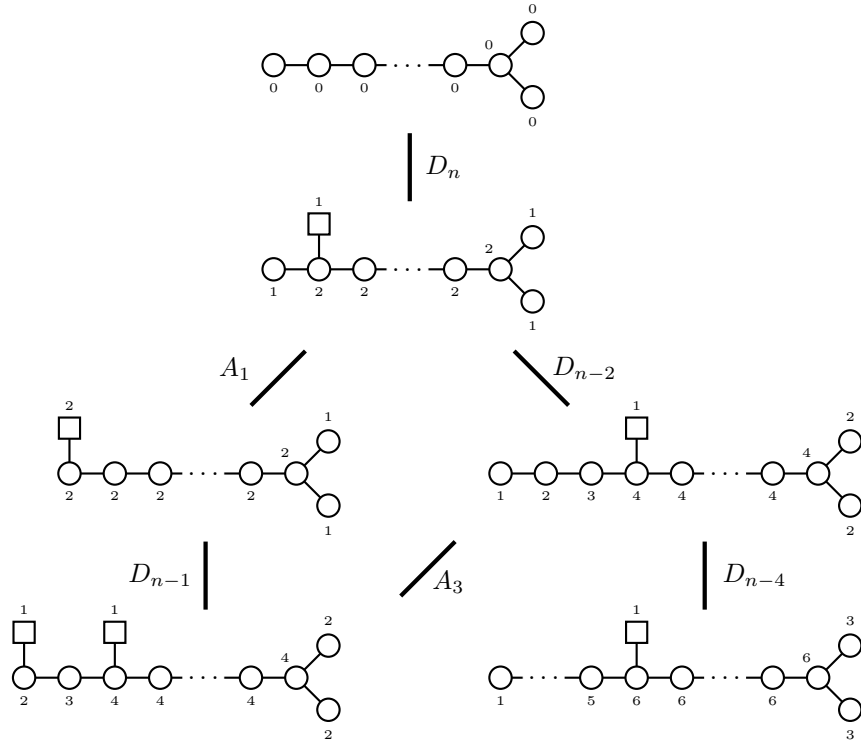


Figure 6.47: More of the Hasse diagram for completely balanced  $D_n$  Dynkin quivers with the added singularities indicated by the labels of the edges. Again, because the quivers' Higgs branches are Slodowy slices, to be consistent with how singularity structure is read from Hasse diagrams, the larger quivers are placed lower.

possibilities are added, Fig. 6.47. Now the only transverse slice that can be added to the right hand theory is  $D_{n-1}$ , whereas the left hand theory could have an  $A_3$  or  $D_{n-4}$  added to it. Note that adding  $D_{n-1}$  to the right hand theory or  $A_3$  to the left hand theory results in the same parent quiver. Each theory should be a single node in the Hasse diagram and so the structure drawn in Fig. 6.47 reflects this. This process may be continued indefinitely but the structure is very regular. For general<sup>8</sup>  $n$  the structure of the balanced  $D_n$  Dynkin quiver Hasse diagram is given in Fig. 6.48.

The structure of the balanced Hasse diagram is that of Hasse diagrams for partitions of even integers with  $D_k$  traversing structure. This provides the means to classify the balanced  $D_n$  Dynkin diagrams very neatly. The problem of classification is now as follows: For a given  $n$ , how can every node of this balanced Hasse diagram be labelled uniquely? The interpretation of the Hasse diagram as even magnitude partition subdiagrams with traversing structure provides an easy answer. Assign to every node in Fig. 6.48 the partition,  $\kappa$ , which denotes the place of that node in its partition Hasse subdiagram<sup>9</sup>. In this way every balanced  $D_n$  Dynkin quiver can be specified with the integer  $n$  and the partition  $\kappa$ . The class of balanced  $D_n$  Dynkin quivers is therefore denoted  $D_\kappa(n)$ .

Assigning these partitions to the theories has a natural interpretation in terms of the distribution of flavours across the quiver. By writing the flavours as in Fig. 6.49, the partition to which the theory is as-

<sup>8</sup>What happens when a specific value of  $n$  is chosen is explored momentarily.

<sup>9</sup>Importantly, these partitions are *not* partitions for the nilpotent varieties of  $\mathfrak{so}_{2n}$ . These even magnitude partitions are not otherwise restricted.

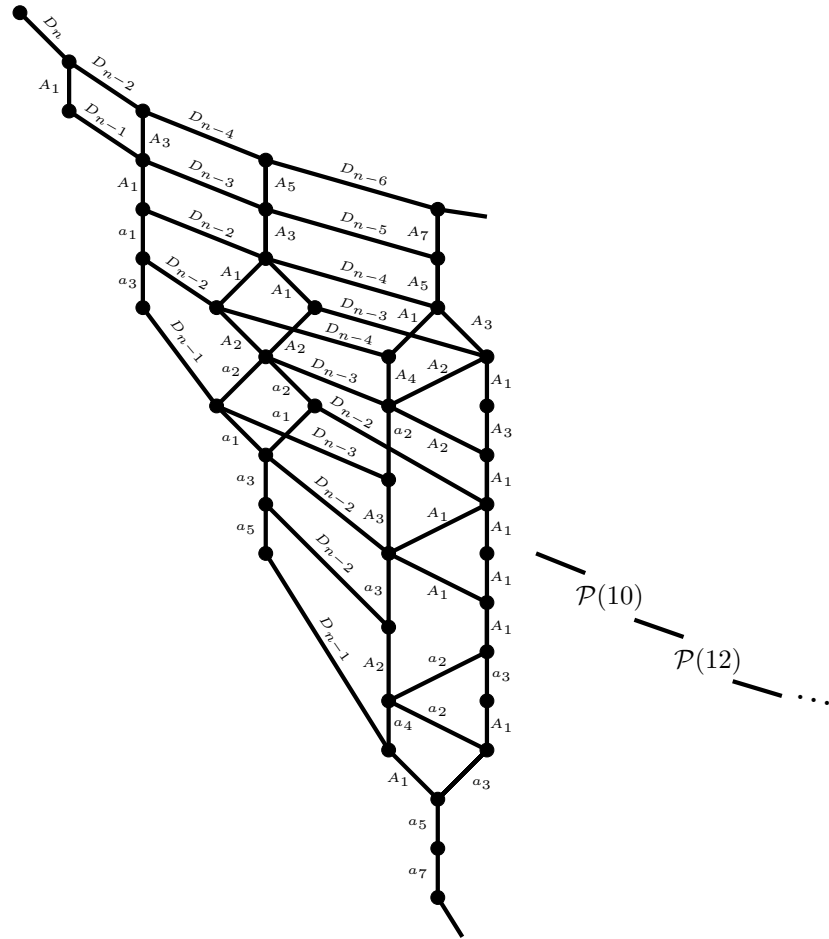


Figure 6.48: The Hasse diagram resulting from balanced quiver addition for a generic  $D_n$  Dynkin quiver. The diagram takes the form of linear subdiagrams of even magnitude partition Hasse diagrams with  $D_k$  singularity traversing structure. The Hasse diagram for the maximal special slice is readily identifiable as the top two lines of traversing structure. Clearly when a specific value of  $n$  is chosen, some of the traversing structure edges become undefined, this is dealt with momentarily via an editing prescription.

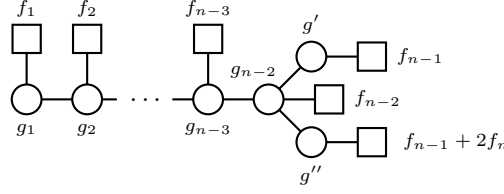
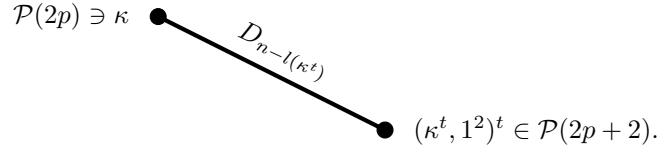


Figure 6.49: The necessary form of a balanced  $D_n$  Dynkin quiver. This naming convention for the flavours is the one used for all the quivers of even type and allows for easy interpretation between a theory's quiver, name and moduli space singularity structure.

signed is

$$\kappa = (n^{f_n}, n-1^{f_{n-1}}, \dots, 2^{f_2}, 1^{f_1}). \quad (6.65)$$

Having labelled the nodes with these partitions the balanced Hasse diagram can be written more compactly as a sequence of partition Hasse diagrams along with an edge diagram capturing the traversing structure:



It is necessary to consider when the construction given in Fig. 6.48 needs editing. For a specific and finite  $n$ , there are obvious issues which arise. For a node  $\kappa$  such that  $n-l(\kappa^t) < 2$ , the traversing edge which descends from the node represents a singularity which is not defined. In such circumstances one needs to edit the construction by removing or replacing some nodes and edges in a systematic way. This will be discussed in a moment.

We begin with a proof that the construction in Fig. 6.48 does indeed contain every balanced  $D_n$  Dynkin quiver by proving that balancing the quiver in Fig. 6.49 requires the flavour to be distributed in the quiver such that the partition (6.65) is of even magnitude. Since two different partitions necessarily give a different flavour distribution, such a proof demonstrates that every balanced  $D_n$  quiver lives at a unique node in Fig. 6.48, and so the classification for balanced quivers is complete.

**Proposition.** A balanced  $D_n$  Dynkin quiver must take the form of Fig. 6.49 with an *even* magnitude partition. Also  $l(\kappa) = g_1$  and  $|\kappa| = 2g''$ .

**Corollary.** The class  $D_\kappa(n)$  contains every balanced  $D_n$  Dynkin quiver.

**Proof.** Proving the proposition and corollary above requires demonstrating that balancing Fig. 6.49 requires  $\kappa$  to have even magnitude, that is,  $|\kappa| = \sum_{i=1}^n i f_i = 2x$  for some  $x$ . Also recall that  $l(\kappa) = \sum_{i=1}^n f_i$ .

The left hand gauge node of Fig. 6.49 is of rank  $g_1$ . Balancing this node requires  $2g_1 = f_1 + g_2$  and so  $g_2 = 2g_1 - f_1$ . Now consider balancing the second node, this requires that  $2g_2 = g_1 + f_2 + g_3$  and so  $g_3 = 2g_2 - g_1 - f_2 = 3g_1 - 2f_1 - f_2$ . Balancing the nodes along the tail one at a time in this manner yields the balance criteria

$$g_k = k g_1 - \sum_{i=1}^{k-1} (k-i) f_i \quad (6.66)$$

for  $k \leq n - 2$ . Applying this to the  $n - 2^{\text{th}}$  node and rearranging terms yields

$$\begin{aligned} g_{n-2} &= (n-2)g_1 - \sum_{i=1}^{n-3} (n-2-i)f_i \\ &= (n-2)g_1 - (n-2) \sum_{i=1}^{n-3} f_i + |\kappa| - \sum_{i=n-2}^n i f_i. \end{aligned} \quad (6.67)$$

This is one of two equations which give a balancing condition on  $g_{n-2}$ . The other comes from balancing  $g_{n-2}$  directly such that  $2g_{n-2} = g_{n-3} + f_{n-2} + g' + g''$ . Using the balance requirements of  $g'$  and  $g''$ , that is,  $2g' = g_{n-2} + f_{n-1}$  and  $2g'' = g_{n-2} + f_{n-1} + 2f_n$ , gives

$$g_{n-2} = g_{n-3} + \sum_{i=n-2}^n f_i \quad (6.68)$$

Writing  $g_{n-3}$  explicitly using (6.66), equating (6.67) to (6.68) and rearranging for  $|\kappa|$  gives

$$\begin{aligned} |\kappa| &= -g_1 - (n-3) \sum_{i=1}^{n-4} f_i + \sum_{i=1}^{n-4} i f_i + \sum_{i=n-2}^n f_i + (n-2) \sum_{i=1}^{n-3} f_i + \sum_{i=n-2}^n i f_i \\ &= -g_1 + \sum_{i=1}^n i f_i - (n-3)f_{n-3} - (n-3) \sum_{i=1}^{n-4} f_i + (n-3) \sum_{i=1}^{n-3} f_i + \sum_{i=1}^{n-3} f_i + \sum_{i=n-2}^n f_i \\ &= -g_1 + l(\kappa) + |\kappa|, \end{aligned}$$

so  $g_1 = l(\kappa)$ . When moving from lines one to two the third and sixth terms go to make the second and third terms. The first, second and fourth terms are pulled through and the fifth term is split into terms five and six. From lines two to three, term two is just  $|\kappa|$ , the last two terms come together to form  $l(\kappa)$ , the middle three terms cancel. Returning to (6.67), rearranging for  $|\kappa|$  and using  $g_1 = l(\kappa)$  gives

$$\begin{aligned} |\kappa| &= g_{n-2} - (n-2)l(\kappa) - (n-2) \sum_{i=1}^{n-3} f_i + \sum_{i=n-2}^n i f_i \\ &= g_{n-2} - (n-2)(f_{n-2} + f_{n-1} + f_n) + (n-2)f_{n-2} + (n-1)f_{n-1} + n f_n \\ &= 2f_n + f_{n-1} + g_{n-2} \\ &= 2g'', \end{aligned} \quad (6.69)$$

where the  $g''$  balance requirement was used in the final line (the  $g'$  balance requirement would have also worked). This completes the proof that balancing the quiver imposes that the magnitude of  $\kappa$  is even, proving the proposition. Every node in the balanced Hasse diagram is a different quiver. Each quiver is determined completely by  $n$  and  $\kappa$ . Therefore exactly one balanced quiver can be associated to each  $(n, \kappa)$  pair, this is the quiver which appears in the balanced Hasse diagram, Fig. 6.48. All balanced  $D_n$  Dynkin quivers are present so the class  $D_\kappa(n)$  contains all balanced  $D_n$  Dynkin quivers exactly once.

There remains the task of establishing a systematic editing of the Fig. 6.48 construction when a specific value of  $n$  is chosen. This can be investigated in a number of corresponding ways. As mentioned already, for  $\kappa$  with  $n - l(\kappa^t) < 2$  the edge labels become undefined. It is also clear that there is no interpretation in the

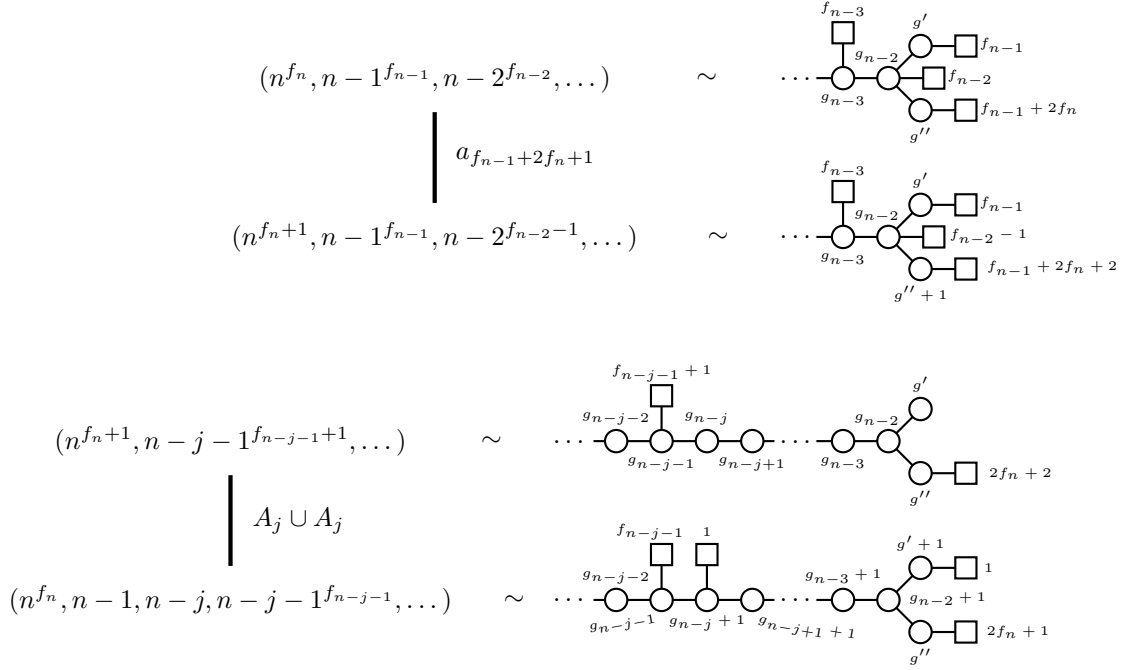


Figure 6.50: The editing prescription for the balanced  $D_n$  Hasse diagram given in Fig. 6.48 when a specific value of  $n$  is chosen and some edges become undefined. Once the offending edges and nodes have been removed, some edges must be added back into the Hasse diagram. This can be calculated from the point of view of the partitions assigned to the nodes between which the edges lie, or by appealing to the structure of the quiver in those circumstances, both are presented here.

style of (6.65) and Fig. 6.49 when the largest part of  $\kappa$  is larger than  $n$ . For  $n - l(\kappa^t) < 2$  to be true, it must be the case that  $\kappa$  contains parts larger than  $n - 2$ . Therefore the traversing structure for the nodes labelled with  $\kappa$  with no parts larger than  $n - 2$  is unaffected in the editing. There is also simply no theory corresponding to partitions with largest part larger than  $n$ . The editing prescription is then as follows:

**Editing prescription** To write down the balanced Hasse diagram for  $D_n$  Dynkin quivers for some specific  $n$ , start with the general construction Fig. 6.48. Identify in this construction all of the nodes with parts larger than  $n$  and delete them and all the edges depending on them. Now identify the partitions with one or more parts equal to  $n$  and/or  $n - 1$ , change the edges coming from these nodes systematically using Fig. 6.50.

An illustrative example of the editing necessary for the Hasse diagram for  $D_\kappa(4)$  for  $|\kappa| \leq 8$  is given in Fig. 6.51. Notice how those  $D_4$  Dynkin quivers which realise  $\mathfrak{so}_8$  nilpotent varieties are the tiny number living at the very top of the final  $D_4$  balanced Hasse diagram. Fig. 6.51 is limited to  $|\kappa| \leq 8$  for practical purposes, the full  $D_4$  balanced Hasse diagram can be expanded using quiver addition forever.

### 6.2.1 Dimension matching for balanced theories

Calculating the dimension of the moduli space branches of balanced  $D_n$  Dynkin quivers gives a useful check of the construction and analysis in Fig. 6.48. The simplest calculation is that of the dimension of the Higgs branch of  $D_\kappa(n)$  using Fig. 6.48. This requires picking a route from the node corresponding to the theory up to the top of Fig. 6.48.

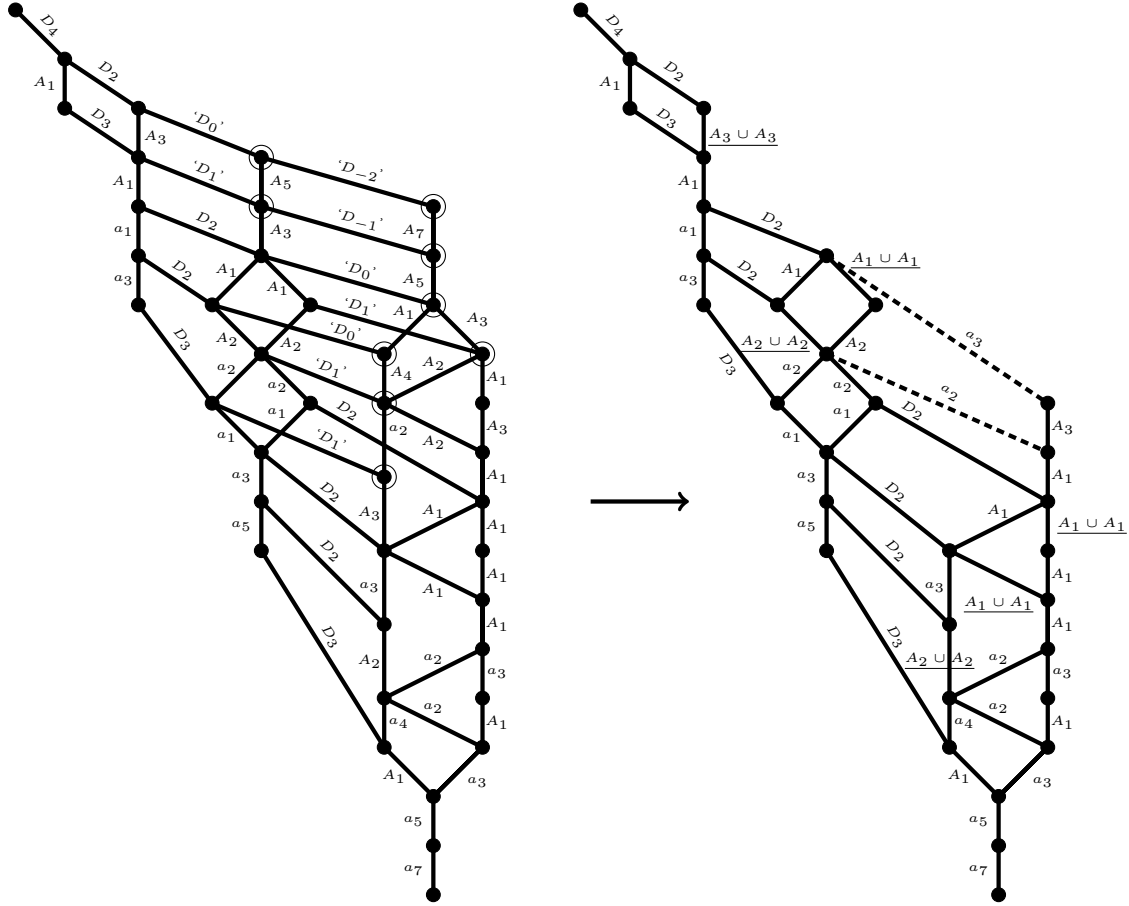


Figure 6.51: An example of the editing prescription for the balanced Hasse diagram to explicitly find the diagram for  $D_\kappa(4)$  for  $|\kappa| \leq 8$ . On the left we draw the general construction from Fig. 6.48 with  $n = 4$ . The nodes corresponding to partitions with parts that are too big are circled and the labels of those edges which are no longer viable are in inverted commas. On the right the nodes with parts that are too large and edges with undefined labels have been removed as per the prescription and the new edges have been edited and added as per Fig. 6.50. This structure can be explicitly verified using quiver addition on  $D_4$  Dynkin quivers. At the very top of the structure, the top five nodes take on the form of the maximal special slice Hasse diagram for  $D_4$ . As observed in Fig. 6.48, the top two lines of traversing structure of the general case gives the Hasse subdiagram for the maximal special slice of the corresponding  $\mathfrak{so}_{2n}$  algebra. When a specific value of  $n$  is chosen, much of this structure is edited away. Since this subdiagram was the only part which appeared in both the Hasse diagram for nilpotent orbits of  $\mathfrak{so}_8$  and in the balanced Hasse diagram for  $D_4$  Dynkin quivers, this once again shows that  $D_4$  Dynkin quivers cannot realise nilpotent varieties of  $\mathfrak{so}_8$  outside the maximal special slice (The  $A_1$  from partitions  $(3, 1)$  to  $(2^2)$  also appears in  $\mathfrak{so}_8$ , but is incidental here and is not a feature repeated for other algebras).



The simple route to choose is to go from the node labelled  $\kappa$  up to the top of the linear subdiagram of nodes (covering the  $\mathfrak{sl}_n$  Slodowy slice to the  $\mathfrak{sl}_n$  nilpotent orbit  $\bar{O}_\kappa$ ) then along the  $D_k$  transitions at the top of the diagram. This gives

$$\dim_{\mathbb{H}}(\mathcal{M}_H(D_\kappa(n))) = \dim_{\mathbb{H}}(\mathcal{S}_\kappa) + \sum_{j=0}^{|\kappa|-2} \dim_{\mathbb{H}}(D_{n-j}) = \frac{1}{2} \left( \sum_i (\kappa_i^t)^2 - |\kappa| \right) + \frac{1}{2} |\kappa| = \frac{1}{2} \sum_i (\kappa_i^t)^2, \quad (6.70)$$

where the sum over  $i$  is the sum over all the nonzero parts of the partition in each summation. The dimension of  $\mathfrak{sl}_n$  nilpotent varieties can be found in [31].

A general calculation requires a general route up through Fig. 6.48 from the node  $\kappa$  to the top. This route will go from  $\kappa$  up to some node in  $\mathcal{P}(|\kappa|)$  which dominates  $\kappa$  and is of the form  $(\eta^t, 1^2)^t$  (this is required by the traversing structure). There the route traverses up to the node  $\eta \in \mathcal{P}(|\kappa| - 2)$  and then up to some other node in  $\mathcal{P}(|\kappa| - 2)$  of appropriate form and across again, and so on up to the top of Fig. 6.48.

Denote the *lowest* visited node in each linear subsystem  $\mathcal{P}(d)$  as  $\lambda_d$ . The highest node in  $\mathcal{P}(d)$  which the route passes through is then specified via the traversing structure by  $\lambda_{d-2}$ . Under this notation  $\lambda_{|\kappa|} = \kappa$  and  $\lambda_0 = (0)$ . Using this notation the dimension of a general route up through Fig. 6.48 is

$$\begin{aligned} \dim_{\mathbb{H}}(\mathcal{M}_H(D_\kappa(n))) &= \sum_{j=0, \text{ even}}^{|\kappa|-2} \left[ \dim_{\mathbb{H}} \left( D_{n-l(\lambda_{|\kappa|-j-2}^t)} \right) + \dim_{\mathbb{H}} \left( \mathcal{S}_{\lambda_{|\kappa|-j}} \cap \bar{O}_{(\lambda_{|\kappa|-j-2}^t, 1^2)^t} \right) \right] \\ &= \frac{1}{2} |\kappa| + \sum_{j=0, \text{ even}}^{|\kappa|-2} \frac{1}{2} \left[ \sum_i ((\lambda_{|\kappa|-j}^t)_i)^2 - \sum_i ((\lambda_{|\kappa|-j-2}^t)_i)^2 - 2 \right] \\ &= \frac{1}{2} \left( \sum_i ((\lambda_{|\kappa|}^t)_i)^2 - \sum_i ((\lambda_0^t)_i)^2 \right) \\ &= \frac{1}{2} \sum_i (\kappa_i^t)^2. \end{aligned} \quad (6.71)$$

Once again, sums over  $i$  mean sums over all the nonzero parts in the partition and the nilpotent varieties are those found in  $\mathfrak{sl}_n$  algebras. The general route agrees with the first, simpler, calculation, as expected since the dimensions ought to be route-independent.

The quaternionic dimension of the Coulomb branch for a unitary quiver gauge theory is the sum of the ranks of the gauge nodes, therefore the dimension of the Coulomb branch for the  $D_p$  singularity quiver is

$$\dim_{\mathbb{H}}(\mathcal{M}_C(\mathbb{Q}_{\mathcal{M}_H}(D_p))) = 2p - 3 = \dim_{\mathbb{H}}(d_p), \quad (6.72)$$

where  $d_p$  is the mirror variety to  $D_p$ .

The construction in Fig. 6.48 can be checked by calculating the dimension of the Coulomb branch of a  $D_n$  Dynkin quiver in two different ways. The first way is to sum over the ranks of all the nodes of a general balanced  $D_n$  Dynkin quiver, Fig. 6.49. The second way is to sum over the mirror varieties of a general route up through Fig. 6.48. For  $\mathfrak{sl}_n$  nilpotent varieties the mirror of  $\mathcal{S}_\rho \cap \bar{O}_\sigma$  is  $\mathcal{S}_{\sigma^t} \cap \bar{O}_{\rho^t}$ .

Before proving the equality of the results of these methods it is worth recalling a small result which will

form an essential step. Given a general partition  $\eta = (z^{y_z}, \dots, 1^{y_1})$ ,

$$\sum_i (((\eta, 1^a)^t)_i)^2 = \left( \sum_{m=1}^z y_m + a \right)^2 + \sum_{q=2}^z \left( \sum_{m=q}^z y_m \right)^2 = a^2 + 2l(\eta)a + \sum_i (\eta_i^t)^2 \quad (6.73)$$

generalizing the result used previously.

**Proposition.** Fig. 6.48 passes the Coulomb branch dimension check, that is,

$$\begin{aligned} \dim_{\mathbb{H}}(\mathcal{M}_C(D_\kappa(n))) &= \sum_{k=1}^{n-2} \left[ kg_1 - \sum_{i=1}^{k-1} (k-i)f_i \right] + g' + g'' \\ &= \sum_{j=0, \text{ even}}^{|\kappa|-2} \left[ \dim_{\mathbb{H}} \left( \mathcal{M}_C \left( \mathcal{Q}_{\mathcal{M}_H} \left( D_{n-l(\lambda_{|\kappa|-j-2}^t)} \right) \right) \right) + \dim_{\mathbb{H}} \left( \text{Mirror}(\mathcal{S}_{\lambda_{|\kappa|-j}} \cap \bar{\mathcal{O}}_{(\lambda_{|\kappa|-j-2}^t, 1^2)^t}) \right) \right]. \end{aligned} \quad (6.74)$$

In fact

$$\dim_{\mathbb{H}}(\mathcal{M}_C(D_\kappa(n))) = \frac{1}{2} |\kappa| (2n-1) - \frac{1}{2} \sum_i (\kappa_i)^2. \quad (6.75)$$

**Proof.** Both lines on the right of (6.74) equal the right side of (6.75). Firstly,

$$\begin{aligned} & \sum_{j=0, \text{ even}}^{|\kappa|-2} \left[ \dim_{\mathbb{H}} \left( \mathcal{M}_C \left( \mathcal{Q}_{\mathcal{M}_H} \left( D_{n-l(\lambda_{|\kappa|-j-2}^t)} \right) \right) \right) + \dim_{\mathbb{H}} \left( \text{Mirror}(\mathcal{S}_{\lambda_{|\kappa|-j}} \cap \bar{\mathcal{O}}_{(\lambda_{|\kappa|-j-2}^t, 1^2)^t}) \right) \right] \\ &= \sum_{j=0, \text{ even}}^{|\kappa|-2} \left[ 2(n-l(\lambda_{|\kappa|-j-2}^t)) - 3 + \dim_{\mathbb{H}} \left( \bar{\mathcal{O}}_{\lambda_{|\kappa|-j}} \cap \mathcal{S}_{(\lambda_{|\kappa|-j-2}^t, 1^2)} \right) \right] \\ &= \sum_{j=0, \text{ even}}^{|\kappa|-2} \left[ 2n-3 - 2l(\lambda_{|\kappa|-j-2}^t) + \frac{1}{2} \left( \sum_i (((\lambda_{|\kappa|-j-2}^t, 1^2)^t)_i)^2 - \sum_i ((\lambda_{|\kappa|-j})_i)^2 \right) \right] \\ &= \sum_{j=0, \text{ even}}^{|\kappa|-2} \left[ 2n-3 - 2l(\lambda_{|\kappa|-j-2}^t) - \frac{1}{2} \left( \sum_i ((\lambda_{|\kappa|-j})_i)^2 \right) \right. \\ & \quad \left. + \frac{1}{2} \left( 4 + 4l(\lambda_{|\kappa|-j-2}^t) + \sum_i ((\lambda_{|\kappa|-j-2})_i)^2 \right) \right] \\ &= \sum_{j=0, \text{ even}}^{|\kappa|-2} \left[ 2n-1 + \frac{1}{2} \sum_i ((\lambda_{|\kappa|-j-2})_i)^2 - \frac{1}{2} \sum_i ((\lambda_{|\kappa|-j})_i)^2 \right] \\ &= \frac{1}{2} |\kappa| (2n-1) + \frac{1}{2} \sum_i ((\lambda_0)_i)^2 - \frac{1}{2} \sum_i ((\lambda_{|\kappa|})_i)^2 \\ &= \frac{1}{2} |\kappa| (2n-1) - \frac{1}{2} \sum_i (\kappa_i)^2. \end{aligned} \quad (6.76)$$

The most important steps in (6.76) are from lines three to four where (6.73) was used and from lines five to six where the sum over  $j$  is assessed, which results in massive cancellation between the  $i$  sums.

For the second part, begin with the realisation that

$$\begin{aligned} \sum_{k=1}^{n-2} \left[ k g_1 - \sum_{i=1}^{k-1} (k-i) f_i \right] + g' + g'' &= g_1 \sum_{k=1}^{n-2} k - \sum_{k=1}^{n-2} \sum_{i=1}^k (k-i) f_i + g' + g'' \\ &= \frac{1}{2} g_1 (n-2)(n-1) + g' + g'' - \sum_{l=1}^{n-3} \left[ f_l \sum_{j=1}^{n-2-l} j \right] \end{aligned} \quad (6.77)$$

which can be found by expanding the second term of the right of the first line directly, and rearranging. Assessing the  $j$  sum and substituting the values of  $g'$  and  $g''$  in terms of  $\kappa$  and  $f_n$  known from balancing yields

$$\begin{aligned} &\frac{1}{2} g_1 (n-2)(n-1) + |\kappa| - f_n - \sum_{l=1}^{n-3} \frac{1}{2} f_l (n-2-l)(n-1-l) \\ &= \frac{1}{2} \left( \sum_{l=1}^n f_l \right) (n-2)(n-1) + |\kappa| - f_n \\ &\quad - \frac{1}{2} \left( \sum_{l=1}^{n-3} f_l \right) (n-2)(n-1) + \frac{1}{2} (2n-3) \sum_{l=1}^{n-3} l f_l - \frac{1}{2} \sum_{l=1}^{n-3} l^2 f_l \\ &= \frac{1}{2} \left( \sum_{l=n-2}^n f_l \right) (n-2)(n-1) + |\kappa| - f_n - \frac{1}{2} (2n-3) \sum_{l=1}^{n-3} l f_l - \frac{1}{2} \sum_{l=1}^{n-3} l^2 f_l \\ &= \frac{1}{2} |\kappa| (2n-1) + \frac{1}{2} \left[ (n^2 - 3n + 2) \left( \sum_{l=n-2}^n f_l \right) - (2n-3) \left( \sum_{l=n-2}^n l f_l \right) - 2f_n - \sum_{l=1}^{n-3} l^2 f_l \right] \\ &= \frac{1}{2} |\kappa| (2n-1) + \frac{1}{2} \left[ - \sum_{l=1}^n l^2 f_l \right] \\ &= \frac{1}{2} |\kappa| (2n-1) - \frac{1}{2} \sum_i (\kappa_i)^2, \end{aligned} \quad (6.78)$$

as required, completing the proof. From line one to two the  $(n-2-l)(n-1-l)$  term was expanded and  $g_1$ ,  $g'$  and  $g''$  written in terms of flavours and  $\kappa$ . From line two to three, terms one and four mostly cancel with one another. From lines three to four

$$\sum_{l=1}^{n-3} l f_l = \sum_{l=1}^n l f_l - \sum_{n-2}^n l f_l = |\kappa| - \sum_{l=n-2}^n l f_l. \quad (6.79)$$

was used. From lines four to five the two sums over  $\{n-2, n-1, n\}$  were assessed and the terms in the square brackets simplify considerably.

### 6.3 From balanced to good quivers

So far the discussion has classified all balanced  $D_n$  Dynkin quivers by appealing to their moduli space singularity structure. The class  $D_\kappa(n)$  of balanced quivers can be ordered into a Hasse diagram as in Fig. 6.48 by appealing to the moduli space inclusion relations. Classification of all *good*  $D_n$  Dynkin quivers can now also be performed. Whereas the gauge node excesses of balanced quivers must be zero, the excesses for good

quivers need only be non-negative. Balanced quivers are therefore a subset of good quivers for a given gauge node topology.

Given a complete set of balanced quivers for a class of quivers with a given gauge node topology, one can construct a set of good quivers fairly easily using quiver subtraction introduced in [64]. A quiver,  $Q_1$ , can only be subtracted from another quiver,  $Q_2$ , to give a third quiver,  $Q_3$ , if  $Q_1$  and  $Q_2$  have the same gauge node topology and if the gauge nodes in  $Q_3$  have non-negative rank<sup>10</sup>.

Consider two balanced quivers  $Q_{\text{bal}}^1$  and  $Q_{\text{bal}}^2$  with gauge nodes with positive rank  $g_i^1$  and  $g_i^2$  respectively<sup>11</sup>. Attached to these gauge nodes are non-negative flavour nodes with label  $f_i^1$  and  $f_i^2$ . Proving that  $Q_{\text{bal}}^1 - Q_{\text{bal}}^2 = Q^3$  is a good quiver is straightforward. Consider that in order for quiver subtraction to make sense requires  $g_i^1 \geq g_i^2$  for all  $i$ . For each gauge node  $g_i$ , consider the set of nodes which are connected to  $g_i$  via an edge. This will be a collection of gauge nodes labelled with indices in the set  $j_i$ . The condition of balance then imposes that the excess  $e$  of every gauge node is zero,

$$e_i^a = f_i^a - 2g_i^a + \sum_{k \in j_i} g_k^a = 0, \quad (6.80)$$

where  $a \in \{1, 2\}$ . From quiver subtraction,  $g_i^3 = g_i^1 - g_i^2 \geq 0$  and  $f_i^3 = f_i^1$ . The excess on the gauge nodes in  $Q_3$  is then,

$$\begin{aligned} e_i^3 &= f_i^3 - 2g_i^3 + \sum_{k \in j_i} g_k^3 \\ &= f_i^1 - 2(g_i^1 - g_i^2) + \sum_{k \in j_i} (g_k^1 - g_k^2) \\ &= 2g_i^2 - \sum_{k \in j_i} g_k^2 \\ &= f_i^2. \end{aligned} \quad (6.81)$$

Flavours are non-negative and so the excess is larger than zero, the result of quiver subtraction amongst balanced quivers is always a good quiver. As we will discuss in the next subsection, those good quivers that are constructable as a difference of balanced quivers are not necessarily all possible good quivers.

## 6.4 Good $D_n$ Dynkin quivers

This section lays out the characterisation and local moduli space analysis of good  $D_n$  Dynkin quivers. Any two balanced quivers where one can be subtracted from the other yield a good quiver. Having already characterised all the balanced  $D_n$  Dynkin quivers, a large number of good quivers can be found by examining all possible subtractions. In the (linear)  $A_n$  Dynkin quiver case this encapsulated all the possible good quivers, however for the  $D_n$  case it does not. When looking at balanced quivers one quickly excluded any quivers with an odd difference in flavour on the end nodes as being unbalanceable. However loosening the restriction to the class of *good* quivers means that they have to be included. The trouble is that the difference of

<sup>10</sup>Note that the rank of some gauge nodes in  $Q_3$  may be zero. This changes the gauge node topology since the rank zero nodes are effectively absent. This includes the possibility that  $Q_3$  is a disjoint quiver.

<sup>11</sup>Where the lower index refers to some ordering of the gauge nodes which is maintained across quivers.

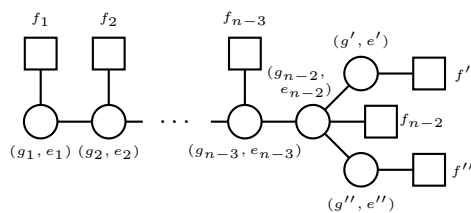


Figure 6.52: The general form for a good  $D_n$  Dynkin quiver. Each gauge node is now labelled with a rank and a non-negative *excess*. Balanced quivers are the subset of good quivers where the excess on all the gauge nodes is zero.

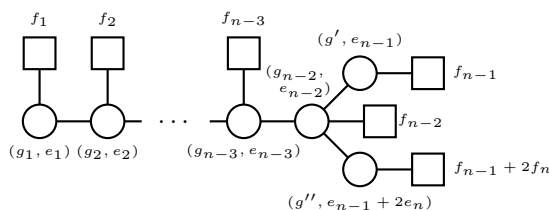


Figure 6.53: The general form of a good  $D_n$  Dynkin quiver of even type. Note that as well as the difference in flavours on the end nodes having to be even, the difference in excess of the end nodes also has to be even.

two balanced quivers must necessarily have an even difference of end flavours, and good quivers with an odd difference in end flavours cannot possibly be found as balanced subtractions. The classification of good  $D_n$  Dynkin quivers therefore necessarily divides into two parts: Those with an even difference in end flavours, *even* type, and those with an odd difference in end flavours, *odd* type.

It will be shown that all good  $D_n$  Dynkin quivers of even type can be found as the subtraction of two balanced  $D_n$  Dynkin quivers. The moduli space singularity structure can be expressed as a *run* from one node down to another node on the balanced Hasse diagram constructed in Fig. 6.48. This is shown by premising an arbitrary good quiver of even type and describing a general method by which the two relevant balanced quivers can be found. This will allow a classification of all good even  $D_n$  Dynkin quivers using two even partitions (not necessarily of the same magnitude) and the integer  $n$ . Attention is then turned to good quivers of odd type. This classification requires very similar methods to even type. Poset structure is established for a class of quivers from which all good odd quivers can be found using quiver subtraction and the completeness of the classification verified using similar methods to the even case.

### 6.4.1 $D_n$ quivers of even type

Each gauge node in a good quiver has associated to it, a flavour, a rank, and an excess. Even quivers have an even difference of flavours on the end nodes. It is simply to establish that the difference in the excess for the end nodes must also be even for an even quiver. Consider Fig. 6.52, the ‘balance’ (while regarding the excess) of the lower node requires  $g_{n-2} + f_{n-1} + 2f_n = 2g'' + e''$ , and the balance of the upper node requires  $g_{n-2} + f_{n-1} = 2g' + e'$ , putting these together requires  $e'' - e' = 2(g' + f_n - g'')$  so the difference is even. A general good  $D_n$  Dynkin quiver of even type is given in Fig. 6.53. Using Fig. 6.53, define the following two

partitions

$$\begin{aligned}\kappa &= (n^{f_n}, n-1^{f_{n-1}}, \dots, 2^{f_2}, 1^{f_1}) \\ \lambda &= (n^{e_n}, n-1^{e_{n-1}}, \dots, 2^{e_2}, 1^{e_1}).\end{aligned}\tag{6.82}$$

In direct analogy with (6.66), it is simply established, by 'balancing' whilst taking into account the excess, that

$$g_k = kg_1 - \sum_{i=1}^{k-1} (k-i)(f_i - e_i).\tag{6.83}$$

for  $k \leq n-2$ . Repeating the analysis of (6.66) - (6.69) with this extra complication yields the analogous results

$$\begin{aligned}g_1 &= l(\kappa) - l(\lambda) \\ 2g'' &= |\kappa| - |\lambda|.\end{aligned}\tag{6.84}$$

Note that all of this analysis reduces to the balanced case when we take  $\lambda$  to be the zero partition which is equivalent to there being zero excess on every node. When it comes to examining the moduli space singularity structure this is the realisation that balanced quivers correspond to a run of edges and nodes in Fig. 6.48 from the very top to some node  $\kappa$  whereas a good quiver corresponds to a run from a node  $\lambda$  down to a node  $\kappa$ .

For a generic good, even  $D_n$  Dynkin quiver one can find two balanced  $D_n$  Dynkin quivers which give the good quiver under quiver subtraction. The larger quiver in quiver subtraction and the resulting quiver have the same flavour. The larger of the balanced quivers is therefore going to have flavour dictated by the partition  $\kappa$ . The clue for the smaller balanced quiver comes from (6.81). The flavour of a given node on the smaller quiver is exactly the excess of the good quiver under construction. The flavour of the smaller quiver is therefore dictated by the partition  $\lambda$ .

A balanced quiver's flavour must be dictated by a partition of even magnitude, however there is nothing about good quivers which restricts (6.82) to be of even magnitude. This must be addressed. Note that the second relationship in (6.84) tells us that either both  $|\kappa|$  and  $|\lambda|$  must be even, or both must be odd.

The result is straight forward when both  $\kappa$  and  $\lambda$  are of even magnitude. In this case one *can* construct balanced quivers using these partitions. The result when both are even is therefore

$$Q_{\text{good, even}}^{|\kappa|, |\lambda| \text{ even}} = Q(D_\kappa(n)) - Q(D_\lambda(n)).\tag{6.85}$$

When both  $|\kappa|$  and  $|\lambda|$  are odd there seems to be an impasse as the analogously defined 'balanced' quivers are unbalanceable. However the gauge node topology of the resulting quiver in quiver subtraction needn't be precisely that of the quivers involved in the subtraction. Nodes of rank zero might result from quiver subtraction which would change the quiver topology. The partitions which correspond to flavour arrangement are considered from the end of the tail of the quiver, premising another gauge node of rank  $g_0 = 0$  on the good quiver changes the magnitude of the defining partitions considerably.

For  $\kappa$  and  $\lambda$  to be of odd magnitude, they must have an odd number of odd parts with odd multiplicity. Adding the zero rank gauge node to the good quiver has the effect of increasing all the parts by one, the odd

number of odd parts with odd multiplicity is changed to an odd number of *even* parts with odd multiplicity, which always gives an even number. However the previously even parts have now been shifted to being odd parts. If  $\kappa$ , for example, had an odd number of even parts with odd multiplicity, the new partition has an odd number of odd parts with odd multiplicity and so is odd. An odd magnitude partition with an odd number of even parts is necessarily of even length. The flavour on the new node can be arbitrary. When  $\kappa$  is odd and  $l(\kappa)$  is even choose the flavour,  $f_0$ , of the new zero node to be odd, and when  $\kappa$  is odd and  $l(\kappa)$  odd, choose  $f_0$  even. This guarantees that the partition associated to the flavour for the new good quiver,  $\kappa'$ , is even. From here construct the quiver of excesses in the normal way. The excess of the new zero node is necessarily  $g_1 + f_0 = l(\kappa) - l(\lambda) + f_0$ . The way  $f_0$  was chosen now guarantees that the new partition on the quiver of excesses is also always even. To see this, note that when  $l(\kappa)$  was odd  $f_0$  was chosen even, therefore if  $l(\lambda)$  was odd (and hence  $\lambda$  had an even number of even parts with odd multiplicity) the flavour on the zeroth node in the excess quiver was even and the magnitude of  $\lambda'$  is even. And if  $l(\lambda)$  was even (and hence  $\lambda$  had an odd number of even parts with odd multiplicity) the flavour on this node is odd and so the magnitude of  $\lambda'$  is even again. In conclusion, when  $\kappa$  and  $\lambda$  as found from Fig. 6.53 are of odd magnitude, the good quiver is realised as

$$Q_{\text{good, even}}^{|\kappa|, |\lambda| \text{ odd}} = Q(D_{\kappa'}(n+1)) - Q(D_{\lambda'}(n+1)). \quad (6.86)$$

where

$$\begin{aligned} \kappa' &= (n + 1^{f_n}, n^{f_{n-1}}, \dots, 2^{f_1}, 1^{f_0}) \\ \lambda' &= (n + 1^{e_n}, n^{e_{n-1}}, \dots, 2^{e_1}, 1^{l(\kappa) - l(\lambda) + f_0}). \end{aligned} \quad (6.87)$$

An important check to make on this construction is that the extra node added does indeed achieve a rank of zero after quiver subtraction. Using that the rank of the first node is the length of the partition for the balanced quivers constructed, the rank of the first node of their difference is

$$\begin{aligned} g_1^{\kappa'} - g_1^{\lambda'} &= l(\kappa') - l(\lambda') \\ &= \sum_{i=0}^n f_i - \sum_{i=1}^n e_i - l(\kappa) + l(\lambda) - f_0 \\ &= l(\kappa) + f_0 - l(\lambda) - l(\kappa) + l(\lambda) - f_0 \\ &= 0 \end{aligned} \quad (6.88)$$

as required.

#### 6.4.2 An alternative for even theories with odd partitions

There is an alternative construction which allows an easier reading of the moduli space singularity structure when  $|\kappa|$  and  $|\lambda|$  are odd as compared to when the quiver is described as the difference of balanced quivers.

In Fig. 6.48, the nodes were all labelled with even magnitude partitions. This can be viewed as arising because the diagram started with a trivial, flavourless quiver with partition (0), and the traversing structure could only shift partition magnitude by an even amount. Starting with the trivial theory with partition (1) (at the top of Fig. 6.54) and employing the same style of traversing structure yields a diagram analogous

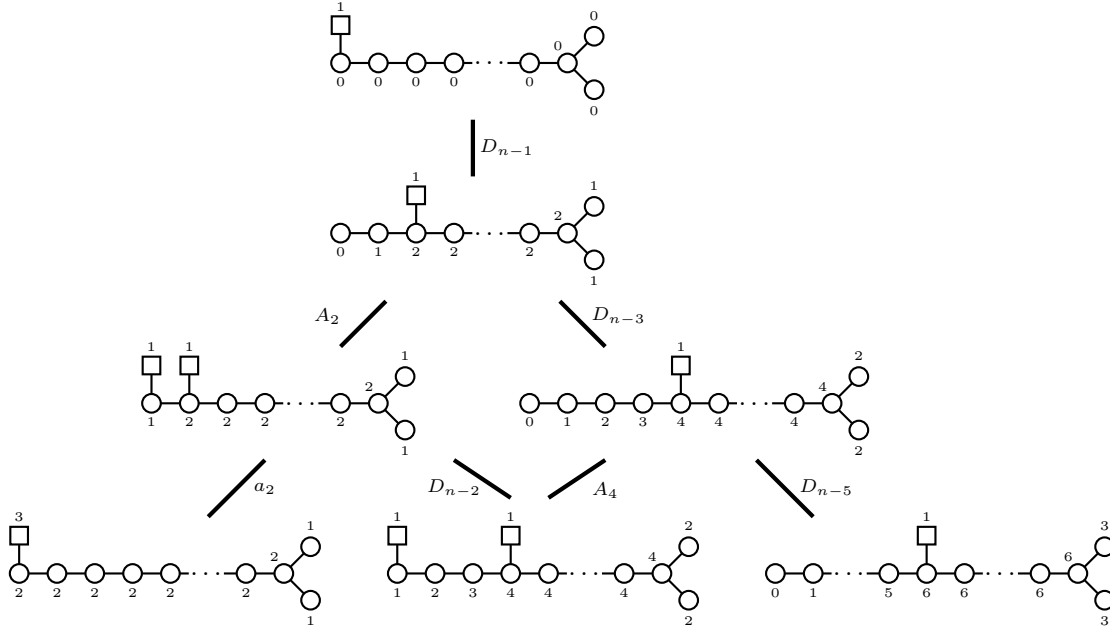


Figure 6.54: The beginning of the Hasse diagram for quiver addition of even theories with an odd magnitude partition. These can be realised as the difference of two balanced quivers with even magnitude partitions, but an easier way to read off the moduli space singularity structure is to perform quiver addition having premised that the node at the end of the tail has an excess of one. This arises because the traversing structure fore even theories necessarily changes the magnitude of the partitions assigned to the theory by an even amount. To cover all possible assignations therefore, it is proper to construct two Hasse diagrams, one starting at the partition (0) and the other at the partition (1). This observation will be important later for the  $\tilde{D}_n$  Dynkin quivers.

to Fig. 6.48 but built entirely of good, even theories with *odd* partitions dictating flavour and whose only non-negative excess appears on the end node of the tail, Fig. 6.55. This exactly gives the even type theories with odd partitions and hence allows a short-cut to their moduli space singularity analysis. As good and even theories with even partition magnitudes can be found as runs in Fig. 6.48, good and even theories with odd partitions can be found as runs Fig. 6.55. Along with the previous discussion regarding identifying odd partitioned theories within Fig. 6.48 this shows that an arbitrarily sized section of Fig. 6.55 can always be found sufficiently far into Fig. 6.48. Reversing the previous discussion also implies the opposite way round. The position of a theory in a partition subdiagram of Fig. 6.55 corresponds to the partitions  $\kappa$  and  $\lambda$  that can be extracted from the quiver in the usual manner via (6.82).

### 6.4.3 Good, even classification

All good, even  $D_n$  Dynkin quivers can be considered as the difference between two balanced quivers. While it is possible to find all good, even quivers when restricted to even magnitude partitions only and using Fig. 6.48, the moduli space analysis is more direct when allowing odd magnitude partitions as well using Fig. 6.55. Either both partitions have an odd magnitude, or both have an even magnitude. All good even type  $D_n$  Dynkin quivers are classified using two partitions (not necessarily of equal magnitude), say  $\mu$  and  $\nu$ , and a value  $n$ . The class is denoted  $D_n^\mu(n)_e$ , where  $e$  denotes even type,  $\mu$  and  $\nu$  are restricted in a number of



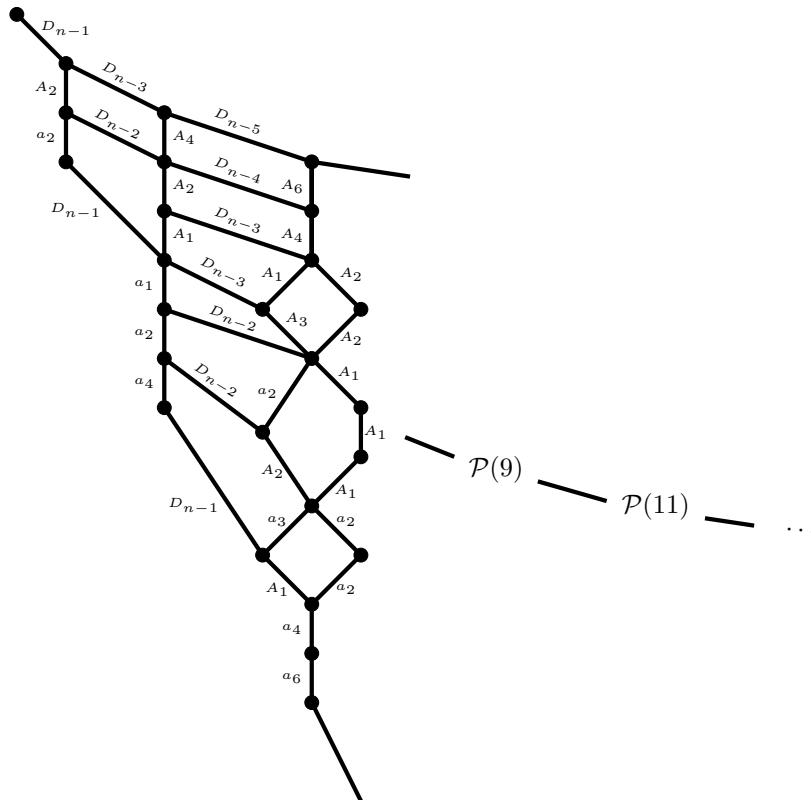


Figure 6.55: The general Hasse diagram for even theories with odd magnitude partitions. This Hasse diagram is similar to Fig. 6.48. Cutting either this or Fig. 6.48 off at an arbitrary point yields a finite Hasse diagram. Finite Hasse subdiagrams of arbitrary size for one can be found *somewhere* in the other. Finding arbitrarily large subdiagrams inside Fig. 6.48 is the same as the statement that even type theories with odd partitions can be found as the difference of two balanced theories (whose partitions must necessarily be even), which we have already seen.

ways such that they are compatible with the value of  $n$  (no part is larger than  $n$ ) and with the need for quiver subtraction to not produce gauge nodes with negative rank.

The moduli space singularity structure for good quivers can then be read off of Fig. 6.48 almost immediately by considering *runs* of nodes and edges. A run on the Hasse diagram is simply a pair of nodes between which there is a Hasse subdiagram. Take a very simple example, the pair of partitions  $(6, 1^2), (3^2, 1^2) \in \mathcal{P}(8)$  form a run as there is a Hasse subdiagram suspended between them, whereas  $(5, 1^3)$  and  $(4^2)$  do not form a run. Runs corresponding to partition Hasse subdiagrams exactly correspond to pairs of partitions where one dominates the other in the usual partition dominance ordering sense. When the Hasse diagram is more complicated the notion of dominance is maintained. Dominance in Fig. 6.48 and Fig. 6.55 also needs to act between partition Hasse subdiagrams as well. For  $\lambda \in \mathcal{P}(2p)$  and  $\kappa \in \mathcal{P}(2p + 2j)$  to define a run corresponding to a variety that is realised as a  $D_n$  Dynkin quiver Higgs branch, it is required that  $(\lambda^t, 1^{2j})^t > \kappa$ . This extension of dominance to Fig. 6.48 and Fig. 6.55 depends on the traversing structure. This is just the usual partition dominance ordering when  $j = 0$ . The relationship for  $\lambda$  and  $\kappa$  is exactly the condition that quiver subtraction needs in order to be well defined (none of the gauge nodes become negative). The edits it is necessary to perform on Fig. 6.48 correspond to the restrictions on the partitions from the value of  $n$ .

#### 6.4.4 Dimension matching for good, even theories

A number of aspects of the analysis can be checked by performing further moduli space dimension calculations. We start with the calculation of the Higgs branch dimensions for a good, even theory. These theories are constructed as differences of balanced theories, so it is expected that

$$\begin{aligned} \dim_{\mathbb{H}}(\mathcal{M}_H(D_\nu^\mu(n)_e)) &= \dim_{\mathbb{H}}(\mathcal{M}_H(D_\nu(n)_e - D_\mu(n)_e)) \\ &= \dim_{\mathbb{H}}(\mathcal{M}_H(D_\nu(n)_e)) - \dim_{\mathbb{H}}(\mathcal{M}_H(D_\mu(n)_e)) \\ &= \frac{1}{2} \left( \sum_i (\nu_i^t)^2 - \sum_i (\mu_i^t)^2 \right) \end{aligned} \quad (6.89)$$

which is indeed the case. It may be confirmed by summing over  $j$  up to  $|\nu| - |\mu| - 2$ , instead of  $|\nu| - 2$  as in (6.71),

$$\begin{aligned} \dim_{\mathbb{H}}(\mathcal{M}_H(D_\nu^\mu(n)_e)) &= \sum_{j=0, \text{ even}}^{|\nu| - |\mu| - 2} \left[ \dim_{\mathbb{H}} \left( D_{n-l(\lambda_{|\nu| - j}^t)} \right) + \dim_{\mathbb{H}} \left( \mathcal{S}_{\lambda_{|\kappa| - j}} \cap \bar{\mathcal{O}}_{(\lambda_{|\kappa| - j - 2}^t, 1^2)^t} \right) \right] \\ &= \frac{1}{2} (|\nu| - |\mu|) + \frac{1}{2} \left( \sum_i ((\lambda_{|\nu|}^t)_i)^2 - \sum_i ((\lambda_{|\mu|}^t)_i)^2 \right) - \frac{1}{2} (|\nu| - |\mu|) \\ &= \frac{1}{2} \left( \sum_i (\nu_i^t)^2 - \sum_i (\mu_i^t)^2 \right). \end{aligned} \quad (6.90)$$

The Coulomb branch dimension check is relatively simple. On the one side the dimension is calculated by a sum of the dimensions of individual edges of Fig. 6.48, this was done for balanced in (6.76). For good theories, replace the sum up to  $|\nu| - 2$  with a sum to  $|\nu| - |\mu| - 2$ , and skip immediately to line 5 of (6.76)

replacing the sum's limits appropriately,

$$\begin{aligned} \dim_{\mathbb{H}}(\mathcal{M}_C(D_\nu^\mu(n)_e)) &= \sum_{j=0, \text{ even}}^{|\nu|-|\mu|-2} \left[ 2n-1 + \frac{1}{2} \sum_i ((\lambda_{|\kappa|-j-2})_i)^2 - \frac{1}{2} \sum_i ((\lambda_{|\kappa|-j})_i)^2 \right] \\ &= \frac{1}{2} (|\nu| - |\mu|)(2n-1) - \frac{1}{2} \left( \sum_i (\nu_i)^2 - \sum_i (\mu_i)^2 \right). \end{aligned} \quad (6.91)$$

When  $\mu = (0)$ , this simplifies to the balanced case exactly as expected.

The other computation of the Coulomb branch dimension check for balanced quivers was (6.77) and (6.78). For good quivers, consider the extra factor of excess as in (6.83), and the analysis is essentially the same. Begin with the generalization of (6.77),

$$\sum_{k=1}^{n-2} \left[ k g_1 - \sum_{i=1}^{k-1} (k-i)(f_i - e_i) \right] + g' + g'' = \frac{1}{2} g_1 (n-2)(n-1) + g' + g'' - \sum_{l=1}^{n-3} \left[ (f_l - e_l) \sum_{j=1}^{n-2-l} j \right], \quad (6.92)$$

and follow the same analysis as (6.78)

$$\begin{aligned} &\frac{1}{2} g_1 (n-2)(n-1) + |\kappa| - (f_n - e_n) - \sum_{l=1}^{n-3} \frac{1}{2} (f_l - e_l)(n-2-l)(n-1-l) \\ &= \frac{1}{2} (|\nu| - |\mu|)(2n-1) + \frac{1}{2} \left[ - \sum_{l=1}^n l^2 (f_l - e_l) \right] \\ &= \frac{1}{2} (|\nu| - |\mu|)(2n-1) - \frac{1}{2} \left( \sum_i (\nu_i)^2 - \sum_i (\mu_i)^2 \right). \end{aligned} \quad (6.93)$$

This matches the result in (6.91) and so the Coulomb branch dimension check is passed for good quivers.

This result generalizes the balanced result where the excesses were zero ( $\mu = (0)$ ).

Explicit calculation of moduli space dimension also allows a consistency check when identifying the theories with an odd partition magnitude as a difference of balanced (and hence even partitioned) theories. The claim is that for  $|\nu|$  and  $|\mu|$  odd,

$$D_\nu^\mu(n)_e = D_{\nu'}(n+1) - (D_{\mu'}(n+1)). \quad (6.94)$$

with

$$\begin{aligned} \nu' &= (n+1^{f_n}, n^{f_{n-1}}, \dots, 2^{f_1}, 1^{f_0}) \\ \mu' &= (n+1^{e_n}, n^{e_{n-1}}, \dots, 2^{e_1}, 1^{l(\nu)-l(\mu)+f_0}). \end{aligned} \quad (6.95)$$

Alternatively these theories could be read from Fig. 6.55. This alternative construction allows a similar analysis as the one performed for Fig. 6.48. (Fig. 6.55 is of the same form, using different partitions. The only change to make is that the  $j$  sum is taken over odd instead of even, values). Therefore, from the alternative

construction in Fig. 6.55, on one hand and from (6.89) and (6.94) on the other, consistency requires

$$\dim_{\mathbb{H}}(\mathcal{M}_H(D_\nu^\mu(n)_e)) = \frac{1}{2} \left( \sum_i (\nu_i^t)^2 - \sum_i (\mu_i^t)^2 \right) = \frac{1}{2} \left( \sum_i ((\nu')_i^t)^2 - \sum_i ((\mu')_i^t)^2 \right). \quad (6.96)$$

for  $\nu$  and  $\mu$  given in the standard way and  $\nu'$  and  $\mu'$  given by (6.95). Note that for  $\nu'$  we have the relation

$$\begin{aligned} \sum_i ((\nu')_i^t)^2 &= \sum_{q=1}^n \left( \sum_{j=q}^n f_j \right)^2 + \left( \sum_{j=0}^n f_j \right)^2 \\ &= \sum_i (\nu_i^t)^2 + (l(\nu) + f_0)^2. \end{aligned} \quad (6.97)$$

Thus

$$\begin{aligned} \frac{1}{2} \left( \sum_i ((\nu')_i^t)^2 - \sum_i ((\mu')_i^t)^2 \right) &= \frac{1}{2} \left( \sum_i (\nu_i^t)^2 - \sum_i (\mu_i^t)^2 \right) \\ &\quad + (l(\nu) + f_0)^2 - (l(\mu) + l(\nu) - l(\mu) + f_0)^2 \\ &= \frac{1}{2} \left( \sum_i (\nu_i^t)^2 - \sum_i (\mu_i^t)^2 \right) \end{aligned} \quad (6.98)$$

as required. A second check of the odd partition even theories is a Coulomb branch dimension consideration which requires

$$\begin{aligned} \frac{1}{2} (|\nu| - |\mu|)(2n - 1) - \frac{1}{2} \left( \sum_i (\nu_i)^2 - \sum_i (\mu_i)^2 \right) \\ = \frac{1}{2} (|\nu'| - |\mu'|)(2(n + 1) - 1) - \frac{1}{2} \left( \sum_i ((\nu')_i)^2 - \sum_i ((\mu')_i)^2 \right). \end{aligned} \quad (6.99)$$

Note that  $|\nu'| = \sum_{j=0}^n (j+1)f_j = |\nu| + l(\nu) + f_0$  and  $|\mu'| = \sum_{j=0}^n (j+1)e_j = |\mu| + l(\mu) + (l(\nu) - l(\mu) + f_0)$  and so it is plain that  $|\nu'| - |\mu'| = |\nu| - |\mu|$ . Also (writing  $e_0 = l(\nu) - l(\mu) + f_0$ ),

$$\begin{aligned} -\frac{1}{2} \left( \sum_i ((\nu')_i)^2 - \sum_i ((\mu')_i)^2 \right) &= -\frac{1}{2} \left( \sum_{j=0}^n (j+1)^2 (f_j - e_j) \right) \\ &= -\frac{1}{2} \left( \sum_{j=0}^n j^2 (f_j - e_j) + 2 \sum_{j=0}^n j (f_j - e_j) + l(\nu') - l(\mu') \right) \\ &= -(|\nu| - |\mu|) - \frac{1}{2} \left( \sum_i (\nu_i)^2 - \sum_i (\mu_i)^2 \right), \end{aligned} \quad (6.100)$$

which completes the equality in (6.99). We used (6.88) in moving from line two to three.

### 6.4.5 Recovering $\mathfrak{so}_{2n}$ nilpotent varieties

The two general quivers given in Fig. 6.45 are those quivers realising nilpotent varieties of  $\mathfrak{so}_{2n}$ . Recasting these quivers under the classification via moduli space given here is straight-forward. Realising  $\mathfrak{so}_{2n}$  nilpotent

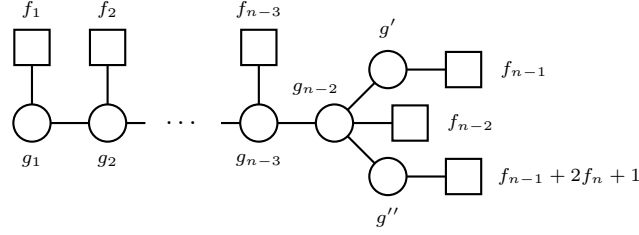


Figure 6.56: The general structure of a  $D_n$  Dynkin quiver of odd type. Note that this quiver is necessarily unbalanceable like in the alternative construction for good, even theories of odd partition magnitude. Because the difference between the end node flavours is odd, it is implicit that for every quiver of odd type there are the options *I* and *II* discussed earlier. For simplicity these won't both be written from here on, however one should always recall that there are two quivers with the same field content at every point.

varieties as  $D_n$  quivers gives

$$\begin{aligned} A(p, q) &= D_{(n-q-2)}^{(n-q-2p-2)}(n)_e = D_{(2p)}(2p+q+2)_e \\ B(p, q) &= D_{(n-q-2,1)}^{(n-q-2p-1)}(n)_e \end{aligned} \quad (6.101)$$

where, in the context of the previous discussion,  $n = m$  or  $m + 1$ .

#### 6.4.6 Odd $D_n$ quiver Hasse diagram

It is time to consider all of the good  $D_n$  quivers which are not captured by  $D_n^\mu(n)_e$ . These are of odd type. Odd  $D_n$  Dynkin quivers have an odd difference in the flavour on the end nodes, and are therefore always unbalanceable. Without loss of generality one can assume the flavours of the end nodes are  $f_{n-1}$  and  $f_{n-1} + 2f_n + 1$  respectively, Fig. 6.56. It can be shown that odd flavour difference requires an odd excess difference for the end nodes.

In order to give the class of good, odd theories with an appropriate poset structure, and so build a Hasse diagram like Fig. 6.48, quiver addition is employed once again. This will yield all possible good  $D_n$  Dynkin quivers of odd type under quiver subtraction in the same manner as even theories were determined.

The positions of flavours on  $D_n$  Dynkin quivers can be associated to partitions as (6.82) as in Fig. 6.56. Note that this time there is an extra flavour on one end node. No singularity changes the fact that the difference of flavour is odd. Therefore the Hasse diagrams from odd theories never connect with the Hasse diagram for even theories. The lowest rank quiver, at the top of the Hasse diagram, is the quiver corresponding to the zero partition. Implicit for odd quivers is the option to swap the flavours and ranks of the end nodes, which formally gives two options, *I* and *II*, for every node in the Hasse diagram. This extra notation is dropped from here for simplicity.

The only first option under quiver addition is to add a single  $A_{n-1} \cup A_{n-1}$  singularity as in Fig. 6.57. Note that whilst the 'extra' flavour has in a sense swapped nodes, the 'extra' excess remains on the lower node.

The full picture is given in Fig. 6.58. Once again a pattern of partition Hasse subdiagram emerges whereby the partition associated to the node in the subdiagram is the same as the partition associated to the flavours in the quiver. For balanced cases the structure traversing from a partition subdiagram to another consisted

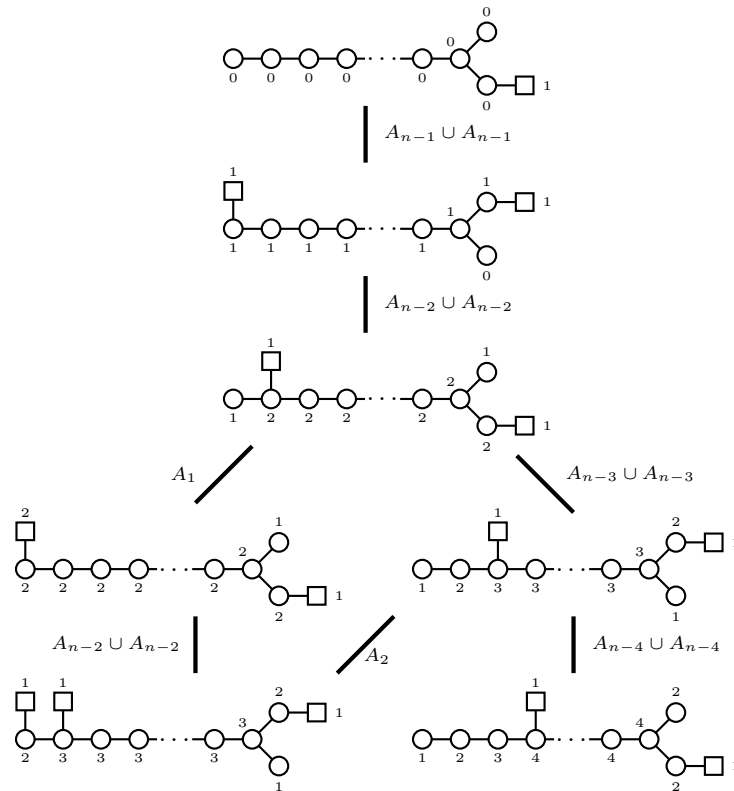


Figure 6.57: The beginning of the quiver addition for odd theories. Recall that at all stages there are options *I* and *II* as discussed previously. Note that because the difference of flavour on the end nodes is odd, the  $D_k$  traversing structure is never possible. There is  $A_k \cup A_k$  traversing structure only. However these transitions change the magnitude of the assigned partition by one each time, this means that all partitions are included in this Hasse diagram and there is no need to use two different starting theories to easily find all of the possible theories. In this sense the Hasse diagram structure for odd theories is simpler than for even theories. Note that whilst the end node with the excess of one is always as assigned at the top of the diagram, the ‘extra flavour’ flips back and forth when only one of the two options is written.

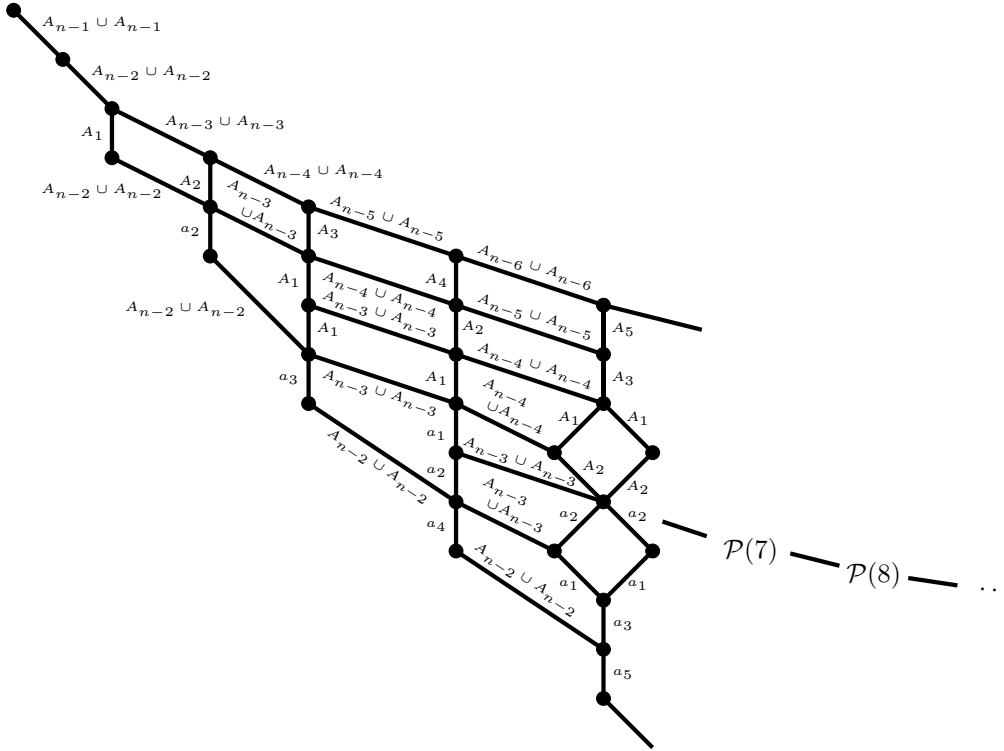


Figure 6.58: The general structure of the quiver addition Hasse diagram for theories of odd type. This is used in the same way as Fig. 6.48 and Fig. 6.55 were used for even quivers to deduce the moduli space singularity structure of any good  $D_n$  theory of odd type.

of  $D_k$  transverse slices which changed the magnitude of the partitions by two. For Fig. 6.58 the traversing structure consists of  $A_k \cup A_k$  singularities which change the partition magnitude by one at a time. This can once again be encapsulated as an edge diagram:

$$\begin{array}{ccc}
 \mathcal{P}(p) \ni \kappa & \bullet & \xrightarrow{A_{n-1-l(\kappa^t)} \cup A_{n-1-l(\kappa^t)}} \\
 & & \bullet \quad (\kappa^t, 1)^t \in \mathcal{P}(p+1).
 \end{array}$$

Observe that when the partition is of odd magnitude, the node with extra flavour and the node with excess are opposite, whereas when the partition is of even magnitude, they are on the same node. Since quiver addition doesn't change the excess of the nodes one can also observe that the end node with excess remains the only node with excess. By repeating the analysis (6.66) - (6.69) it can be shown that indeed when the excess and flavour are on opposite nodes,  $|\kappa| = 2g'' - 1$ . When they are on the same node  $|\kappa| = 2g''$ .

Like in the balanced case, the choice of a concrete  $n$  will inevitably necessitate editing of the general structure presented in Fig. 6.58. Once again this can be determined in a systematic way by observing which quivers and transitions are defined in the Hasse diagram or are possible at the level of the quivers and exploring what happens in the fringe cases.

**Editing prescription** To write down the Hasse diagram for good, odd  $D_n$  Dynkin quivers for some specific  $n$  one starts with the general construction in Fig. 6.58, identifies in this construction all of the nodes with parts larger than  $n$  and deletes them. Also delete any badly defined traversing edges. The final step is to put

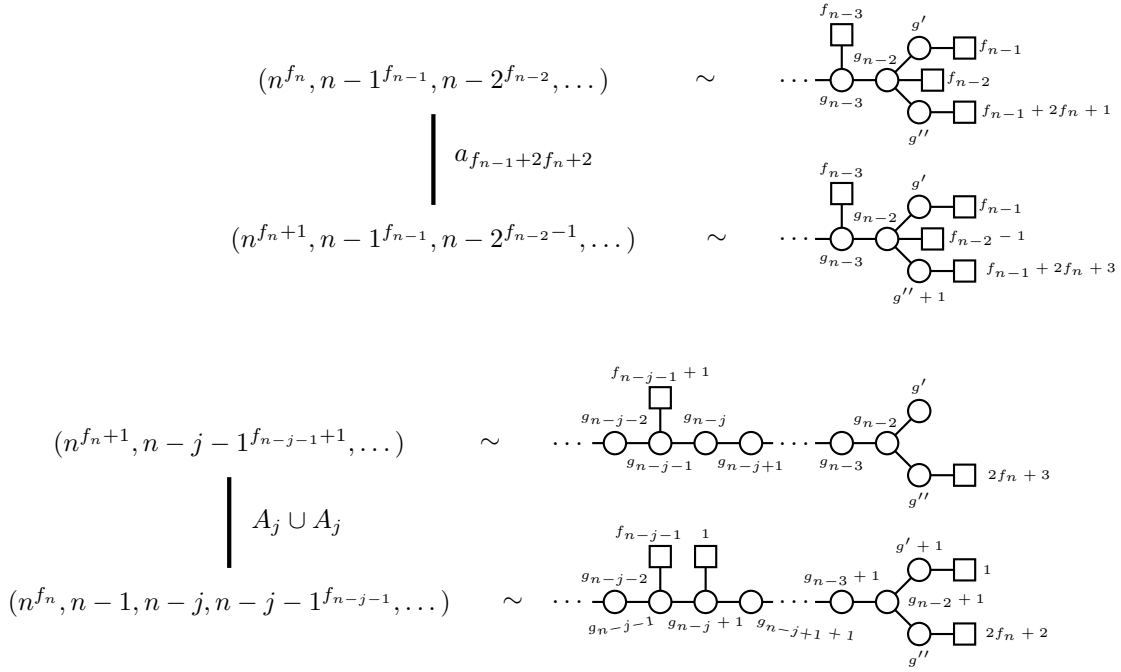


Figure 6.59: The editing prescription for the quiver addition Hasse diagram for theories of odd type presented in the same manner as Fig. 6.50.

in edges following Fig. 6.59.

An example of performing this editing for  $n = 4$  theories and partitions  $\kappa$  with  $|\kappa| \leq 5$  is given in Fig. 6.60

Theories living at the nodes of Fig. 6.58, while not balanced, play the same role as balanced quivers in the even case and may be classified using just one partition and the number  $n$ ,  $D_\kappa(n)_o$ . The moduli space singularity structure for the theory  $D_\kappa(n)_o$  is given by the run on the general construction, after editing, from the very top to the node labelled with the partition  $\kappa$ . The difference between two quivers in Fig. 6.58 is a good, odd  $D_n$  Dynkin quiver. Taking differences of quivers in Fig. 6.58 will encompass all good, odd  $D_n$  Dynkin quivers, as we will discuss now.

### 6.4.7 Good $D_n$ quivers of odd type

Any good  $D_n$  Dynkin quiver of odd type can be realised as the difference between two quivers living at nodes in Fig. 6.58 and hence we need to know the two partitions  $\mu$  and  $\nu$  (not necessarily of equal magnitude) and the integer  $n$ .

The general good  $D_n$  Dynkin quiver of odd type is given in Fig. 6.61, however there is a subtlety that must be addressed. Since there exist two equivalent quivers at every node, for quiver subtraction to work in the desired way, the extra single end flavour must be on the same node in the subtraction. This is always possible since there are always two options,  $I$  and  $II$ , for odd quivers.

It was previously recognised that the ‘extra’ flavour and the extra excess needn’t be on the same node. But in Fig. 6.61 it is drawn such that they are both associated to the bottom node. This is allowed because of the extra freedom in the general good case. A quiver like Fig. 6.61 but with the ‘extra’ end flavour on the upper



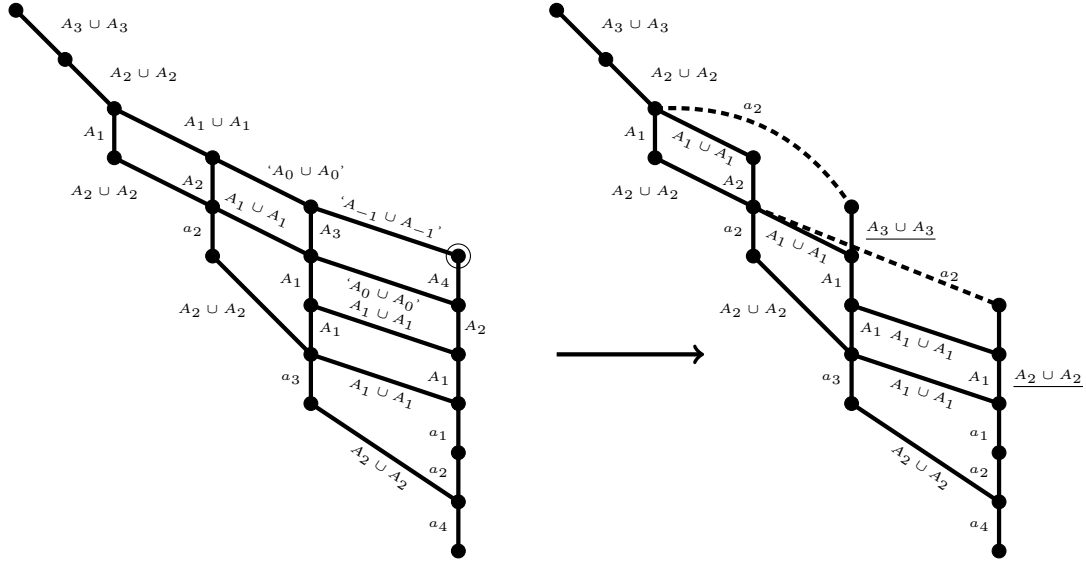


Figure 6.60: An example of the application of the odd type editing prescription to explicitly find the Hasse diagram for odd  $D_4$  Dynkin quivers with  $|\kappa| \leq 5$ . This can be checked explicitly using quiver arithmetic.

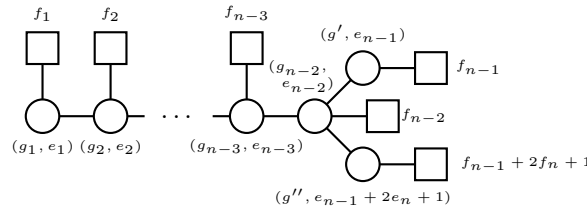


Figure 6.61: The general form of a good, odd  $D_n$  Dynkin quiver. These can all be found as the difference of two odd  $D_n$  Dynkin quivers from Fig. 6.58 and their moduli space singularity structure is given by the appropriate run on Fig. 6.58.

node would in fact be of the form of Fig. 6.61 with  $f_{n-1} \rightarrow f_{n-1} + 1$  and  $f_n \rightarrow f_n - 1$ . When  $f_n = 0$  this transformation isn't possible which sets the 'extra' flavour and excess as having to be on the same node, so all cases are covered.

The partitions associated to the general good, odd  $D_n$  Dynkin quiver are

$$\begin{aligned} \kappa &= (n^{f_n}, n - 1^{f_{n-1}}, \dots, 2^{f_2}, 1^{f_1}) \\ \lambda &= (n^{e_n}, n - 1^{e_{n-1}}, \dots, 2^{e_2}, 1^{e_1}), \end{aligned} \tag{6.102}$$

in the usual manner. From here it follows that we have

$$Q_{\text{good, odd}} = Q(D_\kappa(n)_o) - Q(D_\lambda(n)_o). \tag{6.103}$$

The singularity structure of the Higgs branch of these theories,  $\mathcal{M}_H(D_\nu^\mu(n)_o)$ , is given by the run in Fig. 6.58, after editing, from a node  $\mu$  down to a node  $\nu$ .

### 6.4.8 Dimension matching for good, odd theories

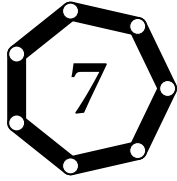
The calculations for odd theories are similar to those for even theories, only the routes have to be defined on Fig. 6.58. This is a matter of replacing the sum over even values of  $j$  to a sum over all values and replacing the manner in which partitions for nodes in different partition subdiagrams are determined by one another in order to be commensurate with the  $A_k \cup A_k$  traversing structure. Otherwise the construction is the same. The Higgs branch calculation for good, odd theories is

$$\begin{aligned}
& \dim_{\mathbb{H}}(\mathcal{M}_H(D_\nu^\mu(n)_o)) \\
&= \sum_{j=0}^{|\nu|-|\mu|-1} \left( \dim_{\mathbb{H}}(A_{n-1-l(\lambda_{|\nu|-j-1}^t) \cup A_{n-1-l(\lambda_{|\nu|-j-1}^t)} + \dim_{\mathbb{H}}(\mathcal{S}_{\lambda_{|\nu|-j}^t} \cap \bar{\mathcal{O}}_{(\lambda_{|\nu|-j-1}^t, 1)^t}) \right) \\
&= \sum_{j=0}^{|\nu|-|\mu|-1} \left( \frac{1}{2} + \frac{1}{2} \left[ \sum_i ((\lambda_{|\nu|-j}^t)_i)^2 - \sum_i ((\lambda_{|\nu|-j-1}^t)_i)^2 - 1 \right] \right) \\
&= \frac{1}{2} \left( \sum_i (\nu_i^t)^2 - \sum_i (\mu_i^t)^2 \right).
\end{aligned} \tag{6.104}$$

For the Coulomb branch calculation one can observe that an odd and even theory with the same partition data have the same ranks on the gauge nodes and so should have the same Coulomb branch dimension. For the even case the partitions either had to be both even or both odd, however for odd theories this needn't be the case. The calculation is

$$\begin{aligned}
& \dim_{\mathbb{H}}(\mathcal{M}_C(\mathcal{Q}_{\mathcal{M}_H}(D_\nu^\mu(n)_o))) \\
&= \sum_{j=0}^{|\nu|-|\mu|-1} \left( \dim_{\mathbb{H}}(\mathcal{M}_C(\mathcal{Q}_{\mathcal{M}_H}(A_{n-1-l(\lambda_{|\nu|-j-1}^t) \cup A_{n-1-l(\lambda_{|\nu|-j-1}^t)} + \dim_{\mathbb{H}}(\mathcal{S}_{(\lambda_{|\nu|-j-1}^t, 1)} \cap \bar{\mathcal{O}}_{\lambda_{|\nu|-j}^t})) \right) \\
&= \sum_{j=0}^{|\nu|-|\mu|-1} \left( n - 1 - l(\lambda_{|\nu|-j-1}^t) - \frac{1}{2} \sum_i ((\lambda_{|\nu|-j}^t)_i)^2 \right. \\
&\quad \left. + \frac{1}{2} \left[ 1 + 2l(\lambda_{|\nu|-j-1}^t) + \sum_i ((\lambda_{|\nu|-j-1}^t)_i)^2 \right] \right) \\
&= \sum_{j=0}^{|\nu|-|\mu|-1} \left( n - \frac{1}{2} + \frac{1}{2} \left[ \sum_i ((\lambda_{|\nu|-j-1}^t)_i)^2 \sum_i ((\lambda_{|\nu|-j}^t)_i)^2 \right] \right) \\
&= \frac{1}{2} (2n - 1)(|\nu| - |\mu|) - \frac{1}{2} \left( \sum_i (\nu_i)^2 - \sum_i (\mu_i)^2 \right).
\end{aligned} \tag{6.105}$$

In the case of even theories, since both of the partitions had to be odd, or both even, this result was guaranteed to be an integer, since the differences were always even. For odd theories, however, there can be one odd and one even partition. In this case, the first term is clearly not an integer. However an odd magnitude partition must contain an odd number of odd parts with odd multiplicity. Since odd numbers square to odd numbers, the sum of the squares of the parts has an odd number of odd numbers in it and so is odd. If one term in (6.105) is a half integer, the other must be a half integer and so the total is an integer.



# Conclusions

## 7.1 Summary

Part I of this thesis has explored topics concerning the vacuum states of  $3d \mathcal{N} = 4$  quiver gauge theories. Building on previous work concerning linear quivers, we have constructed descriptions of the local geometric structure of the moduli spaces of vacua for two generalisations of linear quivers. Firstly circular quivers where there is an additional gauge node and additional bifundamental hypermultiplets related to the two ends of a linear quiver. Secondly, D-type Dynkin quivers wherein an extra gauge node is connected to the penultimate node of a linear quiver via bifundamental hypermultiplets. Nilpotent varieties in semi-simple Lie algebras have played a central role, as has the physical realisation of the associated singularity structures known as the Kraft-Procesi transition. For circular quivers we also made extensive use of the realisation of the theories in question as the infrared dynamics of certain brane constructions.

For circular quivers we first had to determine an appropriate set of theories from which we could perform Kraft-Procesi transitions in order to uncover the local singularity structure of the moduli spaces of vacua. This turned out to be significantly more involved than for the linear quiver case, made more complicated by the fact that a global description, in the spirit of nilpotent orbits for the linear case, was unavailable for the circular case. Once we had settled on an appropriate such minimal set of maximal theories, we set about making extensive use of realisation of the Kraft-Procesi transition in an appropriate brane construction to uncover the Hasse diagram for the moduli space of vacua for these theories. We also provided the necessary editing procedures which should be employed when dealing with specific cases. We made use of detailed checks of the dimension of the varieties under construction along the way in order to be sure of the results of our work.

For D-type Dynkin quivers we dispensed with the construction of appropriate brane systems (despite their existence in the literature) in order to begin to develop a notion of quiver addition. In quiver addition we begin with a certain quiver which has a certain moduli space of vacua. A quiver whose moduli space of vacua is an appropriate transverse slice is then added, following a prescribed set of rules, to the first quiver. The resulting quiver's moduli space of vacua is then properly described as a larger singular variety wherein the entire moduli space of vacua of the initial quiver is singular within a transverse structure given by the moduli

space of vacua of the quiver being added. In this way we were able to build up a Hasse diagram describing the moduli space of vacua of larger and larger quivers. Indeed for the case of strictly D-type Dynkin quivers we were able to give general descriptions using this method, and therefore classify all of the quivers of interest using a minimal set of data. We performed numerous checks of our construction using multiple different calculations of the dimension of the algebraic varieties under construction. Our results successfully passed all of these checks.

The work in this Part has resulted in the publication of two papers, one concerning circular quivers [1], and one concerning D-type Dynkin quivers [2]. Both papers have received praise and criticism and we take time to mention the latter here.

The work on circular quivers is incomplete. This is a small matter, hinted at by the fact that there are circular quivers which can be written down, with accompanying brane constructions, but whose moduli space description was inaccessible by the methods presented here. These theories were given in Fig. 5.21 and are called  $\pi(1, 2, 2, L)$  and  $\pi(3, 2, 2, L)$ . It is clear that the algebraic variety given by the moduli space branches of the  $3d \mathcal{N} = 4$  quiver gauge theory describing the lower energy dynamics of the brane system given in Fig. 5.21 is not constructed from the transverse slices we are familiar with. This is what it is for it to be impossible to perform Kraft-Procesi transitions in the familiar way. Indeed, for these constructions, an entire wrapped brane must be pushed out at a time. For larger quivers this was also the case, we could choose to push an entire wrapped brane from one moduli space branch into the other in a single go. However for larger brane systems this manoeuvre was always explicable in terms of familiar Kraft-Procesi transitions, and so the finer structure could be uncovered. Note that the quiver describing these pathological theories is in fact not *simply-laced*, that is, there are multiple sets of bifundamental hypermultiplets transforming in a given pair of gauge node factors (multiple edges between a given pair of nodes). This feature complicates matters and moves us away from the techniques used and developed here, and is a ripe area of current and future study.

The work on D-type Dynkin quivers is complete in its initial target. This target was the construction of the moduli space of vacua for unitary quiver gauge theories whose gauge nodes and bifundamental hypermultiplets strictly form a D-type Dynkin diagram. However the method it attempts to set in motion, quiver addition, is far from complete as a result. In this section we fixed rigid the D-type Dynkin diagram structure of the quiver, and so ignored any of the transverse slices it may have been possible to add to the quiver which involved connecting gauge nodes not already connected. This was important for our strict requirement that the quiver remain of D-type Dynkin. We determined all of those nilpotent varieties of  $\mathfrak{so}_{2n}$  which could be realised as Higgs branches of quivers which were strictly of D-type Dynkin shape and found these to be those appearing in the *special slice*. From there we moved away from strictly using  $\mathfrak{so}_{2n}$  nilpotent varieties in order to determine the moduli space of vacua singularity structure for all D-type Dynkin quivers. However a potentially more interesting and complicated question is to turn this on its head. Instead of asking which varieties could be realised with strictly D-type Dynkin quivers, ask which quivers realise the further nilpotent varieties of  $\mathfrak{so}_{2n}$  outside of the special slice. We will say more about future work next.

## 7.2 Future directions

Numerous open questions exist in quiver gauge theory [65]. There is a huge amount of recent, current, and inevitable future work to be done on matters related to the topics we have discussed. These especially concern the relationship that  $3d\mathcal{N} = 4$  quiver gauge theory moduli spaces have to the moduli spaces of other theories with eight supercharges in a diverse range of dimensions. There is also much to be done on the subject of *quiver manipulations*. We have discussed the first steps towards a notion of quiver addition here, however quivers maybe added, glued, folded, and perhaps have other procedures applied to them. All of these are promising lines of research and forays are already being made into them and the associated geometric manipulations of the moduli spaces of vacua. Furthermore, the study of mixed branches in the moduli space is in its relative infancy as compared to the Higgs and Coulomb branches specifically, and this may lead on to a better study of *bad* quiver gauge theories, which cannot undergo complete Higgsing. An extensive but not strictly comprehensive list of current efforts is [63–83].

Now we shall discuss some of those potential future directions which the author would find most personally satisfying. These are not necessarily those mentioned above which represent the direction in which the thrust of this topic is moving. We mentioned in the criticism section above that a great deal more effort has been put into realising certain geometric structures as the moduli spaces of vacua of quiver gauge theories (the geometry is fixed) than has been put into finding the moduli space of vacua of specific classes of quivers (the quiver shape is fixed, as with our discussion of D-type Dynkin quivers). The work presented here most naturally generalises to the fixed quiver, not the fixed geometry, scenario. There are two main generalisations to consider, different gauge groups and different quiver shapes. Different gauge groups are already considered in some simple cases (such as linear quivers) in the resources mentioned above and we shall not dwell on them here.

The study of different quiver shapes is a vast untapped area however. There are two main ways in which the quiver can be changed, shape and lacings. The study of non-simply laced (more than one edge between two given nodes) quivers with unitary gauge nodes touches upon several topics already mentioned including the realisation of the nilpotent varieties of other classical Lie algebras as moduli space branches, and the encompassing of the pathological quivers encountered in the circular case above (whose quiver is really non-simply laced). It also touches upon some present work by way of quiver foldings, non-simply laced quivers being realisable as a *folding* of a simply laced quiver. The full generalisation of quiver shape has been largely left untouched so far. The geometry-first approach naturally focuses in on quivers whose shape is a Dynkin diagram because (some of) these quivers realise nilpotent varieties (and associated varieties) as moduli space branches. It is clear though that the study of the deep connection between quiver shape, moduli space geometry, and nilpotent varieties (used as building blocks) is only just beginning. From our work with circular (which can be thought of as the *affine* A-type Dynkin) quivers, and D-type Dynkin quivers, it is plain that linear quivers can be thought of as building blocks for more complicated quivers. Since the moduli spaces of vacua for linear quivers are nilpotent varieties, these nilpotent varieties can be seen as building blocks of sorts for the moduli spaces of vacua of the more complicated quivers. Tackling the simply-laced exceptional cases and further affine cases is the obvious next port-of-call. The main impediment to the use of the techniques here is identifying all of the possible singularities associated to minimal degenerations which it is possible

to add to or remove from a given quiver. For example, for the simply laced exceptional cases there are the quivers whose moduli spaces of vacua are the closures of the smallest non-trivial nilpotent orbits of the associated exceptional Lie algebras. These didn't appear in either circular or D-type considerations, but would be necessary to consider there. Before tackling all possible quiver shapes (as surely must be the ultimate goal of any such line of work) one must be certain of having all of the possible minimal quivers (associated to fundamental types of singularity in the moduli space) with which one can play.

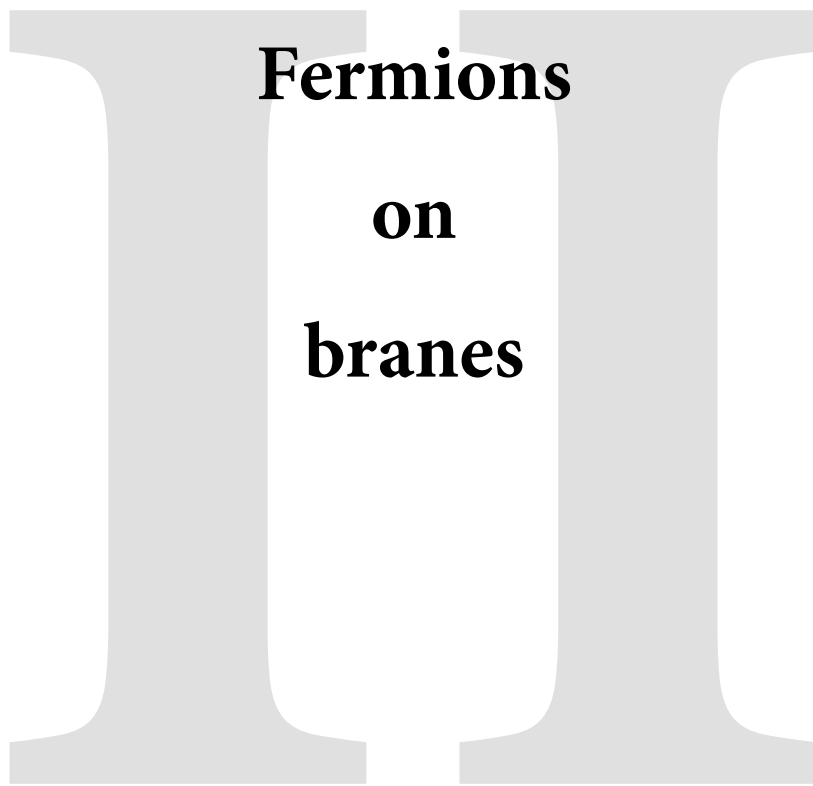
Further work in and around the topics with which we have concerned ourselves for the last 100 or so pages are appearing rapidly and regularly. While the work contained in this thesis is about to make a hard gear-change onto a different subject, the author will always have a fondness for these quiver gauge theories, and will keep at least tokenly abreast of developments for years to come.

**Chainsaw poem 5**

*by Giacomo Pope*

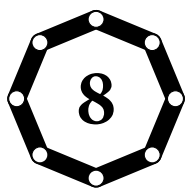
Learning that  
you don't saw  
something  
in half.

There's this piece  
in the middle  
that gets all  
gobbled up.



**Fermions  
on  
branes**





# Introduction

The specific cluster within the Theoretical Physics Division at Liverpool in which I have spent the last four years is that of *String Phenomenology*. The work I performed for over half of my PhD, and which forms Part I, has hardly lived up to this cluster's line of work in an obvious fashion. In the first term of my third year, however, I was encouraged and guided to branch out into areas away from quivers, and pursue a more string phenomenological topic.

String Theory represents a bewilderingly vast, complicated, and difficult set of tools for someone trying to do phenomenology. It can be inordinately difficult to extract 'realistic' physics, not necessarily because strings couldn't hypothetically provide reality, but because finding a 'nice' answer amongst what strings can do is such a herculean task. Compounding this is the fact that full String Theory is indeed extraordinarily complex and our understanding is far from complete. Indeed, throughout this Part we won't *really* be using String Theory, but supergravity (which arises in the low energy limit)<sup>12</sup> as a stand-in for something that in actuality is more complicated. Nevertheless even working with eleven and ten dimensional supergravity theories can prove quite brutal enough. This Part, and the paper [3] that was the result of the work underlying it, pursues an improved understanding of a single type of ingredient in string phenomenology, namely the fermionic couplings for field theories living on branes. This type of ingredient appears prominently in many of the most promising phenomenological pursuits in String Theory today.

Despite the ubiquity of branes in String Theory and the prominent position of fermions in physics, the fermionic fields living on branes are often less well understood than their bosonic counterparts due in no small part to their inherent technical complexities. Nevertheless, many phenomena in high-energy physics involve fermions, and in a large variety of string theoretic scenarios branes are crucial tools, therefore a detailed understanding of fermions on branes is very important.

Ever since the discovery that branes are objects intrinsic to string theories [84], they have been extensively studied in a multitude of contexts. In type II theories, D-branes provide string theoretic realizations of gauge theories (an example of which was already discussed at length in Part I), supersymmetry breaking, and inflation, among others. In many of these studies their worldvolume fermions play central roles in the mech-

---

<sup>12</sup>The irony of the fact that four years of work in *high energy physics* has persistently involved chasing zero- and low- energy limits has not escaped the author.

anisms under investigation. Of particular interest recently is the KKLT scenario [85], a proposal to generate de Sitter vacua in String Theory, where branes are crucial for multiple purposes. The KKLT construction was originally described at an effective 4-dimensional level and so the viability of the proposal has now got to be scrutinized at the 10-dimensional level. This has been done from many perspectives (see e.g. [86–104]). Initially, KKLT-related works considering fermions on branes focused on counting zero modes of brane instantons (see e.g. [105–107]). More recently new developments in this sector have led to an interest in higher order fermion terms on brane actions [108–115], bringing to this context open questions first posed by Hořava and Witten [116–118]. In the well-understood case of non-localized gauginos, supersymmetry gives rise to a ‘perfect square’ structure in the action [119], and it is not currently known how this structure extends to the case of localized gauginos. Shedding light on these terms has been one of the main motivations that has led to the study of higher-order fermionic couplings in  $Dp$ -brane actions pursued in this Part. Another feature that makes branes extremely promising tools for model building resides in the fact that they break half of the bulk supersymmetries (this was first observed in [17, 18]). Supersymmetry breaking is still not completely understood in String Theory proposals, but  $Dp$ -branes are good candidates to provide ways to achieve it without spoiling the solution to the Hierarchy Problem since their fermionic degrees of freedom can realize supersymmetry non-linearly [17, 18, 120–122]. This is a key reason for devoting our interest to the topic from a very general point of view. In [107, 123–127], the worldvolume action of  $Dp$ - and  $Mp$ -branes in an arbitrary bosonic background has been determined up to quadratic terms in fermions. Our aim is to understand more deeply the mathematical structure underlying the action of a  $Dp$ -brane, independently of the fermionic order of interest, and to set the stage for a concrete determination of the order-4 fermionic terms in the imminent future. A fundamental feature will be the structure inherited by the  $Dp$ -branes from the more fundamental underlying theory, the M2-brane theory, as part of the web of string dualities. It would also be possible to inherit the structure from the M5-brane action, but the simplicity of the M2-brane action makes this choice more practical.

It has been understood for quite some time that the five initially distinct-looking superstring theories are in fact limiting cases of a single fundamental theory, M-theory [128]. The five string theories and M-theory are related to each other via a web of *dualities* that we sketch in Fig. 8.62. In this Part, we are going to concentrate on three of these related theories, the dualities which connect them, and the fermions on the branes that the theories contain. We will be investigating the M2-brane from M-theory and the  $Dp$ -branes from the type IIA and type IIB superstring theories (more properly, we will be working with the low-energy supergravity limit of these theories, i.e. 11-dimensional supergravity, from M-theory, and type IIA and type IIB supergravities, from type IIA and type IIB string theories). Compactifying the 11-dimensional spacetime of M-theory on a circle transforms the M2-brane into a D2-brane (when the circle is orthogonal to the brane), and then an arbitrary number of T-dualizations along directions wrapped by the brane, or orthogonal to it, allow us to investigate descriptions of any  $Dp$ -brane. Our goal when it comes to these branes is to explore how to explicitly obtain the terms in the single-brane abelian actions corresponding to high-order couplings for the fermions. Of critical importance to us is the requirement that our methods are, at least in principle, applicable to arbitrary order in the fermions. As we will show, a central development consists of understanding how to dimensionally reduce and T-dualize the theories into each other in a manifestly supersymmetric way,

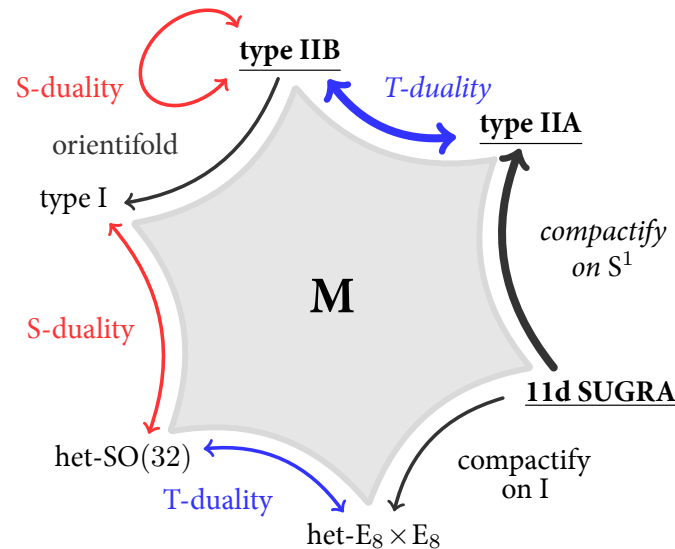


Figure 8.62: A schematic of the web of dualities between the five 10-dimensional string theories and 11-dimensional supergravity (and M-theory). We will use the superspace generalization of this web to investigate the expansion in fermions of the superfields in different theories, and the expansion in fermions of the actions for the branes those theories contain. The parts of the web relevant for this Part have been highlighted with thicker arrows. We begin with the superspace formulation of 11-dimensional supergravity. We find the expansion in fermions of the superfields therein, and use these to find the fermionic expansion of the M2-brane action. Compactification on  $S^1$  is then performed in order to obtain the fermionic expansion of the fields in type IIA, and of the D2-brane action. Finally, T-duality between type IIA and type IIB is used repeatedly to obtain expansions of the fields in type IIB, and so the expansions for  $Dp$ -branes for all  $p$ .

by working in superspace.

## Strategy

We now outline the core details of the strategy that we follow. Due to the existence of the string duality web, if we have a method for obtaining the high-order fermion couplings in one theory it can in principle be extended to the others. We start with 11-dimensional supergravity which has a particularly simple formulation in superspace, wherein the usual dimensions of spacetime are augmented with anticommuting dimensions with Grassman-valued coordinates. In this formulation the usual fields are combined into superfields which contain both bosonic and fermionic degrees of freedom. What we then require is a way of systematically extracting information about the fermionic degrees of freedom from the superfield formulation. The technique used to do this in a complete way is called the ‘normal coordinate’ method,<sup>13</sup> first developed in superspace in [129], and often simply referred to as NORCOR. The question of determining fermionic couplings is turned into a question of differential geometry in superspace in a way that is both elegant and powerful. In [130], many of the results necessary for finding the expansion of the M2-brane action to fourth order in fermions were developed, this is also the order up to which we will expand in the examples which accompany our analysis. The NORCOR method can be applied to determine expansions of the superfields of 11-dimensional supergravity at all orders in fermions [131]. Nevertheless, we show that the usefulness of the approach can be

<sup>13</sup>We shall see in chapter 10 that for our purposes this name is an anachronism and that for the physics we investigate we do not require the specific use of a normal coordinate system.

limited because the size of the formulae grows quickly as one computes terms of higher  $\theta$ -order in the superfields. This is the main obstacle we find in our computations, and it will bring us to the conclusion that unless one succeeds in combining terms obtained with NORCOR together into simple and manageable formulae, it remains extremely challenging to extract information valuable for physics.

After setting up the problem in M-theory we are going to use the web of string dualities to carry the information about fermionic expansions to the type II theories. However, in order to use the superspace formalism when considering the web of dualities, we promote the duality procedures to superspace as well. This circumvents some of the difficulties in applying NORCOR directly to the type II theories by instead only requiring the explicit use of NORCOR in the relatively simple world of 11-dimensional supergravity. In this way a circle compactification will provide us with the superspace formulation of the D2-brane action and T-dualities will allow us to obtain the  $Dp$ -brane actions in superspace for an arbitrary value of  $p$ , in both type IIA and type IIB string theories. We will take advantage of the T-duality rules for fermions [132–134] and express them in a convenient formalism for our superspace approach, spinor doublet notation.

While our motivations are certainly braney in origin, the techniques we investigate and develop are far more broadly applicable. The actions of the single M2-brane and for single  $Dp$ -branes are just some examples of composite superfields that can be built from the fundamental superfields of their respective theories, although, as we have discussed, even these abelian cases are particularly relevant and interesting. We will structure our discussion, therefore, to concentrate on obtaining the  $\theta$ -expansions of certain superfields in each theory, and investigate how they can be combined in order to obtain the brane action expansions in separate examples.

## Outline

This Part is organized as follows. In chapter 9, we review background information about branes which motivates the analysis of later chapters. We concentrate on viewing branes as hypersurfaces in curved superspace, and the role of the Goldstone fermions arising from the broken supersymmetry caused by the presence of a brane. In chapter 10, we review the use of the ‘normal coordinate’ method to provide an expansion in orders of fermions starting with the superspace formulation of the fields of 11-dimensional supergravity. In chapter 11, we consider the application of the normal coordinate expansion to the superspace formulation of the M2-brane action and we obtain expansions to quartic order in fermions. In chapter 12, we investigate the superspace generalization of the dimensional reduction of fields in 11-dimensional supergravity to type IIA. We use this to determine the D2-brane action to quartic order in fermions. In chapter 13, we discuss the superspace generalization of the T-duality relation between fields in type IIA and type IIB string theories. We demonstrate how this can be used in principle to move from the action for the D2-brane at a given order in fermions, to that for any  $Dp$ -brane at the same order, and give explicit examples at second order. We end in chapter 14 with a summary of our results, our conclusions, and a discussion of future lines of inquiry. Our discussion is complemented by several appendices. Appendix 15.1 summarizes our spinor conventions. Appendix 15.2 reviews 11-dimensional supergravity. Appendix 15.3 contains details about quartic-order fermionic expansions in superspace. Appendix 15.4 contains a catalogue of useful identities for the dimen-

sional reduction from eleven to ten dimensions. Appendix 15.5 is reserved for a discussion of topics related to T-duality.

## Notes on notation

Throughout this Part we perform a large number of steps on a large number of quantities. Making our full discussion as clear as possible by avoiding notational clashes therefore necessitates the use of a large range of notation. It is worth our time to take a moment to mention a few of the most consequential choices and changes we make in this regard.

### Indices

We are going to be working with many different sets of indices throughout. We collect details about all of these index choices here for easy reference. For easy reading we will repeat our conventions in the context of the chapters when appropriate.

In chapters 9, 10 and 11, we will be working with (11|32)-dimensional superspace. Our superspace conventions are the following. Superspace coordinates are  $Z^M = (x^m, \theta^\mu)$ , where upper-case letters in the middle of the alphabet are used to denote superspace coordinates, lower-case Latin letters denote spacetime indices,  $m = 0, 1, \dots, 10$ , and lower-case Greek letters stand for Grassmann indices,  $\mu = 1, \dots, 32$ . We will use Latin and Greek indices in the beginning of the alphabet to refer to tangent space directions as  $A = (a, \alpha)$ , with  $a = \underline{0}, \underline{1}, \dots, \underline{10}$  and  $\alpha = \underline{1}, \dots, \underline{32}$ . We will use lower-case Latin indices like  $i, j, k$  for worldvolume directions, because we work only with the M2-brane this means that  $i = 0, 1, 2$ .

In chapter 12, we will perform dimensional reduction from (11|32)-superspace to (10|32)-superspace. All 11-dimensional spacetime or tangent spacetime indices will now receive hats such that  $\hat{m} = 0, 1, \dots, 10$  and  $\hat{a} = \underline{0}, \underline{1}, \dots, \underline{10}$  whereas the 10-dimensional indices will not receive hats so that  $m = 0, 1, \dots, 9$  and  $a = \underline{0}, \underline{1}, \dots, \underline{9}$ . Under the dimensional reduction which we perform the M2-brane gets taken to the D2-brane. Therefore in chapter 12, where only the D2-brane is discussed, we still have  $i = 0, 1, 2$ . The Grassman indices will remain unchanged.

Finally, in chapter 13 we perform T-duality on (10|32)-superspace. This involves singling out a direction to take as a circle, which we will take to be the direction  $x^9$ . We will then maintain the convention that 10-dimensional indices will not receive hats so that  $m = 0, 1, \dots, 9$ , and we shall use a dotted index if referring only to the directions transverse to the T-duality circle so that  $\dot{m} = 0, 1, \dots, 8$ . We will also shift to using double spinor notation; however a detailed explanation of this change is given in the chapter itself. When dealing with  $Dp$ -branes, T-duality maps the brane content of the type IIA theory and the brane content of the type IIB theory into one another, changing the dimensionality. As such, the worldvolume indices  $k, l$  run over all the  $p + 1$  worldvolume directions, whereas indices  $m', n'$  span the complementary transverse directions, with  $p$  always being clear in context. If the brane wraps the T-dual direction, we will employ a dot-notation  $\dot{k}, \dot{l}$  when referring to all the worldvolume directions other than the T-dual one<sup>14</sup>.

<sup>14</sup>Starting now at  $\dot{k}$  to avoid the notational abominations that would be  $\dot{i} \dot{j}$ .

*Hats*

In chapters 10 and 11, we will be working in eleven spacetime dimensions. Then, in chapter 12, we will be reducing to ten dimensions many of the quantities from previous chapters, and we will also work with them in chapter 13. In order to distinguish 11-dimensional quantities from 10-dimensional ones when performing dimensional reduction in chapter 12 we place hats on all 11-dimensional objects and indices. However, because our use of 11-dimensions is implicit in chapters 10 and 11, and to avoid swamping the notation in those chapters with hats, we do not use the convention of hatting 11-dimensional quantities until chapter 12 itself. Similarly, in appendices 15.1 and 15.4, where we discuss both 11-dimensional and 10-dimensional quantities, we are sure to distinguish them from one another with the hatting convention, however in appendices 15.2 and 15.3 where everything is implicitly 11-dimensional, we drop them.



# Branes, fermions, and superspace

In this chapter we provide some general background information about both M2-branes and  $Dp$ -branes. This will motivate our discussion in the coming chapters. For concreteness we mostly focus on the case of a single M2-brane, but the ideas apply in a similar way for  $Dp$ -branes as well. The ideas in this chapter also hold for the M5-brane and the Green-Schwarz string, but as we already mentioned we will restrict ourselves to the M2-brane and  $Dp$ -brane cases.

## 9.1 Braney fermions

M2-branes and  $Dp$ -branes are solitonic solutions of M-theory and type II supergravities, respectively. ‘Brane-only’ solutions are characterized by the breaking of the 11- or 10-dimensional Poincaré symmetry group down to the Poincaré group on the directions spanned by the brane times the group of rotations in the transverse space, i.e.  $ISO(1, 10) \rightarrow ISO(1, 2) \times SO(8)$  for M2-branes and  $ISO(1, 9) \rightarrow ISO(1, p) \times SO(9 - p)$  for  $Dp$ -branes. The Goldstone modes associated to the breaking of the Poincaré symmetry become bosonic degrees of freedom living on the brane worldvolume [135]. In these cases, the brane solution also triggers a spontaneous breaking of half of the bulk supersymmetries and the associated fermionic Goldstone modes turn into fermionic degrees of freedom on the brane.

### 9.1.1 Superspace perspective and the M2-brane action

In this Part we are interested in the action describing these localized branes, with a particular interest in fermionic modes living on them and their couplings in the brane worldvolumes. For this purpose it is convenient to approach branes from a slightly different perspective, that of the superspace formulation of the supergravity theories. In this formulation, branes can be regarded as extended objects in curved superspace. This is the approach taken in [136, 137] to construct the action of the M2-brane: the M2-brane is a  $(2 + 1)$ -dimensional object in  $(11|32)$ -dimensional superspace and its action consists of a brane worldvolume term, coupling the brane to the background metric, and a Wess-Zumino term, coupling the brane to the background

gauge sector. Denoting the coordinates that span the worldvolume as  $\zeta^i$ , with  $i = 0, 1, 2$ , this action reads

$$S_{M2} = -T_{M2} \int d^3\zeta \sqrt{-\det(P[G](Z))} + \mu_{M2} \int P[A](Z), \quad (9.106)$$

where  $T_{M2}$  is the M2-brane tension,  $\mu_{M2} = T_{M2}$  is the brane charge, and  $P[G](Z)$  and  $P[A](Z)$  are the pullbacks of the 11-dimensional supermetric and three-form gauge potential onto the brane worldvolume respectively, with  $Z^M$  representing the superspace coordinates. The pulled-back superfields are built out of components of the supervielbein  $E_M^A(Z)$  and the super-three-form  $A_{ABC}(Z)$ .

The above action is a superspace generalization of the standard bosonic action of the M2-brane, where all fields in the latter are replaced by their superfield counterparts. A product of superfields is a superfield itself, so what we have above is the M2-brane action superfield. Of course, since all superfields depend on superspace Grassmann coordinates  $\theta^\mu$ , so does the action, and both allow for finite expansions in  $\theta$ . Concretely, because the superfields in the action are the supervielbein  $E_M^A(Z)$  and the super three-form gauge potential  $A_{ABC}(Z)$ , if one knows the  $\theta$ -expansion of these superfields, one can obtain the expansion of the action superfield. Both 11-dimensional supergravity, and the type II supergravities in ten dimensions considered in this Part, have 32 supercharges and so the fermionic expansion of the superfields goes up to order 32 in Grassmann coordinates  $\theta^\mu$ . Note that although we are dealing with the brane action, and although the presence of the brane leads to partial supersymmetry breaking, we construct the brane action using off-shell superfields.

## 9.2 The bulk and $\kappa$ -symmetry

We mentioned before that, from the perspective of the bulk, the presence of the brane in the brane-only solutions only preserves half of the supersymmetries. Let us consider the bulk supercharges that are preserved in this type of solution separately from those that are spontaneously broken. The Goldstone modes associated to the latter are fermionic degrees of freedom localized on the brane, arising from the  $\theta^\mu$ -directions that the broken supercharges generate on the (off-shell) superfields. The other supercharges are not affected by the presence of the brane, and so the brane action must be invariant under the shifts they generate in the corresponding Grassmann directions. Combining these ideas together, we see that the superspace Grassmann coordinates on the brane action superfield are lifted to localized fermions living on the brane  $\theta^\mu(\zeta^i)$ , with only half of them (the ones generated by spontaneously broken supercharges) being physical and the other half being associated to transformations that leave the action invariant. From the brane worldvolume perspective, when we lift the Grassmann coordinates  $\theta^\mu$  to fermions living on the brane, because we use the bulk off-shell superfields to write the action, we find that half of these fermions are physical whereas the other half are not physical and instead correspond to redundancies. The existence of these redundancies implies a fermionic gauge symmetry of the action, commonly known as  $\kappa$ -symmetry. In [136] it was shown that the action (9.106) is indeed invariant under  $\kappa$ -symmetry transformations. More comments about the interplay between bulk supersymmetry and  $\kappa$ -symmetry are in chapter 11.



### 9.3 Our approach

These arguments provide a clear approach for obtaining the fermion couplings of the M2-brane action. One needs to obtain the  $\theta$ -expansion of the superfields involved, plug them into the action (9.106), and then lift the Grassmann coordinates to fermionic fields on the brane  $\theta^\mu(\zeta^i)$ . We will follow this approach in order to obtain the M2-brane action at order  $(\theta)^4$ , and so obtain fermionic interaction terms up to quartic order. The approach can in principle be used to obtain the action at all orders in fermions.

Note that we used the brane-only solution to illustrate how to obtain fermion couplings on the brane worldvolume, but our interest includes much more general solutions with the only demand being that they include branes. Many points made above change when moving from the brane-only solution to more general solutions with branes, for example some of the fermions on the brane can be massive and not correspond to the goldstinos of the solution (points of this kind can be found in e.g. [138]). Crucial for our purposes, the fermion couplings that are obtained in the superspace formulation are completely general and do not restrict to couplings on the brane-only solution.

In the above analysis we focused on the M2-brane case, but the same ideas can be extended to all other branes, and in particular to  $Dp$ -branes in type II supergravities. Hence, in order to obtain the  $Dp$ -brane action superfields, one ‘only’ needs to know the superfields involved. Unfortunately, there is no known *simple* approach to obtain the  $\theta$ -expansion of superfields that appear in any of the theories in which we are interested. The method we will use, based on a normal coordinate expansion, is systematic but has limitations in its current form. While effective for the expansion of the M2-brane action, computing the expansion of all superfields using this method turns out *not* to be the best strategy for all  $Dp$ -branes, as we will explain in more detail later. In fact, our strategy will be to use the ‘normal coordinate’ method to obtain the  $\theta$ -expansion of the M2-brane action superfield, and then pursue the results for  $Dp$ -branes using the superspace generalization of the duality web in Fig. 8.62.



# The ‘normal coordinate’ method

In chapter 9 we explained that in order to obtain a fermionic expansion of the M2-brane action one requires the  $\theta$ -expansions of the superfields involved. In this chapter we review a systematic approach to obtain these  $\theta$ -expansions. Later we will specialize and apply this approach to obtain the expansion of some superfields in 11-dimensional supergravity, but the approach discussed here is completely general.

Supergravity in eleven dimensions [139] has a well-established formulation in superspace<sup>15</sup> [140, 141]. From this perspective, the  $\theta$ -expansion of the superfields is just a Taylor expansion describing the dependence of the superfields on the superspace Grassmann coordinates  $\theta^\mu$ . We will use this geometric interpretation in order to obtain the  $\theta$ -expansions we are after. This approach is known as the ‘normal coordinate method’, or NORCOR, because the normal coordinate system was very useful for performing the Taylor expansion of fields in spacetime when the method was originally proposed. We will show, however, that the superspace analysis in which we are interested does not require any special coordinate system. The normal coordinate method is a variant of the background field method to obtain covariant expressions in Taylor expansions of fields. Relevant literature on the development and application of NORCOR is [129, 130, 142–146]. In particular, [130] proposed the use of this method to obtain the  $\theta$ -expansion of the M2-brane action. In this chapter we provide an intuitive and self-contained description of the method.

## 10.1 Generalities

The purpose of the NORCOR approach is to obtain the value of a (super)field at a point  $z_1^M$  in (super)space by starting from the value of the (super)field, and its derivatives, at another point,  $z_0^M$ , which is close to  $z_1^M$ , with

$$z_1^M = z_0^M + \Sigma^M. \quad (10.107)$$

In other words, we obtain the value of the superfield at points in the proximity of a point  $z_0^M$  by performing a Taylor expansion around  $z_0^M$ . This approach is useful when we have plenty of information about the value of the superfield and its derivatives at the *origin*  $z_0^M$ , but the information available at  $z_1^M$  is much more limited.

---

<sup>15</sup>Appendix 15.1 reports our spinor and  $\Gamma$ -matrix conventions. Appendix 15.2 provides notes on the supergravity constraints and Bianchi identities necessary to carry out the analysis in this work.

In our case, we want to Taylor-expand superfields in the Grassmann directions  $\theta^\mu$ : we will take the space-time, i.e. the subspace  $z_0^M = (x^m, \theta^\mu = 0)$ , to be the origin, and perform the expansion along a direction  $\Sigma^M$  that is purely Grassmannian. Let  $S = S(Z)$  be any superfield, and let  $z_0^M = (x^m, 0)$  be the starting point. In order to determine the value  $S(z_1^M)$ , we demand that there exists a geodesic  $Z^M(t)$  with parameter  $t$  connecting  $z_0^M$  and  $z_1^M$ , such that  $Z^M(t=0) = z_0^M$  and  $Z^M(t=1) = z_1^M$ . The tangent vector of the geodesic is  $y^M(t) \equiv dZ^M(t)/dt$ . This tangent vector obeys the geodesic equation

$$y^M(t)\nabla_M y^A(t) = \frac{dy^A(t)}{dt} + y^M(t)\omega_{M^A}^B y^B(t) = 0, \quad (10.108)$$

where  $y^A(t) = y^M(t)E_M^A(Z^N(t))$  is written with the tangent superspace index because the superspace covariant derivative  $\nabla$  comes with a superconnection  $\omega$  generalizing the spin-connection, but nothing analogously comparable to the affine connection. We are expanding along a purely Grassmannian direction, so we want the tangent vector at the origin to point in Grassmann directions, i.e.  $y^M(t=0) = (y^m = 0, y^\mu)$ .

Before proceeding, let us explain why our approach does not need the normal coordinate system. The point of the normal coordinate system is to simplify the geodesic equation at the origin. This is usually achieved because the (affine) connection vanishes there. In our case of interest, however, we can use local Lorentz transformations to set some components of the superconnection to vanish at the origin of Grassmann coordinates, i.e.  $\omega_{\mu^A}^B(\theta^\mu = 0) = 0$ . So for us the geodesic equation simplifies at  $\theta = 0$  regardless of the coordinate system used.

Moreover, Lorentz transformations also permit us to fix the supervielbein in the Wess-Zumino-gauge, such that  $E_{\mu^A}^{\alpha}(\theta = 0) = \delta_{\mu^A}^{\alpha}$ . Then, the solution to the geodesic equation at the origin and its surroundings, in the region where the approximation is valid, is  $Z^M(t) = z_0^M + y^M(t=0)t$ . The point  $z_1^M = (x^m, \theta^\mu)$  is at  $t=1$  on the geodesic, and this allows us to effectively identify the Grassmann coordinate and the origin tangent vector  $y^\mu(t=0) \leftrightarrow \theta^\mu$ .

We are now ready to obtain the  $\theta$ -expansion of any superfield  $S(z_0)$ . To do so, we first use the geodesic above to compute the Taylor expansion with respect to the parameter  $t$  around the point at  $t=0$ , i.e.

$$S(Z^M(t))|_{t=0} = \sum_{k=0}^{\infty} \frac{t^k}{k!} \left( \frac{\delta}{\delta t} \right)^k S(Z^M(t=0)). \quad (10.109)$$

Computing variations in  $t$  means comparing the superfield at the origin with the superfield after dragging it along the geodesic, so we can replace the  $t$  variations with Lie derivatives, denoted  $\mathcal{L}_y$ , along the tangent vector field  $y^M(t)$ . Because we evaluate the derivatives at  $t=0$  the vector  $y$  that appears in the Lie derivatives will also be evaluated at this point. From here on we simply write it as  $y$  and drop that it is evaluated at  $t=0$ , where it only has components in Grassmann directions. Finally, we are interested in obtaining the value of the superfield at the point  $z_1^M$ , where  $t=1$ . Putting these things together we find that

$$S(Z^M(t=1))|_{t=0} = \sum_{k=0}^{\infty} \frac{(\mathcal{L}_y)^k}{k!} S(Z^M(t=0)) = (e^{\mathcal{L}_y} S)|_{t=0}. \quad (10.110)$$

This means that the  $\theta$ -expansion of any superfield in this approach is obtained by repeatedly acting with the Lie derivative. This is effectively the approach followed in [129, 130, 142–146]. It is interesting to point out

that we can write the expansion using the exponential of a differential operator, because this agrees with the fact that a product of superfields is a superfield itself: if  $S$  is a product of superfields, using the Leibniz rule and the exponential expansion one finds that there will be an exponential acting on each superfield involved in the product.

## 10.2 A note on extra complexities

For applying the NORCOR procedure it is important to note that in superspace we have the superconnection (that generalizes the spin connection), and we defined a Lorentz covariant derivative, but we did not define the notion of an affine connection or a fully covariant derivative. For this reason we are often interested in writing superfields with Lorentz indices. Regular Lie derivatives acting on Lorentz tensors do not lead to Lorentz tensors. To fix this problem, we need to replace the regular Lie derivative by the Lie-Lorentz derivative (see e.g. [147, 148] and the original reference [149]). This is a Lorentz covariantization of the regular Lie derivative, wherein partial derivatives are replaced by their Lorentz-covariant counterparts, complemented with the inclusion of an extra term that gives an infinitesimal Lorentz transformation. The effect of this Lorentz transformation is to trivialize the effect on the holonomy group driven by the inclusion of spin-connection terms in the covariantization. For practical purposes we observe that in (9.106) there are no free Lorentz indices, so the extra terms demanded by the Lie-Lorentz derivative will cancel each other in the expansions of the objects we are interested in. For this reason we can (and will) safely ignore the presence of these extra terms. Physics provides an alternative (and, dare we say it, more intuitive) description of the same idea: the Lorentz-Lie derivative above is a combination of a supersymmetry transformation and a local Lorentz transformation, and we will ignore the latter because brane actions have no free Lorentz indices. The  $\theta$ -expansion is therefore obtained by repeatedly taking supersymmetry variations of the fields.

Note that we have turned a problem about worldvolume couplings on branes into a differential geometry problem in superspace, and there is a price to pay for it. If we wish to obtain the superfield expansion systematically using this technique we are also required to do some extra work. On the one hand, we need the value of the superfield at the origin of Grassmann coordinates  $\theta = 0$ , and on the other hand we need to be able to manipulate the outcome of the repeated application of the Lie derivative to write the results in terms of familiar objects. This is substantially easier to accomplish when we focus on computing the expansion of the individual superfields appearing in the action, rather than trying to treat the full action superfield directly. We will use some examples to illustrate these points.

## 10.3 Specifics

As a first example consider the expansion of the 11-dimensional supervielbein that appears in the M2-brane action. We will employ the conventions and the definitions of 11-dimensional supergravity that are reviewed in appendix 15.2. For the first term in the expansion one needs the Lie derivative

$$\mathcal{L}_y E_M^A = \nabla_M y^A + y^C E_M^B T_{BC}^A. \quad (10.111)$$

This formula is obtained via integration by parts, and involves the (Lorentz) covariant exterior derivative,  $\nabla y^A = dy^A - y^B E^C \omega_{BC}{}^A$  (where  $y^A = y^M E_M{}^A$ ), and the (superspace) torsion tensor  $T$ , whose definition is given in (15.256). Note that we wrote the torsion tensor with all indices in tangent space by introducing a supervielbein for convenience. Obtaining the order- $(\theta)^1$  term in the expansion requires evaluating this expression at  $\theta = 0$ , which in turn requires knowledge of the superspace torsion tensor and the supervielbein evaluated on this subspace. We will shortly explain how to perform this evaluation. For now let us point out that without the notion of e.g. the superspace torsion tensor, the Lie derivative would be meaningless, and this makes manifest the need for extra structure to obtain any useful information from this approach.

Let us provide some further formulae necessary to compute higher order terms of the supervielbein expansion. In particular, we will need

$$\mathcal{L}_y G = y^A \nabla_A G, \quad (10.112)$$

$$\mathcal{L}_y y^A = 0, \quad (10.113)$$

$$\mathcal{L}_y (\nabla_M y^A) = -y^B E_M{}^C y^D R_{DCB}{}^A. \quad (10.114)$$

The first formula indicates how the Lie derivative acts on any Lorentz tensor  $G$ . For the second formula we used the previous one together with the geodesic equation. The last formula is also obtained by using integration by parts and the geodesic equation, and  $R$  there is the superspace Riemann tensor defined in (15.257). Again, we find the need of extra structure in order to make sense of certain Lie derivatives. It turns out that the four expressions provided are enough to obtain the  $\theta$ -expansion of the supervielbein at any order. We perform computations up to order four in chapter 11 and appendix 15.3.1.

Once the necessary Lie derivatives have been computed, the next step is to evaluate them at the reference point for the Taylor expansion, that we choose to be  $\theta = 0$ . Again, we concentrate on the 11-dimensional supervielbein for concreteness. The first object to evaluate at this point is the supervielbein itself. We use Lorentz transformations to fix the so-called Wess-Zumino (WZ) gauge<sup>16</sup>, i.e.

$$E_M{}^A(\theta = 0) = \begin{pmatrix} e_m{}^a(x) & \psi_m^\alpha(x) \\ 0 & \delta_\mu^\alpha \end{pmatrix}, \quad (10.115)$$

where  $e_m{}^a(x)$  is the 11-dimensional vielbein and  $\psi_m^\alpha(x)$  the 11-dimensional gravitino. For all other terms appearing in the derivatives, there are a few steps to follow. First we must decide which component of the superfield we are assessing by choosing which of the free indices we would like to be bosonic or Grassmann. Contractions over superspace indices involve both kind of indices, upon expansion we will often find that only one of these kinds contributes. This can be for a number of the reasons including: (1) The supervielbein in the WZ-gauge has some vanishing component. (2) The vector tangent to the geodesic at the origin is constrained to be  $y^M = (0, y^\mu)$  for our particular expansion. Note that the WZ-gauge means that this is  $y^A = (0, y^\alpha)$ . (3) The tangent space structure means no mixing between bosonic and fermionic indices in the superconnection (and so also no mixing in the superspace Riemann tensor). This means  $\omega_\gamma{}^d = \omega_d{}^\gamma = R_{AB\gamma}{}^d = R_{ABd}{}^\gamma = 0$ .

For the terms that survive all of these constraints, one needs to evaluate the superspace tensors involved

<sup>16</sup>We previously used the WZ-gauge to set to zero the  $\omega_\mu{}^{AB}$  component of the superconnection. These two choices are not independent [6] (equation (5.6.8)).

and write them in terms of spacetime fields. To do this we make use of the supergravity constraints and superspace Bianchi identities. It turns out that many components of superspace tensors vanish (for example  $T_{\alpha b}^c = 0$ ) or are constant (for example  $T_{\alpha\beta}^c$ ) all over superspace [141]. Fixing the value of the latter is a matter of conventions. The value of all other components of these superspace tensors can be obtained from superspace Bianchi identities. A list of supergravity constraints can be found in (15.261a - 15.261d) and a list of useful formulae derived from Bianchi identities is given in (15.263a - 15.263c).

As a clarifying example, we evaluate some components of (10.111), at  $\theta = 0$ , using the ideas above. In both cases we consider that the index  $M$  will be restricted to spacetime, and we evaluate the cases where the tangent space index  $A$  is spacetime and Grassmann separately. We obtain,

$$\mathcal{L}_y E_m^a = \nabla_m y^a + y^\gamma E_m^B T_{B\gamma}^a = \nabla_m y^a + y^\gamma E_m^\beta T_{\beta\gamma}^a \stackrel{\theta=0}{=} -iy^\gamma (\Gamma^a)_{\beta\gamma} \psi_m^\beta, \quad (10.116a)$$

$$\mathcal{L}_y E_m^\alpha = \nabla_m y^\alpha + y^\gamma E_m^B T_{B\gamma}^\alpha = \nabla_m y^\alpha + y^\gamma E_m^b T_{b\gamma}^\alpha \stackrel{\theta=0}{=} \nabla_m y^\alpha + y^\gamma e_m^b T_{b\gamma}^\alpha. \quad (10.116b)$$

In both cases we first fixed as many indices as possible to be either spacetime or Grassmann, leaving only the contraction of  $B$  with both types involved, then we got rid of vanishing contributions by using  $T_{b\gamma}^a = T_{\beta\gamma}^\alpha = 0$ . Finally we evaluated the surviving terms using the WZ-gauge for the vielbein (10.115) and our convention for the constant torsion component  $T_{\beta\gamma}^a = -i(\Gamma^a)_{\beta\gamma}$ . We left  $T_{b\gamma}^\alpha$  untouched here, but it is a simple combination of  $\Gamma$ -matrices and four-form flux, as shown in (15.264a).

Once the formulae for the Lie derivatives have been evaluated at the origin of Grassmann coordinates, and re-written as described above, one can write the superfield expansion. In order to do so one must replace the tangent vector  $y$  by the Grassmann coordinate  $\theta$  (this happens when we evaluate the geodesic at  $t = 1$ ). For the components of the supervielbein in the above example this gives the expansions up to order  $(\theta)^1$ , i.e.

$$E_m^a(Z) = e_m^a(x) - i\bar{\theta}\Gamma^a\psi_m(x) + \dots, \quad (10.117a)$$

$$E_m^\alpha(Z) = \psi_m^\alpha(x) + (D_m(x)\theta)^\alpha + \dots. \quad (10.117b)$$

In the first formula we wrote the fermion bilinear with the Dirac conjugate  $\bar{\theta} = \theta^T C$ , with  $C$  being the charge conjugation matrix, see appendix 15.1 for our conventions. For the second formula, we noted that the torsion can be manipulated and combined with the covariant derivative into the *supercovariant* derivative  $D_m = \nabla_m + \check{T}_m$ , where  $\check{T}_m$  is related to  $T_m$  by a transposition. An alert reader will notice that the first order terms in the expansion are (unsurprisingly) the expressions that appear in the supersymmetry variations of the vielbein and the gravitino.

The above method gives rise to a superfield expansion in terms of familiar objects. This is not the end of the story, however. The method relies on writing all contractions in terms of tangent space indices. This often requires including numerous supervielbeins, and these can result in a rapidly growing number of terms when one computes higher and higher order Lie derivatives of any superfield. Higher-order terms, written in terms of spacetime fields, therefore involve an increasing number of contributions. This can cause the expansion to become enormously cumbersome unless one finds a way to put contributions at each level together into more compact and tractable combinations. As a simple example, recall that in the supervielbein expansion we combined the covariant derivative of  $\theta$  together with the term related to the torsion into the supercovariant

derivative. At higher orders it becomes increasingly complicated to combine terms together into manageable expressions. This will be the primary cause of the limitations we find in our computations. We will make further comments about this when we can make more precise statements.

Finally, we will be concentrating on determining expressions for the case where the background is bosonic. Practically speaking, we do this by turning to zero all the terms involving the 11-dimensional gravitino. This means that we also turn to zero all superspace tensors with an odd number of Grassmann indices, since they involve the gravitinos when written in terms of spacetime objects. This restriction causes many more terms in the expansions to vanish. The Lie derivative applied to a bosonic field (a superspace tensor with an even number of Grassmann indices) an odd number of times will always vanish in bosonic backgrounds, as will the expression for the Lie derivative applied to a fermionic field an even number of times. In order to study completely general backgrounds, one would simply not perform this step and maintain all the gravitino terms in the discussion as well.

Now that we have explained the approach, we are ready to spell out why it is more convenient to only use NORCOR in eleven dimensions. In ten dimensions there are more fields and more superspace tensors involved. This means that one needs to work harder in order to obtain all the supergravity constraints and useful formulae from Bianchi identities in each theory, and of course applying them to re-write the Taylor expansions requires performing even more computations. Moreover, the ‘simplicity’ of 11-dimensional supergravity enables us to more clearly capture the structure of the terms involved, and we will show later that this structure is, in a sense, ‘inherited’ by the 10-dimensional theories. We will make this statement more precise later. Nevertheless, we already mentioned that even in this ‘more simple’ theory we encounter difficulties when manipulating higher-order terms. Clearly this problem does not improve for 10-dimensional type II theories. Computing NORCOR expansions in eleven dimensions is substantially cleaner and allows us to make insights and extract information about structure more easily. It is a better strategy, then, to obtain all expansions in this theory and then obtain expansions in ten dimensions via the superspace duality web, as we describe below.

A final compelling reason to use the method in eleven dimensions only is that higher order expansions of the M2-brane action can be obtained with essentially just the 11-dimensional supervielbein expansion, whereas in all other cases one must compute the expansions of more fields. In order to explain what we mean by ‘essentially’, we can consider the M2-brane action. We can first note that in the volume term of the M2-brane action we find the (super)metric, whose expansion follows directly from the supervielbein. For the Wess-Zumino term, what we find is a combination of the supervielbein and of the super-three-form gauge potential. If we compute the Lie derivative of this combination we find

$$\mathcal{L}_y(E_{[m}{}^A E_n{}^B E_p]{}^C A_{ABC}) = E_{[m}{}^A E_n{}^B E_p]{}^C y^D H_{DABC} \quad (10.118)$$

up to total derivatives. This formula is a consequence of how the flux field-strength superfield is defined, in (15.260). We now apply supergravity constraints (15.261c - 15.261d) which tell us that the only components of the field-strength superfield that are non-vanishing are  $H_{abcd}$  and  $H_{\alpha\beta ab} = i(\Gamma_{ab})_{\alpha\beta}$ , which is constant. This has important consequences for expansions of the above combination, and the M2-brane action as a

whole, namely

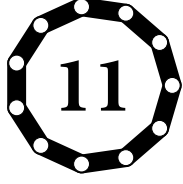
$$(\mathcal{L}_y)^n (y^D H_{DABC}) = 0, \quad \text{for } n \geq 1. \quad (10.119)$$

Hence, if we apply more Lie derivatives on the combined superfield appearing in the WZ-part of the M2-brane action, only the terms with Lie derivatives acting on the supervielbeins survive. This means that knowledge of the supervielbein expansion is sufficient for computing the expansion of the whole M2-brane action. This is the final argument supporting our general strategy.

For ease of use, we summarize the computational steps of the strategy here:

1. Compute the derivatives in the superfield expansion superfield. In practice this means using (10.111 - 10.114).
2. Evaluate the expressions at the origin,  $\theta = 0$ .
3. Apply the relevant supergravity constraints from (15.261a - 15.261d) and those arising as a consequence of superspace Bianchi Identities (15.264a - 15.267b) in order to write formulae in terms of familiar fields.
4. Apply the constraints of the bosonic background if appropriate.





# Eleven dimensional supergravity and the M2-brane

The expansion of the M2-brane action up to order four in fermions was first performed in [130]. In this chapter, with the aid of appendices, we review and correct the main results; appendix 15.2 contains a review of the 11-dimensional supergravity conventions and appendix 15.3 discusses useful superfield expansions up to fermionic order four. Our conventions are described in appendices 15.1 and 15.4.

Let the M2-brane worldvolume coordinates be defined as  $\zeta^i$ , with  $i = 0, 1, 2$ . The superfield action for the M2-brane in terms of the superspace embedding coordinates  $Z^M(\zeta) = (x^m(\zeta), \theta^\mu(\zeta))$  is given in (9.106) which can be written as

$$S_{M2}(Z) = -T_{M2} \int d^3\zeta \left[ \sqrt{-\det(G_{ij}(Z))} - \frac{1}{6} \varepsilon^{ijk} A_{ijk}(Z) \right], \quad (11.120)$$

where, using the pullback of the supervielbein

$$E_i^A(Z) = \frac{\partial Z^M}{\partial \zeta^i} E_M^A(Z), \quad (11.121)$$

we wrote the Dirac-Born-Infeld (DBI) term in terms of the pullback of the metric and the Wess-Zumino (WZ) term in terms of the three-form pullback, which respectively read

$$G_{ij}(Z) = E_i^a(Z) E_j^b(Z) \eta_{ab}, \quad (11.122)$$

$$A_{ijk}(Z) = E_i^A(Z) E_j^B(Z) E_k^C(Z) A_{ABC}(Z). \quad (11.123)$$

We explained in chapter 9 that in order to obtain the  $\theta$ -expansion of the action we need to obtain the  $\theta$ -expansions of the superfields involved. For the M2-brane we also showed that, because of (10.118), the only superfield expansion we need is that of the supervielbein. Nevertheless, it is more practical to work with Lorentz-invariant objects, so in what follows we will compute the expansion of the (super)metric and the (super)three-form, that appear in the brane action. Obtaining the action expansion from these is then

simple. Working with these superfields is sufficient and is a convenient middle-ground between dealing with the full action and dealing with the numerous supervielbeins individually. For a large proportion of the coming chapters we will compute the Lorentz-invariant superfield expansions.

We start by applying the method to compute the metric superfield expansion. In order to write the brane action up to order four in fermions, we need to expand the supermetric to the same order. We write the necessary Lie derivatives acting on the supermetric in terms of Lie derivatives acting on the supervielbeins involved and take into account the fact that we consider a bosonic background, which means that several terms will actually vanish. With the understanding that everything outside of Lie derivatives is evaluated at the origin, the relevant relations are

$$(\mathcal{L}_y)^2 G_{mn} = 2 [(\mathcal{L}_y)^2 E_{(m}{}^a] e_n{}^b \eta_{ab}, \quad (11.124a)$$

$$(\mathcal{L}_y)^4 G_{mn} = 2 [(\mathcal{L}_y)^4 E_{(m}{}^a] e_n{}^b \eta_{ab} + 6 [(\mathcal{L}_y)^2 E_{(m}{}^a] [(\mathcal{L}_y)^2 E_n{}^b] \eta_{ab}. \quad (11.124b)$$

For the WZ-term, the analysis is slightly more involved because one has both the supervielbein and the three-form in the combination  $(E_M{}^A E_N{}^B E_P{}^C A_{ABC})(Z)$ . We saw in the discussion around (10.118) how to deal with this combination, so here we simply use those ideas and then follow the same procedure as we did for the metric. The relevant relations up to fermionic order four in bosonic backgrounds are

$$(\mathcal{L}_y)^2 A_{mnp} = -3i y^\alpha [\mathcal{L}_y E_{[m}{}^\beta] e_n{}^c e_p{}^d (\Gamma_{cd})_{\beta\alpha}, \quad (11.125a)$$

$$(\mathcal{L}_y)^4 A_{mnp} = -3i y^\alpha [(\mathcal{L}_y)^3 E_{[m}{}^\beta] e_n{}^c e_p{}^d (\Gamma_{cd})_{\beta\alpha} - 18i y^\alpha [\mathcal{L}_y E_{[m}{}^\beta] [(\mathcal{L}_y)^2 E_n{}^c] e_p{}^d (\Gamma_{cd})_{\beta\alpha}. \quad (11.125b)$$

We see that we require different components of the supervielbein expansion for the metric and the three-form. Happily, using the supergravity constraints it can be shown that in bosonic backgrounds these components are related by the condition, [131],

$$(\mathcal{L}_y)^{2l+2} E_m{}^a = -i y^\beta (\Gamma^a)_{\beta\gamma} [(\mathcal{L}_y)^{2l+1} E_m{}^\gamma], \quad (11.126)$$

where  $l$  is a natural number. Therefore, in order to obtain the action at order four in fermions, we only require two terms in the expansion of the supervielbein. These are

$$\mathcal{L}_y E_m{}^\alpha = (D_m)^\alpha{}_\gamma y^\gamma, \quad (11.127a)$$

$$(\mathcal{L}_y)^3 E_m{}^\alpha = -y^\beta e_m{}^c y^\delta y^\epsilon \nabla_\epsilon (R_{\delta c\beta}{}^\alpha - \nabla_\delta T_{c\beta}{}^\alpha) - y^\beta (D_m y^\gamma) y^\delta R_{\delta\gamma\beta}{}^\alpha - i (\bar{y} \Gamma^c D_m y) y^\beta T_{c\beta}{}^\alpha. \quad (11.127b)$$

Here the first equation involves the supercovariant derivative that was discussed around (10.117b). The supercovariant derivative will turn out to be a very important operator for our purposes. In (11.127b) we have left the expression written in terms of superspace components of the torsion and curvature tensors. Manipulating this expression using superspace Bianchi identities in order to write it in terms of spacetime fields, though important for our purposes, is a computation that does not add any insight to the present discussion. For this reason we present the details of that analysis in appendix 15.3.2. The outcome of our manipulations

is the expression

$$(\mathcal{L}_y)^3 E_m^\alpha = i(\Gamma^{bc}y)^\alpha (\bar{y}\mathcal{W}_{mbc}y) + i(\check{\mathcal{T}}_b^{dfgh}y)^\alpha (\bar{y}\mathcal{H}_{m}^b{}_{dfgh}y) \quad (11.128)$$

where we have defined

$$\mathcal{H}_{m}^b{}_{dfgh} = \Gamma^b H_{dfgh} D_m - 6e_m{}^b \Gamma_{df} [D_g, D_h], \quad (11.129a)$$

$$\mathcal{W}_{mbc} = \mathcal{R}_{bc} D_m + \frac{1}{8} \Gamma_m [D_b, D_c] + \frac{1}{4} \Gamma_b [D_m, D_c], \quad (11.129b)$$

$$\mathcal{R}_{bc} = \frac{1}{576} \left( \Gamma_{bc} \Gamma^{dfgh} - 8\delta_{[c}^{[d} \Gamma_{b]} \Gamma^{fgh]} - 12\delta_{[c}^{[d} \delta_{b]}^f \Gamma^{gh]} \right) H_{dfgh}, \quad (11.129c)$$

$$\check{\mathcal{T}}_c^{dfgh} = \frac{1}{288} \left( \Gamma_c \Gamma^{dfgh} - 12\delta_c^{[d} \Gamma^{fgh]} \right). \quad (11.129d)$$

There are some important points that need to be made about these formulae. First of all, manipulations lead to some terms involving commutators of supercovariant derivatives. It can be seen in appendix 15.3.2 that these arise from the first term in (11.127b). There are also terms involving a single supercovariant derivative and  $H^{(4)}$ -flux. These contributions are the outcome of manipulating the last two terms in (11.127b). We have so far been unable to write these parts of the expressions strictly in terms of the supercovariant derivative. Note that this problem appears for the first time at order  $(\theta)^4$  for the M2-brane in bosonic backgrounds, and was therefore not observed in the order- $(\theta)^2$  analysis carried out in [125–127, 150] where everything can be packaged up in a tidy and supercovariant way. The result (11.128) agrees with [151], but there are strong indications that these formulae should allow for further manipulation into a more compact expression where supercovariance is made manifest. We will see later that dealing with these complicated objects is the chief source of the difficulty limiting our computational ability when performing dimensional reduction of the M2-brane action to obtain the D2-brane action. Put plainly, our manipulation of the higher order expansion of the supervielbein probably needs to be completed into a manifestly supercovariant formulation that we would expect to be more compact and more manageable than the one presented above.

## 11.1 M2-brane at fermionic order two

Now we review the M2-brane action at order two in fermions. We will use this ‘simple’ analysis for two main purposes. First, it is a warm-up exercise that nicely illustrates how to proceed at higher orders. Second, we will use it to make more precise the relation between  $\kappa$ -symmetry and bulk supersymmetry discussed in chapter 9.

Recall that we decided to perform expansions of Lorentz-invariant superfields in the action since obtaining the full action expansion from these is simple. We begin with the metric expansion. We ignore order- $(\theta)^1$  terms since they involve the gravitino and we are interested in bosonic backgrounds. For the order- $(\theta)^2$  terms, we combine (11.124), (11.126), and (11.127) to obtain  $(\mathcal{L}_y)^2 G_{mn} \stackrel{\theta=0}{=} -2i\bar{y}\Gamma_{(m} D_{n)}y$ . We can use this to write a truncation of the metric superfield which includes only the terms relevant for the brane action. We will use a boldface notation to refer to these truncated superfields. For the metric, the combination is

$$\mathbf{g}_{mn} \equiv g_{mn}(x) - i\bar{\theta}\Gamma_{(m} D_{n)}\theta. \quad (11.130)$$

The expansion of the three-form superfield can be similarly obtained. In fact, (11.125) and (11.127) combine to give the order-2 correction in the combination  $A_{mnp}(Z)$ , whose truncated expansion reads

$$\mathbf{A}_{mnp} \equiv A_{mnp}(x) - \frac{3i}{2} \bar{\theta} \Gamma_{[mn} D_p] \theta. \quad (11.131)$$

These combinations of bosonic and fermionic fields first appeared in [125, 150] in what was called a ‘superfield-like form of the action’, allowing one to write the order- $(\theta)^2$  expansion of the M2-brane action in a compact way. Similar combinations appearing in other  $Dp$ -brane actions were found and these allowed these actions to be written in a compact way as well.

Our discussion makes it manifest that the appearance of the truncated superfields is not a mere trick valid only for the action up to this order, but rather a consequence of how the action superfield is built in the superspace formulation of supergravity. This means it is valid at *any* order in fermions. Therefore in what follows our goal is to provide a systematic approach to compute truncated superfields of this type appearing in all brane actions. For practical purposes we will often refer to the metric and three form without specifying if we refer to the field, the superfield, or the truncated superfield, as this will always be clear from context.

We are now ready to write the M2-brane action at order  $(\theta)^2$ . Plugging the truncated superfields (11.130) and (11.131) into the action (9.106) and then Taylor-expanding up to order  $(\theta)^2$ , we get

$$\begin{aligned} \mathcal{S}_{\text{M2}}^{(2)} &= -T_{\text{M2}} \int d^3\zeta \left[ \sqrt{-\det(g)} - \frac{1}{6} \varepsilon^{ijk} \mathbf{A}_{ijk} \right] \\ &= -T_{\text{M2}} \int d^3\zeta \left[ \sqrt{-\det(g)} - \frac{1}{6} \varepsilon^{ijk} A_{ijk} \right] + iT_{\text{M2}} \int d^3\zeta \sqrt{-\det(g)} \left[ \bar{\theta} P_-^{(0)} \Gamma^i D_i \theta \right]. \end{aligned} \quad (11.132)$$

In the last line, we combined the order- $(\theta)^2$  terms together forming the so-called  $\kappa$ -symmetry projector at order  $(\theta)^0$ , i.e.

$$P_-^{(0)} = \frac{1}{2} (1 - \Gamma_{\text{M2}}^{(0)}), \quad (11.133)$$

where the  $\Gamma$ -matrix combination defining the operator is

$$\Gamma_{\text{M2}}^{(0)} = \frac{\varepsilon^{ijk} \Gamma_{ijk}}{6\sqrt{-\det(g)}}. \quad (11.134)$$

This allows us to see explicitly the manifestation of  $\kappa$ -symmetry in the M2-brane action at fermionic order  $(\theta)^2$ . We comment on  $\kappa$ -symmetry in detail now.

## 11.2 Supersymmetry and $\kappa$ -symmetry

We are now in a position to make more precise comments about bulk supersymmetry and  $\kappa$ -symmetry. As we already mentioned, it is worth taking two perspectives. First, from the bulk perspective, the brane-only solution spontaneously breaks half of the supersymmetries, while the other half are preserved on-shell. The corresponding goldstinos turn into the fermionic degrees of freedom on the brane,  $\theta^\mu(\zeta)$ . Alternatively, from the brane worldvolume perspective, we construct the brane action using off-shell superfields with all 32 Grassmann coordinates, therefore only half of them correspond to actual degrees of freedom on the brane

while the rest are redundancies. This means that there must exist a fermionic gauge symmetry, known as  $\kappa$ -symmetry, that gets rid of these redundant directions. The presence of such a fermionic gauge symmetry in the M2-brane action (9.106) was shown in [136]. The  $\kappa$ -symmetry variations are

$$(\delta_\kappa Z^M) E_M{}^a(Z) = 0, \quad (11.135a)$$

$$(\delta_\kappa Z^M) E_M{}^\alpha(Z) = (1 + \Gamma_{\text{M2}}(Z))^\alpha{}_\beta \kappa^\beta, \quad (11.135b)$$

where the operator

$$\Gamma_{\text{M2}}(Z) = \frac{\varepsilon^{ijkl} \Gamma_{ijk}(Z)}{6\sqrt{-\det(G(Z))}} \quad (11.136)$$

is a hermitian traceless matrix squaring as  $(\Gamma_{\text{M2}}(Z))^2 = 1$ . In the transformations,  $\kappa$  is an arbitrary 32-component Majorana fermion in 11-dimensional spacetime. Note that these expressions are valid all over superspace. If we evaluate them at the origin of Grassmann coordinates, using the WZ-gauge (10.115) for the supervielbein, these variations read

$$\delta_\kappa x^m = 0, \quad (11.137a)$$

$$(\delta_\kappa \theta^\mu) \delta_\mu^\alpha = (1 + \Gamma_{\text{M2}}^{(0)})^\alpha{}_\beta \kappa^\beta, \quad (11.137b)$$

with the matrix  $\Gamma_{\text{M2}}^{(0)}$  defined as in (11.134). Hence it is possible to use  $\kappa$ -symmetry transformations to project out half of the Grassmann coordinates  $\theta^\mu$ . We see that the appearance of the orthogonal projector  $P_-^{(0)}$  in the M2-brane action at order  $(\theta)^2$  is not a coincidence, but rather it is a consequence of  $\kappa$ -symmetry and what we did there was to write the action in such a way as to make this symmetry manifest.

Let us now derive some bulk supersymmetry properties. We start with the M2-brane-only solution, where the brane spontaneously breaks half of the supersymmetries. Here we use  $\kappa$ -symmetry to determine whether a supersymmetry is preserved by the brane or spontaneously broken, following [152, 153]. To make this point explicit, we need some of the symmetries of the M2-brane action (see e.g. [137]). To start, recall that superfields transform under global supersymmetry variations, and so does the brane action. Off-shell, supersymmetry variations are shifts in any Grassmann direction(s)  $\theta^\mu$ . On-shell, in a background where the brane is present, only some of those shifts leave the background invariant. We denote the variation generated by the surviving killing spinors in this background  $\delta_\epsilon \theta = \epsilon_{\text{M2}}$ . The combination of surviving global supersymmetry and  $\kappa$ -symmetry leads to a total variation (at the origin of Grassmann coordinates in order to connect with the above discussion)

$$\delta_{\epsilon, \kappa} \theta = \epsilon_{\text{M2}} + (1 + \Gamma_{\text{M2}}^{(0)}) \kappa. \quad (11.138)$$

In order to get rid of the fermionic redundancies on the brane, we write the  $\kappa$ -symmetry gauge-fixing condition as  $P\theta = 0$ , where  $P$  is a projector independent of background fields. This implies that the physical fermions on the brane are such that  $\theta = (1 - P)\theta$ . Once the gauge is fixed, in order to preserve it, it is necessary that  $\delta_{\epsilon, \kappa}(P\theta) = P\delta_{\epsilon, \kappa}\theta = 0$  holds, and so  $\delta_{\epsilon, \kappa}\theta = 0$ . The latter formula, together with (11.138) implies that the surviving global supersymmetry transformations that are compatible with this fact must satisfy

$$\epsilon_{\text{M2}} = -(1 + \Gamma_{\text{M2}}^{(0)}) \kappa \quad (11.139)$$

on the brane locus. Using this relation, one easily finds that any surviving supersymmetry must satisfy  $P_+^{(0)}\epsilon_{M2} = \epsilon_{M2}$  (equivalently  $\Gamma_{M2}^{(0)}\epsilon_{M2} = \epsilon_{M2}$ ) on the brane locus, where  $P_+^{(0)} = (1 + \Gamma_{M2}^{(0)})/2$ . On the other hand, the orthogonal projector  $P_-^{(0)}$  selects Grassmann coordinates generated by spontaneously broken supercharges, the goldstinos on the brane-only solution. This is the reason why the combination  $P_-^{(0)}\theta$  appears on the brane action. (11.139) also shows that preserved bulk supersymmetries are of the same aspect as  $\kappa$ -symmetry transformations (they both involve  $P_+^{(0)}$ ) and so also leave the M2-brane action invariant thanks to the presence of  $P_-^{(0)}$  in the brane action.

This physical picture is valid not only for the M2-brane, but also for all  $Dp$ -branes. In order to study each case one must replace  $\Gamma_{M2}$  by the corresponding matrix  $\Gamma_{Dp}$ . In [126, 127] it was shown that all  $Dp$ -brane actions at quadratic fermionic order can be written with the corresponding  $\kappa$ -symmetry projector. In [122] the breaking of supersymmetry by  $Dp$ -branes was shown to correspond to a non-linear realization of supersymmetry, generalizing first results of this type [17, 18].

The brane-only solution is illuminating for deriving multiple facts regarding bulk supersymmetry and  $\kappa$ -symmetry, but our interest is in more general setups. In the previous configuration all fermions on the brane are massless goldstinos and many fermionic couplings on the brane vanish. In general, those couplings do not vanish and are physically relevant. For example, depending on the particular solution, some (or all) worldvolume fermions will become massive and will no longer correspond to goldstinos of the solution. The superspace approach in this paper includes all such couplings and therefore captures all of the relevant physical features of these general solutions. Moreover, the argument above, telling which supersymmetries survive in the solutions involving branes, is also valid for such solutions.

Finally, it is worth noting that we evaluated our expressions at the origin of Grassmann coordinates and so formulae involved the zeroth order  $\kappa$ -symmetry matrix  $\Gamma_{M2}^{(0)}$  and the projectors  $P_{\pm}^{(0)}$ , that we used to connect with what we found for the brane action at order  $(\theta)^2$ . Nevertheless, the above arguments work all over superspace and so the general formulas about preserved supercharges and  $\kappa$ -symmetry involve  $\Gamma_{M2}(Z)$  and  $P_{\pm}(Z)$ .

### 11.3 M2-brane at fermionic order four

In this section we apply what we learned at the second fermionic order to build the action at order four in quite a direct way. We saw that in order to do so we need to find the metric and 3-form superfield truncations up to order  $(\theta)^4$ .

We already provided all of the relevant formulae to write the supervielbein expansion at order  $(\theta)^4$  in (11.126) and (11.128). By plugging those results into (11.124) and (11.125), one finds the metric and three-form superfields up to order  $(\theta)^4$ . The metric is

$$\begin{aligned} g_{mn} = & g_{mn} - i(\bar{\theta}\Gamma_{(m}D_n)\theta) - \frac{1}{4}(\bar{\theta}\Gamma_a D_{(m}\theta)(\bar{\theta}\Gamma^a D_n)\theta) \\ & + \frac{1}{12}(\bar{\theta}\Gamma_{(m|}\check{\mathcal{T}}_b{}^{dfgh}\theta)(\bar{\theta}\mathcal{H}^b{}_{|n)dfgh}\theta) + \frac{1}{12}(\bar{\theta}\Gamma_{(m|}\Gamma^{bc}\theta)(\bar{\theta}\mathcal{W}_{|n)bc}\theta), \end{aligned} \quad (11.140)$$

where we used the operators defined in (11.129), and, similarly, the three-form is

$$\begin{aligned} \mathbf{A}_{mnp} &= A_{mnp} - \frac{3}{2}i(\bar{\theta}\Gamma_{[mn}D_p]\theta) - \frac{3}{4}(\bar{\theta}\Gamma_{a[m}D_n\theta)(\bar{\theta}\Gamma^a D_p]\theta) \\ &\quad + \frac{1}{8}(\bar{\theta}\Gamma_{[mn]}\check{\mathcal{T}}_b{}^{dfgh}\theta)(\bar{\theta}\mathcal{H}^b{}_{|p]dfgh}\theta) + \frac{1}{8}(\bar{\theta}\Gamma_{[mn}\Gamma^{bc}\theta)(\bar{\theta}\mathcal{W}_{p]bc}\theta). \end{aligned} \quad (11.141)$$

In the same way as we did at second order, these expressions can be plugged into the action and then we can perform a Taylor expansion to find the action at quartic order

$$\begin{aligned} \mathbf{S}_{\text{M2}}^{(4)} &= -T_{\text{M2}} \int d^3\zeta \left[ \sqrt{-\det(g)} - \frac{1}{6}\varepsilon^{ijk} \mathbf{A}_{ijk} \right] \\ &= -T_{\text{M2}} \int d^3\zeta \sqrt{-\det(g)} \left[ 1 - \frac{1}{6} \frac{\varepsilon^{ijk}}{\sqrt{-\det(g)}} \mathbf{A}_{ijk} \right] \\ &\quad + T_{\text{M2}} \int d^3\zeta \sqrt{-\det(g)} \left[ i(\bar{\theta}P_-^{(0)}\Gamma^i D_i\theta) \right. \\ &\quad \quad + \frac{1}{8}(\bar{\theta}\Gamma^i D_i\theta)^2 - \frac{1}{8}(\bar{\theta}\Gamma_i D_j\theta)(\bar{\theta}\Gamma^i D^j\theta) - \frac{1}{8}(\bar{\theta}\Gamma_i D_j\theta)(\bar{\theta}\Gamma^j D^i\theta) \\ &\quad \quad + \frac{1}{8}(\bar{\theta}\Gamma_m D^i\theta)(\bar{\theta}\Gamma^m D_i\theta) - \frac{1}{8} \frac{\varepsilon^{ijk}}{\sqrt{-\det(g)}} (\bar{\theta}\Gamma_{m[i} D_j\theta)(\bar{\theta}\Gamma^m D_{k]}\theta) \\ &\quad \quad \left. - \frac{1}{12}(\bar{\theta}P_-^{(0)}\Gamma^i\check{\mathcal{T}}_b{}^{dfgh}\theta)(\bar{\theta}\mathcal{H}^b{}_{idfg}h\theta) - \frac{1}{12}(\bar{\theta}P_-^{(0)}\Gamma^i\Gamma^{bc}\theta)(\bar{\theta}\mathcal{W}_{ibc}\theta) \right]. \end{aligned} \quad (11.142)$$

We see that some of the fourth-order terms, like the second-order terms, may be organized around zeroth-order  $\kappa$ -symmetry projectors, whereas some cannot be. Those terms which cannot be (coming with a factor of  $1/8$ ) are related to the higher-order fermionic expansion of the  $\kappa$ -symmetry projector superfield. We leave the study of this for future work, and for now continue on without organising these terms around a  $\kappa$ -symmetry principle.

This completes the expansion of the bosonic background M2-brane action to quartic order. In the next chapter we will examine the dimensional reduction of these expansions to determine the D2-brane action up to order four in fermions.



# Superspace dimensional reduction and the D2-brane

We now know how to obtain the fermion couplings in the M2-brane action up to arbitrary order, and we have calculated them explicitly up to order four. Our plan is to use this knowledge to compute equivalent couplings on all  $Dp$ -branes. The first step in doing this is compactifying M-theory on a circle, connecting the M2-brane in 11-dimensional supergravity to the D2-brane in type IIA supergravity. Then, by T-dualizing the theory, move to branes of arbitrary dimension in both type IIA and IIB theories.

$Dp$ -branes are solutions of 10-dimensional type II supergravities and it is therefore possible to construct their action using the superspace formulation of those supergravity theories. This is indeed what we will do in this chapter and the next one. However, as we previously explained, the approach we will use to obtain the  $Dp$ -brane action superfields will not be a direct application of the NORCOR approach of chapter 10. Instead, in this chapter we use a superspace generalization of the dimensional reduction relating M2-branes and D2-branes. We start by quickly reviewing the  $S^1$ -compactification of the 11-dimensional spacetime that reproduces type IIA supergravity starting from 11-dimensional supergravity. We then consider the M2-brane and its dimensional reduction to the D2-brane. After revisiting the purely bosonic calculation, we then extend the compactification method to superspace.

For a detailed account of the notation employed, see appendix 15.1. See appendix 15.4 for an overview of the relevant dimensional reductions.

## 12.1 Reduction of 11-dim supergravity to type IIA supergravity

Type IIA string theory can be obtained by dimensional reduction of 11-dimensional supergravity. In this section we quickly review the main features of this dimensional reduction.

The notation for the dimensional reduction is as follows: 11-dimensional indices are hatted whereas 10-dimensional indices are not and 11-dimensional objects are also hatted whereas 10-dimensional objects are not; indices  $a, b, \dots$  are tangent space and  $m, n, \dots$  are spacetime indices, with explicit number indices un-



derlined for tangent space and unadorned for spacetime, while  $i, j, \dots$  are M2- and D2-brane worldvolume indices; 11-dimensional spacetime coordinates are  $\hat{x}^{\hat{m}}$  and they split as  $(x^m, x^{10})$ , while worldvolume coordinates are  $\zeta^i$ ; we will leave implicit that the pull-back to the brane of an 11-dimensional object is a different operation than the pull-back to the brane of a 10-dimensional object, but we will keep track of this by observing whether the object is hatted or not, objects always being pulled back in the appropriate way. Background fields are independent of  $x^{10}$ .

To begin the dimensional reduction, we first deal with bosonic fields. Given the 11-dimensional metric  $\hat{g}_{\hat{m}\hat{n}} = \hat{e}_{\hat{m}}^{\hat{a}} \hat{e}_{\hat{n}}^{\hat{b}} \hat{\eta}_{\hat{a}\hat{b}}$ , where  $\hat{e}_{\hat{m}}^{\hat{a}}$  is the 11-dimensional vielbein, the  $S^1$ -compactification ansatz for the vielbein leading to the type IIA action in the string frame is

$$\hat{e}_{\hat{m}}^{\hat{a}} = \begin{pmatrix} e^{-\frac{\phi}{3}} e_m^a & e^{\frac{2\phi}{3}} C_m \\ 0 & e^{\frac{2\phi}{3}} \end{pmatrix}, \quad (12.143)$$

where  $e_m^a$  is the 10-dimensional vielbein,  $\phi$  is the dilaton, and  $C_m$  is the Ramond-Ramond one-form. The 10-dimensional metric is  $g_{mn} = e_m^a e_n^b \eta_{ab}$ . The 11-dimensional three-form gauge potential decomposes as

$$\hat{A}_{mnp} = C_{mnp}, \quad (12.144a)$$

$$\hat{A}_{mn10} = B_{mn}, \quad (12.144b)$$

where  $C_3$  is the Ramond-Ramond three-form potential and  $B_2$  is the Kalb-Ramond potential. Notice that our RR-field sign conventions differ from those used in [125, 126]. There are many objects for which we need the dimensional reduction. Those calculations are crucial, but laborious, so we provide a catalogue of the dimensional reduction results in appendix 15.4.

Fermions are of course highly relevant for our purposes and so we need many details from the dimensional reduction of fermionic fields. The ansatz for the 11-dimensional gravitino  $\hat{\psi}_{\hat{m}}$  is

$$\hat{\psi}_m = e^{-\phi/6} \left[ \psi_m - \frac{1}{6} \Gamma_m \lambda + \frac{1}{3} e^\phi C_m \Gamma^* \lambda \right], \quad (12.145a)$$

$$\hat{\psi}_{10} = e^{-\phi/6} \left[ \frac{1}{3} e^\phi \Gamma^* \lambda \right], \quad (12.145b)$$

where  $\psi_m$  is the 10-dimensional gravitino,  $\lambda$  is the dilatino, and  $\Gamma^*$  is the 10-dimensional chirality matrix. Recall that we start with 11-dimensional Majorana fermions. Upon dimensional reduction, these will split into pairs of 10-dimensional Majorana-Weyl fermions of opposite chiralities, so each 10-dimensional fermion above should be interpreted as a pair of Majorana-Weyl fermions of opposite chirality, e.g.  $\lambda = \lambda_+ + \lambda_-$ , where  $\Gamma^* \lambda_\pm = \pm \lambda_\pm$ . This dimensional reduction leads to the type IIA action in the fermionic frame of [154]. Moreover, any 11-dimensional Majorana fermion, like the supersymmetry parameter or the fermions on the M2-brane, need to be dimensionally reduced like the gravitino, with a rescaling involving the dilaton, and further need splitting into pairs of 10-dimensional Majorana-Weyl fermions, so

$$\hat{\theta} = e^{-\phi/6} \theta, \quad \theta = \theta_+ + \theta_-. \quad (12.146)$$

Next, we are interested in the type IIA gravitino and dilatino supersymmetry variations arising in the resulting 10-dimensional action. In 11-dimensional supergravity, the gravitino supersymmetry variation reads

$$\delta_\epsilon \hat{\psi}_{\hat{m}} = \hat{D}_{\hat{m}} \hat{\epsilon}. \quad (12.147)$$

In the type IIA theory, the supersymmetry variations of fermionic fields are

$$\delta_\epsilon \psi_m = D_m \epsilon, \quad (12.148a)$$

$$\delta_\epsilon \lambda = \Delta \epsilon, \quad (12.148b)$$

with the 10-dimensional supercovariant derivative  $D_m$  and the operator  $\Delta$  being defined as,

$$D_m = \nabla_m + \frac{1}{4} \underline{H}_m^{(3)} \Gamma^* - \frac{1}{8} e^\phi (\underline{F}^{(2)} \Gamma^* + \underline{F}^{(4)}) \Gamma_m, \quad (12.149a)$$

$$\Delta = \partial \phi + \frac{1}{2} \underline{H}^{(3)} \Gamma^* - \frac{1}{8} e^\phi \Gamma^m (\underline{F}^{(2)} \Gamma^* + \underline{F}^{(4)}) \Gamma_m. \quad (12.149b)$$

Using these definitions, the 11- and 10-dimensional operators are related as

$$\hat{D}_m = D_m - \frac{1}{6} \Gamma_m \Delta + \frac{1}{3} e^\phi C_m \Gamma^* \Delta + \frac{1}{6} \partial_m \phi, \quad (12.150a)$$

$$\hat{D}_{10} = \frac{1}{3} e^\phi \Gamma^* \Delta. \quad (12.150b)$$

We see that the 11-dimensional supercovariant derivative essentially splits in terms of the operators determining the type IIA gravitino and dilatino variations. Recall that we defined these operators from the supersymmetry variations of the type IIA gravitinos and dilatinos, which depend on the chosen fermionic frame. Therefore if one makes a different dimensional reduction ansatz for the 11-dimensional gravitino (or equivalently some redefinition in the fermionic sector of type IIA), the definition of these operators will be modified accordingly.

## 12.2 Bosonic D2-brane action

Once we know how to dimensionally reduce the background, we can dimensionally reduce the M2-brane action. We compactify along one direction that is not spanned by the M2-brane, therefore the result is the D2-brane of type IIA supergravity. We start from the bosonic part of the M2-brane action (9.106). Following our compactification ansatz, the pull-backs of the 11-dimensional metric and of the three-form can be written in terms of pullbacks of 10-dimensional fields as

$$\hat{g}_{ij} = e^{-2\phi/3} g_{ij} + e^{4\phi/3} p_i p_j, \quad (12.151)$$

$$\hat{A}_{ijk} = C_{ijk} - 3 C_{[i} B_{jk]} + 3 p_{[i} B_{jk]}, \quad (12.152)$$

where we defined the combination  $p_i = \partial_i x^{10} + \partial_i x^m C_m$ . In terms of these fields, the bosonic M2-brane action becomes the D2-brane action and it reads

$$S_{\text{D2}}^{(0)} = -T_{\text{D2}} \int d^3\zeta e^{-\phi} \sqrt{-\det(g)} \sqrt{1 + e^{2\phi} p^2} + \frac{T_{\text{D2}}}{6} \int d^3\zeta \varepsilon^{ijk} [C_{ijk} - 3C_i B_{jk} + 3p_i B_{jk}], \quad (12.153)$$

where  $T_{\text{D2}} = T_{\text{M2}}$  is the D2-brane tension. We would like to obtain the action for the D2-brane in a fully 10-dimensional formulation. Currently, however, (12.153) contains factors of  $p_i$  and so that formulation of the action implicitly knows about the M-theory circle. We need to get rid of  $p_i$ . We do this by including a Lagrange multiplier term involving the one form  $p_1$  and its worldvolume dual, the exact 2-form  $F_2 = dA_1$ , where  $A_1$  is the D2-brane worldvolume gauge field. This Lagrange multiplier is

$$S_{\text{LM}} = \frac{T_{\text{D2}}}{2} \int d^3\zeta \varepsilon^{ijk} (p_i - C_i) F_{jk}. \quad (12.154)$$

A fully 10-dimensional D2-brane action follows from including this term in the action, and then integrating out  $p_i$  by plugging the solutions to its equation of motion back into the action. After doing this, and with a little massaging, we arrive at the familiar form of the bosonic D2-brane action

$$S_{\text{D2}}^{(0)} = -T_{\text{D2}} \int d^3\zeta e^{-\phi} \sqrt{-\det(g + f)} + T_{\text{D2}} \int (C_3 - C_1 \wedge f_2), \quad (12.155)$$

where we made the definition  $f_{ij} = B_{ij} + F_{ij}$ . This action, obtained from the M-theory dimensional reduction, is in string frame. It is worth noting explicitly here that the worldvolume field  $f_{ij}$  is built using one field that is pulled back from the bulk,  $B_{ij}$ , and one that specifically lives only on the worldvolume,  $F_{ij}$ .

We have calculated a fully 10-dimensional formulation of the D2-brane *bosonic* action. Our next goal is to find fermion couplings on the brane worldvolume. Therefore we turn to the superspace generalization of the  $S^1$ -compactification we have just used.

## 12.3 Superspace dimensional reduction and fermions on the D2-brane

In this section we obtain the fermion couplings on the D2-brane action. Following the same reasoning as in the case of the M2-brane action discussed in chapter 11, this can be done by moving to the superspace formulation of type IIA supergravity. One must promote fields in the bosonic action to superfields and then find the corresponding  $\theta$ -expansions. From the expansions of the constituent superfields, the expansion of the brane action superfield may then be determined.

A possible method to obtain the superfield expansions would be to construct all the necessary superfields using the same geometrical strategy as we applied to the M2-brane, i.e. NORCOR. However this requires more hard work than is necessary and there exists a better strategy. The key of our approach is the following observation: the superspace formulation of M-theory is in  $(11|32)$ -dimensional superspace, and the superspace formulation of type IIA strings is in  $(10|32)$ -superspace. It is therefore natural to expect that, as for the basic spacetime case, both superspaces are related via an  $S^1$ -compactification of a bosonic direction. This superspace compactification and knowledge of 11-dimensional superfields in the M2-brane action are all we need to obtain the expansion of the type IIA superfields that appear in the D2-brane action.

Now we have to determine those 10-dimensional superfields. Same as in the M2-brane case, at zeroth order in the  $\theta$ -expansion, the superfields are simply the bosonic fields. Those 10-dimensional bosonic fields are related to the bosonic fields of 11-dimensional supergravity by the dimensional reduction ansatzes (12.143) and (12.144). The spacetime dimensional reduction is described by those equations, and it is natural to interpret all fields appearing there (both 11- and 10-dimensional fields) as the leading-order terms of the corresponding superfield  $\theta$ -expansions. The superspace dimensional reduction must be described by the superspace generalization of those equations. Our method to compute the 10-dimensional superfields of interest will therefore be to use this superfield generalization together with knowledge of the 11-dimensional superfields we already gleaned in the previous chapter. Before we write the superspace compactification ansatz, recall that in eleven dimensions we did not compute the whole expansion of superfields, but rather we restricted to even  $\hat{\theta}$  powers because we were interested in bosonic backgrounds and we considered truncations to quartic order in the fermions. The same holds in ten dimensions, namely we are interested in explicitly obtaining the same type of restricted and truncated superfield expansions. We promote (12.143) and (12.144) to the superfield level and use bold notation to indicate that in practice we will expand and truncated them. We obtain the promoted 11-dimensional metric

$$\hat{g}_{\hat{m}\hat{n}} = \begin{pmatrix} e^{-2\phi/3}(\mathbf{g}_{mn} + e^{2\phi}\mathbf{C}_m\mathbf{C}_n) & e^{4\phi/3}\mathbf{C}_m \\ e^{4\phi/3}\mathbf{C}_n & e^{4\phi/3} \end{pmatrix} \quad (12.156)$$

and the promoted 11-dimensional three-form<sup>17</sup>

$$\hat{\mathbf{A}}_{mnp} = \mathbf{C}'_{mnp}, \quad (12.157)$$

$$\hat{\mathbf{A}}_{mn\ 10} = \mathbf{B}_{mn}, \quad (12.158)$$

where  $\mathbf{g}_{mn}$  is the truncated 10-dimensional supermetric,  $\phi$  is the truncated dilaton superfield,  $\mathbf{B}_{mn}$  is the truncated Kalb-Ramond superfield, and  $\mathbf{C}_m$  and  $\mathbf{C}'_{mnp}$  are the truncated Ramond-Ramond one- and three-form superfields, respectively.

With these relations in hand, we are ready to obtain the  $\theta$ -expansions of the 10-dimensional superfields. We are going to first compute the expansions of the 10-dimensional superfields up to order  $(\theta)^2$  as an illustrative example. We will do this in detail. Then we will plug the expressions we find into the expression for D2-brane action superfield, expand, and compare our findings with previous results for the D2-brane in bosonic backgrounds at second order in fermions obtained with alternative methods. The results match, confirming the validity of our approach. Finally, we will compute the order- $(\theta)^4$  terms of the truncated superfields. We will use these results to support the point we made in previous chapters, i.e. that combining the terms in  $\theta$ -expansions into a more compact and manifestly supercovariant formulation is crucial. We argue strongly that this is the cornerstone of plausible methods for making the calculation of high-order fermionic couplings in brane actions viable in the future.

<sup>17</sup>For future convenience, we place a prime on the 10-dimensional RR three-form superfield here. Indulge this for the time being, the reason will be made clear. The motivation of this choice is explained in (13.228).

## 12.4 Order- $(\theta)^2$ terms

The superfield relations in (12.156 - 12.158) can be Taylor-expanded, and these expansions can be truncated at a desired fermion order. This will lead to relations between 11- and 10-dimensional fields. We will use the number of fermions (both in eleven and ten dimensions) as an ordering principle to relate those 11- and 10-dimensional fields. At leading order, one finds the original bosonic ansatz, which does not have any new information. For the bosonic backgrounds we are considering, at next order, in eleven dimensions one finds fermion bilinears with  $\hat{\Gamma}$ -matrices and the 11-dimensional supercovariant derivative in which several bosonic fields appear. It is natural to expect a similar behaviour in ten dimensions, namely that at this order each superfield involves a bilinear in  $\theta$  as well as  $\Gamma$ -matrices and operators involving 10-dimensional fields. We can therefore make an ansatz for each truncated superfield involving a (for now) unknown fermion bilinear, i.e.

$$\mathbf{g}_{mn} = g_{mn} + \gamma_{mn}, \quad (12.159a)$$

$$\phi = \phi + \rho, \quad (12.159b)$$

$$\mathbf{B}_{mn} = B_{mn} + \beta_{mn}, \quad (12.159c)$$

$$\mathbf{C}_m = C_m + \tau_m, \quad (12.159d)$$

$$\mathbf{C}'_{mnp} = C_{mnp} + \alpha'_{mnp}. \quad (12.159e)$$

We now need to obtain expressions for the unknown 10-dimensional bilinears. Our procedure is to take each component of the 11-dimensional fields in (12.156) - (12.158) and then perform a Taylor expansion in fermions. We do this by NORCOR for the 11-dimensional left-hand side and by plugging in the ansatzes (12.159) for the 10-dimensional right-hand side. Then we identify the corresponding 11-dimensional bilinears with the unknown 10-dimensional ones. At that stage one has relations between fermion bilinears in different theories. The equations indicate expressions for the unknown 10-dimensional bilinears in terms of 11-dimensional fields. In order to write the results for the 10-dimensional bilinears in terms of 10-dimensional fields, we are required to dimensionally reduce the 11-dimensional expressions. To properly elucidate this procedure, which is critical to our overall method, we will provide several examples at varying levels of technical complexity by calculating the bilinear terms for some of fields in (12.159).

### Example 1: dilaton

The simplest example case is that of the dilaton, for which we will provide every detail. We read from (12.156) that it is related to the (10, 10)-component of the 11-dimensional supermetric as  $\hat{\mathbf{g}}_{10\,10} = e^{4\phi/3}$ . We Taylor-expand both sides of this relation. For the 11-dimensional left-hand side we use the result (11.130) from the NORCOR procedure. For the 10-dimensional right-hand side we use the expansion ansatz for the dilaton superfield in (12.159b). Equating the fermion bilinear terms from each side, we find that

$$-i\hat{\theta}\hat{\Gamma}_{10}\hat{D}_{10}\hat{\theta} = e^{4\phi/3}\frac{4\rho}{3}, \quad (12.160)$$

In order to determine an expression for  $\rho$  in terms of 10-dimensional fields we are required to dimensionally reduce the 11-dimensional bilinear. All the necessary results are given in appendix 15.4. We can eventually write

$$-i\hat{\theta}\hat{\Gamma}_{10}\hat{D}_{10}\hat{\theta} = \frac{-i}{3}e^{4\phi/3}\bar{\theta}\Delta\theta, \quad (12.161)$$

which means the dilaton superfield fermion bilinear contribution is

$$\rho = -\frac{i}{4}\bar{\theta}\Delta\theta. \quad (12.162)$$

We have found an expression for the bilinear  $\rho$  that is associated to the operator  $\Delta$  which appears in the supersymmetry variation of the dilatino. This was to be expected: recall that we obtain the  $\theta$ -expansion by taking supersymmetry variations. In the first supersymmetry variation of the dilaton one finds the dilatino and so the supersymmetry variation of the dilatino appears when we take a second variation (on the dilaton). It is also worth remembering again at this point that, in ten dimensions,  $\theta$  represents a pair of Majorana-Weyl fermions of opposite chirality.

### Example 2: Ramond-Ramond one-form

For this next example we will move through the steps a little faster. We read from (12.156) that the Ramond-Ramond one-form superfield in ten dimensions is related to the  $(m, 10)$ -component of the 11-dimensional supermetric as  $\hat{g}_{m10} = e^{4\phi/3}C_m$ . Taylor-expanding both sides using (11.130) and (12.159d), and keeping fermion bilinear terms, we obtain

$$-i\hat{\theta}\hat{\Gamma}_{(m}\hat{D}_{10)}\hat{\theta} = e^{4\phi/3}\tau_m - \frac{i}{3}e^{4\phi/3}(\bar{\theta}\Delta\theta)C_m. \quad (12.163)$$

Note that because the superfield relation involved both the dilaton and the Ramond-Ramond one-form, we were obliged to use (12.162). After a little work for the dimensional reduction of the 11-dimensional bilinear (again, all the relevant results are given in appendix 15.4), we arrive at

$$-i\hat{\theta}\hat{\Gamma}_{(m}\hat{D}_{10)}\hat{\theta} = -\frac{i}{2}e^{\phi/3}\bar{\theta}\Gamma^*(D_m - \frac{1}{2}\Gamma_m\Delta)\theta - \frac{i}{3}e^{4\phi/3}(\bar{\theta}\Delta\theta)C_m, \quad (12.164)$$

which indicates that the bilinear  $\tau_m$  must be

$$\tau_m = -\frac{i}{2}e^{-\phi}\bar{\theta}\Gamma^*(D_m - \frac{1}{2}\Gamma_m\Delta)\theta. \quad (12.165)$$

### Example 3: metric

The most complicated superfield relation is that of the  $(m, n)$ -component of the 11-dimensional supermetric. We read from (12.156) that it is related to the 10-dimensional supermetric, the Ramond-Ramond one-form, and the dilaton as  $\hat{g}_{mn} = e^{-2\phi/3}(g_{mn} + e^{2\phi}C_m C_n)$ . With the ansatz (12.159a) and the previous results

(12.162) and (12.165) for  $\rho$  and  $\tau_m$ , Taylor-expanding in exactly the way we have in previous examples yields

$$-i\hat{\theta}\hat{\Gamma}_{(m}\hat{D}_n)\hat{\theta} = -ie^{-2\phi/3} \left[ -\frac{1}{6}(\bar{\theta}\Delta\theta)(g_{mn} + e^{2\phi}C_mC_n) + i\gamma_{mn} + e^{2\phi} \left( \frac{1}{2}(\bar{\theta}\Delta\theta)C_mC_n + C_{(m}e^{-\phi}\bar{\theta}\Gamma^*(D_n) - \frac{1}{2}\Gamma_n\Delta)\theta \right) \right]. \quad (12.166)$$

Once more applying the results of appendix 15.4, the dimensional reduction of the 11-dimensional bilinear can be determined to be

$$-i\hat{\theta}\hat{\Gamma}_{(m}\hat{D}_n)\hat{\theta} = -ie^{-2\phi/3} \left[ -\frac{1}{6}(\bar{\theta}\Delta\theta)(g_{mn} + e^{2\phi}C_mC_n) + \bar{\theta}\Gamma_{(m}D_n)\theta + e^{2\phi} \left( \frac{1}{2}(\bar{\theta}\Delta\theta)C_mC_n + C_{(m}e^{-\phi}\bar{\theta}\Gamma^*(D_n) - \frac{1}{2}\Gamma_n\Delta)\theta \right) \right]. \quad (12.167)$$

By comparison, we are immediately able to discern the result

$$\gamma_{mn} = -i\bar{\theta}\Gamma_{(m}D_n)\theta. \quad (12.168)$$

One should observe that the metric superfield expansion takes on the same shape for the 11- and the 10-dimensional metrics. In each case the fields and operators involved are not the same, but equivalent objects appear in the same place. This is once again to be expected. The first-order  $\theta$ -expansion of the metric involves the (corresponding) gravitino, and we obtain the expansion by taking supersymmetry variations. Upon a second variation we are therefore not surprised to find the supersymmetry operator on the gravitino variation.

Application of our approach to the case of the relations (12.157) and (12.158) connecting the 11-dimensional three-form superfield to the 10-dimensional superfields is essentially straightforward and we leave the details of the calculation to the interested reader.

## Full results

At the end of the day, the expansions of the 10-dimensional superfields for type IIA supergravity up to quadratic order in fermions are

$$\mathbf{g}_{mn} = g_{mn} - i\bar{\theta}\Gamma_{(m}D_n)\theta, \quad (12.169)$$

$$\phi = \phi - \frac{i}{4}\bar{\theta}\Delta\theta, \quad (12.170)$$

$$\mathbf{B}_{mn} = B_{mn} - i\bar{\theta}\Gamma^*\Gamma_{[m}D_n]\theta, \quad (12.171)$$

$$\mathbf{C}_m = C_m - \frac{i}{2}e^{-\phi}\bar{\theta}\Gamma^*(D_m - \frac{1}{2}\Gamma_m\Delta)\theta, \quad (12.172)$$

$$\mathbf{C}'_{mnp} = C_{mnp} - \frac{i}{2}e^{-\phi}\bar{\theta}\left(3\Gamma_{[mn}D_p] - \frac{1}{2}\Gamma_{mnp}\Delta\right)\theta - 3iC_{[m}\bar{\theta}\Gamma^*\Gamma_nD_p]\theta. \quad (12.173)$$

All bilinears involve one or both of the operators appearing in the supersymmetry variation of the type IIA gravitino and dilatino, i.e. the supercovariant derivative  $D_m$  and the operator  $\Delta$ , respectively. The Ramond-Ramond potential  $C^{(1)}$  is also present in the expansion of  $C'^{(3)}$ . We asked earlier that the reader indulge us in defining the three-form superfield with a prime for the moment. The reason for this is that it will later

become advantageous to consider the three-form superfield expansion restricted to that bilinear which does *not* come multiplied with  $C^{(1)}$ , and for notational convenience it will be this restricted expansion which we shall call  $C^{(3)}$ . We will say more on this in the next chapter.

Our results precisely match with those used in [125],<sup>18</sup> where, however, the approach followed was morally quite different. They used the results of [126], where all  $Dp$ -brane actions at order  $(\theta)^2$  were computed using a brute-force approach, and noticed that all  $Dp$ -brane actions could be written in a particularly compact and convenient way using field combinations like the ones above. The authors there labelled their observation a ‘superfield-like’ formulation. Using our more conceptually sophisticated approach we can now confidently remove the ‘like’. We can see clearly that the reason these particular field combinations proved to be so useful to previous authors is that they are indeed born out of superfield considerations, namely the use of truncated superfield expansions as we have developed here. Moreover, the brute force approach is very complicated to manage at higher orders in  $\theta$ . Our approach, though still somewhat complicated, does allow such computations to be performed.

## D2-brane action at order $(\theta)^2$

What bosonic fields do, the superfields do better. Or rather, the superfields do morally the same thing but carry with them all of the information about the fermion terms. So it went for the dimensional reduction of individual (super)fields, and so it goes for manipulations of the (super)field quantities built from these constituent (super)fields. The composite quantity we are concerned with now is the D2-brane action.

In section 12.2 we provided many details of the dimensional reduction of the bosonic M2-brane action to the bosonic D2-brane one. Now its usefulness is apparent: we are going to interpret the bosonic action as the zeroth-order fermionic expansion of the corresponding superfield. Based on this idea, we start with the M2-brane superaction (11.132) and write it in terms of 10-dimensional superfields by using the superspace dimensional reduction ansatzes (12.156) and (12.157, 12.158). The appearance of pullbacks works exactly as in the bosonic case, and so the outcome is the D2-brane super action written as

$$S_{D2}^{(2)} = -T_{D2} \int d^3\zeta e^{-\phi} \sqrt{-\det(\mathbf{g})} \sqrt{1 + e^{2\phi} \mathbf{p}^2} + \frac{T_{D2}}{6} \int d^3\zeta \varepsilon^{ijk} \left[ C'_{ijk} - 3C_i B_{jk} + 3\mathbf{p}_i B_{jk} \right], \quad (12.174)$$

where  $\mathbf{p}_i = \partial_i x^{10} + \partial_i x^m C_m$ . Once again we would like to write this action in a fully 10-dimensional formulation, and so need to get rid of the explicit dependence on  $\mathbf{p}_i$  (which knows about the M-theory  $S^1$ ). We do this by once again introducing the Lagrange multiplier (12.154). Notice that the bilinears in the truncated expansions of  $\mathbf{p}_i$  and  $C_i$  cancel in the Lagrange multiplier which depends on the difference  $(\mathbf{p}_i - C_i)$  and so in effect we can promote these bosonic fields to truncated superfields for free. Integrating out  $\mathbf{p}_i$  proceeds in formally the same way as integrating out  $p_i$  did in the bosonic case. After doing so, we arrive at the D2-brane action superfield

$$S_{D2}^{(2)} = -T_{D2} \int d^3\zeta e^{-\phi} \sqrt{-\det(\mathbf{g}_{ij} + \mathbf{f}_{ij})} + \frac{T_{D2}}{6} \int d^3\zeta \varepsilon^{ijk} (C'_{ijk} - 3C_i \mathbf{f}_{jk}), \quad (12.175)$$

where we have defined  $\mathbf{f}_{ij} = B_{ij} + F_{ij}$ . Note the worldvolume flux  $F_2 = dA_1$  remains purely bosonic

<sup>18</sup>What we give as  $C'_{ijk}$  here is denoted  $C_{ijk}^{\text{standard}}$  there.



because it is a brane worldvolume field, not a superfield.

Let us once again stress that this procedure is valid at *any* order in  $\theta$ . The right-hand side of (12.175) is the correct structure from which to obtain the D2-brane action to any order. All one needs to do is plug in the expansions of the superfields truncated at a given order in  $\theta$ . The problem of obtaining the D2-brane action up to a given order in  $\theta$  has been reduced to the problem of determining the expansions of the individual superfields involved. Once these superfield expansions are known, the D2-brane action can be written down immediately.

To elaborate further on this claim, we reproduce the familiar form for the D2-brane action at second order in fermions. Starting with (12.175), in order to obtain explicit couplings we need only plug in the truncated superfields (12.169 - 12.173). We successfully reproduce the quadratic D2-brane action

$$\mathbf{S}_{\text{D2}}^{(2)} = -T_{\text{D2}} \int d^3\zeta e^{-\phi} \left[ \sqrt{-\det(g+f)} \left[ 1 - i\bar{\theta} P_-^{(0)} \left( \mathcal{M}^{ij} \Gamma_i D_j - \frac{1}{2} \Delta \right) \theta \right] - (C_3 - C_1 \wedge f_2) \right], \quad (12.176)$$

where  $\mathcal{M}^{ij}$  is the inverse of the combination  $\mathcal{M}_{ij} = (g_{ij} + \Gamma^* B_{ij})$  and we defined the (zeroth order) D2-brane  $\kappa$ -symmetry projector

$$P_-^{(0)} \equiv \frac{1}{2} (1 - \Gamma_{\text{D2}}), \quad (12.177)$$

where

$$\Gamma_{\text{D2}} = \frac{1}{\sqrt{-\det(g+f)}} \varepsilon^{ijk} \left( \frac{1}{6} \Gamma_{ijk} - \frac{1}{2} \Gamma^* \Gamma_i f_{jk} \right). \quad (12.178)$$

Notice that this is slightly more involved than in the M2-brane case because of the inclusion of worldvolume flux  $f_2$ . The outcome is the full D2-brane action at second order in fermions, and it matches exactly with the results in [126, 127]. This completes the fermionic second-order analysis to exemplify our alternative approach to obtain the D2-brane action at any fermion level.

## 12.5 Order- $(\theta)^4$ terms

We have developed an improved approach for determining superfield fermionic expansions of fields in type IIA supergravity. We did this via NORCOR in 11-dimensional supergravity and the string duality that gives the type IIA theory via an  $S^1$ -compactification. In the above section we demonstrated in detail how our approach can be used to obtain the known results at second order in fermions with much less hassle than previous approaches. In this chapter we move to use our approach to calculate the *quartic*  $\theta$  terms for those same type IIA superfield expansions.

As we discussed above, using our approach, the problem of determining the D2-brane action superfield expansion gets reduced to the problem of determining the fermionic expansion of the constituent superfields. Once these expansions have been found, the D2-brane action follows immediately from plugging them into (12.175). All of the necessary details for this to work function at fourth order just as well as second order, and indeed at every order.

Since our method is applicable at every fermion order, to find the superfield expansions of the type IIA fields we can proceed in the same way as we did for the quadratic case above. To start, we make ansatzes for the order-four terms in the truncated expansions of the 10-dimensional superfields. We have already determined

the bilinear terms and so can include them immediately. We use the same symbols as we did for the ansatzes in the order-two case, but now label the unknown quantities with their fermion order. We have

$$\mathbf{g}_{mn} = g_{mn} - i\bar{\theta}\Gamma_{(m}D_n)\theta + \gamma_{mn}^{(4)}, \quad (12.179a)$$

$$\phi = \phi - \frac{i}{4}\bar{\theta}\Delta\theta + \rho^{(4)}, \quad (12.179b)$$

$$\mathbf{B}_{mn} = B_{mn} - i\bar{\theta}\Gamma^*\Gamma_{[m}D_n]\theta + \beta_{mn}^{(4)}, \quad (12.179c)$$

$$\mathbf{C}_m = C_m - \frac{i}{2}e^{-\phi}\bar{\theta}\Gamma^*\left(D_m - \frac{1}{2}\Gamma_m\Delta\right)\theta + \tau_m^{(4)}, \quad (12.179d)$$

$$\mathbf{C}'_{mnp} = C_{mnp} - \frac{i}{2}e^{-\phi}\bar{\theta}\left(3\Gamma_{[mn}D_p] - \frac{1}{2}\Gamma_{ijk}\Delta\right)\theta - 3iC_{[m}\bar{\theta}\Gamma^*\Gamma_nD_p]\theta + \alpha'_{mnp}{}^{(4)}. \quad (12.179e)$$

Once again, we must determine the expressions for these unknown shifts by Taylor-expanding both sides of (12.156) and (12.157, 12.158), now to quartic order in  $\theta$ . Again, we appeal to the results of the NORCOR procedure to Taylor-expand the left-hand side, whereas we plug our quartic ansatzes in to Taylor-expand the right-hand side. Upon rearrangement, this will result in expressions for the unknowns which contain both 10- and 11-dimensional fields. We must then once again dimensionally reduce the 11-dimensional quantities that appear in order to determine expressions for the unknowns that are entirely in terms of 10-dimensional quantities.

The mixing of the 10-dimensional metric, the dilaton and the Ramond-Ramond one-form in (12.156) causes the expressions for the quartic ansatzes to be quite complicated to deal with practically. For ease of notation, let us denote the quartic terms in the truncated expansion of the 11-dimensional supermetric (11.140) as  $\hat{\gamma}_{\hat{m}\hat{n}}^{(4)}$ . Now, Taylor-expanding the relation  $\hat{\mathbf{g}}_{10\,10} = e^{4\phi/3}$  and keeping only the terms up to quartic order in fermions allows us to find that

$$\rho^{(4)} = \frac{1}{24}(\bar{\theta}\Delta\theta)^2 + \frac{3}{4}e^{-4\phi/3}\hat{\gamma}_{10\,10}^{(4)}. \quad (12.180)$$

Determining a 10-dimensional expression for  $\rho^{(4)}$  now requires us to perform dimensional reduction on  $\hat{\gamma}_{10\,10}^{(4)}$ . Before that though we also note the results of Taylor-expanding and rearranging the relations that allow us to determine expressions for  $\tau_m^{(4)}$  and  $\gamma_{mn}^{(4)}$ . First, expanding both sides of the equation  $\hat{\mathbf{g}}_{m\,10} = e^{4\phi/3}C_m$  yields that the quartic shift on the 10-dimensional Ramond-Ramond one-form superfield is given by

$$\begin{aligned} e^\phi\tau_m^{(4)} = & \frac{1}{6}(\bar{\theta}\Delta\theta)(\bar{\theta}\Gamma^*D_m\theta) - \frac{1}{12}(\bar{\theta}\Delta\theta)(\bar{\theta}\Gamma^*\Gamma_m\Delta\theta) + \frac{1}{18}e^\phi(\bar{\theta}\Delta\theta)^2C_m \\ & - \frac{4}{3}e^\phi\rho^{(4)}C_m + e^{-\phi/3}\hat{\gamma}_{m\,10}^{(4)}. \end{aligned} \quad (12.181)$$

As with the quadratic case, the mixing of 10-dimensional superfields in the right-hand side of the supermetric relation in (12.156) means we are required to use the expressions for the dilaton superfield expansion in this calculation. Second, we Taylor-expand the relation  $\hat{\mathbf{g}}_{mn} = e^{-2\phi/3}(\mathbf{g}_{mn} + e^{2\phi}C_mC_n)$  in order to determine

an expression for the quartic fermion term of the expansion of the 10-dimensional supermetric, obtaining

$$\begin{aligned}
\gamma_{mn}^{(4)} = & \frac{2}{3}g_{mn}\rho^{(4)} + \frac{1}{4}(\bar{\theta}\Gamma^*D_{(m}\theta)(\bar{\theta}\Gamma^*D_{n)}\theta) - \frac{1}{4}(\bar{\theta}\Gamma^*D_{(m}\theta)(\bar{\theta}\Gamma^*\Gamma_{n)}\Delta\theta) \\
& + \frac{1}{16}(\bar{\theta}\Gamma^*\Gamma_{(m}\Delta\theta)(\bar{\theta}\Gamma^*\Gamma_{n)}\Delta\theta) - \frac{1}{6}(\bar{\theta}\Delta\theta)(\bar{\theta}\Gamma_{(m}D_{n)}\theta) + \frac{1}{72}g_{mn}(\bar{\theta}\Delta\theta)^2 \\
& - 2e^{2\phi}C_{(m}\tau_{n)}^{(4)} + \frac{1}{3}e^\phi C_{(m}(\bar{\theta}\Delta\theta)(\bar{\theta}\Gamma^*D_{n)}\theta) - \frac{1}{6}e^\phi C_{(m}(\bar{\theta}\Delta\theta)(\bar{\theta}\Gamma^*\Gamma_{n)}\Delta\theta) \\
& - \frac{4}{3}e^{2\phi}C_{(m}C_{n)}\rho^{(4)} + \frac{1}{18}e^{2\phi}C_{(m}C_{n)}(\bar{\theta}\Delta\theta)^2 + e^{2\phi/3}\hat{\gamma}_{mn}^{(4)}.
\end{aligned} \tag{12.182}$$

The mixing of 10-dimensional superfields in the relation for the 11-dimensional supermetric has again meant that we must include the previously calculated quartic terms for the dilaton and the Ramond-Ramond one-form when making this expansion. Already we can see that the relative complexity of the relation of the 11-dimensional supermetric to the 10-dimensional superfields results in expressions of some length even before we turn our attention to the dimensional reduction step of our procedure.

As with the quadratic case, the initial Taylor expansion and rearrangement of the relations in (12.157, 12.158) concerning the 11-dimensional three-form at quartic order are essentially straightforward. Denoting the quartic terms in the NORCOR expansion of the 11-dimensional super three-form (11.141) as  $\hat{\alpha}_{\hat{m}\hat{n}\hat{p}}^{(4)}$ , it is clear that the quartic terms in the truncated expansion of the 10-dimensional Ramond-Ramond three-form superfield is given by  $\alpha_{mnp}^{(4)} = \hat{\alpha}_{mnp}^{(4)}$ , and for the 10-dimensional Kalb-Ramond form superfield we have  $\beta_{mn}^{(4)} = \hat{\alpha}_{mn10}^{(4)}$ .

At this point, ‘all’ that is left to do in order to obtain expressions for the quartic terms in the expansions of the 10-dimensional superfields is to dimensionally reduce the 11-dimensional quantities that appear, namely the components of  $\hat{\gamma}_{\hat{m}\hat{n}}^{(4)}$  and  $\hat{\alpha}_{\hat{m}\hat{n}\hat{p}}^{(4)}$ . The calculation is very lengthy, so we provide all of the necessary tools and results in appendix 15.4. Despite their cumulative length, all the steps are the simple application of the dimensional reduction procedure with which we are now very familiar. For this reason, we place an example of the calculation in the case of the dilaton in appendix 15.4.5, but otherwise just report the results of the calculations here.

## Quartic $\theta$ -terms for type IIA superfield expansions

In order to simplify the statement of the results, it is convenient to first make a few definitions. Along with the familiar  $D_m$  and  $\Delta$ , we will use the combinations

$$\mathcal{D}_m \equiv D_m - \frac{1}{6}\Gamma_m\Delta, \tag{12.183}$$

$$K_q \equiv [\mathcal{D}_q, \Gamma^*\Delta] + (\partial_q\phi)\Gamma^*\Delta, \tag{12.184}$$

$$K_{pq} \equiv [\mathcal{D}_p, \mathcal{D}_q] + \frac{1}{3}e^\phi F_{pq}^{(2)}\Gamma^*\Delta, \tag{12.185}$$

as well as

$$\begin{aligned} R_{mn} &\equiv \frac{1}{24} \left[ \Gamma_{mn} (e^\phi \underline{F}^{(4)} + \underline{H}^{(3)} \Gamma^*) - 2 \Gamma_m (e^\phi \underline{F}_n^{(4)} + \underline{H}_n^{(3)} \Gamma^*) + (e^\phi \underline{F}_{mn}^{(4)} + \underline{H}_{mn}^{(3)} \Gamma^*) \right], \\ R_m &\equiv \frac{1}{24} \left[ \Gamma_m \Gamma^* e^\phi \underline{F}^{(4)} + \Gamma^* e^\phi \underline{F}_m^{(4)} \right]. \end{aligned} \quad (12.186)$$

We are now ready to list the quartic terms in the superfield expansion of the 10-dimensional superfields using only 10-dimensional operators. The quartic fermionic terms in the dilaton are given by

$$\begin{aligned} \rho^{(4)} &= -\frac{1}{768} (\bar{\theta} \Gamma^{mnpq} \theta) (\bar{\theta} \Gamma_{mn} K_{pq} \theta) + \frac{1}{576} (\bar{\theta} \Gamma^* \Gamma^{mnp} \theta) \left[ \bar{\theta} [3 \Gamma^* \Gamma_m K_{np} - \Gamma_{mn} K_p] \theta \right] \\ &+ \frac{1}{384} (\bar{\theta} \Gamma^* \Gamma^{mn} \theta) \left[ \bar{\theta} [3 \Gamma^* K_{mn} - 2 \Gamma_m K_n] \theta \right] + \frac{1}{48} (\bar{\theta} \Gamma^* \Gamma^{mn} \theta) (\bar{\theta} R_{mn} \Gamma^* \Delta \theta) \\ &- \frac{1}{48} (\bar{\theta} \Gamma_m \Gamma^* \Delta \theta) (\bar{\theta} \Gamma^m \Gamma^* \Delta \theta) - \frac{1}{576} \left[ \bar{\theta} [2 \Gamma^* e^\phi \underline{F}_m^{(4)} - \Gamma_m \underline{H}^{(3)}] \theta \right] (\bar{\theta} \Gamma^m \Gamma^* \Delta \theta) \\ &+ \frac{1}{48} (\bar{\theta} \Delta \theta)^2 + \frac{1}{576} \left[ \bar{\theta} [e^\phi \underline{F}^{(4)} - 2 \underline{H}^{(3)} \Gamma^*] \theta \right] (\bar{\theta} \Delta \theta). \end{aligned} \quad (12.187)$$

The quartic fermionic terms in the Ramond-Ramond one-form superfield are

$$\begin{aligned} e^\phi \tau_m^{(4)} &= + \frac{1}{576} [\bar{\theta} \Gamma_m \Gamma^{npq} \theta] \left[ \bar{\theta} [3 \Gamma^* \Gamma_n K_{pq} - \Gamma_{np} K_q] \theta \right] \\ &+ \frac{1}{192} [\bar{\theta} \Gamma^* \Gamma^{npq} \theta] \left[ \bar{\theta} [\Gamma_{mn} K_{pq} + \Gamma_{np} K_{mq}] \theta \right] \\ &+ \frac{1}{576} [\bar{\theta} \Gamma_m \Gamma^{np} \theta] \left[ \bar{\theta} [3 \Gamma^* K_{np} - 2 \Gamma_n K_p] \theta \right] + \frac{1}{72} [\bar{\theta} \Gamma_m \Gamma^{np} \theta] [\bar{\theta} R_{np} \Gamma^* \Delta \theta] \\ &+ \frac{1}{192} [\bar{\theta} \Gamma^* \Gamma^{np} \theta] \left[ \bar{\theta} [\Gamma_m K_{np} + 2 \Gamma_n K_{mp}] \theta \right] + \frac{1}{24} [\bar{\theta} \Gamma^* \Gamma^{np} \theta] [\bar{\theta} R_{np} \mathcal{D}_m \theta] \\ &+ \frac{1}{144} [\bar{\theta} \Gamma_m \Gamma^n \Gamma^* \theta] [\bar{\theta} \Gamma^* K_n \theta] + \frac{1}{36} [\bar{\theta} \Gamma_m \Gamma^n \Gamma^* \theta] [\bar{\theta} R_n \Gamma^* \Delta \theta] \\ &+ \frac{1}{12} [\bar{\theta} \Delta \theta] [\bar{\theta} \Gamma^* \mathcal{D}_m \theta] - \frac{1}{18} [\bar{\theta} \Delta \theta] [\bar{\theta} \Gamma^* \Gamma_m \Delta \theta] - \frac{1}{12} [\bar{\theta} \Gamma_n \Gamma^* \Delta \theta] [\bar{\theta} \Gamma^n \mathcal{D}_m \theta] \\ &+ \frac{1}{288} \left[ \bar{\theta} [e^\phi \underline{F}^{(4)} - 2 \underline{H}^{(3)} \Gamma^*] \theta \right] [\bar{\theta} \Gamma^* \mathcal{D}_m \theta] + \frac{1}{864} \left[ \bar{\theta} \Gamma_m \Gamma^* [e^\phi \underline{F}^{(4)} - 2 \underline{H}^{(3)} \Gamma^*] \theta \right] [\bar{\theta} \Delta \theta] \\ &+ \frac{1}{288} \left[ \bar{\theta} [\Gamma^* \Gamma_n e^\phi \underline{F}^{(4)} + \Gamma_n \underline{H}^{(3)} - 3 \Gamma^* e^\phi \underline{F}_n^{(4)}] \theta \right] [\bar{\theta} \Gamma^n \mathcal{D}_m \theta] \\ &- \frac{1}{864} \left[ \bar{\theta} \Gamma_m [3 \underline{H}_n^{(3)} \Gamma^* - \Gamma_n e^\phi \underline{F}^{(4)} + 3 e^\phi \underline{F}_n^{(4)} - \Gamma_n \underline{H}^{(3)} \Gamma^*] \theta \right] [\bar{\theta} \Gamma^n \Gamma^* \Delta \theta]. \end{aligned} \quad (12.188)$$

The quartic fermionic terms for the 10-dimensional metric expansion read

$$\begin{aligned}
\gamma_{mn}^{(4)} = & -\frac{1}{384}g_{mn}(\bar{\theta}\Gamma^{pqrs}\theta)(\bar{\theta}\Gamma_{pq}K_{rs}\theta) + \frac{1}{96}[\bar{\theta}\Gamma_{(m}\Gamma^{pqr}\theta][\bar{\theta}[\Gamma_{|n}K_{qr} + \Gamma_{pq}K_{|n}r]\theta] \\
& + \frac{1}{288}[\bar{\theta}\Gamma_{(m}\Gamma^{pq}\Gamma^*\theta][\bar{\theta}[2\Gamma_{|n}K_q + \Gamma_{pq}K_{|n}] + 3\Gamma_{|n}\Gamma^*K_{pq} - 6\Gamma_p\Gamma^*K_{|n}q]\theta] \\
& + \frac{1}{576}g_{mn}(\bar{\theta}\Gamma^*\Gamma^{pq}\theta)[\bar{\theta}[3\Gamma^*K_{pq} - 2\Gamma_pK_q]\theta] + \frac{1}{72}g_{mn}(\bar{\theta}\Gamma^*\Gamma^{pq}\theta)(\bar{\theta}R_{pq}\Gamma^*\Delta\theta) \\
& + \frac{1}{96}[\bar{\theta}\Gamma_{(m}\Gamma^{pq}\theta][\bar{\theta}[\Gamma_{|n}K_{pq} + 2\Gamma_pK_{|n}q]\theta] + \frac{1}{12}[\bar{\theta}\Gamma_{(m}\Gamma^{pq}\theta][\bar{\theta}R_{pq}\mathcal{D}_{|n}]\theta] \\
& + \frac{1}{144}[\bar{\theta}\Gamma_{(m}\Gamma^p\Gamma^*\theta][\bar{\theta}[\Gamma_{|n}K_p + \Gamma_pK_{|n}] - 3\Gamma^*K_{|n}p]\theta] + \frac{1}{6}[\bar{\theta}\Gamma_{(m}\Gamma^p\Gamma^*\theta][\bar{\theta}R_p\mathcal{D}_{|n}]\theta] \\
& - \frac{1}{72}g_{mn}(\bar{\theta}\Gamma_p\Gamma^*\Delta\theta)(\bar{\theta}\Gamma^p\Gamma^*\Delta\theta) - \frac{1}{4}[\bar{\theta}\Gamma_p\mathcal{D}_{(m}\theta][\bar{\theta}\Gamma^p\mathcal{D}_{n)}\theta] \\
& + \frac{1}{36}(\bar{\theta}\Gamma^*\Gamma_{(m}\Delta\theta)(\bar{\theta}\Gamma^*\Gamma_{n)}\Delta\theta) - \frac{1}{6}(\bar{\theta}\Gamma^*\Gamma_{(m}\Delta\theta)(\bar{\theta}\Gamma^*\mathcal{D}_{n)}\theta) - \frac{1}{6}(\bar{\theta}\Delta\theta)(\bar{\theta}\Gamma_{(m}\mathcal{D}_{n)}\theta) \\
& - \frac{1}{864}g_{mn}[\bar{\theta}[2\Gamma^*e^\phi\underline{F}_p^{(4)} - \Gamma_p\underline{H}^{(3)}]\theta](\bar{\theta}\Gamma^p\Gamma^*\Delta\theta) \\
& - \frac{1}{144}[\bar{\theta}\Gamma_{(m}[3\underline{H}_p^{(3)}\Gamma^* - \Gamma_p e^\phi\underline{F}^{(4)} - \Gamma_p\underline{H}^{(3)}\Gamma^* + 3e^\phi\underline{F}_p^{(4)}]\theta][\bar{\theta}\Gamma^p\mathcal{D}_{|n}]\theta] \\
& - \frac{1}{144}[\bar{\theta}\Gamma_{(m}\Gamma^*[2\underline{H}^{(3)}\Gamma^* - e^\phi\underline{F}^{(4)}]\theta][\bar{\theta}\Gamma^*\mathcal{D}_{|n}]\theta] \\
& + \frac{1}{864}g_{mn}(\bar{\theta}\Delta\theta)[\bar{\theta}[e^\phi\underline{F}^{(4)} - 2\underline{H}^{(3)}\Gamma^*]\theta].
\end{aligned} \tag{12.189}$$

The quartic fermionic terms for the Kalb-Ramond two-form are

$$\begin{aligned}
\beta_{mn}^{(4)} = & -\frac{1}{384}(\bar{\theta}\Gamma^*\Gamma_{mn}\Gamma^{pqrs}\theta)[\bar{\theta}\Gamma_{pq}K_{rs}\theta] - \frac{1}{96}(\bar{\theta}\Gamma_{[m}\Gamma^*\Gamma^{pqr}\theta)[\bar{\theta}[\Gamma_{|n}K_{qr} + \Gamma_{pq}K_{|n}r]\theta] \\
& + \frac{1}{576}(\bar{\theta}\Gamma_{mn}\Gamma^{pq}\theta)[\bar{\theta}[3\Gamma^*K_{pq} - 2\Gamma_pK_q]\theta] + \frac{1}{72}(\bar{\theta}\Gamma_{mn}\Gamma^{pq}\theta)[\bar{\theta}R_{pq}\Gamma^*\Delta\theta] \\
& - \frac{1}{96}(\bar{\theta}\Gamma_{[m}\Gamma^*\Gamma^{pq}\theta)[\bar{\theta}[\Gamma_{|n}K_{pq} + 2\Gamma_pK_{|n}q]\theta] - \frac{1}{12}(\bar{\theta}\Gamma_{[m}\Gamma^*\Gamma^{pq}\theta)[\bar{\theta}R_{pq}\mathcal{D}_{|n}]\theta] \\
& - \frac{1}{288}(\bar{\theta}\Gamma_{[m}\Gamma^{pq}\theta)[\bar{\theta}[2\Gamma_{|n}K_q + \Gamma_{pq}K_{|n}] + 3\Gamma_{|n}\Gamma^*K_{pq} - 6\Gamma_p\Gamma^*K_{|n}q]\theta] \\
& + \frac{1}{144}(\bar{\theta}\Gamma_{mn}\Gamma^p\Gamma^*\theta)[\bar{\theta}\Gamma^*K_p\theta] + \frac{1}{36}(\bar{\theta}\Gamma_{mn}\Gamma^p\Gamma^*\theta)[\bar{\theta}\check{R}_p\Gamma^*\Delta\theta] + \frac{1}{6}(\bar{\theta}\Gamma_{[m}\Gamma^p\theta)[\bar{\theta}R_p\mathcal{D}_{|n}]\theta] \\
& + \frac{1}{144}(\bar{\theta}\Gamma_{[m}\Gamma^p\theta)[\bar{\theta}[\Gamma_{|n}K_p + \Gamma_pK_{|n}] - 3\Gamma^*K_{|n}p]\theta] - \frac{1}{12}(\bar{\theta}\Gamma_p\Gamma_{[m}\mathcal{D}_{n)}\theta)(\bar{\theta}\Gamma^p\Gamma^*\Delta\theta) \\
& - \frac{1}{4}(\bar{\theta}\Gamma_p\Gamma^*\mathcal{D}_{[m}\theta)(\bar{\theta}\Gamma^p\mathcal{D}_{n)}\theta) + \frac{1}{12}(\bar{\theta}\Gamma_p\Gamma_{[m}\Gamma^*\Delta\theta)(\bar{\theta}\Gamma^p\mathcal{D}_{n)}\theta) - \frac{1}{12}(\bar{\theta}\Gamma^*\Gamma_{[m}\mathcal{D}_{n)}\theta)(\bar{\theta}\Delta\theta) \\
& - \frac{1}{12}(\bar{\theta}\Gamma_{[m}\Delta\theta)(\bar{\theta}\Gamma^*\mathcal{D}_{n)}\theta) - \frac{1}{12}(\bar{\theta}\Gamma^*\Delta\theta)(\bar{\theta}\Gamma_{[m}\mathcal{D}_{n)}\theta) - \frac{1}{12}(\bar{\theta}\mathcal{D}_{[m}\theta)(\bar{\theta}\Gamma_{n)}\Gamma^*\Delta\theta) \\
& - \frac{1}{144}[\bar{\theta}\Gamma_{[m}[ \Gamma^*\Gamma_p e^\phi\underline{F}^{(4)} + \Gamma_p\underline{H}^{(3)} - 3\Gamma^*e^\phi\underline{F}_p^{(4)} - 3\underline{H}_p^{(3)}]\theta][\bar{\theta}\Gamma^p\mathcal{D}_{|n}]\theta] \\
& + \frac{1}{864}[\bar{\theta}\Gamma_{mn}[\Gamma_p e^\phi\underline{F}^{(4)} + \Gamma_p\underline{H}^{(3)}\Gamma^* - 3\underline{H}_p^{(3)}\Gamma^* - 3e^\phi\underline{F}_p^{(4)}]\theta][\bar{\theta}\Gamma^p\Gamma^*\Delta\theta] \\
& - \frac{1}{144}[\bar{\theta}\Gamma_{[m}\Gamma^*[e^\phi\underline{F}^{(4)} + 2\underline{H}^{(3)}]\theta][\bar{\theta}\Gamma^*\mathcal{D}_{|n}]\theta] \\
& + \frac{1}{864}[\bar{\theta}\Gamma_{mn}[\Gamma^*e^\phi\underline{F}^{(4)} + 2\underline{H}^{(3)}]\theta][\bar{\theta}\Delta\theta].
\end{aligned} \tag{12.190}$$

Finally, the quartic fermionic terms for the Ramond-Ramond three-form superfield can be written as

$$\alpha'_{mnp}{}^{(4)} = \alpha''_{mnp}{}^{(4)} + 3\beta_{[mn}{}^{(4)} C_p], \quad (12.191)$$

where  $\alpha''_{mnp}{}^{(4)}$  is given by the expression,

$$\begin{aligned} e^\phi \alpha''_{mnp}{}^{(4)} = & -\frac{1}{384} (\bar{\theta} \Gamma_{mnp} \Gamma^{qrst} \theta) [\bar{\theta} \Gamma_{qr} K_{st} \theta] - \frac{1}{576} (\bar{\theta} \Gamma_{mnp} \Gamma^{qrs} \Gamma^* \theta) [\bar{\theta} [\Gamma_{qr} K_s - 3 \Gamma^* \Gamma_q K_{rs}] \theta] \\ & + \frac{1}{64} (\bar{\theta} \Gamma_{[mn} \Gamma^{qr} \theta) [\bar{\theta} [\Gamma_{|p} K_{rs} + \Gamma_{qr} K_{|p} s] \theta] \\ & + \frac{1}{192} (\bar{\theta} \Gamma_{[mn} \Gamma^{qr} \Gamma^* \theta) [\bar{\theta} [2 \Gamma_{|p} K_r + \Gamma_{qr} K_{|p} + 3 \Gamma_{|p} \Gamma^* K_{qr} - 6 \Gamma_q \Gamma^* K_{|p} r] \theta] \\ & + \frac{1}{64} (\bar{\theta} \Gamma_{[mn} \Gamma^{qr} \theta) [\bar{\theta} [\Gamma_{|p} K_{qr} + 2 \Gamma_q K_{|p} r] \theta] + \frac{1}{8} (\bar{\theta} \Gamma_{[mn} \Gamma^{qr} \theta) [\bar{\theta} R_{qr} \mathcal{D}_{|p} \theta] \\ & + \frac{1}{96} (\bar{\theta} \Gamma_{[mn} \Gamma^q \Gamma^* \theta) [\bar{\theta} [\Gamma_{|p} K_q + \Gamma_q K_{|p} - 3 \Gamma^* K_{|p} q] \theta] + \frac{1}{4} (\bar{\theta} \Gamma_{[mn} \Gamma^q \Gamma^* \theta) (\bar{\theta} R_q \mathcal{D}_{|p} \theta) \\ & - \frac{3}{4} (\bar{\theta} \Gamma_q \Gamma_m \mathcal{D}_n \theta) (\bar{\theta} \Gamma^q \mathcal{D}_p \theta) - \frac{3}{4} (\bar{\theta} \mathcal{D}_{[m} \theta) (\bar{\theta} \Gamma_n \mathcal{D}_p \theta) - \frac{3}{4} (\bar{\theta} \Gamma^* \Gamma_m \mathcal{D}_n \theta) (\bar{\theta} \Gamma^* \mathcal{D}_p \theta) \\ & + \frac{1}{96} [\bar{\theta} \Gamma_{[mn} [\Gamma_q e^\phi \underline{F}^{(4)} + \Gamma_q \underline{H}^{(3)} \Gamma^* - 3 e^\phi \underline{F}_q^{(4)} - 3 \underline{H}_q^{(3)} \Gamma^*] \theta] [\bar{\theta} \Gamma^q \mathcal{D}_{|p} \theta] \\ & + \frac{1}{96} [\bar{\theta} \Gamma_{[mn} [2 \underline{H}^{(3)} + \Gamma^* e^\phi \underline{F}^{(4)}] \theta] [\bar{\theta} \Gamma^* \mathcal{D}_{|p} \theta]. \end{aligned} \quad (12.192)$$

A few comments are due, as in the above formulae the 10-dimensional quartic fermionic terms look complicated and have an enormous length. With current understanding, the quartic fermion expansions of type IIA superfields seem unavoidably lengthy, as also seen in [155]. We will discuss some promising avenues for improving this quality of these results in what follows. On the other hand, the most prominent feature of these results is their completeness. The robustness and systematicity of the methods we have employed *guarantee* that these are the full and complete quartic fermion terms for the type IIA superfield expansions. This is the first time that some of these terms have been calculated and our results will serve as a foundation for future understanding of such expansions.

### Avenues to simplification

Our current expressions for the results for the quartic order fermion terms in the type IIA superfield expansions are unwieldy. It is therefore worthwhile to discuss how they might be made more manageable.

The first thought that might occur is to try and tidy up the large number of ‘loose’ flux terms in the expansions. One would do this by attempting to package these terms up using the operators  $D_m$  and  $\Delta$  (or combinations thereof) just as everything at second order was packaged neatly. Indeed, this idea is met with some initial success, for example, with a little effort, one can see that three of the terms appearing above in the dilaton shift come together to give

$$\begin{aligned} & \frac{1}{128} (\bar{\theta} \Gamma^* \Gamma^{mn} \theta) (\bar{\theta} \Gamma^* K_{mn} \theta) + \frac{1}{48} (\bar{\theta} \Delta \theta)^2 + \frac{1}{576} [\bar{\theta} [e^\phi \underline{F}^{(4)} - 2 \underline{H}^{(3)} \Gamma^*] \theta] (\bar{\theta} \Delta \theta) = \\ & = \frac{1}{128} (\bar{\theta} \Gamma^* \Gamma^{mn} \theta) (\bar{\theta} \Gamma^* [D_m, D_n] \theta) + \frac{1}{72} (\bar{\theta} \Delta \theta)^2. \end{aligned} \quad (12.193)$$

However, reorganizations along these lines often require spotting tricks in the calculations, for example with

$\Gamma$ -matrix identities, with the symmetry properties of bilinears, and potentially with Fierz identities. It rapidly becomes utterly impractical to hope to significantly reorganize these shifts as they currently stand in this way. We must try and find a better strategy.

We can see in the quadratic and quartic cases that the process of dimensional reduction sharply increases the number and complexity of terms in the expansions. However, dimensional reduction will not generate the capacity for any significant recombination or reorganization of terms all by itself. Any game-changing reorganizational principle for the 10-dimensional quartic terms should be identifiable in the simpler quartic terms in the 11-dimensional description. The most promising line, therefore, is not to try and massage the many terms appearing in ten dimensions, but to return to 11 dimensions and fix them there. The quartic fermion terms in the expansions of the supermetric and super three-form in 11-dimensional supergravity are given in (11.140) and (11.141). We saw in our discussion of the M2-brane that in actuality the only 11-dimensional superfield we need to expand using NORCOR in order to obtain the expansions required for the brane action is the supervielbein  $E_M{}^A(Z)$ . All the components of the expansion of this superfield that we require to get to quartic fermion order for the M2-brane are given in (11.127) in conjuncture with (11.126). Recall that we also performed significant manipulation of the higher-order expansions using Bianchi identities until we arrived at (11.128). We can see then that it is the relative unwieldiness of *these* expressions for components of the NORCOR expansion of the 11-dimensional supervielbein where the vastness of the quartic 10-dimensional terms has its origin. Meaningful rearrangement or simplification of the quartic terms in the type IIA superfield expansion will be identifiable at the level of improvements of (11.128). These improvements have the potential to come from a couple of different lines of reasoning. The most obvious is by improving the application of the Bianchi identities (and litany of other subtle identities that emerge in their combination) when moving from (11.127) to (11.128). Another direction might be to improve the NORCOR procedure itself, or making significant geometrical insight there, such that the left-hand side of (11.128) can be made more and more amenable.

Crucial to note, however, is that even with these improvements to the treatment of the 11-dimensional supervielbein, the best subsequent method for obtaining the type IIA quartic terms is still the one we have presented here, when applied to the improved formulation. We will say some more about how the quartic results might be improved once we have explored the next step in our procedure and obtained information about both type II supergravities.



# Superspace T-duality and Dp-branes

In this chapter we complete the task initiated in chapter 12 and provide a systematic method to compute fermion couplings on all Dp-branes. The method is based on ideas analogous to the ones in chapter 12, and for this reason we will make reference to explanations there when possible to avoid repetition.

Let us briefly summarize the approach. Our proposal relies on two facts. First, Dp-branes are solutions of type II supergravities related by T-dualities. Second, fermion couplings on Dp-brane actions arise naturally in the superspace formulation of the corresponding supergravity theory. For reasons analogous to the ones in the previous chapter, here we combine those two facts and extend the relation between the T-dual geometries to the superspace level. Using this generalization we find relations between superfields in curved superspaces that are T-dual to each other. We use those relations to find the  $\theta$ -expansions of superfields appearing in Dp-brane actions. We already explained that this is equivalent to finding fermion couplings on all Dp-brane actions.

## 13.1 T-duality toolkit

With the general picture in mind, we can move into the details. In type II theories,<sup>19</sup> T-duality represents the equivalence of type IIA strings on a background with an isometry along a non-trivial circle  $S^1$  of size  $R$  and type IIB strings compactified on another background also with an isometric on a non-trivial circle  $\tilde{S}^1$ , this time with size  $\tilde{R} = l_s^2/R$  (in our conventions, the string length is  $l_s = 2\pi\sqrt{\alpha'}$ ). We are interested in this underlying structure that connects the two theories. The relations for Neveu-Schwarz fields were first given by Buscher [156, 157] and expanded to Ramond-Ramond fields in [158], and then they were extended to fermionic fields in [132–134].

### 13.1.1 Bosons

Analogously to the dimensional reduction, we begin with a reminder of the standard T-duality relations for bosonic fields. We take the T-duality  $S^1$ -direction to be  $x^9$ . Our notation will be the following: the indices

---

<sup>19</sup>T-duality is a more general concept in String Theory and it also relates heterotic strings, but here we are interested in type II theories only.



$m, n = 0, \dots, 9$  run through all spacetime directions, and the indices  $\dot{m}, \dot{n} = 0, \dots, 8$  through all but the circle  $S^1$ , that we take to be  $x^9 \sim x^9 + R$ . We indicate which fields belong to each theory by introducing a tilde for fields in one theory and no adornment of symbols for fields in the other one. All fields are independent of the T-duality direction. We start by providing the well-known Buscher rules<sup>20</sup>

$$\tilde{\phi} = \phi - \frac{1}{2} \ln g_{99}, \quad (13.194a)$$

$$\tilde{g}_{\dot{m}\dot{n}} = g_{\dot{m}\dot{n}} - g_{99}^{-1} (g_{\dot{m}9} g_{\dot{n}9} - B_{\dot{m}9} B_{\dot{n}9}), \quad (13.194b)$$

$$\tilde{g}_{\dot{m}9} = g_{99}^{-1} B_{\dot{m}9}, \quad (13.194c)$$

$$\tilde{g}_{99} = g_{99}^{-1}, \quad (13.194d)$$

$$\tilde{B}_{\dot{m}\dot{n}} = g_{\dot{m}\dot{n}} - g_{99}^{-1} (B_{\dot{m}9} g_{\dot{n}9} - g_{\dot{m}9} B_{\dot{n}9}), \quad (13.194e)$$

$$\tilde{B}_{\dot{m}9} = g_{99}^{-1} g_{\dot{m}9}. \quad (13.194f)$$

The Ramond-Ramond gauge potentials are related by the mutually implicative expressions

$$\tilde{C}_{9\dot{m}_2 \dots \dot{m}_n}^{(n)} = C_{\dot{m}_2 \dots \dot{m}_n}^{(n-1)} - (n-1) g_{99}^{-1} g_{9[\dot{m}_2} C_{|\dot{m}_3 \dots \dot{m}_n]}^{(n-1)}, \quad (13.195a)$$

$$\tilde{C}_{\dot{m}_1 \dots \dot{m}_n}^{(n)} = C_{9\dot{m}_1 \dots \dot{m}_n}^{(n+1)} - n B_{9[\dot{m}_1} C_{\dot{m}_2 \dots \dot{m}_n]}^{(n-1)} + n(n-1) g_{99}^{-1} g_{9[\dot{m}_1} B_{9|\dot{m}_2} C_{\dot{m}_3 \dots \dot{m}_n]}^{(n-1)}. \quad (13.195b)$$

### 13.1.2 Spinors, supersymmetry operators, and spinor doublet notation

When fermions are involved, T-duality becomes somewhat more subtle and complicated. The groundwork for the treatment of fermions under T-duality is represented by the Hassan rules [132–134].

The intricate world of fermion T-duality begins with making an observation concerning the T-duality rules for fields in the Neveu-Schwarz sector: there are two different vielbeins that are dual to the original one. Properly dealing with this fact requires the introduction of some extra structure. We denote the ‘initial’ vielbein as  $e_a{}^m$ , and the two possible ‘final’ dual vielbeins as  $(\tilde{e}_+){}_a{}^m$  and  $(\tilde{e}_-){}_a{}^m$ . Both choices give the correct T-dual metric. The initial and final vielbeins are related according to the T-duality rules

$$(\tilde{e}_\pm)_a{}^n = e_a{}^m (Q_\pm)_m{}^n, \quad (13.196a)$$

$$(\tilde{e}_\pm)_m{}^a = (Q_\pm^{-1})_m{}^n e_n{}^a, \quad (13.196b)$$

where we have defined

$$(Q_\pm)_m{}^n = \begin{pmatrix} \delta_{\dot{m}}{}^{\dot{n}} & \mp (g_{9\dot{m}} \pm B_{9\dot{m}}) \\ 0 & \mp g_{99} \end{pmatrix}, \quad (13.197a)$$

$$(Q_\pm^{-1})_m{}^n = \begin{pmatrix} \delta_{\dot{m}}{}^{\dot{n}} & -g_{99}^{-1} (g_{9\dot{m}} \pm B_{9\dot{m}}) \\ 0 & \mp g_{99}^{-1} \end{pmatrix}. \quad (13.197b)$$

Notice that  $(\tilde{Q}_\pm^{-1})_m{}^n = (Q_\pm)_m{}^n$ . The two vielbeins  $(\tilde{e}_+){}_m{}^a$  and  $(\tilde{e}_-){}_m{}^a$  are related to one another by a local

<sup>20</sup>Notice that fields are dimensionless in this setup, e.g.  $g_{99} = (R/l_s)^2$ . Forms therefore have length dimension with the string length  $l_s$  as a reference length. Integrals such as  $\int_0^1 dx^9 \sqrt{g_{99}} = R$  give dimensionful volumes with the appropriate dimension.

Lorentz transformation as  $(\tilde{e}_+)_{m^a} = \Lambda^a_b (\tilde{e}_-)_{m^b}$ , with  $\Lambda^a_b = e_b^m (Q_-)_m^p (Q_+^{-1})_p^n e_n^a$ . This is irrelevant for the Lorentz-invariant quantities in the bosonic analysis, but it plays a vital role when considering fermions. For example there are now two choices for  $\Gamma$ -matrices in the dual theory, i.e.

$$(\tilde{\Gamma}_{\pm})_m = (Q_{\pm}^{-1})_m^n \Gamma_n = (\tilde{e}_{\pm})_m^a \Gamma_a. \quad (13.198)$$

These are naturally related by a spinorial representation  $\Omega$  of the Lorentz transformation  $\Lambda$ , defined via  $\Omega \Gamma_a \Omega^{-1} = \Gamma_b (\Lambda^{-1})^b_a$ , as

$$\Omega (\tilde{\Gamma}_+) \Omega^{-1} = (\tilde{\Gamma}_-). \quad (13.199)$$

It can be determined that this matrix reads (also notice it squares as  $\Omega^2 = -1$ )

$$\Omega = \tilde{\Omega} = \frac{1}{\sqrt{g_{99}}} \Gamma^* \Gamma_9. \quad (13.200)$$

The extra complication when T-dualizing objects that are sensitive to the difference between the two choices of vielbein, such as spinors and  $\Gamma$ -matrices, is that for self-consistency it is necessary that all Lorentz tensors in the dual theory are computed with respect to the same vielbein. We will choose  $(\tilde{e}_-)_{n^a}$  as our reference dual vielbein. Let us point out that this does not imply that we will write all duality relations using  $Q_-$ : we will often find it convenient to transform objects using  $Q_+$  and then perform Lorentz transformations.

With these tools in hand, we are in principle ready to provide all of the rules for fermion T-dualization introduced by Hassan. Before doing so, however, we introduce a new notation that allows us to perform computations in a clean and compact way: the spinor doublet notation. The spinor doublet notation we introduce has differences to the ones found in the literature, e.g. in [102, 125–127, 159]. These differences will make performing the necessary T-duality computations cleaner. The motivation for this new notation is the following: in type II theories spinors come in doublets of Majorana-Weyl spinors. In type IIA these have opposite chirality whereas in IIB they have the same chirality, which we take to be positive for the gravitinos and supersymmetry parameters, and negative for dilatinos. It is therefore convenient to use spinor doublet in the latter in order to write most combinations, such as fermion bilinears, in a compact way. We define the IIB doublets

$$\epsilon^B = \begin{pmatrix} \epsilon_1 \\ \epsilon_2 \end{pmatrix}, \quad \psi_m^B = \begin{pmatrix} \psi_{1m} \\ \psi_{2m} \end{pmatrix}, \quad \lambda^B = \begin{pmatrix} \lambda_1 \\ \lambda_2 \end{pmatrix}. \quad (13.201)$$

It is also convenient to do the same in the type IIA theory. In this case, we must bear in mind that chirality plays a crucial role in organizing fermion bilinears in this theory, and so we need to use chirality as an organizing principle. Our convention will be to have positive chirality fermions on the top of type IIA fermion doublets. We can now define

$$\epsilon^A = \begin{pmatrix} \epsilon_+ \\ \epsilon_- \end{pmatrix}, \quad \psi_m^A = \begin{pmatrix} \psi_{+m} \\ \psi_{-m} \end{pmatrix}, \quad \lambda^A = \begin{pmatrix} \lambda_+ \\ \lambda_- \end{pmatrix}. \quad (13.202)$$

Given these doublets, the natural matrices that act on them can always be written in terms of the 2-dimensional identity  $1_2$  and the Pauli matrices  $\sigma^1, \sigma^2, \sigma^3$ . This also comes with further implications. For instance, chirality matrices in type IIA theory can always be replaced by  $\sigma^3$  in our conventions, as in  $\Gamma^* \epsilon^A = \sigma^3 \epsilon^A$ . Also, to

account for the fact that multiplications by a  $\Gamma$ -matrix flip chiralities, one must introduce a  $\sigma^1$  matrix for each  $\Gamma$ -matrix when moving to the spinor doublet notation from the one in the previous section. The appearance of multiple Pauli matrices in this notation change can make formulae more complicated to read. In order to make them more readable, we compute the product of Pauli matrices and just give the resulting one, such that all other operators appearing in the expressions now come with  $1_2$ . For example, the type IIA product  $\Gamma_m \Gamma^* \epsilon$  leads to  $(\sigma^1 \otimes \Gamma_m) \sigma^3 \epsilon^\Lambda = (1_2 \otimes \Gamma_m) (-i\sigma^2) \epsilon^\Lambda = (-i\sigma^2) \otimes \Gamma_m \epsilon^\Lambda$  in our doublet notation. We will omit ' $\otimes$ ' symbols from now on. Hence operators implicitly come with  $1_2$ . We will also write  $\mathbb{F}_m = 1_2 \otimes \Gamma_m$ . In type IIB strings, chirality cannot be used as an organizing principle, instead the Pauli-matrix structure is inherited from type IIA.

As clarifying examples, and because they will be useful for later purposes, we provide here the second-order truncated superfields (12.169 - 12.173) that appeared in the D2-brane action with fermion bilinears written in this notation. These are

$$\mathbf{g}_{mn} = g_{mn} - i \bar{\theta}^\Lambda \sigma^1 \mathbb{F}_{(m} \mathbb{D}_{n)}^\Lambda \theta^\Lambda, \quad (13.203)$$

$$\phi = \phi - \frac{i}{4} \bar{\theta}^\Lambda \Delta^\Lambda \theta^\Lambda, \quad (13.204)$$

$$\mathbf{B}_{mn} = B_{mn} - i \bar{\theta}^\Lambda (i\sigma^2) \mathbb{F}_{[m} \mathbb{D}_{n]}^\Lambda \theta^\Lambda, \quad (13.205)$$

$$\mathbf{C}_m = C_m - \frac{i}{2} e^{-\phi} \bar{\theta}^\Lambda \sigma^3 \left( \mathbb{D}_m^\Lambda - \frac{1}{2} \sigma^1 \mathbb{F}_m \Delta^\Lambda \right) \theta^\Lambda, \quad (13.206)$$

$$\mathbf{C}'_{mnp} = C_{mnp} - \frac{i}{2} e^{-\phi} \bar{\theta}^\Lambda \left( 3 \mathbb{F}_{[mn} \mathbb{D}_{p]}^\Lambda - \frac{1}{2} \sigma^1 \mathbb{F}_{mnp} \Delta^\Lambda \right) \theta^\Lambda - 3i C_{[m} \bar{\theta}^\Lambda (i\sigma^2) \mathbb{F}_{n} \mathbb{D}_{p]}^\Lambda \theta^\Lambda. \quad (13.207)$$

In order to write the superfields, we used the operators appearing in the type IIA gravitino and dilatino supersymmetry variations, that in the spinor doublet notation are

$$\delta_\epsilon \psi_m^\Lambda = \mathbb{D}_m^\Lambda \epsilon^\Lambda, \quad (13.208)$$

$$\delta_\epsilon \lambda^\Lambda = \Delta^\Lambda \epsilon^\Lambda, \quad (13.209)$$

with

$$\mathbb{D}_m^\Lambda \equiv 1_2 \nabla_m + \frac{1}{4} \sigma^3 \underline{H}_m^{(3)} - \frac{1}{8} e^\phi [i\sigma^2 \underline{F}^{(2)} + \sigma^1 \underline{F}^{(4)}] \Gamma_m, \quad (13.210)$$

$$\Delta^\Lambda \equiv \sigma^1 \partial \phi + \frac{1}{2} i\sigma^2 \underline{H}^{(3)} - \frac{1}{8} e^\phi \Gamma^m [\sigma^3 \underline{F}^{(2)} + 1_2 \underline{F}^{(4)}] \Gamma_m. \quad (13.211)$$

We also need to define the equivalent operators in type IIB. For doing so we first give the supersymmetry variations in the spinor doublet notation

$$\delta_\epsilon \psi_m^B = \mathbb{D}_m^B \epsilon^B, \quad (13.212)$$

$$\delta_\epsilon \lambda^B = \Delta^B \epsilon^B, \quad (13.213)$$

and this time

$$\mathbb{D}_m^{\mathbb{B}} \equiv 1_2 \nabla_m + \frac{1}{4} \sigma^3 \underline{H}_m^{(3)} + \frac{1}{8} e^\phi \left[ i \sigma^2 \left( \underline{F}^{(1)} + \underline{F}^{(5)} \right) + \sigma^1 \underline{F}^{(3)} \right] \Gamma_m, \quad (13.214)$$

$$\Delta^{\mathbb{B}} \equiv \sigma^1 \underline{\partial} \phi + \frac{1}{2} i \sigma^2 \underline{H}^{(3)} + \frac{1}{8} e^\phi \Gamma^m \left[ \sigma^3 \left( \underline{F}^{(1)} + \underline{F}^{(5)} \right) + 1_2 \underline{F}^{(3)} \right] \Gamma_m. \quad (13.215)$$

Now we have to express the basic T-duality relations in this spinor doublet notation. The extensions of  $Q_\pm$  and  $\Omega$  can be simply achieved by defining

$$(Q_\pm)_m{}^n = \begin{pmatrix} (Q_\pm)_m{}^n & 0 \\ 0 & (Q_\mp)_m{}^n \end{pmatrix} \quad (13.216)$$

and

$$\Upsilon = \begin{pmatrix} 1 & 0 \\ 0 & \Omega \end{pmatrix}. \quad (13.217)$$

These definitions allow us to extend the T-duality rules for many objects to the spinor doublet notation which will be used later on. For instance, once we take  $(\tilde{e}_-)_m{}^a$  as the reference frame in the dual theory, the  $\Gamma$ -matrix rule can be manipulated to give

$$\tilde{\Gamma}_m = (Q_-^{-1})_m{}^n \Upsilon \Gamma_n \Upsilon^{-1}. \quad (13.218)$$

Adapting the notation of [125, 126, 132–134] to our conventions, spinors in type IIA and type IIB theories are related to each other by the T-duality rules

$$\epsilon^{\mathbb{B}} = \Upsilon \epsilon^{\mathbb{A}}, \quad (13.219)$$

$$\psi_m^{\mathbb{B}} = (Q_+^{-1})_m{}^n \Upsilon \psi_n^{\mathbb{A}}, \quad (13.220)$$

$$\lambda^{\mathbb{B}} = (\sigma^1 \Upsilon \sigma^1) [\lambda^{\mathbb{A}} - 2 g_{99}^{-1} \sigma^1 \Gamma_9 \psi_9^{\mathbb{A}}], \quad (13.221)$$

Related to the above formulae, it is convenient to define the Dirac conjugate doublets because these appear in fermion bilinears. Based on chirality arguments above this is  $\bar{\epsilon}^{\mathbb{A}} = (\bar{\epsilon}_-, \bar{\epsilon}_+)$  for type IIA and we extend the structure to IIB by defining  $\bar{\epsilon}^{\mathbb{B}} = (\bar{\epsilon}_2, \bar{\epsilon}_1)$ . The T-duality relation between them is  $\bar{\epsilon}^{\mathbb{B}} = \bar{\epsilon}^{\mathbb{A}} \sigma^1 \Upsilon^{-1} \sigma^1$ .

A point worth making here is that if we invert the relations above, the outcome is similar but involves  $\Upsilon^{-1}$ , instead of  $\Upsilon$  itself, so there is a slight difference between going from type IIA to type IIB or taking the opposite route. This did not happen for bosonic fields above, where the relations found worked the same regardless of the direction taken to perform the duality. To conclude, the T-duality rules between the supersymmetry operators read

$$\mathbb{D}_m^{\mathbb{B}} = (Q_+^{-1})_m{}^n \Upsilon \mathbb{D}_n^{\mathbb{A}} \Upsilon^{-1}, \quad (13.222a)$$

$$\Delta^{\mathbb{B}} = \sigma^1 \Upsilon \sigma^1 [\Delta^{\mathbb{A}} - 2 g_{99}^{-1} \sigma^1 \Gamma_9 \mathbb{D}_9^{\mathbb{A}}] \Upsilon^{-1}, \quad (13.222b)$$

The above results are in precise agreement with the existing literature. As should be apparent, the spinor doublet notation approach we have employed here is highly successful in compactly capturing the T-duality relationships for the fermions and supersymmetry variations in type IIA and type IIB supergravity.

### 13.1.3 T-duality and bosonic D $p$ -branes

We will now review how bosonic D $p$ -brane actions are related to each other under T-duality. This is instrumental in explaining our superspace approach below. In general, the basic idea is that T-dualising a theory with a D $p$ -brane produces a theory with a D $(p \pm 1)$ -brane, depending on whether the original brane wraps the T-duality circle  $S^1$  or not. This is consistent with the fact that type IIA and type IIB theories are exchanged, as the former only admits even- $p$  branes and the latter only odd- $p$  ones. Starting from the bosonic D2-brane action, one can repeatedly T-dualise the theory to infer that the bosonic action of a generic D $p$ -brane is

$$S_{Dp}^{(0)} = -T_{Dp} \int d^{p+1}\zeta e^{-\phi} \sqrt{-\det(g+f)} + T_{Dp} \int C e^{-f}, \quad (13.223)$$

where the brane tension is  $T_{Dp} = 2\pi/l_s^{p+1}$ . All bulk fields are pulled-back onto the brane worldvolume. The WZ-term contains a formal sum  $C = \sum_q C^{(q)}$  over forms of all degrees and we let the integral pick out the appropriate forms each time.

In order to show in some detail how the machinery of T-duality works for D $p$ -branes, we consider a bosonic D $p$ -brane wrapping the T-duality circle  $S^1$  in the direction  $x^9$  and, with simple manipulations, we integrate its action over the circle  $S^1$  to obtain the action of the dual D $(p-1)$ -brane that is localized on the dual circle. The initial D $p$ -brane wraps a  $(p+1)$ -cycle  $\Sigma_{p+1}$  that is an  $S^1$ -fibration over  $\Sigma_p$ , which is the cycle wrapped by the final D $(p-1)$ -brane. Indices  $k = 0, \dots, p-1, 9$  span the D $p$ -brane worldvolume and indices  $\dot{k} = 0, \dots, p-1$  are parallel to the D $(p-1)$ -brane, excluding the direction  $x^9$ . For simplicity, we fix the static gauge for the brane embedding, with all fields independent of the  $S^1$ -direction. For clarity, we manipulate the DBI- and the WZ-terms of the action separately. See [160, 161] for details.

First, we deal with the DBI-action. Integrating over the circle  $S^1$  goes as

$$\begin{aligned} S_{Dp}^{\text{DBI}} &= -T_{Dp} \int_{\Sigma_{p+1}} d^{p+1}\zeta e^{-\phi} \sqrt{-\det[\varphi(g+f)_{kl}]} \\ &= -T_{Dp} \int_{\Sigma_p} d^p\zeta \int_0^1 dx^9 e^{-\phi} \sqrt{g_{99}} \sqrt{-\det[\varphi(g+f)_{\dot{k}\dot{i}} - g_{99}^{-1} \varphi(g+f)_{\dot{k}9} \varphi(g+f)_{9\dot{i}}]} \quad (13.224) \\ &= -\tilde{T}_{D(p-1)} \int_{\Sigma_p} d^p\zeta e^{-\tilde{\phi}} \sqrt{-\det[\tilde{\varphi}(\tilde{g} + \tilde{f})_{\dot{k}\dot{i}}]}. \end{aligned}$$

To achieve this, we first expressed the determinant of the block matrix singling out the  $S^1$ -direction and observed that, once the T-dualized fields are defined, the leftover terms coming from the off-diagonal blocks allow the writing of the pullback  $\varphi$  in terms of the pullback  $\tilde{\varphi}$ . Finally, we integrated over the circle, whose volume reads  $\text{vol } \tilde{S}^1 = \int_0^1 dx^9 \sqrt{g_{99}} = \tilde{R}$  and recognised the D $(p-1)$ -brane tension  $T_{Dp} \tilde{R} / \sqrt{g_{99}} = l_s T_{Dp} = \tilde{T}_{D(p-1)}$ . The outcome of these manipulations is the DBI-term in the resulting D $(p-1)$ -brane action, also in the static gauge, as expected. This approach provides an alternative derivation of the Buscher rules (13.194).

We can proceed analogously for the WZ-term. This calculation is greatly simplified by the fact that the

WZ-term depends on the combination  $K = C e^{-B}$ . We have

$$\begin{aligned}
S_{Dp}^{\text{WZ}} &= T_{Dp} \sum_{n=0}^{\infty} \frac{(-1)^n}{n!} \int_{\Sigma_{p+1}} (\varphi K)^{(p+1-2n)} \mathbf{F}^n \\
&= T_{Dp} \sum_{n=0}^{\infty} \frac{(-1)^n (p+1)}{2^n n! (p+1-2n)!} \int_0^1 dx^9 \int_{\Sigma_p} d^p \zeta \tilde{\epsilon}^{i_1 \dots i_p} \left[ (\varphi K)_{9i_1 \dots i_{p-2n}}^{(p+1-2n)} \mathbf{F}_{i_{p-2n+1} i_{p-2n+2} \dots i_{p-1} i_p} \right] \\
&= l_s T_{Dp} \sum_{n=0}^{\infty} \frac{(-1)^n}{2^n n! (p-2n)!} \int_{\Sigma_p} d^p \zeta \tilde{\epsilon}^{i_1 \dots i_p} \left[ (\tilde{\varphi} \tilde{K})_{i_1 \dots i_{p-2n}}^{(p-2n)} \mathbf{F}_{i_{p-2n+1} i_{p-2n+2} \dots i_{p-1} i_p} \right] \\
&= \tilde{T}_{D(p-1)} \int_{\Sigma_p} (\tilde{\varphi} \tilde{K}) e^{-\tilde{F}}.
\end{aligned} \tag{13.225}$$

We have expanded out the integrand and we have expressed the T-duality rules as  $\tilde{K}_{9\tilde{m}_2 \dots \tilde{m}_n}^{(n)} = K_{\tilde{m}_2 \dots \tilde{m}_n}^{(n-1)}$  and  $\tilde{K}_{\tilde{m}_1 \dots \tilde{m}_n}^{(n)} = K_{9\tilde{m}_1 \dots \tilde{m}_n}^{(n+1)}$ . This allows one to map the WZ-term of  $Dp$ -branes into  $D(p-1)$ -branes directly. These T-duality rules are in fact equivalent to the Ramond-Ramond gauge potential relations (13.195), as shown by [134], which means that the calculation above can also be seen as an alternative derivation of them.

In detail, we have used the general identity  $X_{[mm_1 \dots m_{n-1}]} = \frac{1}{n} \sum_{j=0}^{n-1} X_{[m_1 \dots m_j | m | m_{j+1} \dots m_{n-1}]}$  to write the integrand for a given  $n$  as

$$\begin{aligned}
(\varphi K)_{9i_1 \dots i_{p-2n}}^{(p+1-2n)} \mathbf{F}_{i_{p-2n+1} i_{p-2n+2} \dots i_{p-1} i_p} &= \frac{1}{p+1} \left[ (p+1-2n) (\varphi K)_{9[i_1 \dots i_{p-2n}]}^{(p+1-2n)} \mathbf{F}_{i_{p-2n+1} i_{p-2n+2} \dots i_{p-1} i_p} \right. \\
&\quad \left. + (-1)^{p-2n} (\varphi K)_{[i_1 \dots i_{p-2n+1}]}^{(p+1-2n)} \mathbf{F}_{i_{p-2n+2} | 9 | \dots i_{p-1} i_p} \right].
\end{aligned} \tag{13.226}$$

Now, given the T-duality rules for  $K^{(n)}$ , it is clear that the  $n = m$  and  $n = m+1$  terms of the sum over  $n$  for this integrand will both contribute to the  $n = m$  term in the sum for our target integrand. Specifically the first term on the right-hand side contributes for  $n = m$  and the second term on the right-hand side contributes for  $n = m+1$ . Concentrating on only these contributing terms for simplicity, we can write

$$\begin{aligned}
&\frac{(-1)^m (p+1)}{2^m m! (p+1-2m)!} \frac{p+1-2m}{p+1} (\varphi K)_{9[i_1 \dots i_{p-2m}]}^{(p+1-2m)} \mathbf{F}_{i_{p-2m+1} i_{p-2m+2} \dots i_{p-1} i_p} \\
&+ \frac{(-1)^{m+1} (p+1)}{2^{m+1} (m+1)! (p-1-2m)!} \frac{(-1)^{p-2m} (m+1)}{p+1} (\varphi K)_{[i_1 \dots i_{p-2m-1}]}^{(p-1-2m)} \mathbf{F}_{i_{p-2m} | 9 | \dots i_{p-1} i_p} = \\
&= \frac{(-1)^m}{2^m m! (p-2m)!} \left[ \frac{\partial x^{m_1}}{\partial \zeta^{[i_1}} \dots \frac{\partial x^{m_{p-2m}}}{\partial \zeta^{i_{p-2m}]} \right] K_{9m_1 \dots m_{p-2m}}^{(p+1-2m)} \mathbf{F}_{i_{p-2m+1} i_{p-2m+2} \dots i_{p-1} i_p} \\
&+ \frac{(-1)^{m+1} (-1)^p (p-2m)}{2^m m! (p-2m)!} \left[ \frac{\partial x^{m_1}}{\partial \zeta^{[i_1}} \dots \frac{\partial x^{m_{p-2m-1}}}{\partial \zeta^{i_{p-2m-1}]} \right] K_{\tilde{m}_1 \dots \tilde{m}_{p-2m-1}}^{(p-1-2m)} \mathbf{F}_{i_{p-2m} | 9 | \dots i_{p-1} i_p} \\
&= \frac{(-1)^m}{2^m m! (p-2m)!} \left[ \frac{\partial x^{\tilde{m}_1}}{\partial \zeta^{[i_1}} \dots \frac{\partial x^{\tilde{m}_{p-2m}}}{\partial \zeta^{i_{p-2m}]} \right] \tilde{K}_{\tilde{m}_1 \dots \tilde{m}_{p-2m}}^{(p-2m)} \mathbf{F}_{i_{p-2m+1} i_{p-2m+2} \dots i_{p-1} i_p} \\
&+ \frac{(-1)^m (p-2m)}{2^m m! (p-2m)!} \left[ \frac{\partial x^{\tilde{m}_1}}{\partial \zeta^{[i_1}} \dots \frac{\partial x^{\tilde{m}_{p-2m-1}}}{\partial \zeta^{i_{p-2m-1}}} \frac{\partial x^9}{\partial \zeta^{i_{p-2m}}} \right] \tilde{K}_{\tilde{m}_1 \dots \tilde{m}_{p-2m-1} | 9}^{(p-2m)} \mathbf{F}_{i_{p-2m+1} i_{p-2m+2} \dots i_{p-1} i_p} \\
&= \frac{(-1)^m}{2^m m! (p-2m)!} (\tilde{\varphi} \tilde{K})_{[i_1 \dots i_{p-2m}}^{(p-2m)} \mathbf{F}_{i_{p-2m+1} i_{p-2m+2} \dots i_{p-1} i_p},
\end{aligned} \tag{13.227}$$

which when considered over all  $m$  delivers the required result. We first wrote the pullbacks explicitly and rearranged factors in a useful way. Then, we performed several tasks at once. We T-dualized the form  $K$  while paying close attention to index ordering to give the correct factors of  $-1$ , we used the T-duality condition  $F_{k9} = \partial_k \varphi^9$ , and we used (anti)symmetry to see that the  $m_j$  indices in the pullbacks of the second line cannot equal 9, and so receive dots. Finally, to move to the final line, we recognised that this resulted in precisely the structure for the appropriate pullback of  $\tilde{K}$ .

This completes our review of the behaviour of the bosonic brane actions under T-duality. One should notice a fundamental fact: T-duality maps the DBI- and WZ-actions of a  $Dp$ -brane into the DBI- and WZ-actions of a  $D(p-1)$ -brane, respectively, and there is no mixing among the two in the transformation. A similar calculation to the ones above may be engineered to move from a  $Dp$ -brane to a  $D(p+1)$ -brane.

### 13.2 A useful rearrangement

We just showed how to obtain all the bosonic  $Dp$ -brane actions by T-dualizing the bosonic D2-brane one. Moreover, in the superspace formulation, the structure of the D2-brane action is formally the same both at zeroth order and in superspace at any fermionic order. Therefore, the structure of fermion couplings on all  $Dp$ -branes just follows from the D2-brane one. Because our goal is to compute these fermionic couplings for all  $Dp$ -branes, here we present a useful rearrangement that simplifies the computation of such couplings. In fact, because the fermion couplings are inherited from the superfield expansions appearing on the brane, the rearrangement is a neat manipulation of the superfields appearing on the D2-brane action that will simplify the computation of those appearing in the rest of  $Dp$ -branes.

In chapter 12, we defined the promoted Ramond-Ramond three-form field in type IIA with a prime symbol. That is the standard three-form superfield obtained from dimensional reduction of 11-dimensional supergravity. Rather than working with that superfield, it will be convenient to work with a related one. We define a new *unprimed* three-form superfield as

$$C_{mnp} = C'_{mnp} - 3C_{[m}(B_{np]} - B_{np}). \quad (13.228)$$

From here on we will work using this unprimed three-form rather than the standard one. This new superfield is such that the last term in the superfield  $C'_{mnp}$  in (13.207) is removed, and at order  $(\theta)^2$  it reads

$$C_{mnp} = C_{mnp} - \frac{i}{2} e^{-\phi} \bar{\theta}^A \left( 3\Gamma_{[mn} \mathbb{D}_p^A - \frac{1}{2} \sigma^1 \Gamma_{mnp} \Delta^A \right) \theta^A. \quad (13.229)$$

The reason why we defined this rearrangement is easily explained: the super-D2-brane action now reads

$$S_{D2} = -T_{D2} \int d^3\zeta e^{-\phi} \sqrt{-\det(\mathbf{g} + \mathbf{f})} + \frac{T_{D2}}{6} \int d^3\zeta \varepsilon^{ijk} (C_{ijk} - 3C_i f_{jk}). \quad (13.230)$$

In other words, we have engineered a superspace action where the Neveu-Schwarz fields appear as superfields in the DBI-term but only as bosonic fields in the WZ-term. Ramond-Ramond fields instead appear as superfields in the WZ-term. From the discussion in section 13.1.3 we conclude that this combination of fields and superfields will hold for any  $Dp$ -brane if we obtain the brane superspace actions by T-dualizing this one.

### 13.3 Superspace T-duality and fermions on $Dp$ -branes

We will once again be following the reasoning of the example already laid out with dimensional reduction in chapter 12. We interpret the bosonic T-duality relations (13.194) and (13.195) as the zeroth-order terms in the fermionic expansions of superspace T-duality relationships and extend them to superspace relations. T-duality in the context of full superfields was also discussed in [162].

Now, since T-duality maps the DBI-action of  $Dp$ -branes into the DBI-action of  $D(p \pm 1)$ -branes, and since this mapping allows one to derive the Buscher rules (13.194), one can simply conclude that the Buscher rules for the Neveu-Schwarz fields in superspace read

$$\tilde{\phi} = \phi - \frac{1}{2} \ln g_{99}, \quad (13.231a)$$

$$\tilde{g}_{\dot{m}\dot{n}} = g_{\dot{m}\dot{n}} - g_{99}^{-1} (g_{\dot{m}9} g_{\dot{n}9} - B_{\dot{m}9} B_{\dot{n}9}), \quad (13.231b)$$

$$\tilde{g}_{\dot{m}9} = g_{99}^{-1} B_{\dot{m}9}, \quad (13.231c)$$

$$\tilde{g}_{99} = g_{99}^{-1}, \quad (13.231d)$$

$$\tilde{B}_{\dot{m}\dot{n}} = g_{\dot{m}\dot{n}} - g_{99}^{-1} (B_{\dot{m}9} g_{\dot{n}9} - g_{\dot{m}9} B_{\dot{n}9}), \quad (13.231e)$$

$$\tilde{B}_{\dot{m}9} = g_{99}^{-1} g_{\dot{m}9}. \quad (13.231f)$$

Some of these rules partially appeared in [150], where they found the T-duality relation between Green-Schwarz superstrings in type IIA and type IIB with fermionic expansions up to quadratic terms.

Similarly, T-duality maps the WZ-action of  $Dp$ -branes into the WZ-action of  $D(p \pm 1)$ -branes and this mapping allows one to derive the T-duality rules for Ramond-Ramond fields (13.232). Because in the WZ-action of (13.230) the Neveu-Schwarz field appear only bosonically and the Ramond-Ramond fields appear as superfields, we conclude that the Ramond-Ramond T-duality rules we will use are

$$\tilde{C}_{9\dot{m}_2 \dots \dot{m}_n}^{(n)} = C_{\dot{m}_2 \dots \dot{m}_n}^{(n-1)} - (n-1) g_{99}^{-1} g_{9[\dot{m}_2} C_{9|\dot{m}_3 \dots \dot{m}_n]}^{(n-1)}, \quad (13.232a)$$

$$\tilde{C}_{\dot{m}_1 \dots \dot{m}_n}^{(n)} = C_{9\dot{m}_1 \dots \dot{m}_n}^{(n+1)} - n B_{9[\dot{m}_1} C_{\dot{m}_2 \dots \dot{m}_n]}^{(n-1)} + n(n-1) g_{99}^{-1} g_{9[\dot{m}_1} B_{9|\dot{m}_2} C_{\dot{m}_3 \dots \dot{m}_n]}^{(n-1)}. \quad (13.232b)$$

This mechanism was used in [126] for the quadratic fermionic action and we have extended that observation to any fermionic order. Note that without our manipulation on the super-three-form, one would have obtained similar results involving Neveu-Schwarz superfields rather than fields. Those are the actual superspace T-duality rules for Ramond-Ramond superfields, but for our purposes it will be more convenient to use (13.232).

#### 13.3.1 Order- $(\theta)^2$ terms

In the following, we will use the promoted T-duality relations (13.231) and (13.232) to calculate the second-order fermionic expansions of all the superfields that appear in type IIA and type IIB under repeated T-dualizations. Just as in section 12.4, we will provide illuminating examples of the necessary calculations before listing the full results.



### Example: type IIB metric

We will now use the simplest superspace T-duality relationships in order to provide an example of how to obtain the fermionic expansions of type IIB operators from type IIA description by using the conventional T-duality rules applied to quadratic fermionic quantities. We will focus on the supermetric.

Consider the superspace T-duality rule (13.231d), i.e.  $\tilde{g}_{99} = g_{99}^{-1}$ . Starting from the type IIA supermetric  $g_{mn}$ , in order to determine an expression for the quadratic fermionic expansion of the type IIB supermetric  $\tilde{g}_{mn}$ , we Taylor-expand both sides, concentrating on the components of interest. On the type IIB left-hand side, we set the ansatz  $\tilde{g}_{99} = \tilde{g}_{99} + \tilde{\gamma}_{99}$ , whereas on the type IIA right-hand side we use the result of the dimensional reduction (13.203). Using the spinor doublet notation and keeping only the second-order fermion terms from both sides (as the zeroth-order terms just reproduce the bosonic identities), one determines an expression for the type IIB shift  $\tilde{\gamma}_{99}$  in terms of type IIA quantities, i.e.

$$\tilde{\gamma}_{99} = i g_{99}^{-2} \bar{\theta}^A \sigma^1 \Gamma_9 D_9^A \theta^A. \quad (13.233)$$

We are now required to perform conventional T-duality on the term on the right-hand side in order to determine an expression for the expansion ansatz of the type IIB metric in terms of type IIB quantities. We can use the basic T-duality rules in spinor doublet notation in section 13.1.2 to write

$$\begin{aligned} \tilde{\gamma}_{99} &= i \tilde{g}_{99}^2 (\bar{\theta}^B \sigma^1 \Upsilon \sigma^1) \sigma^1 [(\tilde{Q}_-^{-1})_9{}^p \Upsilon^{-1} \tilde{\Gamma}_p \Upsilon] [(\tilde{Q}_+^{-1})_9{}^q \Upsilon^{-1} D_q^B \Upsilon] \Upsilon^{-1} \theta^B \\ &= i \tilde{g}_{99}^2 \bar{\theta}^B \sigma^1 (\tilde{Q}_-^{-1})_9{}^p (\tilde{Q}_+^{-1})_9{}^q \tilde{\Gamma}_p D_q^B \theta^B \\ &= i \tilde{g}_{99}^2 \bar{\theta}^B \sigma^1 (-\tilde{g}_{99}^{-1} \sigma^3) (\tilde{g}_{99}^{-1} \sigma^3) \tilde{\Gamma}_9 D_9^B \theta^B \\ &= -i \bar{\theta}^B \sigma^1 \tilde{\Gamma}_9 D_9^B \theta^B. \end{aligned} \quad (13.234)$$

The result is exactly as expected. The quadratic terms in the expansions of the type IIB metric take precisely the same form as the type IIA metric, just with all of the operators and spinors being the type IIB ones and not the type IIA versions. One can proceed analogously to get the generic second-order shift of the type IIB dilaton and Kalb-Ramond superfields.

### Example: Ramond-Ramond two-form

The superspace promotion of the dimensional reduction from 11-dimensional supergravity to type IIA supergravity allowed us to determine the fermionic expansions for the Ramond-Ramond superfields of degrees one and three. Now that we are considering T-duality between type IIA and type IIB, we must confront the requirement that we calculate the fermionic expansions of Ramond-Ramond superfields of any degree.

Our strategy will be to take the promoted Ramond-Ramond T-duality rule (13.232a), expand in orders of fermions and keep only the quadratic contribution. Writing  $C^{(q)} = C^{(q)} + \chi^{(q)}$ , where  $\chi^{(q)}$  is the corresponding fermion bilinear, we are interested in obtaining  $\chi^{(2)}$ . Following our standard procedure, from

(13.232a) we find

$$\begin{aligned}\tilde{\chi}_{9\dot{m}}^{(2)} &= \chi_{9\dot{m}}^{(1)} - g_{99}^{-1} g_{9\dot{m}} \chi_9^{(1)} \\ &= -\frac{i}{2} e^{-\phi} \bar{\theta}^A \sigma^3 \left[ (\mathbb{D}_{\dot{m}}^A - g_{99}^{-1} g_{9\dot{m}} \mathbb{D}_9^A) - \frac{1}{2} (\mathbb{F}_{\dot{m}} - g_{99}^{-1} g_{9\dot{m}} \mathbb{F}_9) \sigma^1 \Delta^A \right] \theta^A\end{aligned}\quad (13.235)$$

where for the one-form shift we have made use of (13.206). We now need to manipulate the right-hand side in order to obtain an expression for the type IIB Ramond-Ramond two-form superfield in terms of type IIB operators. We will use identities similar to (13.218)

$$\Upsilon (\mathbb{D}_{\dot{m}}^A - g_{99}^{-1} g_{9\dot{m}} \mathbb{D}_9^A) \Upsilon^{-1} = \mathbb{D}_{\dot{m}}^B - \tilde{g}_{99}^{-1} \tilde{g}_{9\dot{m}} \mathbb{D}_9^B, \quad (13.236)$$

$$\Upsilon (\mathbb{F}_{\dot{m}} - g_{99}^{-1} g_{9\dot{m}} \mathbb{F}_9) \Upsilon^{-1} = \tilde{\mathbb{F}}_{\dot{m}} - \tilde{g}_{99}^{-1} \tilde{g}_{9\dot{m}} \tilde{\mathbb{F}}_9. \quad (13.237)$$

and  $\sqrt{\tilde{g}_{99}} \sigma^1 \Upsilon \sigma^1 \sigma^3 \Upsilon^{-1} = \Gamma^* \tilde{\mathbb{F}}_9$ . Splitting the first and the second term in (13.235), using (13.236) and (13.237), we find

$$e^{-\phi} \bar{\theta}^A \sigma^3 (\mathbb{D}_{\dot{m}}^A - g_{99}^{-1} g_{9\dot{m}} \mathbb{D}_9^A) \theta^A = e^{-\tilde{\phi}} \bar{\theta}^B \Gamma^* (\tilde{\mathbb{F}}_9 \mathbb{D}_{\dot{m}}^B - \tilde{g}_{99}^{-1} \tilde{g}_{9\dot{m}} \tilde{\mathbb{F}}_9 \mathbb{D}_9^B) \theta^B, \quad (13.238)$$

$$e^{-\phi} \bar{\theta}^A \sigma^3 \sigma^1 (\mathbb{F}_{\dot{m}} - g_{99}^{-1} g_{9\dot{m}} \mathbb{F}_9) \Delta^A \theta^A = e^{-\tilde{\phi}} \bar{\theta}^B \Gamma^* \left[ \sigma^1 \tilde{\mathbb{F}}_{9\dot{m}} \Delta^B + 2 \tilde{g}_{99}^{-1} (\tilde{\mathbb{F}}_9 \tilde{g}_{9\dot{m}} - \tilde{\mathbb{F}}_{\dot{m}} \tilde{g}_{99}) \mathbb{D}_9^B \right] \theta^B. \quad (13.239)$$

Therefore, putting together the expressions we have

$$\tilde{\chi}_{9\dot{m}}^{(2)} = \frac{i}{2} e^{-\tilde{\phi}} \bar{\theta}^B \left[ 2 \tilde{\mathbb{F}}_{[9} \mathbb{D}_{\dot{m}}^B - \frac{1}{2} \sigma^1 \tilde{\mathbb{F}}_{9\dot{m}} \Delta^B \right] \theta^B. \quad (13.240)$$

One can proceed analogously to obtain all the type IIA and type IIB bilinears in Ramond-Ramond superfields, going up in the degree of the T-dualized form one at a time. Alternatively, a generalised discussion of the Ramond-Ramond superfields in appendix 15.5 demonstrates that all of these expansions can be calculated together.

## Full results

To conclude, we list all the relevant superfields up to quadratic order both in the Neveu-Schwarz and Ramond-Ramond sectors.

The expansions for the Neveu-Schwarz superfields at order  $(\theta)^2$  look same in both theories in our spinor doublet notation. They are

$$\mathbf{g}_{mn} = g_{mn} - i \bar{\theta}^{\text{II}} \sigma^1 \mathbb{F}_{(m} \mathbb{D}_{n)}^{\text{II}} \theta^{\text{II}}, \quad (13.241)$$

$$\phi = \phi - \frac{i}{4} \bar{\theta}^{\text{II}} \Delta^{\text{II}} \theta^{\text{II}}, \quad (13.242)$$

$$\mathbf{B}_{mn} = B_{mn} - i \bar{\theta}^{\text{II}} (i\sigma^2) \mathbb{F}_{[m} \mathbb{D}_{n]}^{\text{II}} \theta^{\text{II}}, \quad (13.243)$$

where the superscript <sup>II</sup> indicates that one must introduce the appropriate object in each theory. The order-

$(\theta)^2$  terms in the Ramond-Ramond superfields in type IIA and type IIB theories can also be written compactly

$$C_{m_1 \dots m_n}^{(n)} = C_{m_1 \dots m_n}^{(n)} - \frac{i}{2} e^{-\phi} \bar{\theta}^{\text{II}} \left[ (-1)^n (\sigma^3)^{1 + \lfloor \frac{n}{2} \rfloor} \right] \left[ n \mathbb{F}_{[m_1 \dots m_n]}^{\text{II}} - \frac{1}{2} \mathbb{F}_{m_1 \dots m_n} \sigma^1 \Delta^{\text{II}} \right] \theta^{\text{II}}, \quad (13.244)$$

where the parity of  $n$  determines whether the spinor doublet and the supersymmetry operators are the type IIA or type IIB ones.

## Dp-branes

Now that we have determined the fermionic expansion of the all the fundamental superfields in type IIA and type IIB theories, we can turn our attention to the composite superfields of greatest interest, namely the worldvolume actions of a Dp-brane for arbitrary  $p$ .

Since the formal structure of purely bosonic Dp-brane is equivalent to the structure of the action in superspace, the T-duality mechanism is also the same as the one leading to the bosonic action (13.223). The only precaution one needs to take regards the fact that the starting point, i.e. the superspace D2-brane action (13.230), and consequently the T-duality rules, are such that the Neveu-Schwarz T-duality rules see all fields in superspace whereas the Ramond-Ramond ones only contain the Ramond-Ramond fields in superspace, as exemplified in (13.231) and (13.232). At the end of the day, the action of any Dp-brane in superspace takes the form

$$S_{\text{D}p} = -T_{\text{D}p} \int d^{p+1} \zeta e^{-\phi} \sqrt{-\det(\mathbf{g} + \mathbf{f})} + T_{\text{D}p} \int \mathbf{C} e^{-f}, \quad (13.245)$$

where  $\mathbf{g}_{ij}$  is the supermetric pullback,  $\mathbf{f}_{ij} = \mathbf{B}_{ij} + \mathbf{F}_{ij}$  is the natural superspace combination of the Kalb-Ramond field with the worldvolume flux term, with  $f_{ij} = B_{ij} + F_{ij}$  being its bosonic component, and where we have defined the formal sum  $\mathbf{C} = \sum_q \mathbf{C}^{(q)}$  over promoted Ramond-Ramond  $q$ -form pulled-back superfields  $\mathbf{C}^{(q)}$ . Once again, this result holds at all orders in fermions. In order to determine the expansion of the Dp-brane action superfield to an arbitrary order in fermions, one needs to plug the expansions of the fundamental superfields from the corresponding type II supergravity into (13.245). The second-order expansions in spinor doublet notation are in (13.241) - (13.244) for both type II theories.

### 13.3.2 Order- $(\theta)^4$ terms

We have already made some comments in section 12.5 regarding the unwieldy size of the expressions obtained for the quartic fermionic couplings after dimensional reduction. There we also discussed how these expressions might be improved and simplified going forward, in order that they become more manageable. In their current formulation the calculation necessary for their full T-dualization is impractically lengthy. Important to note, however, is that there is no technical impediment. Just like the quadratic fermionic couplings, the quartic couplings may in principle be T-dualized using the techniques and results we have reviewed and developed in this chapter. Actively pursuing this full calculation is better delayed until such a time that the possible simplifying procedures for the quartic terms have been implemented.

Nevertheless there are some observations that can be made concretely at quadratic fermion level that we can fully expect to also happen at quartic level. Firstly, the NS superfield expansions take on the same shape in both type II supergravities. The same holds for the expansion of the 11-dimensional supermetric, that at

order two has the same structure as the 10-dimensional supermetrics. This is not a coincidence: the supervielbein expansion looks schematically the same in all these theories (even though in each theory there is a different notion of what the gravitino or the supercovariant derivative are) and the outcome of manipulations at quadratic order makes this point manifest. Moreover, the existing relations go beyond that. The type IIA metric and  $B_2$  superfield expansions came from different 11 dimensional superfields but at quadratic order turned out to be very similar. If it were not for this, it would have been impossible to find again this structure in type IIB upon T-duality. This extends to the whole NSNS sector, that allowed us to write those superfields up to quadratic order at once both for type IIA and type IIB (13.241 - 13.243). In principle there is no argument against the structure extending to all levels in  $\theta$ , but unfortunately, the current form of quartic terms did not quite allow us to make this point manifest. For example, the 10 dimensional metric expansion and the 11-dimensional one do not seem to allow for such comparisons in their order  $(\theta)^4$  terms. On the other hand, there are indeed many similarities between the metric and the  $B_2$ -field order  $(\theta)^4$  terms (modulo (anti)symmetry of indices and chirality matrices), which is a positive observation, but there are also differences on certain terms (that maybe could be manipulated to make them similar to each other). These ideas could also be used e.g. to obtain quartic terms of NSNS fields in type IIB by ‘simply’ writing type IIA formulae (12.187), (12.189), and (12.190) in spinor doublet notation. It would be nice to compare that with the outcome of performing the computation using the Hassan rules.

Finally, something that might be possible given the current formulation of the quartic order fermionic couplings for the D2-brane is to identify those parts of the expressions which would lead to particularly sought-after terms in  $Dp$ -brane actions. For example, the work in [115] posits a particular quartic term in the action of the D7-brane. It could be possible to hunt for this term via T-dualization without laboriously T-dualizing everything appearing after dimensional reduction, however we leave this possibility for future study.



# Conclusions

In Part II of this thesis we have developed an understanding of the mathematical structures involved when examining the fermionic degrees of freedom which live on the M2-brane and  $Dp$ -branes. We have drawn our primary motivation from the fact that the current level of knowledge about the fermions living on branes requires significant improvement. One of the core reasons that fermions on branes are under-studied is that obtaining their couplings explicitly turns out to be surprisingly difficult. Higher-order couplings of fermions in brane actions have been invoked recently [108–114], however the impracticality of the existing methods used to obtain these terms limited their use. Even more recently, a proposal for obtaining specific quartic couplings on D7-branes that can be pertinent for understanding KKLT has also been put forward [115]. Over the course of two years of initial study and late research we have made significant progress in improving both the conceptual understanding and the practical techniques needed to pursue these terms. Furthermore, the insights we have had and connections we have made are applicable far beyond the calculation of specific couplings in brane worldvolume theories. In fact we have presented the calculation of these terms as a single, if pertinent, example of a place where our more general methods come into use.

## 14.1 Summary

The structure at the heart of this Part is the web of string dualities given in Fig. 8.62. The approaches that we have developed, and used to obtain brane actions, rest upon the superspace generalizations of the connections in this web. Such connections allowed us to take advantage of the elegance of techniques more easily applicable to a theory in one part of the web in order to achieve progress in others. More concretely, the connections we have concentrated on are the circle compactification linking 11-dimensional to type IIA supergravity and the T-duality relating type IIA and type IIB theories to each other. Fig. 14.63 presents a map of the concepts used.

The reasons for which this particular generalization has proved to be so useful are twofold. First, our starting point of 11-dimensional supergravity has a particularly elegant formulation in  $(11|32)$ -superspace. Second, we have access to a systematic, complete, and *manageable* geometrical method for determining explicit fermionic expansions of this theory's superfields, namely NORCOR. The small number of superfields in

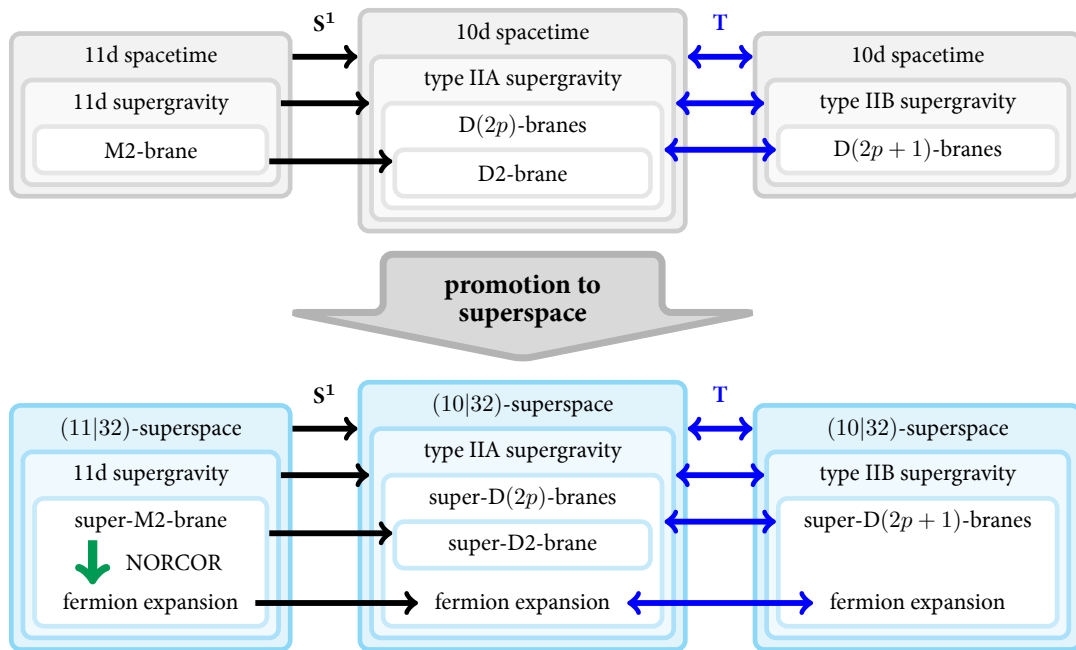


Figure 14.63: A schematic map of the procedures investigated. We work in superspace, and in order to do so profitably we generalize the string duality web to superspace. We generalize the  $S^1$  compactification from 11-dimensional supergravity to type IIA, and we generalize the T-duality procedure connecting type IIA and type IIB to superspace. This allows us to carry the elegant geometric treatment of the ‘normal coordinate’ (NORCOR) method in 11-dimensional supergravity over to type II supergravity, circumventing the difficulty in applying that treatment directly in those theories. This method allows us to calculate the expansion of actions of branes in orders of the worldvolume fermions. We have presented example calculations up to quartic order in fermions for the M2-brane and the D2-brane in this work, although the methods we have presented are in principle applicable to any order in fermions.

11-dimensional supergravity in conjunction with NORCOR means we can readily obtain the fermionic expansions of all the fundamental superfields in the theory. Obtaining the fermionic expansions for composite superfields built out of these fundamental superfields is then a conceptually simple matter. The example composite superfield we have chosen to concentrate on in this case is the action for a single M2-brane. This action is constructed using the pullbacks of the supervielbein and super three-form in 11-dimensional supergravity.

With our starting point of 11-dimensional supergravity and the M2-brane firmly in hand, we then pursued the superspace generalization of the  $S^1$ -compactification to type IIA supergravity and the D2-brane. Our goal was to use the expansion of the 11-dimensional superfields together with this connection in the web to determine the expansion of the type IIA superfields. The regular dimensional reduction ansatz relates the 11-dimensional vielbein and three-form to the 10-dimensional vielbein, dilaton, Ramond-Ramond one-form, Kalb-Ramond two-form and Ramond-Ramond three-form. We took the view that these bosonic relations represented the ‘zeroth-order’ fermionic expansion of the corresponding superfield relations. As such, we promoted the dimensional reduction ansatz relations to superfields, taking the fermionic expansions of the 10-dimensional superfields (to some desired order) as unknowns to be determined. We then used the NORCOR results of the Taylor expansion of the 11-dimensional fields to determine explicit expressions for these 10-dimensional unknowns in terms of 11-dimensional fields. Finally we dimensionally reduced the 11-dimensional fermionic terms and compared the results with the expansion in terms 10-dimensional unknown fermionic terms in order to read off the desired results. We demonstrated how known second-order results for fundamental superfield expansions in type IIA can be recovered painlessly using this method. Furthermore we demonstrated how labourious manipulations of the D2-brane action can be completed almost trivially in this superfield paradigm, and how the form for the quadratic fermion terms on the D2-brane can be recovered, again relatively painlessly. Finally we calculated the fermionic expansion of the type IIA fields relevant for the D2-brane all the way up to order four in fermions. Unfortunately these terms, while systematic and complete, are unwieldy in their present formulation. We discussed some promising lines of research regarding their simplification, something we will come back to in a moment.

Finally we turned our attention to the second strand on the web of dualities that we sought to generalize to superspace. This was the T-duality relation between type IIA and type IIB theories. The structure of work mirrored that of the generalization of the dimensional reduction just discussed. We first observed the relations the T-duality demanded of the bosonic fields in either theory. These were the Buscher rules and the Ramond-Ramond field rules. We once again interpreted these relations as representing the ‘zeroth-order’ fermionic expansion of the corresponding superfield relations, and as such promoted these T-duality rules to superfields. This required observing that the discussion of the Ramond-Ramond sector can be substantially simplified by conveniently arranging the D2-brane action. Then it was the repeated application of these promoted rules which we used to determine the fermion terms in the superfield expansions for all the superfields in both type II supergravities. When we performed the T-duality transformations, we had to become familiar with precisely how fermions behaved. This transpired to be an area of much subtle complexity, but one which we greatly streamlined by moving to spinor doublet notation. Once again, we chose as a crucial example case the calculation of the fermionic expansion of brane actions. In this case repeated T-duality transformations allowed us to leverage the knowledge we had built about the D2-brane in the previous stage to determine features of the  $D_p$ -brane actions in general. We once again wrote down a form of the action which will yield

the fermion couplings on the  $Dp$ -brane to any order if provided with the expansions of the fundamental fields of the type II supergravity in which the brane lives. We noticed that in this formulation Ramond-Ramond fields of every degree are used implicitly, yet the first dimensional reduction step had furnished us with only degree 1 and 3. This is where the careful study of fermions under T-duality became invaluable as explicit T-dualization of these two superfield expansions allowed us to determine the expansions for all the fields we desired to quadratic order. The only remaining impediments to a full calculation at quartic order for all  $Dp$ -branes are then of a practical nature. The expressions we have obtained, since they represent all couplings of the brane fermions to an arbitrary bosonic background, have many terms, and the calculation for each term is non-trivial. There is no technical impediment to T-dualization and we provide all the necessary tools, however we consider it prudent to first make a proper investigation of how the expressions we have obtained for type IIA fields and D2-brane might be improved. We discuss this, and other future lines of work, next.

## 14.2 Future directions

The directions in which this work will progress in the future come in two main classes: those directions that improve and build upon the work and those that use it.

The most obvious direction in which the present work might be improved is in seeking to simplify the results at quartic order in fermions. We have already discussed at the end of section 12.5 how significant simplifications of the current formulation of the complete quartic order terms for the superfield expansions in type II supergravities will have their roots in a better treatment of the 11-dimensional supervielbein expansion. This might be achieved via something as simple as a more adroit rearrangement and application of the constraints imposed by Bianchi identities than we have managed here, or it could require an improvement at a higher level in the set-up of NORCOR. Pursuing such a better treatment is an obvious and tantalising direction of future study.

For the brane actions specifically, these results might be improved by getting a firmer grasp of how to arrange higher order fermionic expansions around a  $\kappa$ -symmetry organizational principle. As early in our process as our expression for the M2-brane action in (11.142), we neglected to explicitly organize all our terms around such a principle. When calculating the quartic terms in the M2 brane, one can interpret all of the different terms as arising from the variation of different parts of the quadratic fermionic term. Those quartic terms that came with the same, ‘zeroth-order’ projector as in the quadratic term are interpreted as arising from varying the supercovariant derivative that appeared in the quadratic term. The remaining quartic terms (coming with a factor  $\frac{1}{8}$ ) can be interpreted as arising from further variations of the projector, inverse metric, etc, appearing at quadratic order. The higher-order expansion of the kappa symmetry projector may be calculated directly by expanding the superfield projector (11.136). Better understanding of the structure here could then be carried over to type II theories using the duality promotion method we have presented. At second order the  $Dp$ -brane actions were able to be organized into a similar form as the M2-brane, that is, a bilinear containing a kappa projector and some operators. The expectation would be that whatever further structure is found in the M2-brane should provide analogous arrangements of the  $Dp$ -brane action through the promoted duality web.

With more agile control over  $Dp$ -brane actions, it becomes natural to revisit the D7-brane quartic gaugino



couplings and compare them with the existing literature, among other things. This would be instrumental in shedding further light on gaugino condensation in the stabilization of volume moduli à la KKLT. A proposal for the specific quartic gaugino terms on D7-branes necessary to achieve this was recently put forward in [115], and hunting for the specific terms which that proposal requires within our results is a promising line of inquiry. In a different area, a further result that is now in reach is the determination of the F1-string action at arbitrary fermionic order. In fact, once the M2-brane action is known at a given order, a circle compactification along a direction wrapped by the brane (a double dimensional reduction) gives the Green-Schwarz-string action [150] in a similar way to the compactification along an unwrapped direction, which gave the D2-brane action. Finally, we have worked in bosonic backgrounds. To do so we simply set to zero those terms proportional to the gravitino in the expansions of the superfields of 11-dimensional supergravity. By keeping these terms, however, the methods we employed can also be used to explore more general backgrounds than purely bosonic ones. In this way, one would obtain the M2-brane couplings to the 11-dimensional gravitino and hence, upon dimensional reduction and T-dualization, the  $Dp$ -brane couplings to the 10-dimensional gravitino and dilatino. Finally, we have concentrated in this work on obtaining the fermion couplings on brane actions in the abelian case of a single brane. Expanding this work to the non-abelian case of multiple branes, or to even more complicated brane set-ups, is yet another promising line of inquiry.



# Appendices

## 15.1 Spinor conventions

We summarize the conventions that we use in the main text regarding spinors defined in 11- and 10-dimensional spacetime. Here we denote terms intrinsically living in 11-dimensional spacetime with a hat in order to distinguish them from the ones defined in 10-dimensional spacetime (with no hats). This is also the case in appendix 15.4, which explains the details about dimensional reduction. In the main text we often drop hats for the sake of clarity, as the spacetime dimension is always clear from the context, only using hats for 11-dimensional objects at the point of performing dimensional reduction.

In the 11-dimensional spacetime, we use real Majorana anticommuting 32-component spinors denoted as  $\hat{\theta}^\mu$ , with  $\mu$  representing spinor indices in the curved superspace manifold and  $\alpha$  representing spinor indices on the corresponding tangent space. Spinor indices can generally be suppressed without loss of clarity. Explicitly, Dirac conjugation is defined in terms of the antisymmetric conjugation matrix  $C = C_{\alpha\beta}$ , with  $C_{\alpha\beta} = -C_{\beta\alpha}$ , as

$$\hat{\theta}_\beta = \hat{\theta}^\alpha C_{\alpha\beta}. \quad (15.246)$$

More generally spinor indices are raised and lowered by the conjugation matrix and its inverse  $C^{-1} = C^{\alpha\beta}$ , with  $C_{\alpha\beta}C^{\beta\gamma} = \delta_\alpha^\gamma$ , according to the rule

$$M_\alpha{}^\beta = C_{\alpha\gamma}M^\gamma{}_\delta C^{\delta\beta}. \quad (15.247)$$

In the index-free notation, one can write  $\hat{\theta} = \hat{\theta}^T C$  and  $\hat{\theta} M \hat{\theta} = \hat{\theta}_\alpha M^\alpha{}_\beta \hat{\xi}^\beta = \hat{\theta}^\alpha M_{\alpha\beta} \hat{\xi}^\beta$ . We work with the mostly-plus Minkowski metric  $\hat{\eta}_{\hat{a}\hat{b}}$ , with signature  $(-1, (+1)^{10})$  and indices running as  $\hat{a} = \underline{0}, \dots, \underline{10}$ , and employ  $\Gamma$ -matrices  $\hat{\Gamma}^{\hat{a}}$  fulfilling the Clifford algebra

$$\{\hat{\Gamma}^{\hat{a}}, \hat{\Gamma}^{\hat{b}}\} = 2\hat{\eta}^{\hat{a}\hat{b}}. \quad (15.248)$$

The antisymmetrized  $\Gamma$ -matrix products are defined as

$$\hat{\Gamma}_{\hat{a}_1 \hat{a}_2 \dots \hat{a}_n} = \hat{\Gamma}_{[\hat{a}_1} \hat{\Gamma}_{\hat{a}_2} \dots \hat{\Gamma}_{\hat{a}_n]}. \quad (15.249)$$

The combinations  $(\hat{\Gamma}_{\hat{a}_1 \hat{a}_2 \dots \hat{a}_n})_{\alpha\beta}$  are symmetrical in their spinor indices for  $n = 1, 2 \pmod 4$  and antisymmetrical otherwise, i.e.

$$(\hat{\Gamma}_{\hat{a}_1 \hat{a}_2 \dots \hat{a}_n})_{\alpha\beta} = +(\hat{\Gamma}_{\hat{a}_1 \hat{a}_2 \dots \hat{a}_n})_{\beta\alpha}, \quad n = 1, 2 \pmod 4; \quad (15.250a)$$

$$(\hat{\Gamma}_{\hat{a}_1 \hat{a}_2 \dots \hat{a}_n})_{\alpha\beta} = -(\hat{\Gamma}_{\hat{a}_1 \hat{a}_2 \dots \hat{a}_n})_{\beta\alpha}, \quad n = 0, 3 \pmod 4. \quad (15.250b)$$

The Majorana nature of the anticommuting fermions  $\hat{\theta}$  means that  $\hat{\theta} \hat{\Gamma}_{\hat{a}_1 \hat{a}_2 \dots \hat{a}_n} \hat{\theta} = 0$  for  $n = 1, 2 \pmod 4$ . The master equation for practical  $\Gamma$ -matrix manipulation (in any number of dimensions) is

$$\hat{\Gamma}^{\hat{a}_1 \dots \hat{a}_m} \hat{\Gamma}_{\hat{b}_1 \dots \hat{b}_n} = \sum_{r=0}^{\min(m,n)} r! \binom{m}{r} \binom{n}{r} \delta_{[\hat{b}_1}^{[\hat{a}_m} \dots \delta_{\hat{b}_r}^{\hat{a}_{m+1-r}]} \hat{\Gamma}^{\hat{a}_1 \dots \hat{a}_{m-r}]_{\hat{b}_{r+1} \dots \hat{b}_n}}. \quad (15.251)$$

After the dimensional reduction to a 10-dimensional space spanned by indices  $a = \underline{0}, \dots, \underline{9}$ , where the direction  $x^{10}$  is compactified, it is necessary to introduce a chirality matrix. In tangent spacetime, the first ten  $\Gamma$ -matrices are the same because the Clifford algebra reads  $\{\hat{\Gamma}^a, \hat{\Gamma}^b\} = 2\hat{\eta}^{ab} = 2\eta^{ab} = \{\Gamma^a, \Gamma^b\}$ , so  $\hat{\Gamma}^a = \Gamma^a$ , where  $\eta_{ab} = \hat{\eta}_{ab}$  is the 10-dimensional Minkowski metric; the last 11-dimensional  $\Gamma$ -matrix defined to be the 10-dimensional chirality matrix  $\hat{\Gamma}^{10} \equiv \Gamma^*$ . All the other rules on spinor indices are unchanged. Because in ten dimensions there is a notion of chirality, we split 11-dimensional Majorana spinors into pairs of 10-dimensional Majorana-Weyl spinors as  $\theta = \theta_+ + \theta_-$ , where  $\Gamma^* \theta_{\pm} = \pm \theta_{\pm}$ . For type IIB strings, we relate the previous pair of Majorana-Weyl spinors to another pair of Majorana-Weyl spinors, but this time with equal chirality, i.e.  $\theta_{1,2}$  with  $\Gamma^* \theta_{1,2} = +\theta_{1,2}$ . In this case it is convenient to rearrange these fermion pairs into a Pauli matrix-valued spinor

$$\theta = \begin{pmatrix} \theta_1 \\ \theta_2 \end{pmatrix}, \quad (15.252)$$

which is acted on by the 2-dimensional identity  $1_2$  and the three Pauli matrices  $\sigma^1, \sigma^2$  and  $\sigma^3$ . All the  $\Gamma$ -matrices and the chirality matrix that need to act on the spinor  $\theta$  can be redefined by means of a tensor product with the 2-dimensional identity  $1_2$  in such a way as to act appropriately on the two spinor components  $\theta_{1,2}$ .

### Note on spinor indices

In dealing with spinor contractions, we often find it useful to rearrange expressions by moving spinor indices. Given a matrix  $M_{\alpha\beta}$  acting on the spinor space, we define its transpose as the matrix  $\check{M}_{\alpha\beta} = M_{\beta\alpha}$ . As an example, consider the torsion  $\hat{T}_{\hat{a}}$  and its transpose  $\hat{\check{T}}_{\hat{a}}$

$$\hat{T}_{\hat{a}} = \frac{1}{288} \left( \hat{\Gamma}_{\hat{a}}^{\hat{b}\hat{c}\hat{d}\hat{e}} + 8\delta_{\hat{a}}^{\hat{b}} \hat{\Gamma}^{\hat{c}\hat{d}\hat{e}} \right) \hat{H}_{\hat{b}\hat{c}\hat{d}\hat{e}},$$

$$\hat{\check{T}}_{\hat{a}} = \frac{1}{288} \left( \hat{\Gamma}_{\hat{a}}^{\hat{b}\hat{c}\hat{d}\hat{e}} - 8\delta_{\hat{a}}^{\hat{b}} \hat{\Gamma}^{\hat{c}\hat{d}\hat{e}} \right) \hat{H}_{\hat{b}\hat{c}\hat{d}\hat{e}}.$$

Notice that it is not the position of the spinor indices that is used to make the distinction between  $\hat{T}_{\hat{a}}$  and  $\hat{\hat{T}}_{\hat{a}}$ : both are defined as in the main text and the position of the indices can be changed with the charge conjugation matrix  $C_{\alpha\beta}$  and its inverse  $C^{\alpha\beta}$ . In fact, we can write for instance  $(\hat{T}_{\hat{m}})_{\alpha}{}^{\beta} = -(\hat{\hat{T}}_{\hat{m}})^{\beta}{}_{\alpha}$ .

## 15.2 11-dimensional supergravity

Here we summarize the set-up and conventions for 11-dimensional supergravity [139–141], including the field content, the constraints on the torsion which are equivalent to the equations of motions, and the Bianchi identities [163].

In 11-dimensional supergravity, let us consider the (11|32)-dimensional supermanifold spanned by coordinates  $Z^M = (x^m, \theta^{\mu})$ , where  $M$  is a generalized superspace index, with  $m = 0, \dots, 10$  representing the original spacetime directions and  $\mu = 1, \dots, 32$  representing the corresponding spinor directions. In this formalism, one defines the supervielbein as

$$E^A(x, \theta) = dZ^M E_M{}^A(x, \theta), \quad (15.253)$$

where the index  $A$  corresponds to the tangent space, with the possibility to introduce local coordinates  $y^A = (y^a, y^{\alpha})$ , with  $a = 0, \dots, 10$  and  $\alpha = 1, \dots, 32$ . Let us also introduce a superconnection, i.e. the super-one-form  $\omega_A{}^B$ , with Lorentzian structure group, in terms of which we define the superspace covariant derivative,

$$\nabla X^{A_1 \dots}_{B_1 \dots} = dX^{A_1 \dots}_{B_1 \dots} + X^{DA_2 \dots}_{B_1 \dots} E^C \omega_{CD}{}^{A_1} \dots + X^{A_1 \dots}_{DB_2 \dots} E^C \omega_{B_1 C}{}^D \dots \quad (15.254)$$

The superconnection is compatible with the structure of the tangent space Lorentz group, and it is related to the spin connection according to

$$\omega_a{}^{\beta} = \omega_{\beta}{}^a = 0 \quad , \quad \omega_{\alpha}{}^{\beta} = \frac{1}{4} \omega_{ab} (\Gamma^{ab})_{\alpha}{}^{\beta} \quad (15.255)$$

We can then define the supertorsion  $T^A$  and the supercurvature  $R_B{}^A$  as

$$T^A = \nabla E^A = dE^A + E^B \omega_B{}^A = \frac{1}{2} E^C E^B T_{CB}{}^A, \quad (15.256)$$

$$R_B{}^A = d\omega_B{}^A + \omega_B{}^C \omega_C{}^A = \frac{1}{2} E^D E^C R_{DCB}{}^A. \quad (15.257)$$

Finally, we define the super-three-form

$$A = \frac{1}{3!} E^C E^B E^A A_{CBA}, \quad (15.258)$$

along with its field-strength, i.e. the super-four-form

$$H = dA = \frac{1}{4!} E^A E^B E^C E^D H_{DCBA}, \quad (15.259)$$

whose components explicitly read

$$H_{DCBA} = \sum_{(ABCD)} \nabla_D A_{CBA} + T_{DC}{}^E A_{EBA}, \quad (15.260)$$

where  $\nabla_A = (E^{-1})_A{}^M \nabla_M$ .

In this formulation, 11-dimensional supergravity has only two dynamical superfields, namely the vielbein  $E_M{}^A(x, \theta)$  and the super-three-form  $A_{MNP}(x, \theta)$ . The equations of motion can be shown to be equivalent to constraints placed upon the components of the supertorsion and the super-four-form [140, 141, 163]. These *supergravity constraints* read

$$T_{\gamma\beta}{}^a = -i(\Gamma^a)_{\gamma\beta}, \quad (15.261a)$$

$$T_{\gamma\beta}{}^\alpha = T_{\gamma b}{}^a = T_{cb}{}^a = 0, \quad (15.261b)$$

$$H_{\delta\gamma\beta\alpha} = H_{\delta\gamma\beta a} = H_{\delta cba} = 0, \quad (15.261c)$$

$$H_{\delta\gamma ba} = i(\Gamma_{ba})_{\delta\gamma}. \quad (15.261d)$$

Using this superspace formulation, the physical fields of 11-dimensional supergravity only appear through their covariant field strengths, namely the top component of the supercurvature  $R_{abc}{}^d$ , the supertorsion component  $T_{ab}{}^\alpha$ , and the four-form  $H_{abcd}$ . To see exactly how this is the case, we must use the Bianchi identities.

It is possible to observe that the supertorsion and the supercurvature obey the Bianchi identities

$$\nabla T^A = E^B R_B{}^A, \quad (15.262a)$$

$$\nabla R_B{}^A = 0. \quad (15.262b)$$

These, along with the closure relationship  $dH = 0$ , can be expressed more explicitly as

$$\sum_{(ABC)} (R_{ABC}{}^D - \nabla_A T_{BC}{}^D - T_{AB}{}^E T_{EC}{}^D) = 0, \quad (15.263a)$$

$$\sum_{(ABCD)} (\nabla_A R_{BCD}{}^E + T_{AB}{}^F R_{FCD}{}^E) = 0, \quad (15.263b)$$

$$\sum_{(ABCDE)} (\nabla_A H_{BCDE} + T_{AB}{}^F H_{FCDE}) = 0. \quad (15.263c)$$

Starting from these identities, we can determine expressions concerning the remaining components of the supertorsion, i.e.

$$T_{c\beta}{}^\alpha = \frac{1}{288} (\Gamma_c{}^{dfgh} + 8\delta_c^d \Gamma^{fgh})_\beta{}^\alpha H_{dfgh} = (\mathcal{T}_c{}^{dfgh})_\beta{}^\alpha H_{dfgh}, \quad (15.264a)$$

$$T_{ab}{}^\alpha = \frac{i}{42} (\Gamma^{cd})^{\alpha\beta} \nabla_\beta H_{abcd}, \quad (15.264b)$$

$$(\Gamma^{abc})_{\alpha\beta} T_{bc}{}^\beta = 0. \quad (15.264c)$$

and the remaining components of the supercurvature, i.e.

$$R_{\delta\gamma ba} = -2i(\Gamma_b \check{\mathcal{T}}_a^{dfgh})_{(\delta\gamma)} H_{dfgh}, \quad (15.265a)$$

$$R_{\delta cba} = \frac{i}{2} [(\Gamma_c)_{\delta\epsilon} T_{ba}{}^\epsilon + 2(\Gamma_{[a})_{\delta\epsilon} T_{b]c}{}^\epsilon], \quad (15.265b)$$

$$R_{dc\beta}{}^\alpha = 2\nabla_{[d} T_{c]\beta}{}^\alpha + 2T_{[d|\beta}{}^\epsilon T_{|c]\epsilon}{}^\alpha + \nabla_\beta T_{dc}{}^\alpha, \quad (15.265c)$$

Note that the Riemann tensor is built from the superconnection and obeys

$$R_{DCa}{}^\beta = R_{DC\beta}{}^a = 0 \quad , \quad R_{DC\beta}{}^\alpha = \frac{1}{4} R_{DCba} (\Gamma^{ba})_\beta{}^\alpha. \quad (15.266)$$

The  $\Gamma$ -matrix combination  $\mathcal{T}$  is defined in (15.264a) and  $\check{\mathcal{T}}$  is its transposition. Finally, the Bianchi identities also give the expressions

$$\nabla_\alpha H_{bcde} = -6i(\Gamma_{[bc})_{\alpha\beta} T_{de]}{}^\beta, \quad (15.267a)$$

$$\nabla_\alpha R_{bcde} = 2\nabla_{[b|} R_{\alpha|c]de} + 2T_{[b|\alpha}{}^\gamma R_{\gamma|c]de} - T_{bc}{}^\gamma R_{\beta\alpha de}. \quad (15.267b)$$

## 15.3 Order-4 vielbein manipulations

Expansion of the M2-brane action only requires knowledge of the expansion of the supervielbein. Therefore we record the expansion of the frame super-form to quartic order.

### 15.3.1 Normal coordinate expansion of frame super-form

Using the expressions for the behaviour of the Lie derivative  $\mathcal{L}_y$  along the tangent field  $y = y^M$ , it can be established that the repeated action on the supervielbein  $E^A$  gives [130]<sup>21</sup>

$$\mathcal{L}_y E^A = \nabla y^A + y^C E^B T_{BC}{}^A, \quad (15.268)$$

$$(\mathcal{L}_y)^2 E^A = -y^B E^C y^D R_{DCB}{}^A + y^C E^B y^D \nabla_D T_{BC}{}^A + y^C (\nabla y^B + y^E E^D T_{DE}{}^B) T_{BC}{}^A, \quad (15.269)$$

$$\begin{aligned} (\mathcal{L}_y)^3 E^A = & -y^D (\nabla y^B + y^F E^G T_{GF}{}^B) y^C R_{CBD}{}^A - y^D E^B y^C y^F \nabla_F R_{CBD}{}^A \\ & + 2y^C (\nabla y^B + y^F E^G T_{GF}{}^B) y^D \nabla_D T_{BC}{}^A + y^C E^B y^D y^E \nabla_E \nabla_D T_{BC}{}^A \\ & + y^C y^G (\nabla y^D + y^E E^F T_{FE}{}^D) T_{DG}{}^B T_{BC}{}^A - y^C y^D E^F y^E R_{EFD}{}^B T_{BC}{}^A \\ & + y^C y^F E^D y^E (\nabla_E T_{DF}{}^B) T_{BC}{}^A, \end{aligned} \quad (15.270)$$

<sup>21</sup>Note that (15.270) corrects (4.7, [130]), in which there is an erroneous extra term.

$$\begin{aligned}
(\mathcal{L}_y)^4 E^A = & + 3y^C y^F (\nabla y^E + y^G E^H T_{HG}{}^E) T_{EF}{}^B y^D \nabla_D T_{BC}{}^A \\
& + 3y^C (\nabla y^B + y^F E^G T_{GF}{}^B) y^D y^E \nabla_E \nabla_D T_{BC}{}^A \\
& - y^C y^D (\nabla y^F + y^G E^H T_{HG}{}^F) y^E R_{EFD}{}^B T_{BC}{}^A \\
& + 2y^C y^F (\nabla y^D + y^E E^G T_{GE}{}^D) y^H (\nabla_H T_{DF}{}^B) T_{BC}{}^A \\
& - y^D y^F (\nabla y^E + y^H E^G T_{GH}{}^E) T_{EF}{}^B y^C R_{CBD}{}^A \\
& - 2y^D (\nabla y^B + y^F E^G T_{GF}{}^B) y^C y^E \nabla_E R_{CBD}{}^A \\
& + y^C y^G y^E (\nabla y^F + y^I E^H T_{HI}{}^F) T_{FE}{}^D T_{DG}{}^B T_{BC}{}^A \\
& + y^D y^E E^F y^G R_{GFE}{}^B y^C R_{CBD}{}^A - y^D y^F E^G y^E (\nabla_E T_{GF}{}^B) y^C R_{CBD}{}^A \\
& - y^D E^B y^C y^E y^F \nabla_F \nabla_E R_{CBD}{}^A + y^C E^B y^D y^E y^F \nabla_F \nabla_E \nabla_D T_{BC}{}^A \\
& - y^C y^D E^F y^E y^G (\nabla_G R_{EFD}{}^B) T_{BC}{}^A - 3y^C y^D E^F y^E R_{EFD}{}^B y^G \nabla_G T_{BC}{}^A \\
& - y^C y^E y^F E^G y^H R_{HGF}{}^D T_{DE}{}^B T_{BC}{}^A + y^C y^G y^E E^F y^H (\nabla_H T_{FE}{}^D) T_{DG}{}^B T_{BC}{}^A \\
& + y^C y^F E^D y^E y^G (\nabla_G \nabla_E T_{DF}{}^B) T_{BC}{}^A + 3y^C y^F E^D y^E (\nabla_E T_{DF}{}^B) y^G \nabla_G T_{BC}{}^A.
\end{aligned} \tag{15.271}$$

Notice that many terms can be rearranged in terms of the supercovariant derivative. However, while the order-1 variation can be written entirely in terms of this (in a bosonic background, one has  $\nabla_m y^\alpha + y^\beta e_m{}^c T_{c\beta}{}^\alpha = D_m y^\alpha$ ), higher orders contain components of the super-Riemann tensor and operators involving the torsion that are difficult to rearrange in compact ways.

### 15.3.2 Rearranging the expanded supervielbein using Bianchi identities

Starting from the order-4 term in (11.127) and using (15.266) to perform some straightforward rearrangement while making use of  $\Gamma$ -matrix symmetries, we may write

$$\begin{aligned}
(\mathcal{L}_y)^4 E_m{}^a = & \frac{i}{4} (y^\delta R_{\delta abc} D_m y^\epsilon) (\bar{y} \Gamma^{abc} y) + (\bar{y} \Gamma^b D_m y) (\bar{y} \Gamma^a \check{T}_b{}^{dfgh} y) H_{dfgh} \\
& + \frac{i}{4} y^\delta y^\chi e_m{}^e y^\delta y^\xi \nabla_\xi (R_{\delta abc} (\Gamma^{bc})_\chi{}^\beta - 4 \nabla_\delta T_{e\chi}{}^\beta) (\Gamma^a)_{\beta\gamma}.
\end{aligned}$$

Now we will use (15.265a) in the first term and (15.264a, 15.265b, 15.267a) in the third term, and we also split the third term. We also use the spinor index symmetry properties of  $\Gamma$ -matrices to write

$$(\Gamma_b \check{T}_c{}^{dfgh})_{(\delta\epsilon)} = \frac{1}{288} \left( \Gamma_{bc} \Gamma^{dfgh} - 8 \delta_{[c}^{[d} \Gamma_b] \Gamma^{fgh]} - 12 \delta_{[c}^{[d} \delta_b^f \Gamma^{gh]} \right)_{\delta\epsilon} H_{dfgh} \equiv 2 \mathcal{R}_{bc}{}^{dfgh} H_{dfgh},$$

so we eventually arrive at

$$\begin{aligned}
(\mathcal{L}_y)^4 E_m{}^a = & [\bar{y} (\mathcal{R}_{bc}{}^{dfgh} H_{dfgh} D_m y)] (\bar{y} \Gamma^{abc} y) + (\bar{y} H_{dfgh} \Gamma^b D_m y) (\bar{y} \Gamma^a \check{T}_b{}^{dfgh} y) \\
& + \frac{1}{8} (\bar{y} \Gamma^{abc} y) e_m{}^e y^\delta [(\Gamma_e)_{\delta\sigma} y^\xi \nabla_\xi T_{bc}{}^\sigma + 2(\Gamma_b)_{\delta\sigma} y^\xi \nabla_\xi T_{ec}{}^\sigma] \\
& - 6 (\bar{y} \Gamma^a \check{T}_b{}^{dfgh} y) e_m{}^b y^\delta (\Gamma_{df})_{\delta\sigma} y^\xi \nabla_\xi T_{gh}{}^\sigma.
\end{aligned}$$

We see that a number of previously nasty-looking curvature and torsion terms are all reducible to expressions involving gamma matrices and the spinor derivative of the supercovariantized gravitino fields strength

$\nabla_\xi T_{gh}{}^\sigma$ .

To assess this we step back to superspace momentarily. Using the superspace covariant derivative

$$\nabla_M v_A{}^B = \partial_M v_A{}^B + v_A{}^C \omega_{MC}{}^B - \omega_{MA}{}^C v_C{}^B,$$

we have  $[\nabla_M, \nabla_N]v_A = -R_{MNA}{}^B v_B$ , and so

$$\begin{aligned} [E_A{}^M \nabla_M, E_B{}^N \nabla_N]v_C &= (E_A{}^M E_B{}^N [\nabla_M, \nabla_N] - 2E_{[A}{}^M E_{B]}{}^N (\nabla_M E_N{}^D) \nabla_D)v_C \\ &= -R_{ABC}{}^D v_D - T_{AB}{}^D \nabla_D v_C. \end{aligned}$$

This means that we have  $R_{ab\gamma}{}^\delta = -[\nabla_a, \nabla_b]_{\gamma}{}^\delta - T_{ab}{}^\mu (\nabla_\mu)_{\gamma}{}^\delta$ , which in bosonic backgrounds is  $R_{ab\gamma}{}^\delta = -[\nabla_a, \nabla_b]_{\gamma}{}^\delta$ . Using Bianchi identity results, we have in bosonic backgrounds,

$$\nabla_\gamma T_{ab}{}^\delta = R_{ab\gamma}{}^\delta - 2\nabla_{[a} T_{b]\gamma}{}^\delta - 2T_{[a|\gamma}{}^\sigma T_{\sigma|b]}{}^\delta = -[\nabla_a + T_a, \nabla_b + T_b]_{\gamma}{}^\delta.$$

In terms of the supercovariant derivative  $D_m$  we can eventually write  $\nabla_\gamma T_{ab}{}^\delta = e_a{}^m e_b{}^n [D_m, D_n]_{\gamma}{}^\delta$ . Applying this result we see that the two objects defined in (11.128) arise naturally by combining terms, as we have

$$\begin{aligned} (\mathcal{L}_y)^4 E_m{}^a &= (\bar{y}\Gamma^{abc}y) \left[ \bar{y} \left( \mathcal{R}_{bc}{}^{dfgh} H_{dfgh} D_m + \frac{1}{8} \Gamma_e e_m{}^e e_b{}^p e_c{}^q [D_p, D_q] + \frac{1}{4} \Gamma_b e_c{}^q [D_m, D_q] \right) y \right] \\ &\quad + (\bar{y}\Gamma^a \check{\mathcal{T}}_b{}^{dfgh} y) \left[ \bar{y} (H_{dfgh} \Gamma^b D_m - 6e_m{}^b \Gamma_{df} e_g{}^p e_h{}^q [D_p, D_q]) y \right], \end{aligned}$$

which means

$$(\mathcal{L}_y)^4 E_m{}^a = (\bar{y}\Gamma^{abc}y)(\bar{y}\mathcal{W}_{mbc}y) + (\bar{y}\Gamma^a \check{\mathcal{T}}_b{}^{dfgh} y)(\bar{y}\mathcal{H}^b{}_{m\,dfgh}y). \quad (15.272)$$

## 15.4 Catalogue of dimensional reductions

In this appendix we catalogue the details of the dimensional reductions of all the terms appearing in the main text.

### Notation

In the M-theory formulation, we consider the 11-dimensional spacetime to be spanned by the coordinates  $x^{\hat{m}}$ . This is reduced to a 10-dimensional string background via the split  $x^{\hat{m}} = (x^m, x^{10})$ . Unless differently stated, 11-dimensional indices are hatted whereas 10-dimensional indices are not; 11-dimensional objects are also hatted and 10-dimensional objects are not. So vectors in the 11- and 10-dimensional spacetimes read  $\hat{\omega} = \hat{\omega}_{\hat{m}} dx^{\hat{m}}$  and  $\omega = \omega_m dx^m$ , respectively, and similarly for tensors of arbitrary rank. Indices  $\hat{a}, \hat{b}$  and  $a, b$  are 11- and 10-dimensional tangent spacetime indices, respectively, with explicit number indices being underlined for tangent space and unadorned for spacetime. Background fields are always independent of the extra M-theory coordinate  $x^{10}$ .

The M2- and D2-brane 3-dimensional worldvolumes are spanned by the coordinates  $\xi^i$ . Pulling an object back from eleven dimensions and pulling an object back from ten dimensions are different manoeuvres: for



ease of notation, instead of writing these pullbacks explicitly, we shall keep track of which is being used by noting whether the object itself is hatted or not. For instance, denoting for a moment the pullback from the 11-dimensional spacetime to the 3-dimensional M2-brane worldvolume with  $\varphi_*$  and the pullback from the 10-dimensional spacetime to the 3-dimensional D2-brane worldvolume with  $\phi_*$ , for two vectors  $\hat{\omega}_{\hat{m}}$  and  $\omega_m$  we will write  $\hat{\omega}_i = (\varphi_* \hat{\omega})_i = \partial_i x^{\hat{m}} \hat{\omega}_{\hat{m}}$  and  $\omega_i = (\phi_* \omega)_i = \partial_i x^m \omega_m$ .

The  $n$ -dimensional Levi-Civita symbol  $\varepsilon_{\mu_1 \dots \mu_n}$  is normalized as  $\varepsilon_{1 \dots n} = +1$  and the Levi-Civita tensor is defined as  $\epsilon_{\mu_1 \dots \mu_n} = (-\det g)^{1/2} \varepsilon_{\mu_1 \dots \mu_n}$ , where  $g_{\mu_1 \mu_2}$  is the associated  $n$ -dimensional metric. Similarly, we define the symbol  $\varepsilon^{\mu_1 \dots \mu_n} \equiv -\varepsilon_{\mu_1 \dots \mu_n}$  and  $\epsilon^{\mu_1 \dots \mu_n} = (-\det g)^{-1/2} \varepsilon^{\mu_1 \dots \mu_n}$ .

Antisymmetric and symmetric combinations of a number  $n$  of indices are denoted by square brackets and parentheses, respectively, and include a normalization factor  $1/n!$ . For instance, we have  $\Gamma_{[1 \dots n]} = \sum_{\sigma \in S_n} \text{sgn}(\sigma) \Gamma_{\sigma(1)} \dots \Gamma_{\sigma(n)}/n!$ , where  $\sigma \in S_n$  are the permutations of  $n$  elements.

### 15.4.1 Basic dimensional reductions

We report details about the dimensional reductions of the essential quantities that are needed in the analysis of M2- and D2-branes.

#### Metric

In terms of 10-dimensional quantities, the 11-dimensional vielbein splits according to the standard ansatz

$$\hat{e}_{\hat{m}}^{\hat{a}} = \begin{pmatrix} e^{-\frac{\phi}{3}} e_m^a & e^{\frac{2\phi}{3}} C_m \\ 0 & e^{\frac{2\phi}{3}} \end{pmatrix}, \quad (15.273)$$

where  $e_m^a$  is the 10-dimensional string frame vielbein,  $\phi$  is the dilaton, and  $C^{(1)} = dx^m C_m$  is the Ramond-Ramond one-form. The vielbein is invertible and its inverse reads

$$\hat{e}_{\hat{a}}^{\hat{m}} = \begin{pmatrix} e^{\frac{\phi}{3}} e_a^m & -e^{\frac{\phi}{3}} C_a \\ 0 & e^{-\frac{2\phi}{3}} \end{pmatrix}. \quad (15.274)$$

The 11-dimensional metric is defined in terms of the vielbein as  $\hat{g}_{\hat{m}\hat{n}} = \hat{e}_{\hat{m}}^{\hat{a}} \hat{e}_{\hat{n}}^{\hat{b}} \hat{\eta}_{\hat{a}\hat{b}}$ , where  $\hat{\eta}_{\hat{a}\hat{b}}$  is the 11-dimensional Minkowski metric, so it reads

$$\hat{g}_{\hat{m}\hat{n}} = \begin{pmatrix} e^{-\frac{2\phi}{3}} g_{mn} + e^{\frac{4\phi}{3}} C_m C_n & e^{\frac{4\phi}{3}} C_m \\ e^{\frac{4\phi}{3}} C_n & e^{\frac{4\phi}{3}} \end{pmatrix},$$

where the 10-dimensional metric is defined as  $g_{mn} = e_m^a e_n^b \eta_{ab}$ , with  $\eta_{ab}$  the 10-dimensional Minkowski metric.

#### Three-form field

We describe the dimensional reduction of the 11-dimensional three-form  $\hat{A} = dx^{\hat{m}} \wedge dx^{\hat{n}} \wedge dx^{\hat{p}} \hat{A}_{\hat{p}\hat{n}\hat{m}}/3!$  in terms of two 10-dimensional form fields  $C^{(3)} = dx^m \wedge dx^n \wedge dx^p C_{pnm}/3!$  and  $B^{(2)} = dx^m \wedge dx^n B_{nm}/2!$

defined as

$$\hat{A}_{mnp} = C_{mnp}, \quad (15.275a)$$

$$\hat{A}_{mn10} = B_{mn}, \quad (15.275b)$$

The 11-dimensional flux is defined as  $\hat{H} = d\hat{A}$ , while in the 10-dimensional formulation we have  $F^{(4)} = dC^{(3)}$  and  $H^{(3)} = dB^{(2)}$ , so the 10-dimensional form field strengths are such that

$$\hat{H}_{mnpq} = F_{mnpq}, \quad (15.276a)$$

$$\hat{H}_{mnp10} = H_{mnp}. \quad (15.276b)$$

An analysis of the dimensional-reduction ansatz shows that the tangent-space 11-dimensional flux is related to the 10-dimensional field-strength tensors as

$$\hat{H}_{abc10} = e^{\frac{\phi}{3}} e_a^m e_b^n e_c^p H_{mnp}, \quad (15.277a)$$

$$\hat{H}_{abcd} = e^{\frac{4\phi}{3}} e_a^m e_b^n e_c^p e_d^q (F_{mnpq} - 4H_{[mnp}C_{q]}) = e^{\frac{4\phi}{3}} e_a^m e_b^n e_c^p e_d^q F_{mnpq}, \quad (15.277b)$$

where we defined the combination  $F^{(4)} = dC^{(3)} - C^{(1)} \wedge H^{(3)}$ .

### $\hat{\Gamma}$ -matrices

In tangent spacetime, the first ten  $\hat{\Gamma}$ -matrices are the same, i.e.  $\hat{\Gamma}^a = \Gamma^a$ , since the Clifford algebra is the same as a consequence of the equality  $\hat{\eta}_{ab} = \eta_{ab}$ ; the last  $\hat{\Gamma}$ -matrix defined as the chirality matrix  $\hat{\Gamma}^{10} \equiv \Gamma^*$ . In curved spacetime, the 11-dimensional  $\hat{\Gamma}$ -matrices and 10-dimensional  $\Gamma$ -matrices are then related as

$$\hat{\Gamma}_m = e^{-\frac{\phi}{3}} (\Gamma_m + e^\phi C_m \Gamma^*), \quad (15.278)$$

$$\hat{\Gamma}_{10} = e^{\frac{2\phi}{3}} \Gamma^*. \quad (15.279)$$

One also finds,

$$\hat{\Gamma}_{mn} = e^{-\frac{2\phi}{3}} (\Gamma_{mn} - 2e^\phi C_{[m} \Gamma_{n]} \Gamma^*), \quad (15.280)$$

$$\hat{\Gamma}_{mnp} = e^{-\phi} (\Gamma_{mnp} + 3e^\phi C_{[m} \Gamma_{np]} \Gamma^*). \quad (15.281)$$

For contractions of the components of a form field  $\omega_p$  with a number  $n$  of 10-dimensional curved-spacetime  $\Gamma$ -matrices  $\Gamma^m$ , we employ the underlined notation

$$\underline{\omega}_{q_1 q_2 \dots q_m} = \frac{1}{n!} \omega_{q_1 \dots q_m p_1 \dots p_n} \Gamma^{p_1 \dots p_n}. \quad (15.282)$$

## 15.4.2 Supercovariant derivatives

### Spin connection

The 11-dimensional spin connection is defined in terms of the anhomology coefficients as

$$\hat{\omega}_{\hat{a}\hat{b}}^{\hat{c}} = \frac{1}{2} \left( \hat{\Omega}_{\hat{a}\hat{b}}^{\hat{c}} - \hat{\Omega}_{\hat{a}\hat{d}}^{\hat{e}} \hat{\eta}^{\hat{c}\hat{d}} \hat{\eta}_{\hat{b}\hat{e}} - \hat{\Omega}_{\hat{b}\hat{d}}^{\hat{e}} \hat{\eta}^{\hat{c}\hat{d}} \hat{\eta}_{\hat{a}\hat{e}} \right), \quad (15.283)$$

where the latter read

$$\hat{\Omega}_{\hat{a}\hat{b}}^{\hat{c}} = \hat{e}_{\hat{a}}^{\hat{m}} \hat{e}_{\hat{b}}^{\hat{n}} \left( \hat{\partial}_{\hat{m}} \hat{e}_{\hat{n}}^{\hat{c}} - \hat{\partial}_{\hat{n}} \hat{e}_{\hat{m}}^{\hat{c}} \right).$$

These allow us to express the 11-dimensional spin connection in terms of 10-dimensional operators as

$$\hat{\omega}_{ab}{}^c = e^{\frac{\phi}{3}} \left[ \omega_{ab}{}^c + \frac{1}{3} \partial_b \phi \delta_a^c - \frac{1}{3} \partial^c \phi \eta_{ba} \right], \quad (15.284a)$$

$$\hat{\omega}_{ab}{}^{10} = \frac{1}{2} e^{\frac{4\phi}{3}} F_{ab}, \quad (15.284b)$$

$$\hat{\omega}_{\underline{10}a}{}^c = \hat{\omega}_{a\underline{10}}{}^c = -\frac{1}{2} e^{\frac{4\phi}{3}} F_a{}^c, \quad (15.284c)$$

$$\hat{\omega}_{\underline{10}a}{}^{10} = -\frac{2}{3} e^{\frac{\phi}{3}} \partial_a \phi, \quad (15.284d)$$

$$\hat{\omega}_{\underline{10}\underline{10}}{}^c = \frac{2}{3} e^{\frac{\phi}{3}} \partial^c \phi, \quad (15.284e)$$

where all the remaining combinations are vanishing, i.e.  $\hat{\omega}_{a\underline{10}}{}^{10} = \hat{\omega}_{\underline{10}\underline{10}}{}^{10} = 0$ .

### Torsion

The 11-dimensional torsion term that appears in the M2-brane action is the  $\Gamma$ -matrix valued term

$$\hat{T}_{\hat{a}} = \frac{1}{288} \left( \hat{\Gamma}_{\hat{a}}{}^{\hat{b}\hat{c}\hat{d}\hat{e}} - 8\delta_{\hat{a}}^{\hat{b}} \hat{\Gamma}^{\hat{c}\hat{d}\hat{e}} \right) \hat{H}_{\hat{b}\hat{c}\hat{d}\hat{e}}. \quad (15.285)$$

In terms of 10-dimensional operators, the 11-dimensional torsion components can be seen to split as

$$\hat{T}_a = \frac{1}{12} e^{\frac{\phi}{3}} \left[ \Gamma_a(e^\phi \underline{F}^{(4)} + \underline{H}^{(3)} \Gamma^*) - 3e_a{}^m (e^\phi \underline{F}_m^{(4)} + \underline{H}_m^{(3)} \Gamma^*) \right], \quad (15.286a)$$

$$\hat{T}_{\underline{10}} = \frac{1}{12} e^{\frac{\phi}{3}} \left[ \Gamma^*(e^\phi \underline{F}^{(4)} - 2\underline{H}^{(3)} \Gamma^*) \right]. \quad (15.286b)$$

### Supercovariant derivative

In dealing with the M2-brane action, the spinor kinetic term contains the worldvolume pullback of the 11-dimensional spacetime operator

$$\hat{D}_{\hat{m}} = \hat{\nabla}_{\hat{m}} - \hat{T}_{\hat{m}}, \quad (15.287)$$

where  $\hat{\nabla}_{\hat{m}}$  is the 11-dimensional spinor covariant derivative and  $\hat{T}_{\hat{m}}$  is the 11-dimensional torsion, which are defined in the tangent spacetime as

$$\nabla_{\hat{a}} = \partial_{\hat{a}} + \frac{1}{4} \hat{\omega}_{\hat{a}}{}^{\hat{b}\hat{c}} \hat{\Gamma}_{\hat{c}\hat{d}}, \quad (15.288a)$$

$$\hat{T}_{\hat{a}} = \frac{1}{288} (\hat{\Gamma}_{\hat{a}}^{\hat{b}\hat{c}\hat{d}\hat{e}} - 8\delta_{\hat{a}}^{\hat{b}} \hat{\Gamma}^{\hat{c}\hat{d}\hat{e}}) \hat{H}_{\hat{b}\hat{c}\hat{d}\hat{e}}. \quad (15.288b)$$

Using the above relations one can dimensionally reduce the 11 dimensional supercovariant derivative and write it in terms of 10 dimensional operators (12.149), recovering the relations (12.150).

### 15.4.3 Pullbacks

We report details about the relationships between pullbacks onto M2- and D2-brane worldvolumes.

#### Metric

Defining the combination

$$p_i = \partial_i x^{10} + \partial_i x^m C_m, \quad (15.289)$$

which is the dual to the world volume flux on the D2-brane, we can express the metric pullback as

$$\hat{g}_{ij} = e^{-\frac{2\phi}{3}} g_{ij} + e^{\frac{4\phi}{3}} p_i p_j. \quad (15.290)$$

Equivalently, the pullback of the vielbein is

$$\hat{e}_i^a = e^{-\frac{\phi}{3}} e_i^a, \quad (15.291a)$$

$$\hat{e}_i^{10} = e^{\frac{2\phi}{3}} p_i. \quad (15.291b)$$

Since the pulled-back metrics are 3-dimensional, using the shorthand  $g^{ij} p_i p_j = p^2$ , we get the exact relationship

$$\det(\hat{g}_{ij}) = e^{-2\phi} \det(g_{ij}) (1 + e^{2\phi} p^2), \quad (15.292)$$

To conclude, the relationship between the inverses of the pulled-back metrics can be seen to be

$$\hat{g}^{ij} = e^{\frac{2\phi}{3}} \left( g^{ij} - \frac{e^{2\phi} p^i p^j}{1 + e^{2\phi} p^2} \right). \quad (15.293)$$

#### Three-form field

For the three-form field, we can write

$$\hat{A}_{ijk} = C_{ijk} - 3C_{[i} B_{jk]} + 3p_{[i} B_{jk]}. \quad (15.294)$$

#### $\hat{\Gamma}$ -matrices

The relationship between the 11-dimensional  $\hat{\Gamma}$ -matrix pullbacks and 10-dimensional  $\Gamma$ -matrix pullbacks is

$$\hat{\Gamma}_i = e^{-\frac{\phi}{3}} (\Gamma_i + e^{\phi} p_i \Gamma^*). \quad (15.295)$$

Starting from this, we can then express the antisymmetric combinations of  $\hat{\Gamma}$ -matrices as

$$\hat{\Gamma}_{ij} = e^{-\frac{2\phi}{3}} (\Gamma_{ij} - 2e^\phi p_{[i}\Gamma_{j]}\Gamma^*), \quad (15.296)$$

$$\hat{\Gamma}_{ijk} = e^{-\phi} (\Gamma_{ijk} + 3e^\phi p_{[i}\Gamma_{jk]}\Gamma^*). \quad (15.297)$$

Matrices with upper indices are defined by use of the metric pullback inverse, i.e.  $\hat{\Gamma}^i = \hat{g}^{ij}\hat{\Gamma}_j$  and  $\Gamma^i = g^{ij}\Gamma_j$ , and they are related as

$$\hat{\Gamma}^i = e^{\frac{\phi}{3}} \left[ \Gamma^i + \frac{e^\phi p^i}{1 + e^{2\phi} p^2} (\Gamma^* - e^\phi \Gamma^k p_k) \right]. \quad (15.298)$$

### Supercovariant derivative pullback

The operator that appears in the M2-brane action is the 11-dimensional spinor covariant derivative pullback  $\hat{D}_i \hat{\theta}$ . By making use of the results above, we can determine that in terms of the D2-brane operators this reads

$$\hat{D}_i \hat{\theta} = e^{-\frac{\phi}{6}} \left[ D_i - \frac{1}{6} \Gamma_i \Delta + \frac{1}{3} e^\phi p_i \Gamma^* \Delta \right] \theta. \quad (15.299)$$

#### 15.4.4 Order-4 combinations

In the order-4 fermion expansions we find combinations of the operators that appear at second order. These are discussed in detail below.

### $\hat{\Gamma}$ -matrices and fluxes

We now treat the term

$$\hat{\mathcal{R}}_{\hat{b}\hat{c}} = \frac{1}{576} (\hat{\Gamma}_{\hat{b}\hat{c}} \hat{\Gamma}^{\hat{d}\hat{f}\hat{g}\hat{h}} - 8\delta_{[\hat{c}}^{\hat{d}} \hat{\Gamma}_{\hat{b}]} \hat{\Gamma}^{\hat{f}\hat{g}\hat{h}} - 12\delta_{[\hat{c}}^{\hat{d}} \delta_{\hat{b}]}^{\hat{f}} \hat{\Gamma}^{\hat{g}\hat{h}}) \hat{H}_{\hat{d}\hat{f}\hat{g}\hat{h}}. \quad (15.300)$$

Upon dimensional reduction, this allows us to define

$$R_{bc} \equiv e^{-\frac{\phi}{3}} \hat{\mathcal{R}}_{bc} = \frac{1}{24} \left[ \Gamma_{bc} (e^\phi \underline{F}^{(4)} + \underline{H}^{(3)} \Gamma^*) - 2\Gamma_{[b} (e^\phi \underline{F}_{c]}^{(4)} + \underline{H}_{c]}^{(3)} \Gamma^*) + (e^\phi \underline{F}_{bc}^{(4)} + \underline{H}_{bc}^{(3)} \Gamma^*) \right], \quad (15.301a)$$

$$R_b \equiv e^{-\frac{\phi}{3}} \hat{\mathcal{R}}_{b\underline{10}} = -\frac{1}{24} e^\phi \Gamma^* \left[ \Gamma_b \underline{F}^{(4)} - \underline{F}_b^{(4)} \right]. \quad (15.301b)$$

### Supercovariant derivative commutator

An operator appearing frequently in the order-4 fermionic expansion is the commutator of supercovariant derivatives on which we must perform dimensional reduction. First of all, we have

$$[\hat{D}_p, \hat{D}_{10}] \hat{y} = \frac{1}{3} e^{-\frac{\phi}{6}} e^\phi K_p \theta,$$

where we have defined the operator

$$K_p \equiv \left[ D_p - \frac{1}{6} \Gamma_p \Delta, \Gamma^* \Delta \right] + (\partial_p \phi) \Gamma^* \Delta. \quad (15.302)$$

The other non-zero commutator reads

$$[\hat{D}_p, \hat{D}_q] \hat{y} = e^{-\frac{\phi}{6}} K_{pq} \theta - \frac{2}{3} e^{-\frac{\phi}{6}} e^\phi C_{[p} K_{q]},$$

where we have defined the operator

$$K_{pq} = \left[ D_p - \frac{1}{6} \Gamma_p \Delta, D_q - \frac{1}{6} \Gamma_q \Delta \right] + \frac{1}{3} e^\phi F_{pq}^{(2)} \Gamma^* \Delta. \quad (15.303)$$

To conclude, we notice that  $\hat{e}_{10}^{\hat{p}} \hat{e}_{10}^{\hat{q}} [\hat{D}_{\hat{p}}, \hat{D}_{\hat{q}}] \hat{y} = \hat{e}_{10}^{10} \hat{e}_{10}^{10} [\hat{D}_{10}, \hat{D}_{10}] \hat{y} = 0$ . From these results, one can immediately derive

$$[\hat{D}_a, \hat{D}_b] \hat{\theta} = e^{\frac{\phi}{2}} e_a^p e_b^q K_{pq} \theta, \quad (15.304a)$$

$$[\hat{D}_a, \hat{D}_{10}] \hat{\theta} = \frac{1}{3} e^{\frac{\phi}{2}} e_a^p K_p \theta. \quad (15.304b)$$

#### 15.4.5 Dimensional reduction of the quartic 11-dimensional shifted fields for the dilaton

In this appendix we provide an example of the dimensional reduction calculation for the quartic fermionic terms. We will concentrate on the dilaton as these terms are the least formidable, however the approach is fundamentally the same for the dimensional reduction for all the quartic fermionic terms in 11 dimensions. We will make heavy use of the results in appendix 15.4.

The relationship between the quartic fermionic expansion of the 11-dimensional metric  $\hat{g}_{\hat{m}\hat{n}}$  and the quartic fermionic expansions of the 10-dimensional metric  $g_{mn}$ , Ramond-Ramond one-form  $C_m^{(1)}$ , and dilaton  $\phi$  is (12.156). The expansion of the 11-dimensional metric is (11.140). Plugging in (11.129) we can write the 11-dimensional shifted metric as

$$\begin{aligned} \hat{g}_{\hat{m}\hat{n}} = & -\frac{1}{4} (\hat{\theta} \hat{\Gamma}_{\hat{a}} \hat{D}_{(\hat{m}} \hat{\theta}) (\hat{\theta} \hat{\Gamma}_{\hat{a}} \hat{D}_{\hat{n})} \hat{\theta}) + \frac{1}{12} (\hat{\theta} \hat{\Gamma}_{(\hat{m}} \hat{T}_{\hat{a}} \hat{\theta}) (\hat{\theta} \hat{\Gamma}_{\hat{a}} \hat{D}_{|\hat{n})} \hat{\theta}) \\ & - \frac{1}{576} \hat{g}_{\hat{m}\hat{n}} (\hat{\theta} \hat{\Gamma}^{\hat{a}\hat{b}\hat{c}\hat{d}} \hat{\theta}) (\hat{\theta} \hat{\Gamma}_{\hat{a}\hat{b}} [\hat{D}_{\hat{c}}, \hat{D}_{\hat{d}}] \hat{\theta}) + \frac{1}{96} (\hat{\theta} \hat{\Gamma}_{(\hat{m}} \hat{\Gamma}^{\hat{a}\hat{b}\hat{c}} \hat{\theta}) (\hat{\theta} \hat{\Gamma}_{\hat{n})\hat{a}} [\hat{D}_{\hat{b}}, \hat{D}_{\hat{c}}] \hat{\theta}) \\ & + \frac{1}{96} (\hat{\theta} \hat{\Gamma}_{(\hat{m}} \hat{\Gamma}^{\hat{a}\hat{b}\hat{c}} \hat{\theta}) (\hat{\theta} \hat{\Gamma}_{\hat{a}\hat{b}} [\hat{D}_{|\hat{n})}, \hat{D}_{\hat{c}}] \hat{\theta}) + \frac{1}{12} (\hat{\theta} \hat{\Gamma}_{(\hat{m}} \hat{\Gamma}^{\hat{a}\hat{b}} \hat{\theta}) (\hat{\theta} \hat{\mathcal{R}}_{\hat{a}\hat{b}} \hat{D}_{|\hat{n})} \hat{\theta}) \\ & + \frac{1}{96} (\hat{\theta} \hat{\Gamma}_{(\hat{m}} \hat{\Gamma}^{\hat{a}\hat{b}} \hat{\theta}) (\hat{\theta} \hat{\Gamma}_{\hat{n})} [\hat{D}_{\hat{a}}, \hat{D}_{\hat{b}}] \hat{\theta}) + \frac{1}{48} (\hat{\theta} \hat{\Gamma}_{(\hat{m}} \hat{\Gamma}^{\hat{a}\hat{b}} \hat{\theta}) (\hat{\theta} \hat{\Gamma}_{\hat{a}} [\hat{D}_{|\hat{n})}, \hat{D}_{\hat{b}}] \hat{\theta}). \end{aligned} \quad (15.305)$$

Plugging this into (12.180) allows us to write the dilaton quartic shift as

$$\begin{aligned} \rho^{(4)} = & -\frac{1}{768} (\hat{\theta} \hat{\Gamma}^{\hat{a}\hat{b}\hat{c}\hat{d}} \hat{\theta}) (\hat{\theta} \hat{\Gamma}_{\hat{a}\hat{b}} [\hat{D}_{\hat{c}}, \hat{D}_{\hat{d}}] \hat{\theta}) + \frac{1}{128} e^{-\frac{4\phi}{3}} (\hat{\theta} \hat{\Gamma}_{10} \hat{\Gamma}^{\hat{a}\hat{b}\hat{c}} \hat{\theta}) \left( \hat{\theta} (\hat{\Gamma}_{10\hat{a}} [\hat{D}_{\hat{b}}, \hat{D}_{\hat{c}}] + \hat{\Gamma}_{\hat{a}\hat{b}} [\hat{D}_{10}, \hat{D}_{\hat{c}}]) \hat{\theta} \right) \\ & + \frac{1}{128} e^{-\frac{4\phi}{3}} (\hat{\theta} \hat{\Gamma}_{10} \hat{\Gamma}^{\hat{a}\hat{b}} \hat{\theta}) \left( \hat{\theta} (\hat{\Gamma}_{10} [\hat{D}_{\hat{a}}, \hat{D}_{\hat{b}}] + 2\hat{\Gamma}_{\hat{a}} [\hat{D}_{10}, \hat{D}_{\hat{b}}]) \hat{\theta} \right) - \frac{3}{16} e^{-\frac{4\phi}{3}} (\hat{\theta} \hat{\Gamma}_{\hat{a}} \hat{D}_{10} \hat{\theta}) (\hat{\theta} \hat{\Gamma}_{\hat{a}} \hat{D}_{10} \hat{\theta}) \\ & + \frac{1}{16} e^{-\frac{4\phi}{3}} (\hat{\theta} \hat{\Gamma}_{10} \hat{T}_{\hat{a}} \hat{\theta}) (\hat{\theta} \hat{\Gamma}_{\hat{a}} \hat{D}_{10} \hat{\theta}) + \frac{1}{16} e^{-\frac{4\phi}{3}} (\hat{\theta} \hat{\Gamma}_{10} \hat{\Gamma}^{\hat{a}\hat{b}} \hat{\theta}) (\hat{\theta} \hat{\mathcal{R}}_{\hat{a}\hat{b}} \hat{D}_{10} \hat{\theta}) + \frac{1}{24} (\bar{\theta} \Delta \theta)^2. \end{aligned}$$

We will demonstrate the dimensional reduction of these terms in detail. The dimensional reduction of the terms involved in the quartic shifts of the other type IIA fields follows in a very similar way, so we will forgo spelling these out. Let us tackle the dilaton shift one term at a time. We will variously require, (15.279), (15.286a), (15.286b), (15.301a), (15.301b), (15.304a), and (15.304b), at different stages of the calculations. In the order in which the terms appear, we have from the first term

$$\begin{aligned} & -\frac{1}{768}(\hat{\theta}\hat{\Gamma}^{\hat{a}\hat{b}\hat{c}\hat{d}}\hat{\theta})(\hat{\theta}\hat{\Gamma}_{\hat{a}\hat{b}}[\hat{D}_{\hat{c}}, \hat{D}_{\hat{d}}]\hat{\theta}) = \\ & = -\frac{1}{768}(\hat{\theta}\hat{\Gamma}^{abcd}\hat{\theta})(\hat{\theta}\hat{\Gamma}_{ab}[\hat{D}_c, \hat{D}_d]\hat{\theta}) - \frac{1}{192}(\hat{\theta}\hat{\Gamma}^{10bcd}\hat{\theta})(\hat{\theta}\hat{\Gamma}_{\underline{10}b}[\hat{D}_c, \hat{D}_d]\hat{\theta}) \\ & = -\frac{1}{768}(\bar{\theta}\hat{\Gamma}^{mnpq}\theta)(\bar{\theta}\hat{\Gamma}_{mn}K_{pq}\theta) - \frac{1}{1152}(\bar{\theta}\hat{\Gamma}^*\hat{\Gamma}^{mnp}\theta)\left[\bar{\theta}[3\hat{\Gamma}^*\hat{\Gamma}_m K_{np} - \hat{\Gamma}_{mn}K_p]\theta\right]. \end{aligned}$$

In moving to the final line we used many of the results derived previously, and we move vielbeins around in order to write everything with spacetime indices rather than tangent space. In the second term, we have

$$\frac{1}{128}e^{-\frac{4\phi}{3}}(\hat{\theta}\hat{\Gamma}_{10}\hat{\Gamma}^{\hat{a}\hat{b}\hat{c}}\hat{\theta})(\hat{\theta}(\hat{\Gamma}_{10\hat{a}}[\hat{D}_{\hat{b}}, \hat{D}_{\hat{c}}] + \hat{\Gamma}_{\hat{a}\hat{b}}[\hat{D}_{10}, \hat{D}_{\hat{c}}])\hat{\theta}) = \frac{1}{384}(\bar{\theta}\hat{\Gamma}^*\hat{\Gamma}^{mnp}\theta)\left[\bar{\theta}[3\hat{\Gamma}^*\hat{\Gamma}_m K_{np} - \hat{\Gamma}_{mn}K_p]\theta\right],$$

where the term with  $\hat{a}\hat{b}\hat{c} \rightarrow 10bc$  vanishes by symmetry of the first bilinear. Next, we have

$$\frac{1}{128}e^{-\frac{4\phi}{3}}(\hat{\theta}\hat{\Gamma}_{10}\hat{\Gamma}^{\hat{a}\hat{b}}\hat{\theta})(\hat{\theta}(\hat{\Gamma}_{10}[\hat{D}_{\hat{a}}, \hat{D}_{\hat{b}}] + 2\hat{\Gamma}_{\hat{a}}[\hat{D}_{10}, \hat{D}_{\hat{b}}])\hat{\theta}) = \frac{1}{384}(\bar{\theta}\hat{\Gamma}^*\hat{\Gamma}^{mn}\theta)\left[\bar{\theta}[3\hat{\Gamma}^*K_{mn} - 2\hat{\Gamma}_m K_n]\theta\right],$$

where symmetry considerations of the first bilinear causes the  $\hat{a}\hat{b} \rightarrow 10b$  terms to vanish. Moving to the fourth term, we have

$$-\frac{3}{16}e^{-\frac{4\phi}{3}}(\hat{\theta}\hat{\Gamma}_{\hat{a}}\hat{D}_{10}\hat{\theta})(\hat{\theta}\hat{\Gamma}^{\hat{a}}\hat{D}_{10}\hat{\theta}) = -\frac{1}{48}(\bar{\theta}\hat{\Gamma}_m\hat{\Gamma}^*\Delta\theta)(\bar{\theta}\hat{\Gamma}^m\hat{\Gamma}^*\Delta\theta) - \frac{1}{48}(\bar{\theta}\Delta\theta)^2.$$

The fifth term gives us

$$\begin{aligned} & \frac{1}{16}e^{-\frac{4\phi}{3}}(\hat{\theta}\hat{\Gamma}_{10}\hat{T}_{\hat{a}}\hat{\theta})(\hat{\theta}\hat{\Gamma}^{\hat{a}}\hat{D}_{10}\hat{\theta}) = \\ & = -\frac{1}{576}\left[\bar{\theta}[2\hat{\Gamma}^*e^\phi\underline{F}_m^{(4)} - \hat{\Gamma}_m\underline{H}^{(3)}]\theta\right](\bar{\theta}\hat{\Gamma}^m\hat{\Gamma}^*\Delta\theta) + \frac{1}{576}\left[\bar{\theta}[e^\phi\underline{F}^{(4)} - 2\underline{H}^{(3)}\hat{\Gamma}^*]\theta\right](\bar{\theta}\Delta\theta), \end{aligned}$$

where we have once again been able to use the symmetries of the  $\hat{\Gamma}$ -matrices to combine some terms together. Finally, we have

$$\frac{1}{16}e^{-\frac{4\phi}{3}}(\hat{\theta}\hat{\Gamma}_{10}\hat{\Gamma}^{\hat{a}\hat{b}}\hat{\theta})(\hat{\theta}\hat{\mathcal{R}}_{\hat{a}\hat{b}}\hat{D}_{10}\hat{\theta}) = \frac{1}{48}(\bar{\theta}\hat{\Gamma}^*\hat{\Gamma}^{mn}\theta)(\bar{\theta}R_{mn}\hat{\Gamma}^*\Delta\theta).$$

We also must not forget the final term  $(\bar{\theta}\Delta\theta)^2/24$  in the dilaton shift, which was already built out of 10-

dimensional fields. If we combine everything together, we obtain the dilaton quartic order shift

$$\begin{aligned}
\rho^{(4)} = & -\frac{1}{768}(\bar{\theta}\Gamma^{mnpq}\theta)(\bar{\theta}\Gamma_{mn}K_{pq}\theta) + \frac{1}{576}(\bar{\theta}\Gamma^*\Gamma^{mnp}\theta)\left[\bar{\theta}\left[3\Gamma^*\Gamma_m K_{np} - \Gamma_{mn}K_p\right]\theta\right] \\
& + \frac{1}{384}(\bar{\theta}\Gamma^*\Gamma^{mn}\theta)\left[\bar{\theta}\left[3\Gamma^*K_{mn} - 2\Gamma_m K_n\right]\theta\right] + \frac{1}{48}(\bar{\theta}\Gamma^*\Gamma^{mn}\theta)(\bar{\theta}R_{mn}\Gamma^*\Delta\theta) \\
& - \frac{1}{48}(\bar{\theta}\Gamma_m\Gamma^*\Delta\theta)(\bar{\theta}\Gamma^m\Gamma^*\Delta\theta) - \frac{1}{576}\left[\bar{\theta}\left[2\Gamma^*e^\phi\underline{F}_m^{(4)} - \Gamma_m\underline{H}^{(3)}\right]\theta\right](\bar{\theta}\Gamma^m\Gamma^*\Delta\theta) \\
& + \frac{1}{48}(\bar{\theta}\Delta\theta)^2 + \frac{1}{576}\left[\bar{\theta}\left[e^\phi\underline{F}^{(4)} - 2\underline{H}^{(3)}\Gamma^*\right]\theta\right](\bar{\theta}\Delta\theta).
\end{aligned} \tag{15.306}$$

This is the shift given in the main text for the dilaton.

For the sake of completion, let us also note here that the expanded expression for the quartic terms in the expansion of the three-form superfield, obtained by plugging (11.129) into (11.141), is

$$\begin{aligned}
\hat{\alpha}_{\hat{m}\hat{n}\hat{p}} = & -\frac{3}{4}(\hat{\theta}\hat{\Gamma}_{\hat{a}[\hat{m}}\hat{D}_{\hat{n}}\hat{\theta})(\hat{\theta}\hat{\Gamma}^{\hat{a}}\hat{D}_{\hat{p}}]\hat{\theta}) + \frac{1}{8}(\hat{\theta}\hat{\Gamma}_{[\hat{m}\hat{n}}\hat{T}_{\hat{a}}\hat{\theta})(\hat{\theta}\hat{\Gamma}^{\hat{a}}\hat{D}_{|\hat{p}}]\hat{\theta}) \\
& - \frac{1}{384}(\hat{\theta}\hat{\Gamma}_{\hat{m}\hat{n}\hat{p}}\hat{\Gamma}^{\hat{a}\hat{b}\hat{c}\hat{d}}\hat{\theta})(\hat{\theta}\hat{\Gamma}_{\hat{a}\hat{b}}[\hat{D}_{\hat{c}},\hat{D}_{\hat{d}}]\hat{\theta}) + \frac{1}{64}(\hat{\theta}\hat{\Gamma}_{[\hat{m}\hat{n}}\hat{\Gamma}^{\hat{a}\hat{b}\hat{c}}\hat{\theta})(\hat{\theta}\hat{\Gamma}_{\hat{p}]\hat{a}}[\hat{D}_{\hat{b}},\hat{D}_{\hat{c}}]\hat{\theta}) \\
& + \frac{1}{64}(\hat{\theta}\hat{\Gamma}_{[\hat{m}\hat{n}}\hat{\Gamma}^{\hat{a}\hat{b}\hat{c}}\hat{\theta})(\hat{\theta}\hat{\Gamma}_{\hat{a}\hat{b}}[\hat{D}_{|\hat{p}}],\hat{D}_{\hat{c}}]\hat{\theta}) + \frac{1}{8}(\hat{\theta}\hat{\Gamma}_{[\hat{m}\hat{n}}\hat{\Gamma}^{\hat{a}\hat{b}}\hat{\theta})(\hat{\theta}\hat{\mathcal{R}}_{\hat{a}\hat{b}}\hat{D}_{|\hat{p}}]\hat{\theta}) \\
& + \frac{1}{64}(\hat{\theta}\hat{\Gamma}_{[\hat{m}\hat{n}}\hat{\Gamma}^{\hat{a}\hat{b}}\hat{\theta})(\hat{\theta}\hat{\Gamma}_{\hat{p}}] [\hat{D}_{\hat{a}},\hat{D}_{\hat{b}}]\hat{\theta}) + \frac{1}{32}(\hat{\theta}\hat{\Gamma}_{[\hat{m}\hat{n}}\hat{\Gamma}^{\hat{a}\hat{b}}\hat{\theta})(\hat{\theta}\hat{\Gamma}_{\hat{a}}[\hat{D}_{|\hat{p}}],\hat{D}_{\hat{b}}]\hat{\theta}).
\end{aligned} \tag{15.307}$$

## 15.5 Further comments on T-duality

Here we discuss the T-duality calculation for the general Ramond-Ramond superfield expansions at second order in fermions. Notice that all three of the quadratic shifts so far calculated have been of the form

$$\mathcal{C}_{m_1\dots m_n}^{(n)} = C_{m_1\dots m_n}^{(n)} - \begin{cases} \frac{i}{2}e^{-\phi}\bar{\theta}^A a_n \left[ n\mathbb{F}_{[m_1\dots m_{n-1}}\mathbb{D}_{m_n]}^A - \frac{1}{2}\mathbb{F}_{m_1\dots m_n}\sigma^1\Delta^A \right] \theta^A, & n = 2p - 1, \\ \frac{i}{2}e^{-\phi}\bar{\theta}^B b_n \left[ n\tilde{\mathbb{F}}_{[m_1\dots m_{n-1}}\mathbb{D}_{m_n]}^B - \frac{1}{2}\tilde{\mathbb{F}}_{m_1\dots m_n}\sigma^1\Delta^B \right] \theta^B, & n = 2p, \end{cases}$$

where the  $a_n$  and  $b_n$  are some Pauli matrix combinations that need to be determined. We will show that this is the form for all the quadratic RR shifts, and determine  $a_n$  and  $b_n$  for all  $n$ , starting from the known results for  $n = 1, 3$ . The key equations to T-dualize these superfields into each other is the Ramond-Ramond superfield T-duality rule (13.232). In particular, defining the quadratic Ramond-Ramond superfield expansions as  $\mathcal{C}^{(n)} = C^{(n)} + \chi^{(n)}$ , one can write

$$\tilde{\chi}_{9\hat{m}_2\dots\hat{m}_{n+1}}^{(n+1)} = \chi_{\hat{m}_2\dots\hat{m}_{n+1}}^{(n)} - n g_{99}^{-1} g_{9[\hat{m}_2}\chi_{9|\hat{m}_3\dots\hat{m}_{n+1}}^{(n)}. \tag{15.308}$$

Let us first concentrate on the terms outside of the square brackets. For now we will neglect to write what appears inside the square brackets after applying (15.308), instead we shall just label it [IIA] or [IIB] to keep track of whether it has yet been T-dualized. Under T-dualization, moving from type IIA to type IIB we can



write,

$$\begin{aligned} -\frac{i}{2} e^{-\phi} \bar{\theta}^A a_{2p-1} [\text{IIA}] \theta^A &= -\frac{i}{2} e^{-\phi} \sqrt{\tilde{g}_{99}} (\bar{\theta}^B \sigma^1 \Upsilon \sigma^1) a_{2p-1} \Upsilon^{-1} \Upsilon [\text{IIA}] \Upsilon^{-1} \theta^B \\ &= -\frac{i}{2} e^{-\phi} \bar{\theta}^B b_{2p} \tilde{\Gamma}_9 \Upsilon [\text{IIA}] \Upsilon^{-1} \theta^B. \end{aligned}$$

We will see shortly that we will require  $\tilde{\Gamma}_9$  when T-dualizing the terms inside the square brackets, so write it separately in line two and treat that part in a moment. Moving from type IIB to type IIA, instead, we can write

$$\begin{aligned} \frac{i}{2} e^{-\phi} \bar{\theta}^B b_{2p} [\text{IIB}] \theta^B &= -\frac{i}{2} e^{-\phi} \sqrt{g_{99}} (\bar{\theta}^A \sigma^1 \Upsilon^{-1} \sigma^1) b_{2p} \Upsilon \Upsilon^{-1} [\text{IIB}] \Upsilon \theta^A \\ &= -\frac{i}{2} e^{-\phi} \bar{\theta}^A a_{2p+1} \Gamma_9 \Upsilon^{-1} [\text{IIB}] \Upsilon \theta^A. \end{aligned}$$

We know from the expansions in (13.244) that  $a_1 = \sigma^3$  and  $a_3 = 1_2$ . We also know from the definitions of the T-duality operators in section 13 that  $\sqrt{\tilde{g}_{99}} \sigma^1 \Upsilon \sigma^1 \sigma^3 \Upsilon^{-1} = \Gamma^* \tilde{\Gamma}_9$ , which allows to conclude that  $\bar{\theta}^B b_2 \tilde{\Gamma}_9 = \bar{\theta}^B \Gamma^* \tilde{\Gamma}_9$ , meaning that  $b_2 = -1_2$ . From  $\bar{\theta}^A a_3 \Gamma_9 = \sqrt{g_{99}} \bar{\theta}^A \sigma^1 \Upsilon^{-1} \sigma^1 b_2 \Upsilon = -\sqrt{g_{99}} \bar{\theta}^A \sigma^1 \Upsilon^{-1} \sigma^1 \Upsilon = \bar{\theta}^A \Gamma_9$ , we recover  $a_3 = 1_2$ . Going on, from  $\bar{\theta}^B b_4 \tilde{\Gamma}_9 = \sqrt{\tilde{g}_{99}} \bar{\theta}^B \sigma^1 \Upsilon \sigma^1 a_3 \Upsilon^{-1} = -\sigma^3 \bar{\theta}^B \Gamma_9$ , we find  $b_4 = -\sigma^3$ . Finally, from the chain of relationships  $\bar{\theta}^A a_5 \Gamma_9 = \sqrt{g_{99}} \bar{\theta}^A \sigma^1 \Upsilon^{-1} \sigma^1 b_4 \Upsilon = -\sqrt{g_{99}} \bar{\theta}^A \sigma^1 \Upsilon^{-1} \sigma^1 \sigma^3 \Upsilon = \sigma^3 \bar{\theta}^A \Gamma_9$ , we obtain  $a_5 = \sigma^3$ . In conclusion we have

$$a_1 = \sigma^3, \quad b_2 = -1_2, \quad a_3 = 1_2, \quad b_4 = -\sigma^3, \quad a_5 = \sigma^3. \quad (15.309)$$

The pattern continues, multiplying by  $-1_2$  when moving from IIB to IIA and by  $-\sigma^3$  when moving from IIA to IIB.

Now let us concentrate on the expressions [IIA] and [IIB] inside the square brackets. Here we will look at moving from type IIA to type IIB, however moving from type IIB to type IIA employs an essentially identical structure. More specifically, when we use (15.308) to determine the shift on  $C_{m_1 \dots m_{n+1}}^{(n+1)}$  from the shift on  $C_{m_1 \dots m_n}^{(n)}$  to move from IIA to IIB, we have to consider  $\tilde{\Gamma}_9 \Upsilon [\text{IIB}] \Upsilon^{-1}$ , and vice versa. The explicit terms are

$$\begin{aligned} [\text{IIA}]_{\tilde{m}_2 \dots \tilde{m}_{n+1}}^{[\tilde{\chi}^{(n+1)}]} &= \tilde{\Gamma}_9 \Upsilon \left[ n \mathbb{F}_{[\tilde{m}_2 \dots \tilde{m}_n] \mathbb{D}_{\tilde{m}_{n+1}}^A} - n(n-1) g_{99}^{-1} g_{9[\tilde{m}_2 | 9] \tilde{m}_3 \dots \tilde{m}_n} \mathbb{D}_{\tilde{m}_{n+1}}^A \right. \\ &\quad \left. - (-1)^{n-1} n g_{99}^{-1} g_{9[\tilde{m}_2 | \tilde{m}_3 \dots \tilde{m}_{n+1}]} \mathbb{D}_9^A \right. \\ &\quad \left. - \frac{1}{2} \left( \mathbb{F}_{\tilde{m}_2 \dots \tilde{m}_{n+1}} - n g_{99}^{-1} g_{9[\tilde{m}_2 | 9] \tilde{m}_3 \dots m_{n+1}} \right) \sigma^1 \Delta^A \right] \Upsilon^{-1}. \end{aligned}$$

After a little work and using  $(-1)^{n-1} n g_{99}^{-1} g_{9[\tilde{m}_2 | \tilde{m}_3 \dots \tilde{m}_{n+1}]} \mathbb{D}_9 = n g_{99}^{-1} g_{9[\tilde{m}_{n+1} | \tilde{m}_2 \dots \tilde{m}_n]} \mathbb{D}_9$ , this can be written as

$$\begin{aligned} [\text{IIA}]_{\tilde{m}_2 \dots \tilde{m}_{n+1}}^{[\tilde{\chi}^{(n+1)}]} &= \tilde{\Gamma}_9 \Upsilon \left[ n \left( \mathbb{F}_{[\tilde{m}_2} - g_{99}^{-1} g_{9[\tilde{m}_2 | \tilde{m}_3]} \Gamma_9 \right) \dots \left( \mathbb{F}_{\tilde{m}_n} - g_{99}^{-1} g_{9[\tilde{m}_n | \tilde{m}_{n+1}]} \Gamma_9 \right) \left( \mathbb{D}_{\tilde{m}_{n+1}}^A - g_{99}^{-1} g_{9[\tilde{m}_{n+1}]} \mathbb{D}_9^A \right) \right. \\ &\quad \left. - \frac{1}{2} \left( \mathbb{F}_{[\tilde{m}_2} - g_{99}^{-1} g_{9[\tilde{m}_2 | \tilde{m}_3]} \Gamma_9 \right) \dots \left( \mathbb{F}_{\tilde{m}_{n+1}} - g_{99}^{-1} g_{9[\tilde{m}_{n+1}]} \Gamma_9 \right) \sigma^1 \Delta^A \right] \Upsilon^{-1}. \end{aligned}$$

At this point, we can use (13.236) and (13.237) to T-dualize almost everything immediately, obtaining

$$\begin{aligned}
[\text{IIA}]_{\dot{m}_2 \dots \dot{m}_{n+1}}^{\tilde{\chi}^{(n+1)}} &= \tilde{\Gamma}_9 \left[ n \left( \tilde{\Gamma}_{[\dot{m}_2 - \tilde{g}_{99}^{-1} \tilde{g}_{9|\dot{m}_2]} \tilde{\Gamma}_9] \dots \left( \tilde{\Gamma}_{\dot{m}_n} - \tilde{g}_{99}^{-1} \tilde{g}_{9|\dot{m}_n} \tilde{\Gamma}_9 \right) \left( \mathbb{D}_{\dot{m}_{n+1}}^{\text{B}} - \tilde{g}_{99}^{-1} \tilde{g}_{9|\dot{m}_{n+1}} \mathbb{D}_9^{\text{B}} \right) \right. \right. \\
&\quad \left. \left. - \frac{1}{2} \left( \tilde{\Gamma}_{[\dot{m}_2 - \tilde{g}_{99}^{-1} \tilde{g}_{9|\dot{m}_2]} \tilde{\Gamma}_9] \dots \left( \tilde{\Gamma}_{\dot{m}_{n+1}} - \tilde{g}_{99}^{-1} \tilde{g}_{9|\dot{m}_{n+1}} \tilde{\Gamma}_9 \right) \left( \sigma^1 \Delta^{\text{B}} - 2\tilde{g}_{99}^{-1} \tilde{\Gamma}_9 \mathbb{D}_9^{\text{B}} \right) \right) \right] \\
&= \left[ n \tilde{\Gamma}_9 \tilde{\Gamma}_{[\dot{m}_2 \dots \dot{m}_n} \left( \mathbb{D}_{\dot{m}_{n+1}}^{\text{B}} - \tilde{g}_{99}^{-1} \tilde{g}_{9|\dot{m}_{n+1}} \mathbb{D}_9^{\text{B}} \right) - n(n-1) \tilde{g}_{9|\dot{m}_2} \tilde{\Gamma}_{\dot{m}_3 \dots \dot{m}_n} \mathbb{D}_{\dot{m}_{n+1}}^{\text{B}} \right. \\
&\quad \left. - \frac{1}{2} \tilde{\Gamma}_9 \tilde{\Gamma}_{\dot{m}_2 \dots \dot{m}_{n+1}} \left( \sigma^1 \Delta^{\text{B}} - 2\tilde{g}_{99}^{-1} \tilde{\Gamma}_9 \mathbb{D}_9^{\text{B}} \right) \right. \\
&\quad \left. + \frac{n}{2} \tilde{g}_{9|\dot{m}_2} \tilde{\Gamma}_{\dot{m}_3 \dots \dot{m}_{n+1}} \left( \sigma^1 \Delta^{\text{B}} - 2\tilde{g}_{99}^{-1} \tilde{\Gamma}_9 \mathbb{D}_9^{\text{B}} \right) \right] \\
&= \left[ n \tilde{\Gamma}_9 [\dot{m}_2 \dots \dot{m}_n \mathbb{D}_{\dot{m}_{n+1}}^{\text{B}}] - n \tilde{\Gamma}_9 [\dot{m}_2 \dots \dot{m}_n | \tilde{g}_{99}^{-1} \tilde{g}_{9|\dot{m}_{n+1}}] \mathbb{D}_9^{\text{B}} \right. \\
&\quad \left. + (-1)^n \tilde{\Gamma}_{\dot{m}_2 \dots \dot{m}_{n+1}} \tilde{g}_{99}^{-1} \tilde{\Gamma}_9 \mathbb{D}_9^{\text{B}} - \frac{1}{2} \tilde{\Gamma}_9 \dot{m}_2 \dots \dot{m}_{n+1} \sigma^1 \Delta^{\text{B}} \right],
\end{aligned}$$

where in the final step we combined some  $\Gamma$ -matrices, distributed the final term and eventually rearranged some indices. A further use of useful  $\Gamma$ -matrix identities and a little further massaging results in some more cancellations, to give

$$\begin{aligned}
[\text{IIA}]_{\dot{m}_2 \dots \dot{m}_{n+1}}^{\tilde{\chi}^{(n+1)}} &= \left[ n \tilde{\Gamma}_9 [\dot{m}_2 \dots \dot{m}_n \mathbb{D}_{\dot{m}_{n+1}}^{\text{B}}] - n \tilde{\Gamma}_9 [\dot{m}_2 \dots \dot{m}_n | \tilde{g}_{99}^{-1} \tilde{g}_{9|\dot{m}_{n+1}}] \mathbb{D}_9^{\text{B}} \right. \\
&\quad \left. + (-1)^n \left( \tilde{\Gamma}_{\dot{m}_2 \dots \dot{m}_{n+1}} \tilde{\Gamma}_9 - n \tilde{\Gamma}_{[\dot{m}_2 \dots \dot{m}_n | \tilde{g}_{99}^{-1} \tilde{g}_{9|\dot{m}_{n+1}}]} \tilde{g}_{99}^{-1} \tilde{\Gamma}_9 \mathbb{D}_9^{\text{B}} - \frac{1}{2} \tilde{\Gamma}_9 \dot{m}_2 \dots \dot{m}_{n+1} \sigma^1 \Delta^{\text{B}} \right) \right] \\
&= \left[ n \tilde{\Gamma}_9 [\dot{m}_2 \dots \dot{m}_n \mathbb{D}_{\dot{m}_{n+1}}^{\text{B}}] + (-1)^n \tilde{\Gamma}_{\dot{m}_2 \dots \dot{m}_{n+1}} \tilde{\Gamma}_9 \tilde{g}_{99}^{-1} \tilde{\Gamma}_9 \mathbb{D}_9^{\text{B}} - \frac{1}{2} \tilde{\Gamma}_9 \dot{m}_2 \dots \dot{m}_{n+1} \sigma^1 \Delta^{\text{B}} \right. \\
&\quad \left. - n \tilde{\Gamma}_9 [\dot{m}_2 \dots \dot{m}_n | \tilde{g}_{99}^{-1} \tilde{g}_{9|\dot{m}_{n+1}}] \mathbb{D}_9^{\text{B}} - (-1)^n n \tilde{\Gamma}_{[\dot{m}_2 \dots \dot{m}_n | \tilde{g}_{99}^{-1} \tilde{g}_{9|\dot{m}_{n+1}}]} \tilde{g}_{99}^{-1} \tilde{\Gamma}_9 \mathbb{D}_9^{\text{B}} \right] \\
&= \left[ n \tilde{\Gamma}_9 [\dot{m}_2 \dots \dot{m}_n \mathbb{D}_{\dot{m}_{n+1}}^{\text{B}}] + (-1)^n \tilde{\Gamma}_{\dot{m}_2 \dots \dot{m}_{n+1}} \mathbb{D}_9^{\text{B}} - \frac{1}{2} \tilde{\Gamma}_9 \dot{m}_2 \dots \dot{m}_{n+1} \sigma^1 \Delta^{\text{B}} \right. \\
&\quad \left. - n \tilde{\Gamma}_9 [\dot{m}_2 \dots \dot{m}_n | \tilde{g}_{99}^{-1} \tilde{g}_{9|\dot{m}_{n+1}}] \mathbb{D}_9^{\text{B}} - (-1)^{2n-1} n \tilde{\Gamma}_9 [\dot{m}_2 \dots \dot{m}_n | \tilde{g}_{99}^{-1} \tilde{g}_{9|\dot{m}_{n+1}}] \tilde{g}_{99}^{-1} \mathbb{D}_9^{\text{B}} \right] \\
&= \left[ n \tilde{\Gamma}_9 [\dot{m}_2 \dots \dot{m}_n \mathbb{D}_{\dot{m}_{n+1}}^{\text{B}}] + (-1)^n \tilde{\Gamma}_{\dot{m}_2 \dots \dot{m}_{n+1}} \mathbb{D}_9^{\text{B}} - \frac{1}{2} \tilde{\Gamma}_9 \dot{m}_2 \dots \dot{m}_{n+1} \sigma^1 \Delta^{\text{B}} \right] \\
&= \left[ (n+1) \tilde{\Gamma}_9 [\dot{m}_2 \dots \dot{m}_n \mathbb{D}_{\dot{m}_{n+1}}^{\text{B}}] - \frac{1}{2} \tilde{\Gamma}_9 \dot{m}_2 \dots \dot{m}_{n+1} \sigma^1 \Delta^{\text{B}} \right],
\end{aligned}$$

which is exactly the desired result. Note that while powers of  $(-1)$  depending on  $n$  appeared, nowhere did we rely on  $n$  being odd for the specific case of moving from type IIA to type IIB, and indeed the derivation moving the other way has precisely the same structure. Thanks to this procedure, one can verify the general second-order Ramond-Ramond shifts in (13.244).

# References

- [1] J. Rogers and R. Tatar, *Moduli space singularities for 3d  $\mathcal{N} = 4$  circular quiver gauge theories*, *JHEP* **11** (2018) [[1807.01754](#)].
- [2] J. Rogers and R. Tatar,  *$D_n$  Dynkin quiver moduli spaces*, *J. Phys. A* **52** (2019) [[1902.10019](#)].
- [3] A. Retolaza, J. Rogers, R. Tatar and F. Tonioni, *Branes, fermions, and superspace dualities*, *JHEP* **10** (2021) 243 [[2106.02090](#)].
- [4] S. Cabrera and A. Hanany, *Branes and the Kraft-Procesi Transition*, *JHEP* **11** (2016) 175 [[1609.07798](#)].
- [5] S. Cabrera and A. Hanany, *Branes and the Kraft-Procesi transition: classical case*, *JHEP* **04** (2018) 127 [[1711.02378](#)].
- [6] S. J. Gates, M. T. Grisaru, M. Rocek and W. Siegel, *Superspace Or One Thousand and One Lessons in Supersymmetry*, vol. 58 of *Frontiers in Physics*. Benjamin-Cummings Publishing, 1983, [[hep-th/0108200](#)].
- [7] J. Wess and J. Bagger, *Supersymmetry and supergravity*. Princeton University Press, Princeton, NJ, USA, 1992.
- [8] D. Z. Freedman and A. Van Proeyen, *Supergravity*. Cambridge Univ. Press, Cambridge, UK, 5, 2012.
- [9] H. Nakajima, *Instantons on ALE spaces, quiver varieties, and Kac-Moody algebras*, *Duke Math. J.* **76** (1994) 365.
- [10] M. R. Douglas and G. W. Moore, *D-branes, quivers, and ALE instantons*, [hep-th/9603167](#).
- [11] P. C. Argyres, M. R. Plesser and N. Seiberg, *The Moduli space of vacua of  $N=2$  SUSY QCD and duality in  $N=1$  SUSY QCD*, *Nucl. Phys. B* **471** (1996) 159 [[hep-th/9603042](#)].
- [12] N. Seiberg and E. Witten, *Monopoles, duality and chiral symmetry breaking in  $N=2$  supersymmetric QCD*, *Nucl. Phys. B* **431** (1994) 484 [[hep-th/9408099](#)].
- [13] N. Seiberg and E. Witten, *Gauge dynamics and compactification to three-dimensions*, in *Conference on the Mathematical Beauty of Physics (In Memory of C. Itzykson)*, pp. 333–366, 6, 1996, [hep-th/9607163](#).
- [14] K. A. Intriligator and N. Seiberg, *Mirror symmetry in three-dimensional gauge theories*, *Phys. Lett. B* **387** (1996) 513 [[hep-th/9607207](#)].
- [15] A. Hanany and E. Witten, *Type IIB superstrings, BPS monopoles, and three-dimensional gauge dynamics*, *Nucl. Phys. B* **492** (1997) 152 [[hep-th/9611230](#)].
- [16] A. Giveon and D. Kutasov, *Brane Dynamics and Gauge Theory*, *Rev. Mod. Phys.* **71** (1999) 983 [[hep-th/9802067](#)].
- [17] J. Hughes and J. Polchinski, *Partially Broken Global Supersymmetry and the Superstring*, *Nucl. Phys. B* **278** (1986) 147.
- [18] J. Hughes, J. Liu and J. Polchinski, *Supermembranes*, *Phys. Lett. B* **180** (1986) 370.

- [19] J. Polchinski, S. Chaudhuri and C. V. Johnson, *Notes on D-branes*, [hep-th/9602052](#).
- [20] V. Borokhov, A. Kapustin and X.-k. Wu, *Topological disorder operators in three-dimensional conformal field theory*, *JHEP* **11** (2002) 049 [[hep-th/0206054](#)].
- [21] V. Borokhov, A. Kapustin and X.-k. Wu, *Monopole operators and mirror symmetry in three-dimensions*, *JHEP* **12** (2002) 044 [[hep-th/0207074](#)].
- [22] V. Borokhov, *Monopole operators in three-dimensional N=4 SYM and mirror symmetry*, *JHEP* **03** (2004) 008 [[hep-th/0310254](#)].
- [23] D. Gaiotto and E. Witten, *S-Duality of Boundary Conditions In N=4 Super Yang-Mills Theory*, *Adv. Theor. Math. Phys.* **13** (2009) 721 [[0807.3720](#)].
- [24] D. Bashkirov and A. Kapustin, *Supersymmetry enhancement by monopole operators*, *JHEP* **05** (2011) 015 [[1007.4861](#)].
- [25] S. Cremonesi, A. Hanany and A. Zaffaroni, *Monopole operators and Hilbert series of Coulomb branches of 3d  $\mathcal{N} = 4$  gauge theories*, *JHEP* **01** (2014) 005 [[1309.2657](#)].
- [26] N. J. Hitchin, A. Karlhede, U. Lindstrom and M. Rocek, *Hyperkahler Metrics and Supersymmetry*, *Commun. Math. Phys.* **108** (1987) 535.
- [27] M. Billo and P. Fre, *Hyperkahler quotients and N=4 gauge theories in D = 2*, *Lect. Notes Phys.* **447** (1995) 145 [[hep-th/9411183](#)].
- [28] I. Antoniadis and B. Pioline, *Higgs branch, hyperKahler quotient and duality in SUSY N=2 Yang-Mills theories*, *Int. J. Mod. Phys. A* **12** (1997) 4907 [[hep-th/9607058](#)].
- [29] S. Benvenuti, B. Feng, A. Hanany and Y.-H. He, *Counting BPS Operators in Gauge Theories: Quivers, Syzygies and Plethystics*, *JHEP* **11** (2007) 050 [[hep-th/0608050](#)].
- [30] S. Benvenuti, A. Hanany and N. Mekareeya, *The Hilbert Series of the One Instanton Moduli Space*, *JHEP* **06** (2010) 100 [[1005.3026](#)].
- [31] D. Collingwood and W. McGovern, *Nilpotent orbits in semisimple Lie algebras*. Van Nostrand Reinhold, 1993.
- [32] E. Brieskorn, *Singular elements of semi-simple algebraic groups*, *Actes, Congres intern. Math.* **2** (1970) 279.
- [33] H. Kraft and C. Procesi, *Closures of conjugacy classes of matrices are normal.*, *Inventiones mathematicae* **53** (1979) 227.
- [34] H. Kraft and C. Procesi, *Minimal singularities in  $gln$ .*, *Inventiones mathematicae* **62** (1980/81) 503.
- [35] H. Kraft and C. Procesi, *On the geometry of conjugacy classes in classical groups.*, *Commentarii mathematici Helvetici* **57** (1982) 539.
- [36] B. Fu, D. Juteau, P. Levy and E. Sommers, *Generic singularities of nilpotent orbit closures*, 2016.
- [37] D. I. Panyushev, *On spherical nilpotent orbits and beyond*, *Annales de l'Institut Fourier* **49** (1999) 1453.
- [38] R. Yamagishi, *Crepant resolutions of a slodowy slice in a nilpotent orbit closure in  $\mathfrak{sl}_n(\mathbb{C})$* , 2016.
- [39] S. Cremonesi, A. Hanany, N. Mekareeya and A. Zaffaroni, *Coulomb branch Hilbert series and Hall-Littlewood polynomials*, *JHEP* **09** (2014) 178 [[1403.0585](#)].
- [40] S. Cremonesi, A. Hanany, N. Mekareeya and A. Zaffaroni, *Coulomb branch Hilbert series and Three Dimensional Sicilian Theories*, *JHEP* **09** (2014) 185 [[1403.2384](#)].

- [41] A. Hanany and R. Kalveks, *Highest Weight Generating Functions for Hilbert Series*, *JHEP* **10** (2014) 152 [[1408.4690](#)].
- [42] S. Cremonesi, G. Ferlito, A. Hanany and N. Mekareeya, *Coulomb Branch and The Moduli Space of Instantons*, *JHEP* **12** (2014) 103 [[1408.6835](#)].
- [43] S. Cremonesi, A. Hanany, N. Mekareeya and A. Zaffaroni,  *$T_\rho^\sigma(G)$  theories and their Hilbert series*, *JHEP* **01** (2015) 150 [[1410.1548](#)].
- [44] S. Cremonesi, G. Ferlito, A. Hanany and N. Mekareeya, *Instanton Operators and the Higgs Branch at Infinite Coupling*, *JHEP* **04** (2017) 042 [[1505.06302](#)].
- [45] A. Hanany and R. Kalveks, *Construction and Deconstruction of Single Instanton Hilbert Series*, *JHEP* **12** (2015) 118 [[1509.01294](#)].
- [46] A. Hanany and M. Sperling, *Coulomb branches for rank 2 gauge groups in  $3d \mathcal{N} = 4$  gauge theories*, *JHEP* **08** (2016) 016 [[1605.00010](#)].
- [47] A. Hanany and M. Sperling, *Algebraic properties of the monopole formula*, *JHEP* **02** (2017) 023 [[1611.07030](#)].
- [48] A. Dey, A. Hanany, P. Koroteev and N. Mekareeya, *On Three-Dimensional Quiver Gauge Theories of Type B*, *JHEP* **09** (2017) 067 [[1612.00810](#)].
- [49] S. Cabrera, A. Hanany and Z. Zhong, *Nilpotent orbits and the Coulomb branch of  $T^\sigma(G)$  theories: special orthogonal vs orthogonal gauge group factors*, *JHEP* **11** (2017) 079 [[1707.06941](#)].
- [50] A. Hanany and N. Mekareeya, *The small  $E_8$  instanton and the Kraft Procesi transition*, *JHEP* **07** (2018) 098 [[1801.01129](#)].
- [51] A. Hanany and D. Miketa, *Nilpotent orbit Coulomb branches of types AD*, *JHEP* **02** (2019) 113 [[1807.11491](#)].
- [52] A. Hanany and R. Kalveks, *Quiver Theories for Moduli Spaces of Classical Group Nilpotent Orbits*, *JHEP* **06** (2016) 130 [[1601.04020](#)].
- [53] A. Hanany and R. Kalveks, *Quiver Theories and Formulae for Nilpotent Orbits of Exceptional Algebras*, *JHEP* **11** (2017) 126 [[1709.05818](#)].
- [54] S. Cabrera, A. Hanany and R. Kalveks, *Quiver Theories and Formulae for Slodowy Slices of Classical Algebras*, *Nucl. Phys. B* **939** (2019) 308 [[1807.02521](#)].
- [55] A. Hanany and R. Kalveks, *Quiver Theories and Hilbert Series of Classical Slodowy Intersections*, *Nucl. Phys. B* **952** (2020) 114939 [[1909.12793](#)].
- [56] A. Giveon and O. Pelc, *M theory, type iia string and  $4d n = 1$  susy  $su(nl) \otimes su(nr)$  gauge theory*, *Nuclear Physics B* **512** (1998) 103–147.
- [57] P. C. Argyres, M. Ronen Plesser and N. Seiberg, *The moduli space of vacua of  $n = 2$  susy qcd and duality in  $n = 1$  susy qcd*, *Nuclear Physics B* **471** (1996) 159–194.
- [58] B. Assel, C. Bachas, J. Estes and J. Gomis, *IIB Duals of  $D=3 N=4$  Circular Quivers*, *JHEP* **12** (2012) 044 [[1210.2590](#)].
- [59] J. de Boer, K. Hori, H. Ooguri, Y. Oz and Z. Yin, *Mirror symmetry in three-dimensional theories,  $SL(2, Z)$  and D-brane moduli spaces*, *Nucl. Phys. B* **493** (1997) 148 [[hep-th/9612131](#)].

- [60] A. Dey, A. Hanany, N. Mekareeya, D. Rodríguez-Gómez and R.-K. Seong, *Hilbert Series for Moduli Spaces of Instantons on  $C^2/Z_n$* , *JHEP* **01** (2014) 182 [[1309.0812](#)].
- [61] N. Mekareeya, *The moduli space of instantons on an ALE space from 3d  $\mathcal{N} = 4$  field theories*, *JHEP* **12** (2015) 174 [[1508.06813](#)].
- [62] A. Kapustin,  *$D(n)$  quivers from branes*, *JHEP* **12** (1998) 015 [[hep-th/9806238](#)].
- [63] A. Hanany and M. Sperling, *Resolutions of nilpotent orbit closures via Coulomb branches of 3-dimensional  $\mathcal{N} = 4$  theories*, *JHEP* **08** (2018) 189 [[1806.01890](#)].
- [64] S. Cabrera and A. Hanany, *Quiver Subtractions*, *JHEP* **09** (2018) 008 [[1803.11205](#)].
- [65] J. Bao, A. Hanany, Y.-H. He and E. Hirst, *Some Open Questions in Quiver Gauge Theory*, [2108.05167](#).
- [66] A. Hanany and M. Sperling, *Discrete quotients of 3-dimensional  $\mathcal{N} = 4$  Coulomb branches via the cycle index*, *JHEP* **08** (2018) 157 [[1807.02784](#)].
- [67] A. Hanany and A. Zajac, *Discrete Gauging in Coulomb branches of Three Dimensional  $\mathcal{N} = 4$  Supersymmetric Gauge Theories*, *JHEP* **08** (2018) 158 [[1807.03221](#)].
- [68] S. Cabrera, A. Hanany and A. Zajac, *Minimally Unbalanced Quivers*, *JHEP* **02** (2019) 180 [[1810.01495](#)].
- [69] S. Cabrera, A. Hanany and F. Yagi, *Tropical Geometry and Five Dimensional Higgs Branches at Infinite Coupling*, *JHEP* **01** (2019) 068 [[1810.01379](#)].
- [70] S. Cabrera, A. Hanany and M. Sperling, *Magnetic quivers, Higgs branches, and 6d  $\mathcal{N}=(1,0)$  theories*, *JHEP* **06** (2019) 071 [[1904.12293](#)].
- [71] A. Bourget, S. Cabrera, J. F. Grimminger, A. Hanany, M. Sperling, A. Zajac et al., *The Higgs mechanism — Hasse diagrams for symplectic singularities*, *JHEP* **01** (2020) 157 [[1908.04245](#)].
- [72] A. Bourget, S. Cabrera, J. F. Grimminger, A. Hanany and Z. Zhong, *Brane Webs and Magnetic Quivers for SQCD*, *JHEP* **03** (2020) 176 [[1909.00667](#)].
- [73] S. Cabrera, A. Hanany and M. Sperling, *Magnetic quivers, Higgs branches, and 6d  $\mathcal{N} = (1, 0)$  theories — orthogonal and symplectic gauge groups*, *JHEP* **02** (2020) 184 [[1912.02773](#)].
- [74] A. Hanany and A. Zajac, *Ungauging Schemes and Coulomb Branches of Non-simply Laced Quiver Theories*, *JHEP* **09** (2020) 193 [[2002.05716](#)].
- [75] J. F. Grimminger and A. Hanany, *Hasse diagrams for 3d  $\mathcal{N} = 4$  quiver gauge theories — Inversion and the full moduli space*, *JHEP* **09** (2020) 159 [[2004.01675](#)].
- [76] A. Bourget, J. F. Grimminger, A. Hanany, M. Sperling and Z. Zhong, *Magnetic Quivers from Brane Webs with O5 Planes*, *JHEP* **07** (2020) 204 [[2004.04082](#)].
- [77] A. Bourget, A. Hanany and D. Miketa, *Quiver origami: discrete gauging and folding*, *JHEP* **01** (2021) 086 [[2005.05273](#)].
- [78] A. Bourget, J. F. Grimminger, A. Hanany, M. Sperling, G. Zafrir and Z. Zhong, *Magnetic quivers for rank 1 theories*, *JHEP* **09** (2020) 189 [[2006.16994](#)].
- [79] A. Bourget, J. F. Grimminger, A. Hanany, R. Kalveks, M. Sperling and Z. Zhong, *Magnetic Lattices for Orthosymplectic Quivers*, *JHEP* **12** (2020) 092 [[2007.04667](#)].

- [80] A. Bourget, S. Giacomelli, J. F. Grimminger, A. Hanany, M. Sperling and Z. Zhong, *S-fold magnetic quivers*, *JHEP* **02** (2021) 054 [[2010.05889](#)].
- [81] A. Bourget, J. F. Grimminger, A. Hanany, M. Sperling and Z. Zhong, *Branes, Quivers, and the Affine Grassmannian*, [2102.06190](#).
- [82] A. Bourget, A. Dancer, J. F. Grimminger, A. Hanany, F. Kirwan and Z. Zhong, *Orthosymplectic implosions*, *JHEP* **08** (2021) 012 [[2103.05458](#)].
- [83] A. Bourget, J. F. Grimminger, A. Hanany, R. Kalveks, M. Sperling and Z. Zhong, *Folding Orthosymplectic Quivers*, [2107.00754](#).
- [84] J. Polchinski, *Dirichlet Branes and Ramond-Ramond charges*, *Phys. Rev. Lett.* **75** (1995) 4724 [[hep-th/9510017](#)].
- [85] S. Kachru, R. Kallosh, A. D. Linde and S. P. Trivedi, *De Sitter vacua in string theory*, *Phys. Rev.* **D68** (2003) 046005 [[hep-th/0301240](#)].
- [86] P. Koerber and L. Martucci, *From ten to four and back again: How to generalize the geometry*, *JHEP* **08** (2007) 059 [[0707.1038](#)].
- [87] P. Koerber and L. Martucci, *Warped generalized geometry compactifications, effective theories and non-perturbative effects*, *Fortsch. Phys.* **56** (2008) 862 [[0803.3149](#)].
- [88] I. Bena, M. Grana and N. Halmagyi, *On the Existence of Meta-stable Vacua in Klebanov-Strassler*, *JHEP* **09** (2010) 087 [[0912.3519](#)].
- [89] D. Baumann, A. Dymarsky, S. Kachru, I. R. Klebanov and L. McAllister, *D3-brane Potentials from Fluxes in AdS/CFT*, *JHEP* **06** (2010) 072 [[1001.5028](#)].
- [90] B. Heidenreich, L. McAllister and G. Torroba, *Dynamic SU(2) Structure from Seven-branes*, *JHEP* **05** (2011) 110 [[1011.3510](#)].
- [91] A. Dymarsky and L. Martucci, *D-brane non-perturbative effects and geometric deformations*, *JHEP* **04** (2011) 061 [[1012.4018](#)].
- [92] J. Blaback, U. H. Danielsson, D. Junghans, T. Van Riet, T. Wrase and M. Zagermann, *(Anti-)Brane backreaction beyond perturbation theory*, *JHEP* **02** (2012) 025 [[1111.2605](#)].
- [93] I. Bena, M. Grana, S. Kuperstein and S. Massai, *Giant Tachyons in the Landscape*, *JHEP* **02** (2015) 146 [[1410.7776](#)].
- [94] I. Bena, J. Blåbäck and D. Turton, *Loop corrections to the antibrane potential*, *JHEP* **07** (2016) 132 [[1602.05959](#)].
- [95] S. Sethi, *Supersymmetry Breaking by Fluxes*, *JHEP* **10** (2018) 022 [[1709.03554](#)].
- [96] J. Moritz, A. Retolaza and A. Westphal, *Toward de Sitter space from ten dimensions*, *Phys. Rev.* **D97** (2018) 046010 [[1707.08678](#)].
- [97] I. Bena, E. Dudas, M. Grana and S. Luest, *Uplifting Runaways*, *Fortsch. Phys.* **67** (2019) 1800100 [[1809.06861](#)].
- [98] L. Randall, *The Boundaries of KKLt*, *Fortsch. Phys.* **68** (2020) 1900105 [[1912.06693](#)].
- [99] R. Blumenhagen, D. Klaewer and L. Schlechter, *Swampland Variations on a Theme by KKLt*, *JHEP* **05** (2019) 152 [[1902.07724](#)].
- [100] I. Bena, M. Graña, N. Kovensky and A. Retolaza, *Kähler moduli stabilization from ten dimensions*, *JHEP* **10** (2019) 200 [[1908.01785](#)].

- [101] M. Demirtas, M. Kim, L. McAllister and J. Moritz, *Vacua with Small Flux Superpotential*, *Phys. Rev. Lett.* **124** (2020) 211603 [[1912.10047](#)].
- [102] M. Graña, N. Kovensky and A. Retolaza, *Gaugino mass term for D-branes and Generalized Complex Geometry*, *JHEP* **06** (2020) 047 [[2002.01481](#)].
- [103] X. Gao, A. Hebecker and D. Junghans, *Control issues of KKLT*, [2009.03914](#).
- [104] F. Carta and J. Moritz, *Resolving spacetime singularities in flux compactifications & KKLT*, [2101.05281](#).
- [105] R. Kallosh, A.-K. Kashani-Poor and A. Tomasiello, *Counting fermionic zero modes on M5 with fluxes*, *JHEP* **06** (2005) 069 [[hep-th/0503138](#)].
- [106] P. K. Tripathy and S. P. Trivedi, *D3 brane action and fermion zero modes in presence of background flux*, *JHEP* **06** (2005) 066 [[hep-th/0503072](#)].
- [107] R. Kallosh and D. Sorokin, *Dirac action on M5 and M2 branes with bulk fluxes*, *JHEP* **05** (2005) 005 [[hep-th/0501081](#)].
- [108] F. F. Gautason, V. Van Hemelryck and T. Van Riet, *The Tension between 10D Supergravity and dS Uplifts*, *Fortsch. Phys.* **67** (2019) 1800091 [[1810.08518](#)].
- [109] Y. Hamada, A. Hebecker, G. Shiu and P. Soler, *On brane gaugino condensates in 10d*, *JHEP* **04** (2019) 008 [[1812.06097](#)].
- [110] R. Kallosh, *Gaugino Condensation and Geometry of the Perfect Square*, *Phys. Rev.* **D99** (2019) 066003 [[1901.02023](#)].
- [111] Y. Hamada, A. Hebecker, G. Shiu and P. Soler, *Understanding KKLT from a 10d perspective*, *JHEP* **06** (2019) 019 [[1902.01410](#)].
- [112] F. F. Gautason, V. Van Hemelryck, T. Van Riet and G. Venken, *A 10d view on the KKLT AdS vacuum and uplifting*, *JHEP* **06** (2020) 074 [[1902.01415](#)].
- [113] F. Carta, J. Moritz and A. Westphal, *Gaugino condensation and small uplifts in KKLT*, *JHEP* **08** (2019) 141 [[1902.01412](#)].
- [114] S. Kachru, M. Kim, L. McAllister and M. Zimet, *de Sitter Vacua from Ten Dimensions*, [1908.04788](#).
- [115] Y. Hamada, A. Hebecker, G. Shiu and P. Soler, *Completing the D7-brane local gaugino action*, [2105.11467](#).
- [116] P. Horava and E. Witten, *Heterotic and type I string dynamics from eleven-dimensions*, *Nucl. Phys. B* **460** (1996) 506 [[hep-th/9510209](#)].
- [117] P. Horava and E. Witten, *Eleven-dimensional supergravity on a manifold with boundary*, *Nucl. Phys. B* **475** (1996) 94 [[hep-th/9603142](#)].
- [118] P. Horava, *Gluino condensation in strongly coupled heterotic string theory*, *Phys. Rev. D* **54** (1996) 7561 [[hep-th/9608019](#)].
- [119] M. Dine, R. Rohm, N. Seiberg and E. Witten, *Gluino Condensation in Superstring Models*, *Phys. Lett.* **156B** (1985) 55.
- [120] R. Kallosh and T. Wrase, *Emergence of Spontaneously Broken Supersymmetry on an Anti-D3-Brane in KKLT dS Vacua*, *JHEP* **12** (2014) 117 [[1411.1121](#)].



- [121] R. Kallosh, B. Vercnocke and T. Wrase, *String Theory Origin of Constrained Multiplets*, *JHEP* **09** (2016) 063 [[1606.09245](#)].
- [122] N. Cribiori, C. Roupec, M. Tournoy, A. Van Proeyen and T. Wrase, *Non-supersymmetric branes*, *JHEP* **07** (2020) 189 [[2004.13110](#)].
- [123] B. de Wit, K. Peeters and J. Plefka, *Superspace geometry for supermembrane backgrounds*, *Nucl. Phys. B* **532** (1998) 99 [[hep-th/9803209](#)].
- [124] M. Grana, *D3-brane action in a supergravity background: The Fermionic story*, *Phys. Rev.* **D66** (2002) 045014 [[hep-th/0202118](#)].
- [125] D. Marolf, L. Martucci and P. J. Silva, *Fermions, T duality and effective actions for D-branes in bosonic backgrounds*, *JHEP* **04** (2003) 051 [[hep-th/0303209](#)].
- [126] D. Marolf, L. Martucci and P. J. Silva, *Actions and Fermionic symmetries for D-branes in bosonic backgrounds*, *JHEP* **07** (2003) 019 [[hep-th/0306066](#)].
- [127] L. Martucci, J. Rosseel, D. Van den Bleeken and A. Van Proeyen, *Dirac actions for D-branes on backgrounds with fluxes*, *Class. Quant. Grav.* **22** (2005) 2745 [[hep-th/0504041](#)].
- [128] P. K. Townsend, *Four lectures on M theory*, in *ICTP Summer School in High-energy Physics and Cosmology*, 12, 1996, [hep-th/9612121](#).
- [129] I. N. McArthur, *Superspace Normal Coordinates*, *Class. Quant. Grav.* **1** (1984) 233.
- [130] M. T. Grisaru and M. E. Knutt, *Norcor versus the abominable gauge completion*, *Phys. Lett. B* **500** (2001) 188 [[hep-th/0011173](#)].
- [131] D. Tsmpis, *Curved 11D supergeometry*, *JHEP* **11** (2004) 087 [[hep-th/0407244](#)].
- [132] S. F. Hassan, *T duality, space-time spinors and RR fields in curved backgrounds*, *Nucl. Phys. B* **568** (2000) 145 [[hep-th/9907152](#)].
- [133] S. F. Hassan, *SO(d,d) transformations of Ramond-Ramond fields and space-time spinors*, *Nucl. Phys. B* **583** (2000) 431 [[hep-th/9912236](#)].
- [134] S. F. Hassan, *Supersymmetry and the systematics of T duality rotations in type II superstring theories*, *Nucl. Phys. B Proc. Suppl.* **102** (2001) 77 [[hep-th/0103149](#)].
- [135] I. Low and A. V. Manohar, *Spontaneously broken space-time symmetries and Goldstone's theorem*, *Phys. Rev. Lett.* **88** (2002) 101602 [[hep-th/0110285](#)].
- [136] E. Bergshoeff, E. Sezgin and P. Townsend, *Supermembranes and Eleven-Dimensional Supergravity*, *Phys. Lett. B* **189** (1987) 75.
- [137] E. Bergshoeff, E. Sezgin and P. K. Townsend, *Properties of the Eleven-Dimensional Super Membrane Theory*, *Annals Phys.* **185** (1988) 330.
- [138] I. Bandos and D. Sorokin, *Aspects of D-brane dynamics in supergravity backgrounds with fluxes, kappa-symmetry and equations of motion: Part IIB*, *Nucl. Phys. B* **759** (2006) 399 [[hep-th/0607163](#)].
- [139] E. Cremmer, B. Julia and J. Scherk, *Supergravity Theory in Eleven-Dimensions*, *Phys. Lett. B* **76** (1978) 409.
- [140] E. Cremmer and S. Ferrara, *Formulation of Eleven-Dimensional Supergravity in Superspace*, *Phys. Lett. B* **91** (1980) 61.

- [141] L. Brink and P. S. Howe, *Eleven-Dimensional Supergravity on the Mass-Shell in Superspace*, *Phys. Lett. B* **91** (1980) 384.
- [142] L. Alvarez-Gaume, D. Z. Freedman and S. Mukhi, *The Background Field Method and the Ultraviolet Structure of the Supersymmetric Nonlinear Sigma Model*, *Annals Phys.* **134** (1981) 85.
- [143] S. Mukhi, *The Geometric Background Field Method, Renormalization and the Wess-Zumino Term in Nonlinear Sigma Models*, *Nucl. Phys. B* **264** (1986) 640.
- [144] J. J. Atick and A. Dhar, *Normal Coordinates,  $\theta$  Expansion and Strings on Curved Superspace*, *Nucl. Phys. B* **284** (1987) 131.
- [145] M. T. Grisaru and D. Zanon, *The Green-schwarz Superstring  $\sigma$  Model*, *Nucl. Phys. B* **310** (1988) 57.
- [146] M. T. Grisaru, M. E. Knutt-Wehlau and W. Siegel, *A Superspace normal coordinate derivation of the density formula*, *Nucl. Phys. B* **523** (1998) 663 [[hep-th/9711120](#)].
- [147] J. M. Figueroa-O'Farrill, *On the supersymmetries of Anti-de Sitter vacua*, *Class. Quant. Grav.* **16** (1999) 2043 [[hep-th/9902066](#)].
- [148] T. Ortin, *A Note on Lie-Lorentz derivatives*, *Class. Quant. Grav.* **19** (2002) L143 [[hep-th/0206159](#)].
- [149] Y. Kosmann, *Derives de Lie des spineurs*, *Annali di Mat. Pura Appl.* (1971) 317.
- [150] L. Martucci and P. J. Silva, *On type 2 superstrings in bosonic backgrounds and their T duality relation*, *JHEP* **04** (2003) 004 [[hep-th/0303102](#)].
- [151] M. Serra, *Membrane dynamics in non-supersymmetric AdS M-theory vacua*, *MSc. Thesis* (2021) .
- [152] E. Bergshoeff, R. Kallosh, T. Ortin and G. Papadopoulos, *Kappa symmetry, supersymmetry and intersecting branes*, *Nucl. Phys. B* **502** (1997) 149 [[hep-th/9705040](#)].
- [153] J. Simon, *Brane Effective Actions, Kappa-Symmetry and Applications*, *Living Rev. Rel.* **15** (2012) 3 [[1110.2422](#)].
- [154] E. Bergshoeff, R. Kallosh, T. Ortin, D. Roest and A. Van Proeyen, *New formulations of  $D = 10$  supersymmetry and  $D8 - O8$  domain walls*, *Class. Quant. Grav.* **18** (2001) 3359 [[hep-th/0103233](#)].
- [155] L. Wulff, *The type II superstring to order  $\theta^4$* , *JHEP* **07** (2013) 123 [[hep-th/1304.6422](#)].
- [156] T. Buscher, *A symmetry of the string background field equations*, *Physics Letters B* **194** (1987) 59.
- [157] T. Buscher, *Path-integral derivation of quantum duality in nonlinear sigma-models*, *Physics Letters B* **201** (1988) 466.
- [158] E. Bergshoeff, C. M. Hull and T. Ortin, *Duality in the type II superstring effective action*, *Nucl. Phys. B* **451** (1995) 547 [[hep-th/9504081](#)].
- [159] D. Luest, F. Marchesano, L. Martucci and D. Tsimpis, *Generalized non-supersymmetric flux vacua*, *JHEP* **11** (2008) 021 [[0807.4540](#)].
- [160] E. Bergshoeff and M. De Roo, *D-branes and T duality*, *Phys. Lett. B* **380** (1996) 265 [[hep-th/9603123](#)].
- [161] R. C. Myers, *Dielectric branes*, *JHEP* **12** (1999) 022 [[hep-th/9910053](#)].
- [162] I. A. Bandos and B. Julia, *Superfield T duality rules*, *JHEP* **08** (2003) 032 [[hep-th/0303075](#)].
- [163] P. S. Howe, *Weyl superspace*, *Phys. Lett. B* **415** (1997) 149 [[hep-th/9707184](#)].